Preparation of Sulfoximines, Sulfoximidoyl Derivatives and Sulfones via Visible-Light Photocatalysis

Dissertation

Zur Erlangung des Doktorgrades der Naturwissenschaften

(Dr. rer. nat.)

an der Fakultät für Chemie und Pharmazie

der Universität Regensburg

vorgelegt von

Alexander Wimmer

aus Bad Griesbach

2019

The experimental work was carried out at the Institute of Organic Chemistry at the University of Regensburg under the supervision of Prof. Dr. Burkhard König between November 2016 and October 2019 and at the Department of Chemistry at the University of Montreal under the supervision of Prof. Dr. Shawn K. Collins between July and September 2019.

Date of submission: 21.10.2019
Date of colloquium: 02.12.2019

Board of examiners:

Chair: Apl. Prof. Dr. Rainer Müller
1st Referee: Prof. Dr. Burkhard König
2nd Referee: Prof. Dr. Frank-Michael Matysik
Examiner: Prof. Dr. Alexander Breder

This thesis is dedicated to

My parents Angela & Adolf

My sister Nadine

„Nicht zur Strafe, nur zur Übung.“

A. A. Wimmer

In anderen Worten / In other words

Fehler passieren – Fehler sind menschlich. Lerne aus ihnen und versuche dich erneut.

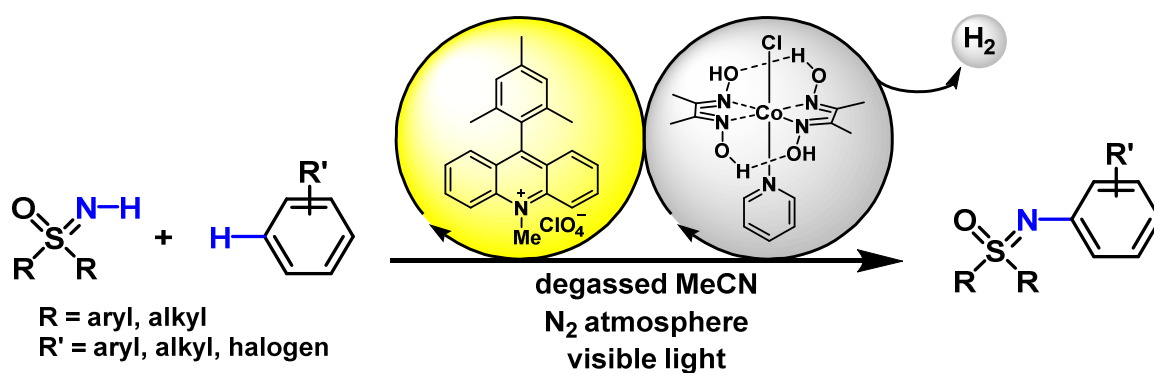*Take chances, make mistakes. Mistakes are human. That's how you grow.*

TABLE OF CONTENTS

1. Visible-Light-Mediated Photoredox-Catalyzed *N*-Arylation of *NH*-Sulfoximines with Electron-Rich Arenes

R = aryl, alkyl
R' = aryl, alkyl, halogen

degassed MeCN
N₂ atmosphere
visible light

CHAPTER 1

Visible-Light-Mediated Photoredox-Catalyzed *N-Arylation* of *NH-Sulfoximines* with Electron-Rich Arenes

1.1 Abstract

The direct C–H/N–H dehydrogenative cross-coupling of *NH*-sulfoximines with electron-rich arenes was realized by oxidative visible-light photoredox catalysis, applying 9-mesityl-10-methylacridinium perchlorate as an organic photocatalyst. Sulfoximines display diverse desirable properties for medicinal chemistry and the pharmaceutical industry. However, their preparation is still challenging.

Our reaction proceeds without sacrificial oxidant, at room temperature and is highly selective for the C–N bond forming reaction. The scope of the reaction includes mono- and multi-alkylated and halogenated arenes, which are reacted with aromatic and aliphatic electron-rich and electron-poor *NH*-sulfoximines, giving moderate to excellent yields of the *N*-arylated sulfoximines. In addition, we successfully conducted the developed reaction on a gram scale in batch as well as in continuous flow.

Mechanistic investigations show that both arene and *NH*-sulfoximine interact with the excited-state of the photocatalyst. We propose a radical-based mechanism, where both the arene and the *NH*-sulfoximine are photo-oxidized to their respective radical intermediates. Radical-radical cross-coupling subsequently leads to the *N*-arylated sulfoximine. Two electrons and two protons are released during the reaction and are subsequently converted into H_2 by a proton-reducing cobalt-catalyst.

Author contributions:

AW developed the reaction, carried out the experiments and wrote the manuscript. BK supervised the project and is the corresponding author.

1.2 Introduction

Sulfoximines, the monoaza analogues of sulfones, are a rather uncommon class of substrates to many chemists, although their discovery goes back into the early 1950s.[1] Due to their chemical and configurational stability, first applications mainly focused on asymmetric reactions or catalysis where they act as chiral auxiliaries or ligands.[2] Only recently, it was realized that the diverse structure of sulfoximines has much more to offer, especially in medicinal chemistry and the pharmaceutical industry. Recent reports attest sulfoximines to be relevant bioactive structures, which display desirable metabolic stability and physicochemical properties in combination with hydrogen-bond acceptor/donor functionalities.[3] Consequently, pharmaceutical companies developed sulfoximine-based drugs or pharmaceutical agents. Several kinase inhibiting drug candidates for the treatment of cancer have already been introduced to clinical trials such as roniciclib, BAY 1143572 and AZD 6738 (Figure 1). Nevertheless, very limited synthetic procedures associated with safety concerns hampered the application of sulfoximines in drug discovery for a long time.[4]
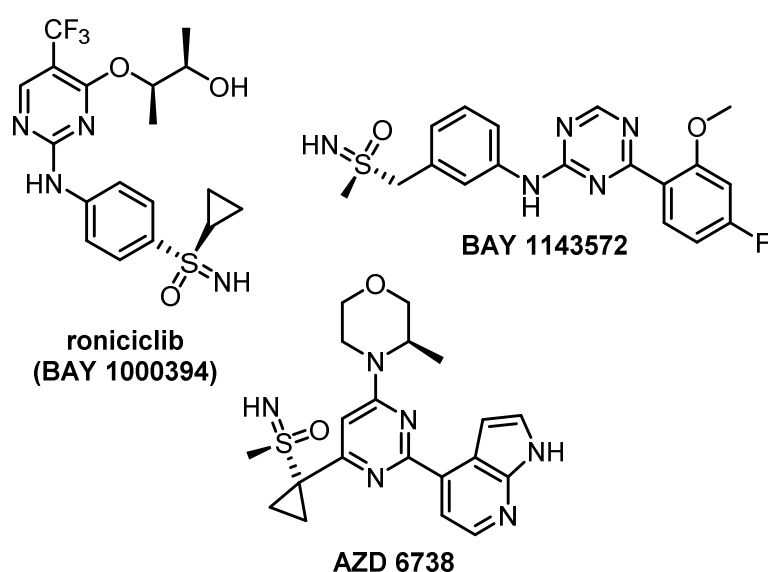

Figure 1. Examples for kinase inhibiting candidates for the treatment of cancer in clinical trials.

Ideal sulfoximines for further functionalization and derivatization are unprotected *NH*-sulfoximines. Classic synthetic strategies proceed *via* three steps including oxidation and imination of sulfides and a final deprotection to the respective unsubstituted

NH-sulfoximine.[5] Very recently, the groups of Bull and Luisi reported the direct synthesis of unsubstituted *NH*-sulfoximines from the respective sulfides in an "one-pot-synthesis".[6] This approach significantly facilitates the access to "free" *NH*-sulfoximines and further *N*-functionalization reactions.

The direct *N*-arylation of *NH*-sulfoximines was first reported by the group of Bolm in 1998. Inspired by the palladium-catalyzed amination of aryl halides with amines by Buchwald[7] and Hartwig,[8] they successfully applied this concept to the cross-coupling of aryl bromides with *NH*-sulfoximines.[9] In the following years, various transition-metal-catalyzed (Pd, Cu, Ni and Fe) approaches have been developed, enabling the cross-coupling also with other aryl halides, aryl triflates, nonaflates, tosylates, arylboronic acids, diaryliodonium salts, arylsiloxanes, sodium arylsulfinates and acyl peroxides.[2i, 2n, 10] In order to avoid the need of pre-activated substrates Bolm and Jeganmohan described the direct transition-metal-catalyzed C–H bond activation and subsequent C–N bond formation with *NH*-sulfoximines (Scheme 1a. and b.).[11] However, such metal-catalyzed processes often require high reaction temperatures, pre-activated substrates or expensive metals combined with special ligands. Furthermore, in late-stage functionalization of complex molecules, the functional group compatibility can be challenging and metal-derived impurities can cause elaborative purification. In this context, it is surprising that only very few metal-free reports for the *N*-arylation of *NH*-sulfoximines have been reported. On one hand electrophilic azine *N*-oxides were found to be reactive enough to be coupled with *NH*-sulfoximines after activation with phosphonium salts.[12] On the other hand, in-situ generated arynes were successfully reacted with nucleophilic *NH*-sulfoximines by the group of Singh and Hosoya very recently.[13]

The reported methods for the *N*-arylation of *NH*-sulfoximines use transition-metal catalysis or require special reactive precursors or reagents. Visible-light photoredox catalysis enables the generation of highly reactive intermediates, but at the same time proceeds under very mild reaction conditions. This may facilitate selective and unique bond formations, which are inaccessible by classic synthetic methods. High-intensity, visible-light emitting diodes are commercially available and simple reaction setups now allow every chemist to conduct photoredox-catalyzed reactions without expended effort or expensive equipment.[14]

Very recently, metal-free organic photoredox catalysts were applied for the direct oxidative *N*-arylation of amines by the groups of Nicewicz and Lei.[15] These approaches demonstrate the advantages of visible-light photoredox catalysis in developing challenging

unique bond formations in a very sustainable and atom-economic manner. To the best of our knowledge, no visible-light photoredox-catalyzed approach for the *N*-arylation of *NH*-sulfoximines exists in the current literature. We therefore focused on developing a new synthetic strategy for the direct oxidative C–H/N–H dehydrogenative cross-coupling of arenes and *NH*-sulfoximines *via* organic visible-light photoredox catalysis (Scheme 1c.).

a. Transition-metal catalyzed *N*-arylation with pre-functionalized arenes

R = aryl, alkyl
X = Hal, OTf, OS(O)$_2$(CF$_2$)$_3$CF$_3$, OTs, B(OH)$_2$, IAr,
    Si(OR)$_3$, SO$_2$Na, C(O)O$_2$C(O)Ar

b. Transition-metal catalyzed *N*-arylation *via* direct C-H bond activation

R = aryl, alkyl
X = Het, directing group

c. Our Work: Photocatalyzed *N*-arylation with electron-rich arenes

R = aryl, alkyl
R' = aryl, alkyl, halogen

Scheme 1. Established transition-metal-catalyzed methods for the *N*-arylation of *NH*-sulfoximines and our new synthetic approach.

1.3 Results and Discussion

1.3.1 Optimization of the Reaction Conditions

Inspired by the group of Lei utilizing a proton-reducing cobalt catalyst[15c, 16] instead of sacrificial electron-donors for their photoredox-catalyzed systems, we wondered if such an approach also could be suitable for our envisioned cross-coupling system. We began our studies by employing *NH*-sulfoximine **1a** (0.1 mmol) and arene **2a** as model substrates for the dehydrogenative cross-coupling, together with 10 mol% 9-mesityl-10-methylacridinium perchlorate (**A**) as organic photocatalyst and 10 mol% proton-reducing catalyst **D** in degassed acetonitrile (0.1 M) under nitrogen-atmosphere and irradiation with blue light of 455 nm for 20 hours at 25 °C (Table 1).

To our delight, the desired product **3a** could be observed in a moderate yield of 41% (Entry 1). Exchanging the counter-anion of **A** to tetrafluoroborate (**B**) did not improve the reaction (Entry 2). It has been previously reported that **A** can be unstable in the presence of nucleophiles or radicals, leading to decomposition of the photocatalyst. *NH*-Sulfoximines are reasonable nucleophilic. Therefore, we decided to exchange **A** by its modified version **C**, which has been reported to be more stable towards nucleophiles.[15a] Unfortunately, the yield of **3a** even decreased to 19% (Entry 3), which indicates that instability of **A** might not be a problem in our reaction.

We further investigated the best ratio and catalyst loadings of **A** and **D** and found that 20 mol% of **A** and 10 mol% of **D** gave 67% of the *N*-arylated product **3a** (Entry 4). Being already quite satisfied with these results, we wondered if we could lower the amount of arene **2a**. Applying only four equivalents of **2a**, still gave a good yield of 55% of **3a**, whereas further decrease to only one equivalent significantly diminishes the reaction efficiency (Entries 5 and 6). Applying 4-fold excess of **1a** and therefore reversing the ratio of the substrates confirmed the observed trend (Entry 7). Considering methyl-arenes as one of the most readily available and cheap raw chemical materials,[17] further experiments were conducted with an excess of 10 equivalents.

Although cobalt-catalyst **D** reacts highly efficient in our developed system, we were also interested if classic terminal oxidants like dioxygen, nitrobenzene or persulfate work as well in our reactions. We observed that the sulfoximine-moiety was not stable in the presence of strong oxidants like dioxygen or persulfate under photo-irradiation conditions, but was transformed into the respective sulfone and sulfoxide, which were identified by GC-MS

analysis (Entries 8 and 10). These results show that an oxygen-free atmosphere is highly important for our reaction system. Using nitrobenzene did not lead to decomposition of **1a**, but gave a yield of only 7% of the desired product (Entry 9).

Further test reactions revealed that solvents like DCM, DCE, DMSO, MeOH or EtOH were not suitable for the reaction and afforded only small amounts of **3a**. Conducting the reaction without **A**, without **D** or without blue light irradiation (reaction in the dark) gave no product, which indicates that the reaction proceeds *via* a light-mediated process (Entries 11, 12 and 4[b)], respectively).

Visible-Light-Mediated Photoredox-Catalyzed *N-Arylation* of *NH-Sulfoximines* with Electron-Rich Arenes

Table 1. Optimization of the reaction conditions.

PC
A: R^1 = Me; R^2 = H; X^- = ClO_4^-
B: R^1 = Me; R^2 = H; X^- = BF_4^-
C: R^1 = Ph; R^2 = *t*-Bu; X^- = BF_4^-

D
Co(dmgH)₂PyCl

Entry	PC [mol%]	Co-cat or oxidant [mol%] or (equiv.)	1a (equiv.)	2a (equiv.)	Yield[a] [%]
1	10 (**A**)	10 (**D**)	1	10	41
2	10 (**B**)	10 (**D**)	1	10	34
3	10 (**C**)	10 (**D**)	1	10	19
4	20 (**A**)	10 (**D**)	1	10	67 (0)[b]
5	20 (**A**)	10 (**D**)	1	4	55
6	20 (**A**)	10 (**D**)	1	1	27
7	20 (**A**)	10 (**D**)	4	1	27
8	20 (**A**)	O_2[c]	1	10	traces
9	20 (**A**)	1 PhNO₂	1	10	7
10	20 (**A**)	1 (NH₄)₂S₂O₈	1	10	0
11	No (**A**)	10 (**D**)	1	10	0
12	20 (**A**)	No (**D**)	1	10	0

[a]Yields were determined by GC analysis with chlorobenzene as internal standard. [b]No yield when the reaction is conducted in the dark. [c]A balloon filled with O_2 was connected to the vial *via* a syringe needle.
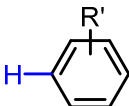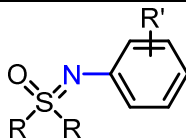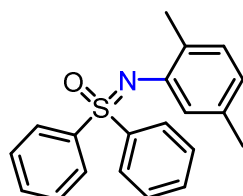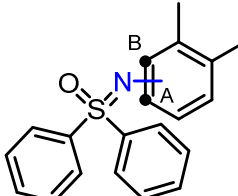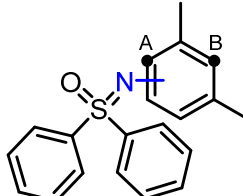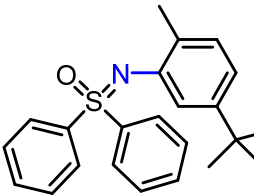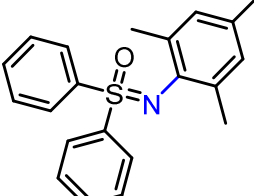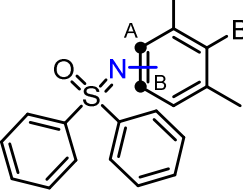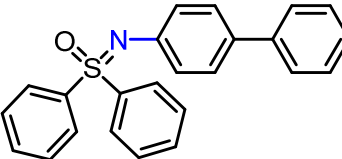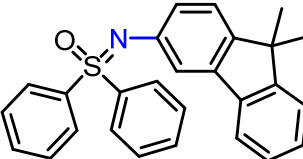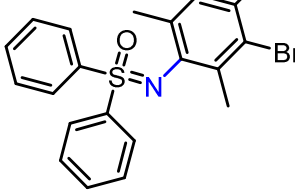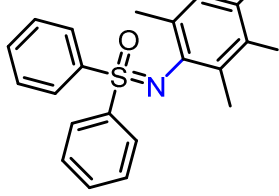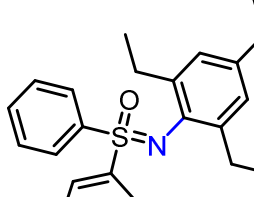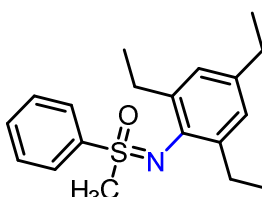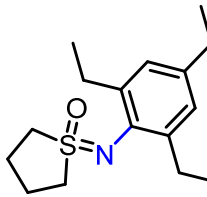
1.3.2   Scope of the Reaction

With the optimized reaction conditions in hand, we were interested in the applicability of our method. Therefore, we first explored the scope of different arenes for the dehydrogenative cross-coupling with *NH*-sulfoximine **1a** (Table 2). Compared to **3a**, which gave 61% of the desired product, the *ortho-* and *meta-*analogues afforded slightly lower, but still moderate yields. We also observed that in these unsymmetrical substrates the inductively more stabilized C–H-position of the arene is favorably functionalized. This also was recently highlighted in several reports and is due to better stabilization of the radical-cationic intermediate.[18]

The coupling product with 4-*tert*-butyltoluene (**1d**) could be obtained in an excellent yield of 94%. We assume that on one hand the *tert*-butyl group donates even more electrons, to stabilize the radical-cationic intermediate, which subsequently leads to a higher yield. On the other hand, it is also bulky enough to block efficiently its *ortho*-C–H-position, giving only one regioisomer. Applying 1,3,5-trimethylbenzene or biphenyl as arene coupling partners, moderate yields of **3e** (44%) and **3g** (42%) could be obtained, whereas only trace amounts of the coupling product **3h** could be observed. To our delight, brominated and iodinated arenes were tolerated under our reaction conditions, giving the opportunity for further product functionalizations. Compound **3i** could be isolated in high yield (80%) while only using 5.3 equivalents, whereas 2-iodo-1,3,5-trimethylbenzene only afforded 10% of the coupling product (**3j**). Applying bulky 1,3,5-triethylbenzene we recognized, that steric hindrance can play a decisive role for our system. The reaction with **1a** did not proceed at all, whereas cross-coupling with smaller *NH*-sulfoximines proceeded well and gave **3l** and **3m** in moderate to high yields. More electron-rich substrates like anisole or heterocyclic substrates like pyrroles and indoles were not suitable for the reaction and the substrates could be re-isolated in quantitative amounts. Simple benzene or toluene also did not react with *NH*-sulfoximine **1a**. The scope of the arene coupling partner is therefore limited to mono- and multi-alkylated and halogenated arenes, affording moderate to high yields.

Table 2. Scope of electron-rich arenes for the *N*-arylation of *NH*-sulfoximines.

3a, 61%

3b, 42%
2.6:1 C_A:C_B

3c, 39%
6.5:1 C_A:C_B

3d, 94%

3e, 44%

3f, 12%
2.6:1 C_A:C_B

3g, 42%

3h, 5%

3i, 80%

3j, 10%

3k, 0%

3l, 87%

3m, 57%

Reactions were carried out under optimized conditions in a scale of 0.1 mmol of *NH*-sulfoximine **1**. Yields of the products are reported as the average yield of two isolated reactions. Isomeric ratios were calculated by ^{1}H-NMR.

Next, we investigated different *NH*-sulfoximines for our *N*-arylation procedure (Table 3). Benzylic positions or a free *S*-methyl substituent in sulfoximines were tolerated and afforded moderate to good yields. In addition, electron-donating *para*-methyl and *para*-methoxy substituents react smoothly. Electron-poor *NH*-sulfoximines containing fluorine-, chlorine- or cyano-substituents were tolerated and gave up to 93% of the cross-coupling products. Even a cyclopropyl moiety was stable under the reaction conditions, yielding *N*-arylated sulfoximine **3w** in an excellent yield of 95%. *NH*-sulfoximine **1x** containing a free hydroxyl-group was selectively converted to the *N*-arylated product, which proves that our method is very selective for the formation of the C–N-bond, instead of a C–O-bond. Furthermore, we could apply various aliphatic *NH*-sulfoximines, giving also moderate to high yields of the desired product. It has to be mentioned, that the reaction with 1,3,5-tri-*tert*-butylbenzene leads to the *ipso*-substituted product **3ac**. The relatively facile replacement of the *tert*-butyl group is well known and can be attributed to the high stability of the respective *tert*-butyl radical cation as leaving group.[19] More complex *NH*-sulfoximines showed low or no conversion to the respective products. Only 10% of **3ad** could be isolated and no **3ae** could be obtained. Again, quantitative amounts of the unconverted substrates could be re-isolated.

In general, a diverse scope of *NH*-sulfoximines was applicable for the cross-coupling reaction with different arenes. Both aromatic and aliphatic *NH*-sulfoximines containing electron-donating and electron-withdrawing functional groups, as well as benzyl, cyclopropyl and free hydroxyl moieties were tolerated and gave moderate to excellent product yields. However, more complex substrates, like **1ad** and **1ae**, showed low or no conversion to the respective *N*-arylated products.

Table 3. Scope of *NH*-sulfoximines for the *N*-arylation of arenes.

3n, 58%   **3o**, 79%   **3p**, 85%

3q, 84%   **3r**, 89%   **3s**, 84%

3t, 63%   **3u**, 78%   **3v**, 93%

3w, 95%   **3x**, 59%   **3z**, 69%

3aa, 84%   **3ab**, 52%   **3ac**, 66%

3ad, 10%   **3ae**, 0%

Reactions were carried out under optimized conditions in a scale of 0.1 mmol of *NH*-sulfoximine **1**. Yields of the products are reported as the average yield of two isolated reactions. Isomeric ratios were calculated by ^{1}H-NMR.
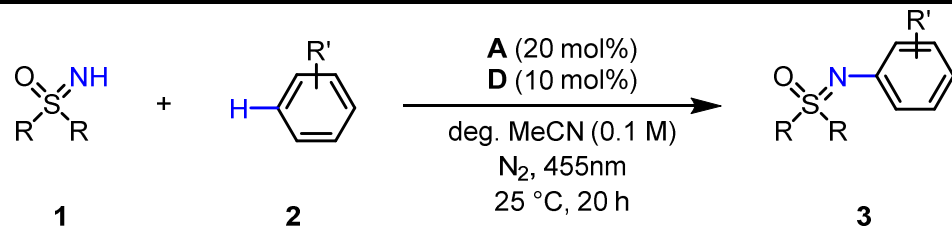
1.3.3 Mechanistic Investigations

1.3.3.1 Fluorescence Quenching Experiments

First, we performed a series of Stern-Volmer emission quenching studies (Figure 2). The applied organic photocatalyst 9-mesityl-10-methylacridinium (Mes-Acr$^+$-Me, **A**) exhibits an excited charge-transfer singlet-state with a reduction potential (E_{Red}^*) of +2.08 V vs. SCE upon irradiation with blue light of 455nm.[20] The single-electron oxidation of **2a** (E_{Red} = +2.01 V vs. SCE[21]) to the corresponding radical cation is therefore thermodynamically feasible. The emission intensity as well as the lifetime of the excited-state of the organic photocatalyst significantly decreases upon titration with **2a**, following a linear Stern-Volmer behavior. In contrast to literature reports,[15a, 15c] where the applied nucleophiles did not quench the excited-state of the photocatalyst, also titration with **1a** decreased the fluorescence intensity and lifetime of the excited-state photocatalyst in a linear Stern-Volmer behavior, however with a smaller rate constant. The observed quenching can be rationalized by the measured reduction potential for **1a** of +2.00 V vs. SCE (see section 1.8.5, Table 5). These results show that the arene and the *NH*-sulfoximine both interact with the excited-state of the photocatalyst and a single-electron oxidation can lead to the respective radical cationic species.

Sulfoximine **1ae** did not react under our reaction conditions. Investigating the excited-state quenching by **1ae**, no decrease of the emission intensity of the photocatalyst was observed. Upon titration, the emission-intensity of the photocatalyst increased, which is explained by an accompanied slight increase of the absorbance in the UV/Vis spectrum (Figure 3). This may be due to changes in polarity in the microenvironment of the photocatalyst upon addition of **1ae**. However, no quenching of the excited-state of the photocatalyst could be observed and the reaction resulted in no product formation. We tried to determine the reduction potential of **1ae** by cyclic voltammetric measurements, but could not observe any corresponding oxidation signal up to +2.4 V vs SCE. We assume that the reduction potential of **1ae** is too high for a reaction with the photocatalyst in the excited-state, therefore no photo-oxidation to the reactive species occurs and consequently no cross-coupling reaction.

These results reveal that *NH*-sulfoximines, which do not quench the emission, cannot be converted in our developed reaction. This gives the opportunity for a facile selection of suitable substrates by emission quenching measurements.

A) Fluorescence Quenching Experiments

Steady-State   **Time-Resolved**

B) Stern-Volmer Plots
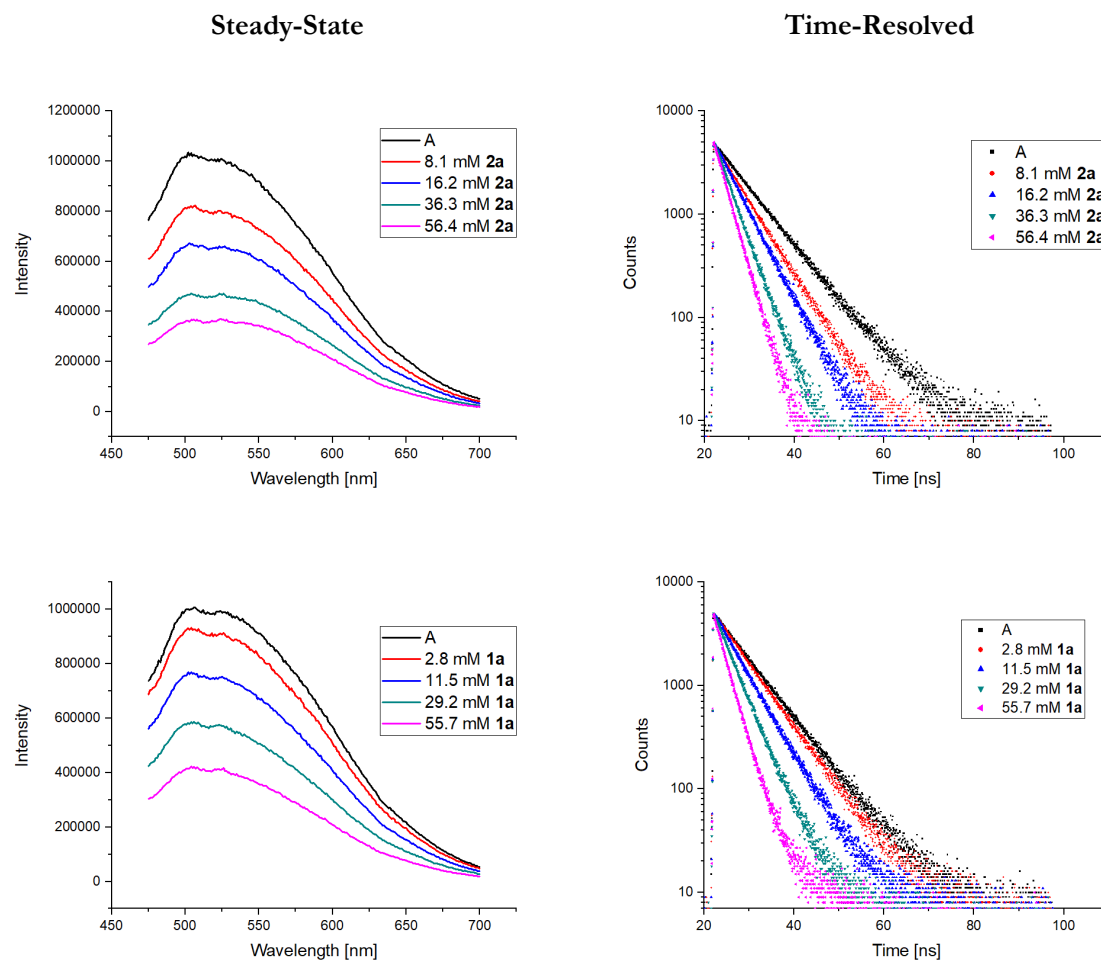
Steady-State   **Time-Resolved**
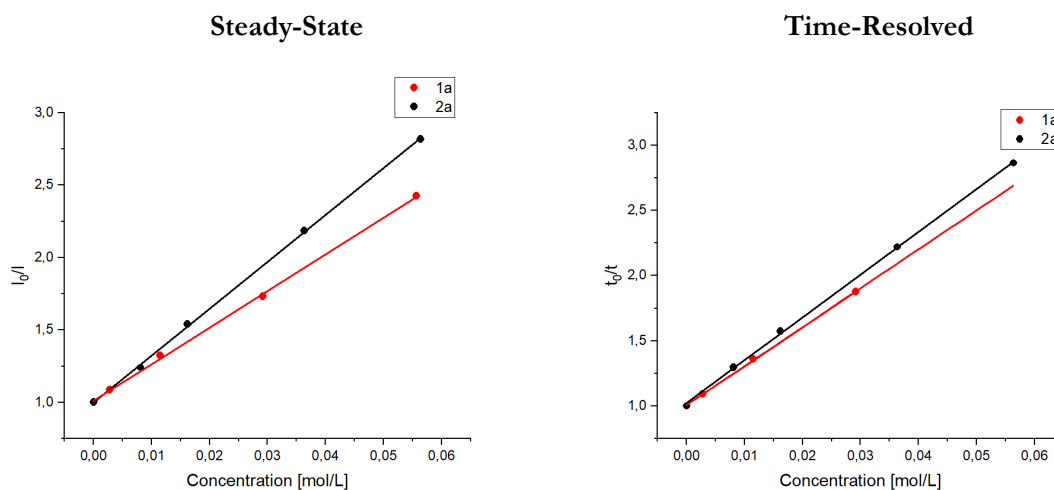
Figure 2. Steady-state (A) and time-resolved (B) fluorescence quenching experiments of Mes-Acr$^+$-Me (1.6μM in degassed MeCN) upon titration with *NH*-sulfoximine 1a or arene 2a and the respective Stern-Volmer plots (C).

A) Steady-State UV/Vis Absorption Measurements
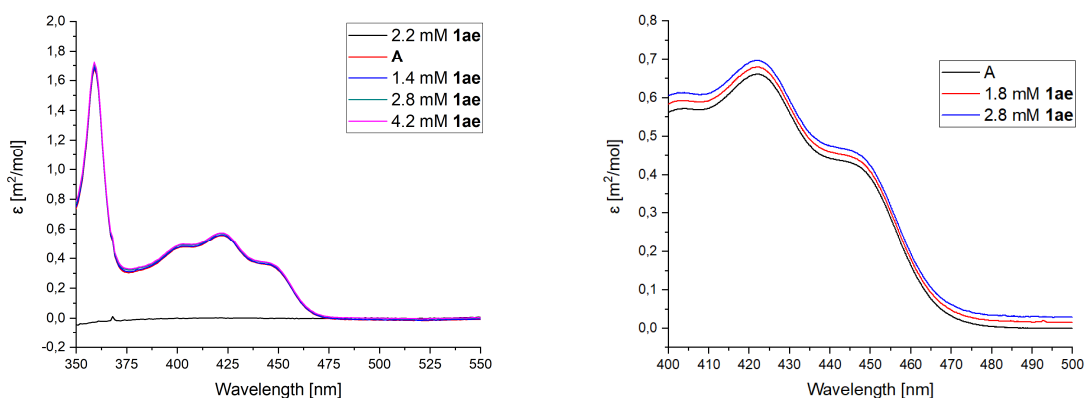
B) Steady-State Fluorescence Measurements
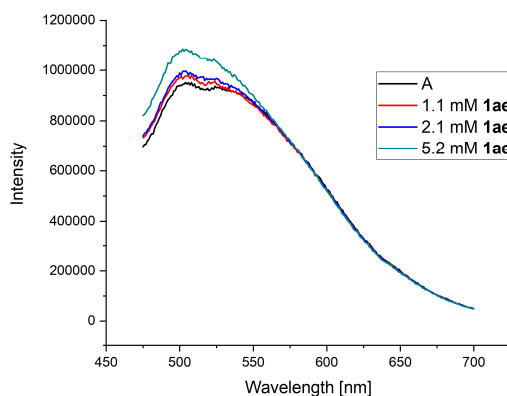
Figure 3. Steady-state UV/Vis absorption measurements (A) of Mes-Acr$^+$-Me (50µM in MeCN) upon titration with *NH*-sulfoximine 1ae (left: full spectra, right: enlarged extract of the full spectra) and steady-state fluorescence measurements (B) of Mes-Acr$^+$-Me (1.6µM in degassed MeCN) upon titration with *NH*-sulfoximine 1ae.

1.3.3.2   Radical Trapping Experiments

Reactive radical intermediates can be trapped by TEMPO, yielding stable adducts of the respective intermediates.[22] As shown in (Scheme 2) we conducted our standard reaction with one equivalent of TEMPO as additive and were able to identify the radical trapping product of TEMPO with the arene radical cation by LC-MS analysis (see section 1.8.4). Unfortunately, we could not observe any coupling with a potential *N*-centered radical of the *NH*-sulfoximine, which may be explained by competing fast hydrogen atom abstraction[23] from the solvent.
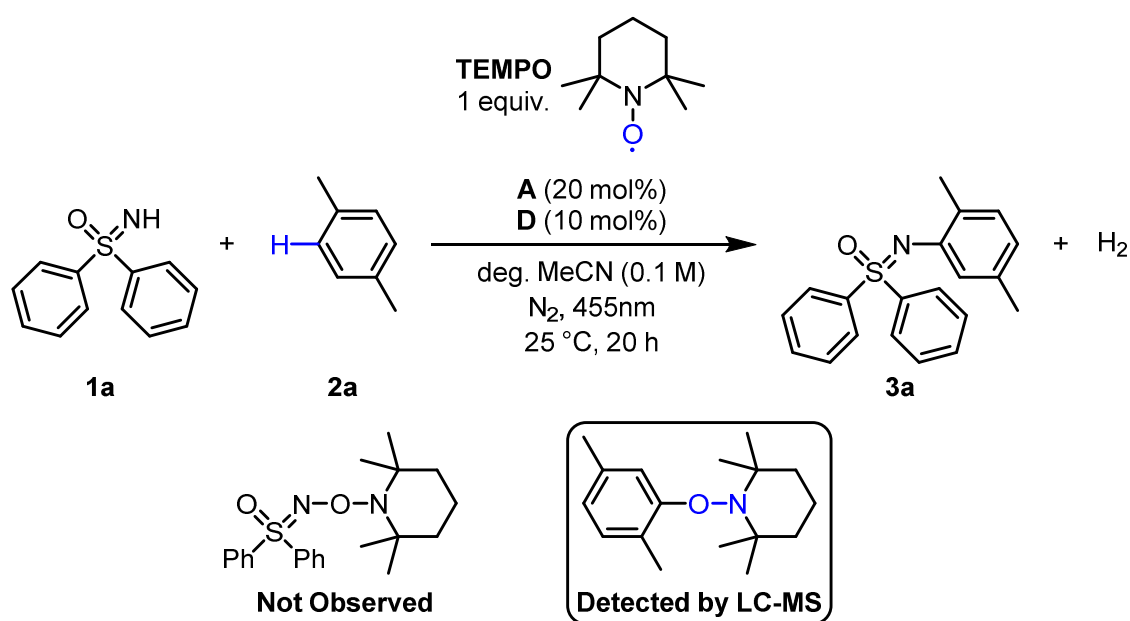
Scheme 2. TEMPO trapping experiment conducted with 1 equivalent of TEMPO under standard conditions.

1.3.3.3   In-Situ, Time-Resolved UV/Vis Absorption Measurements

Regarding the cobalt-catalyzed part of the mechanism, it is reported that step-wise reduction of the Co(III) complex leads to Co(II) and Co(I) species.[15c, 16, 24] We were able to visualize the formed Co(II) and Co(I) species by in-situ, time-resolved UV/Vis absorption measurements (Figure 4). At the beginning of the reaction, the UV/Vis spectrum solely reflects the spectrum of the pure catalyst. Upon irradiation, characteristic absorption bands at 450 nm and 550 – 700 nm arise, which can be attributed to Co(II) and Co(I) species[25], respectively.
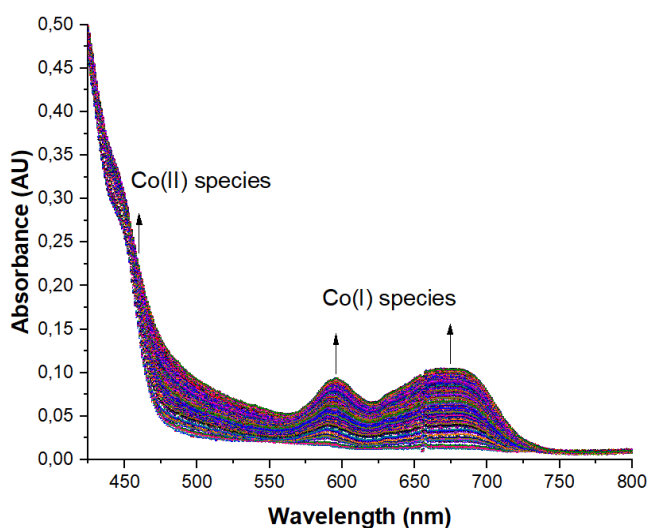
Figure 4. In-situ, time-resolved UV/Vis investigation of the reaction of **1a** with **2a** at a reaction concentration scale dependent on the photocatalyst concentration (**A**, 50μM). Spectra are recorded every 10 seconds over a period of 30 minutes.

1.3.4 Mechanistic Proposal

Based on the reported mechanism for the C–H/N–H dehydrogenative cross-coupling applying the Co(III) complex as proton-reducing catalyst, recent literature on radical-radical cross-coupling reactions and our experiments, we propose the following mechanism for the *N*-arylation of *NH*-sulfoximines (Scheme 3[26]): Upon irradiation with blue light the photocatalyst is excited to its charge-transfer singlet-state (**Mes•+-Acr•-Me**). Single-electron oxidation of arene **2** leads to the arene radical cation **2•+** and Mes-Acr•-Me radical. The photocatalytic cycle is closed *via* oxidation by the Co(III) complex, generating the ground-state Mes-Acr+-Me and a Co(II) species. In addition, *NH*-sulfoximine **1** is photo-oxidized by the excited photocatalyst, leading first to the radical cationic intermediate **1•+**, which can undergo fast deprotonation to the respective neutral *N*-centered radical intermediate **1•**. Now electrophilic **2•+** can cross-couple[27] with **1•**, yielding the cationic intermediate **3+**. The final product **3** is formed *via* deprotonation and rearomatization. The Co(II) complex again is reduced to Co(I) by Mes-Acr•-Me to close the photocatalytic cycle. Addition of a proton leads to a Co(III)-hydride complex and releases H_2 upon addition of a second proton. Nearly equimolar amounts of H_2 (89%) could be detected by headspace GC-TCD measurements in the cross-coupling reaction yielding **3r**.
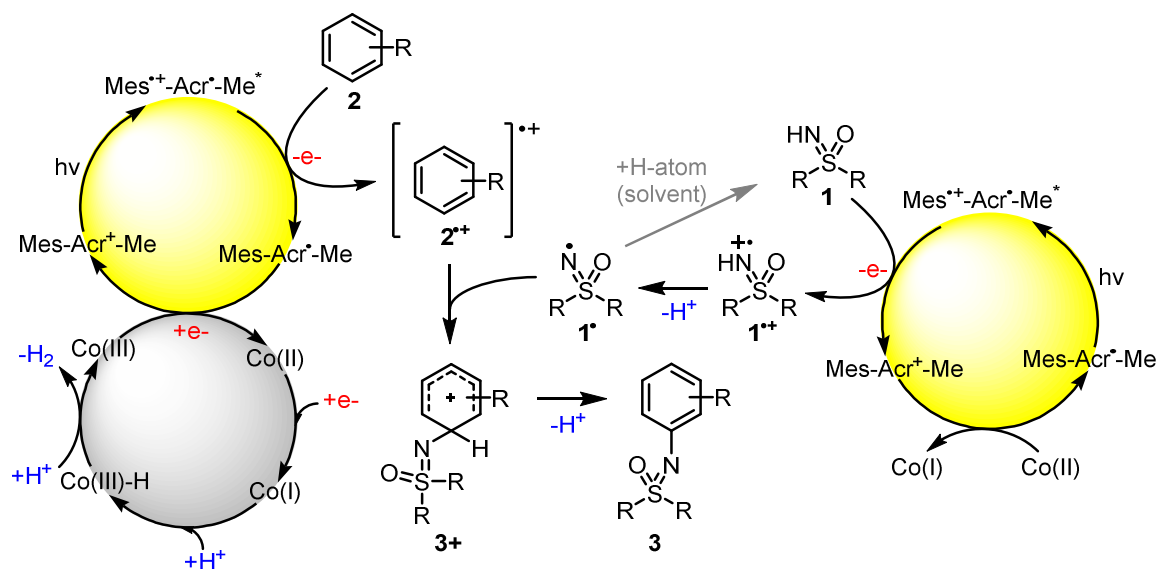
Scheme 3. Proposed mechanism for the *N*-arylation of *NH*-sulfoximines with electron-rich- arenes.

1.4 Preparative-Scale in Batch and Continuous Flow

1.4.1 Large-Scale Batch Reactor

We also were interested in performing our reaction on a larger preparative scale. Therefore, we conducted the reaction shown in Scheme 4 with 1.0 g of *NH*-sulfoximine **1a** (4.6 mmol, 1.0 equiv.) in a large-scale reactor developed in our laboratories (Figure 5). After 24 hours of irradiation with blue LEDs (455 nm) 1.5 g (79%) of the *N*-arylated sulfoximine **3i** were isolated. The result shows that larger scale reactions can be realized for the developed reaction without decrease in yield or prolonged reaction times.
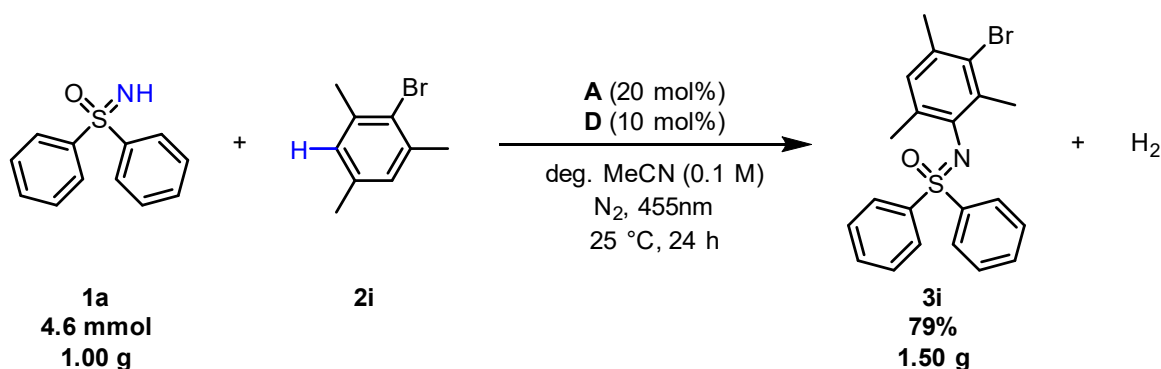
Scheme 4. Photoredox-catalyzed *N*-arylation reaction of **1a** in preparative scale
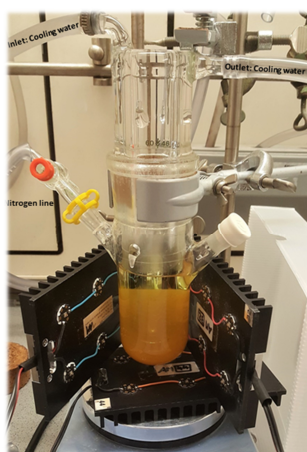
Figure 5. Large-scale reactor developed in our laboratories.

.

1.4.2   *N*-Arylation of *NH*-Sulfoximines in Continuous Photo–Flow

Continuous flow chemistry serves as an ideal scale-up technique especially in the field of industrial organic synthesis, where grams or kilograms of substrates need to be processed in a safe and controllable manner. The inherent advantage of processing chemical synthesis in a continuous flow regime compared to classic batch lies in the unique control of the reaction parameters like temperature, pressure or mixing. Exemplarily, the small inner diameter of commonly used flow-tubes (1 – 3 mm) provides a significantly increased surface-to-volume ratio. Product selectivity can be enhanced in endothermic reactions due to narrow, defined temperature profiles along the flow reactor and exothermic reactions can be cooled very efficiently, minimizing the risk of a thermal runaway. Furthermore, short diffusion length in tubes leads to higher efficiency in the mixing of reagents and therefore to increased product selectivity and faster reaction times. Complete automation approaches for the overall flow process result in reliable reproducibility and in-line or on-line analysis of the reagent stream can be used to control or adjust the outcome of the reaction in real-time (automated feedback optimization).[28]

In particular, photoredox catalysis can greatly benefit from the flow-tube's small inner diameter. Since the transmission (T) of excitation-light relies on the Bouguer–Lambert–Beer law (Equation 1), it decreases exponentially with the depth (l) in a given reaction medium. As a result, reaction vessels in batch are often only illuminated efficiently in the very first millimeters when strong absorbing photocatalysts are used.[28b, 29]

Equation 1. Bouguer–Lambert–Beer law.

$$A = -log_{10}\, T = \, log_{10}\, \frac{I_0}{I} = \, \varepsilon * c * l$$

A = absorbance; T = light transmittance; I = light intensity; ε = molar extinction coefficient; c = concentration of attenuating species; l = optical path length

Continuous flow chemistry conducted in transparent small inner diameter tubing is an ideal setup to ensure efficient light exposure and penetration depth in photoredox catalysis. In this context, we decided to adapt the photoredox-catalyzed *N*-arylation of *NH*-sulfoximines to continuous flow conditions and develop a large-scale preparative method.

Table 4. Screening for optimal reaction conditions in continuous flow.

Entry	Reactor	c (1l) [mol/L]	ν [μL/min]	t_R [min]	Yield [%]	Productivity [mg/h]
1	batch	0.10		20h	85[a]	1.5
2	batch	0.10		20h	63	1.2
3	batch	0.25		20h	46	2.0
4	continuous	0.10	450	31	28	262
5	continuous	0.10	1000	41	34	720
6	continuous	0.10	200 (1000)[b]	191	53	224
7	continuous	0.25	200 (1000)[b]	191	51	544
8	continuous	0.25	1000	69	41	2160
9	continuous	0.20	750	91	54	1710
10	continuous	0.25	750	91	54	2138

Yields of the products are isolated amounts after purification *via* flash-column chromatography. [a]Reaction carried out with photocatalyst **A** (see Table 3, **3p**). [b]The suspension was loaded onto the photoreactor–coil at an initial flowrate of 1000 μL/min. After the loading process, the processing flowrate was 200 μL/min.

The general reaction is shown in Table 4. We applied the less potent photocatalyst **B** instead of **A**, due to better availability at the moment when we conducted the experiments. Entries 1 and 2 were set as benchmarks of the batch reaction, applying **A** or **B** as photocatalyst, affording 85% and 63% of the desired *N*-arylated sulfoximine **3p**, respectively, in degassed acetonitrile (0.1 M), under nitrogen-atmosphere and irradiation with blue light of 455 nm for 20 hours at 25 °C (Table 4). It has to be mentioned, that cobalt-catalyst **D** is insoluble in the reaction mixture, which results in the formation of a light suspension as reaction media (Figure 6). However, upon irradiation with blue light, conversion of the substrates is initiated and insoluble Co(III)-species are converted into soluble Co(II)- and Co(I)-species (Scheme 3). Consequently, a clear reaction solution is obtained usually after 5

minutes of irradiation (Figure 7). Up-concentration of the reaction mixture to 0.25 M led to the formation of a thick suspension, resulting in diminished light-penetration and decreased yield (Table 4, entry 3).
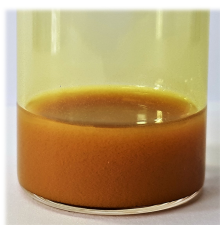
Figure 6. Suspension of Co(dmgH)$_2$PyCl (**D**), **1l**, **2i** in degassed MeCN, sonicated for 15 minutes.
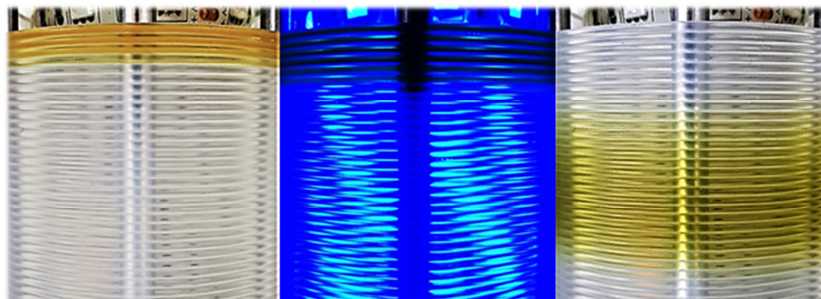
Figure 7. Left: Reaction mixture pumped into the coil-reactor as suspension, before being irradiated. Middle: Irradiation of the reaction mixture. Right: Clear, solubilized reaction mixture after being irradiated for 5 minutes.

The general flow setup used for our experiments consist of a solvent delivery feed, a 2.0 mL sonicated sample loop, a coil-reactor with transparent FEP tubing (1.0 mm inner diameter) and LEDs as light source, a 100 psi back-pressure regulator and a fraction collector (Scheme 5).

24
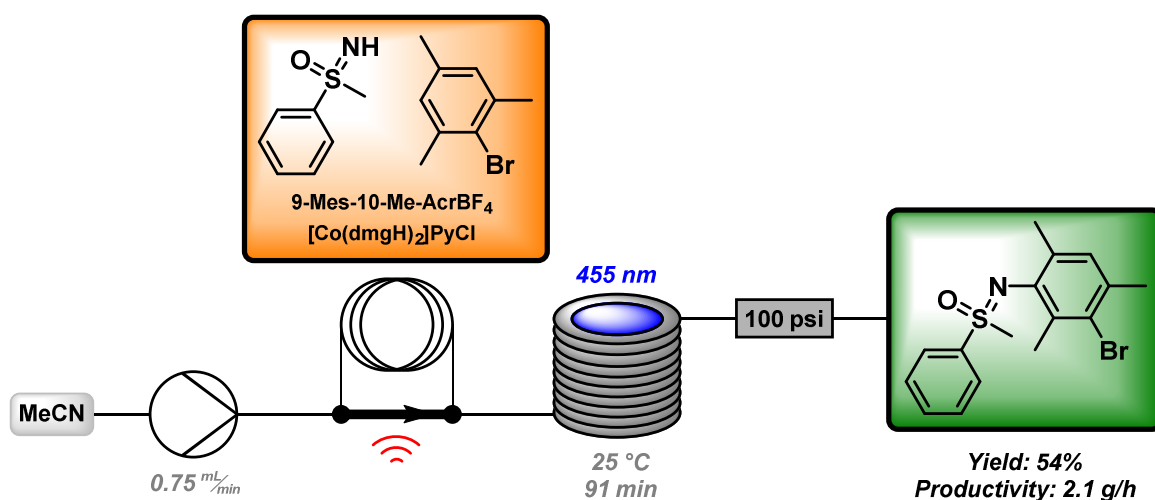
Scheme 5. *N*-arylation of *NH*-sulfoximines processed in continuous photo-flow.

As a first experiment, the reaction mixture was processed at a flowrate of 450 µL/min and 31 minutes of residence time in the illuminated coil-reactor. We observed, that the Co(III)-catalyst was not carried efficiently by the solvent stream and started to drag within the tubing. This created a lack of cobalt-catalyst in the leading sequence of the reaction mixture and resulted in poor overall conversion to the product (Table 4, entry 4). Next, we increased the flowrate to 1000 µL/min and observed efficient and homogenous transport of the suspension through the tubing. We obtained a slightly increased yield of 34% of **3p** within a similar residence time of 41 minutes (Table 4, entry 5). In order to validate the influence of increasing residence time, we performed a non-continuous experiment where the suspension was first loaded onto the reactor-coil at 1000 µL/min, irradiated until a clear solution was obtained and then processed at 200 µL/min. After a total residence time of 191 minutes, a significantly increased overall yield of 53% was isolated. Even a 2.5-fold higher concentrated reaction mixture could be processed under these conditions, affording 51% of **3p** (Table 4, entries 6 and 7). Finally, we found that a flowrate of 750 µL/min and a residence time of 91 minutes are the optimal conditions for the *N*-arylation reaction (Table 4, entries 8 – 10). We could isolate an overall yield of 54% at 2-fold and even 2.5-fold substrate concentrations compared to standard batch conditions. Furthermore, the developed continuous photo-flow process operates at a significantly enhanced productivity of about 2.14 g/h – 1782 times as high as the benchmark in batch.

1.5   Conclusion

In conclusion, we report the first visible-light photoredox-catalyzed direct *N*-arylation of *NH*-sulfoximines with alkylated arenes. A series of mono- and multi-alkylated and halogenated arenes react in the C–H/N–H cross-coupling with a diverse scope of aromatic and aliphatic electron-rich and electron-poor *NH*-sulfoximines.

We conducted the reaction on a gram scale (1.5 g, 4.6 mmol) in a custom-built batch reactor and furthermore developed a continuous photo-flow approach. We were able to reach similar isolated overall yields in continuous flow compared to batch and could even increase the process productivity by a factor of x1782 to 2.14 g/h of the desired product.

We could show, that our reaction proceeds *via* single-electron transfer steps initiated by the excited state of the photocatalyst 9-mesityl-10-methylacridinium perchlorate. A second, cobalt-catalyzed cycle closes the photocatalytic cycle and produces H_2 as the only byproduct. Stern-Volmer emission quenching studies indicate that both, arene and *NH*-sulfoximine interact with the excited state of the photocatalyst. Therefore, we propose a radical-radical cross-coupling mechanism initiated by visible-light photocatalysis.

Our method can serve as a mild and selective synthetic tool for accessing *N*-arylated sulfoximines, which are of increasing importance in drug development and crop protection compounds.

1.6   Acknowledgements

1.7 References

[1]   a) H. R. Bentley, E. E. McDermott, J. Pace, J. K. Whitehead, T. Moran, Nature, 1950, 165, 150-151; b) H. R. Bentley, E. E. McDermott, J. Pace, J. K. Whitehead, T. Moran, Nature, 1949, 163, 675.

[2]   a) S. Otocka, M. Kwiatkowska, L. Madalinska, P. Kielbasinski, Chem. Rev., 2017, 117, 4147-4181; b) X. Shen, Q. Liu, W. Zhang, J. Hu, Eur. J. Org. Chem., 2016, 906-909; c) X. Shen, W. Miao, C. Ni, J. Hu, Angew. Chem. Int. Ed., 2014, 53, 775-779; d) D. Craig, F. Grellepois, A. J. White, J. Org. Chem., 2005, 70, 6827-6832; e) M. Langner, P. Remy, C. Bolm, Chem. Eur. J., 2005, 11, 6254-6265; f) M. T. Reetz, O. G. Bondarev, H. J. Gais, C. Bolm, Tetrahedron Lett., 2005, 46, 5643-5646; g) H. J. Gais, G. S. Babu, M. Gunter, P. Das, Eur. J. Org. Chem., 2004, 2004, 1464-1473; h) M. Langner, C. Bolm, Angew. Chem. Int. Ed., 2004, 43, 5984-5987; i) M. Harmata, X. Hong, J. Am. Chem. Soc., 2003, 125, 5754-5756; j) S. Koep, H. J. Gais, G. Raabe, J. Am. Chem. Soc., 2003, 125, 13243-13251; k) C. Bolm, M. Martin, O. Simic, M. Verrucci, Org. Lett., 2003, 5, 427-429; l) C. Bolm, M. Verrucci, O. Simic, P. G. Cozzi, G. Raabe, H. Okamura, Chem. Commun., 2003, 2826-2827; m) C. Bolm, O. Simić, J. Am. Chem. Soc., 2001, 123, 3830-3831; n) M. Harmata, S. K. Ghosh, Org. Lett., 2001, 3, 3321-3323; o) M. Reggelin, C. Zur, Synthesis, 2000, 1-64; p) C. Bolm, M. Felder, J. Müller, Synlett, 1992, 439-441; q) C. R. Johnson, Acc. Chem. Res., 1973, 6, 341-347.

[3]   U. Lucking, Angew. Chem. Int. Ed., 2013, 52, 9399-9408.

[4]   a) J. A. Sirvent, U. Lucking, ChemMedChem, 2017, 12, 487-501; b) M. Frings, C. Bolm, A. Blum, C. Gnamm, Eur. J. Med. Chem., 2017, 126, 225-245.

[5]   a) R. Luisi, J. Bull, L. Degennaro, Synlett, 2017, 28, 2525-2538; b) V. Bizet, C. M. Hendriks, C. Bolm, Chem. Soc. Rev., 2015, 44, 3378-3390; c) H. Okamura, C. Bolm, Chem. Lett., 2004, 33, 482-487.

[6]   A. Tota, M. Zenzola, S. J. Chawner, S. S. John-Campbell, C. Carlucci, G. Romanazzi, L. Degennaro, J. A. Bull, R. Luisi, Chem. Commun., 2016, 53, 348-351.

[7]   A. S. Guram, R. A. Rennels, S. L. Buchwald, Angew. Chem. Int. Ed., 1995, 34, 1348-1350.

[8]   M. S. Driver, J. F. Hartwig, J. Am. Chem. Soc., 1996, 118, 7217-7218.

[9]   C. Bolm, J. P. Hildebrand, Tetrahedron Lett., 1998, 39, 5731-5734.

[10]   a) M. Harmata, N. Pavri, Angew. Chem. Int. Ed., 1999, 38, 2419-2421; b) C. Bolm, J. P. Hildebrand, J. Org. Chem., 2000, 65, 169-175; c) C. Bolm, J. P. Hildebrand, J. Rudolph, Synthesis, 2000, 911-913; d) C. Bolm, M. Martin, L. Gibson, Synlett, 2002, 832-834; e) M. Harmata, X. Hong, S. K. Ghosh, Tetrahedron Lett., 2004, 45, 5233-5236; f) N. Yongpruksa, N. L. Calkins, M. Harmata, Chem. Commun., 2011, 47, 7665-7667; g) G. Y. Cho, P. Remy, J. Jansson, C. Moessner, C. Bolm, Org. Lett., 2004, 6, 3293-3296; h) J. Sedelmeier, C. Bolm, J. Org. Chem., 2005, 70, 6904-6906; i) A. Correa, C. Bolm, Adv. Synth. Catal., 2007, 349, 2673-2676; j) Y. Macé, B. Pégot,

R. Guillot, C. Bournaud, M. Toffano, G. Vo-Thanh, E. Magnier, Tetrahedron, 2011, 67, 7575-7580; k) Z. J. Liu, J. P. Vors, E. R. F. Gesing, C. Bolm, Green Chem., 2011, 13, 42-45; l) C. Moessner, C. Bolm, Org. Lett., 2005, 7, 2667-2669; m) B. Vaddula, J. Leazer, R. S. Varma, Adv. Synth. Catal., 2012, 354, 986-990; n) A. Correa, C. Bolm, Adv. Synth. Catal., 2008, 350, 391-394; o) J. Kim, J. Ok, S. Kim, W. Choi, P. H. Lee, Org. Lett., 2014, 16, 4602-4605; p) H. Zhu, F. Teng, C. Pan, J. Cheng, J.-T. Yu, Tetrahedron Lett., 2016, 57, 2372-2374.

[11]   a) M. Miyasaka, K. Hirano, T. Satoh, R. Kowalczyk, C. Bolm, M. Miura, Org. Lett., 2011, 13, 359-361; b) L. Wang, D. L. Priebbenow, W. Dong, C. Bolm, Org. Lett., 2014, 16, 2661-2663; c) R. K. Chinnagolla, A. Vijeta, M. Jeganmohan, Chem. Commun., 2015, 51, 12992-12995.

[12]   S. K. Aithagani, M. Kumar, M. Yadav, R. A. Vishwakarma, P. P. Singh, J. Org. Chem., 2016, 81, 5886-5894.

[13]   a) S. K. Aithagani, S. Dara, G. Munagala, H. Aruri, M. Yadav, S. Sharma, R. A. Vishwakarma, P. P. Singh, Org. Lett., 2015, 17, 5547-5549; b) S. Yoshida, H. Nakajima, K. Uchida, T. Yano, M. Kondo, T. Matsushita, T. Hosoya, Chem. Lett., 2017, 46, 77-80.

[14]   a) B. König, Eur. J. Org. Chem., 2017, 2017, 1979-1981; b) J. K. Matsui, S. B. Lang, D. R. Heitz, G. A. Molander, ACS Catal., 2017, 7, 2563-2575; c) N. A. Romero, D. A. Nicewicz, Chem. Rev., 2016, 116, 10075-10166; d) I. Ghosh, L. Marzo, A. Das, R. Shaikh, B. Konig, Acc. Chem. Res., 2016, 49, 1566-1577; e) J. J. Douglas, M. J. Sevrin, C. R. J. Stephenson, Org. Process Res. Dev., 2016, 20, 1134-1147; f) A. Wimmer, B. Konig, Beilstein J. Org. Chem., 2018, 14, 54-83; g) C. K. Prier, D. A. Rankic, D. W. MacMillan, Chem. Rev., 2013, 113, 5322-5363; h) J. Xuan, W. J. Xiao, Angew Chem Int Ed Engl, 2012, 51, 6828-6838.

[15]   a) N. A. Romero, K. A. Margrey, N. E. Tay, D. A. Nicewicz, Science, 2015, 349, 1326-1330; b) K. A. Margrey, A. Levens, D. A. Nicewicz, Angew. Chem. Int. Ed., 2017, 56, 15644-15648; c) L. Niu, H. Yi, S. Wang, T. Liu, J. Liu, A. Lei, Nat. Commun., 2017, 8, 14226.

[16]   G. Zhang, C. Liu, H. Yi, Q. Meng, C. Bian, H. Chen, J. X. Jian, L. Z. Wu, A. Lei, J. Am. Chem. Soc., 2015, 137, 9273-9280.

[17]   R. Vanjari, K. N. Singh, Chem. Soc. Rev., 2015, 44, 8062-8096.

[18]   a) K. A. Margrey, J. B. McManus, S. Bonazzi, F. Zecri, D. A. Nicewicz, J. Am. Chem. Soc., 2017, 139, 11288-11299; b) N. E. S. Tay, D. A. Nicewicz, J. Am. Chem. Soc., 2017, 139, 16100-16104.

[19]   R. B. Moodie, K. Schofield, Acc. Chem. Res., 1976, 9, 287-292.

[20]   N. A. Romero, D. A. Nicewicz, J. Am. Chem. Soc., 2014, 136, 17024-17035.

[21]   P. B. Merkel, P. Luo, J. P. Dinnocenzo, S. Farid, J. Org. Chem., 2009, 74, 5163-5173.

[22]   A. U. Meyer, S. Jager, D. P. Hari, B. Konig, Adv. Synth. Catal., 2015, 357, 2050-2054.

[23] H. Wang, D. Zhang, C. Bolm, Angew. Chem. Int. Ed., 2018, 10.1002/anie.201801660.

[24] X. Hu, G. Zhang, F. Bu, X. Luo, K. Yi, H. Zhang, A. Lei, Chem. Sci., 2018, 9, 1521-1526.

[25] a) J. J. Zhong, Q. Y. Meng, B. Liu, X. B. Li, X. W. Gao, T. Lei, C. J. Wu, Z. J. Li, C. H. Tung, L. Z. Wu, Org. Lett., 2014, 16, 1988-1991; b) J. J. Zhong, C. J. Wu, Q. Y. Meng, X. W. Gao, T. Lei, C. H. Tung, L. Z. Wu, Adv. Synth. Catal., 2014, 356, 2846-2852; c) T. Lazarides, T. McCormick, P. Du, G. Luo, B. Lindley, R. Eisenberg, J. Am. Chem. Soc., 2009, 131, 9192-9194.

[26] A mechanism where both photo-oxidized intermediates are generated in catalytic amounts and then react with the respective neutral coupling partners should also be considered and could not be ruled out so far.

[27] a) Y. T. Zhao, B. B. Huang, C. Yang, B. Li, B. Q. Gou, W. J. Xia, ACS Catal., 2017, 7, 2446-2451; b) E. Fava, A. Millet, M. Nakajima, S. Loescher, M. Rueping, Angew Chem Int Ed Engl, 2016, 55, 6776-6779; c) M. Chen, X. Zhao, C. Yang, W. Xia, Org. Lett., 2017, 19, 3807-3810; d) H. Wang, Q. Lu, C. W. Chiang, Y. Luo, J. Zhou, G. Wang, A. Lei, Angew Chem Int Ed Engl, 2017, 56, 595-599.

[28] a) M. B. Plutschack, B. Pieber, K. Gilmore, P. H. Seeberger, Chem. Rev., 2017, 117, 11796-11893; b) D. Cambié, C. Bottecchia, N. J. W. Straathof, V. Hessel, T. Noël, Chem. Rev., 2016, 116, 10276-10341; c) L. D. Elliott, J. P. Knowles, P. J. Koovits, K. G. Maskill, M. J. Ralph, G. Lejeune, L. J. Edwards, R. I. Robinson, I. R. Clemens, B. Cox, D. D. Pascoe, G. Koch, M. Eberle, M. B. Berry, K. I. Booker-Milburn, Chem. Eur. J., 2014, 20, 15226-15232; d) F. M. Akwi, P. Watts, Chem. Commun., 2018, 54, 13894-13928; e) H.-W. Hsieh, C. W. Coley, L. M. Baumgartner, K. F. Jensen, R. I. Robinson, Organic Process Research & Development, 2018, 22, 542-550.

[29] in Visible Light Photocatalysis in Organic Chemistry, pp. 389-413.

1.8 Experimental Part

1.8.1 General Information

Starting materials and reagents were purchased from commercial suppliers (Sigma Aldrich, Alfa Aesar, Acros, Fluka or VWR) and were used without further purification. All reactions were performed with degassed solvents by bubbling nitrogen for 15 minutes before used. Yields are generally isolated amounts of products after column chromatography. Industrial grade of solvents was used for automated flash-column chromatography. All reactions with oxygen- or moisture-sensitive reagents were carried out in glassware, which was dried before use by heating under vacuum. Dry nitrogen was used as inert gas atmosphere. Liquids were added *via* syringe, needle and septum technique unless otherwise stated. All NMR spectra were measured at room temperature using a Bruker Avance 300 (300 MHz for ^{1}H, 75 MHz for ^{13}C)[1] or a Bruker Avance 400 (400 MHz for ^{1}H, 101 MHz for ^{13}C) NMR spectrometer. All chemical shifts are reported in δ-scale as parts per million [ppm] (multiplicity, coupling constant J, number of protons) relative to the solvent residual peaks as the internal standard.[2] Coupling constants J are given in Hertz [Hz]. Abbreviations used for signal multiplicity: ^{1}H-, ^{13}C-NMR: b = broad, s = singlet, d = doublet, t = triplet, q = quartet, dd = doublet of doublets, dt = doublet of triplets, dq = doublet of quartets, and m = multiplet. The mass spectrometrical measurements were performed at the Central Analytical Laboratory of the University of Regensburg. All mass spectra were recorded on a Finnigan MAT 95, ThermoQuest Finnigan TSQ 7000, Finnigan MAT SSQ 710 A or an Agilent Q-TOF 6540 UHD instrument. GC measurements were performed on a GC 7890 from Agilent Technologies. Data acquisition and evaluation was done with Agilent ChemStation Rev.C.01.04.. GC-MS measurements were performed on a 7890A GC system from Agilent Technologies with an Agilent 5975 MSD Detector. Data acquisition and evaluation was done with MSD ChemStation E.02.02.1431.. GC measurements were made and analyzed *via* integration of the signal obtained with respect to the calibration with a suitable internal standard. Head-space GC measurements were performed on INFICON 3000 Micro GC equipped with MS-5A column using argon as carrier gas. Analytical TLC was performed on silica gel coated alumina. Visualization was done by UV light (254 or 366 nm). If necessary, potassium permanganate or vanillin was used for chemical staining. Purification of the crude substrates was performed by automated flash-column chromatography. CV measurements were performed with the three-electrode potentiostat galvanostat PGSTAT302N from Metrohm Autolab using a glassy carbon working electrode, a platinum

wire counter electrode, a silver wire as a reference electrode and TBATFB 0.1 M as supporting electrolyte. Prior to the measurement the solvent is degassed with argon. All experiments are performed under argon atmosphere. Ferrocene is used as an internal reference for determining the reduction and oxidation potentials. The photochemical setup for experiments in regular scale consists of 455 nm LEDs (OSRAM Oslon SSL 80 royal-blue, 455 nm (±15 nm), 3.5 V, 700 mA) which illuminate from the bottom and a custom made aluminum cooling block connected to a thermostat which cools from the side (Figure 8).
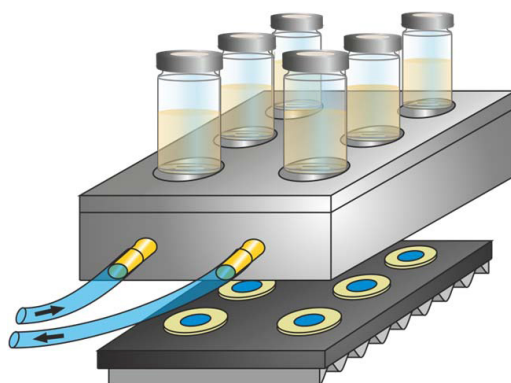
Figure 8. Photochemical reaction setup.

1.8.2   General Procedures

1.8.2.1   General Procedure for the Photoredox-Catalyzed N-Arylation of NH-Sulfoximines

A 5 mL crimp cap vial was equipped with solid *NH*-sulfoximine **1** (0.10 mmol, 1.0 equiv.), solid arene **2** (1.00 mmol, 10 equiv.; except **1i**, 0.53 mmol, 5.3 equiv.), 9-mesityl-10-methylacridinium perchlorate (**A**) (0.02 mmol, 20 mol%) as organic photocatalyst, Co(dmgH)$_2$PyCl (**D**) (0.01 mmol, 10 mol%) as co-catalyst and a magnetic stirring bar and was capped with a septum. All liquid substrates were added *via* syringe after degassing. Nitrogen atmosphere was introduced *via* three cycles vacuum/nitrogen (2 min at 7 mbar/2 min nitrogen atmosphere). Degassed MeCN (0.1 M, 1 mL) was added *via* syringe under nitrogen atmosphere. The reaction mixture was stirred and irradiated using a blue LED (455 nm) for 20 hours at 25 °C under nitrogen atmosphere in a typical irradiation setup used in our laboratories (**Figure 8**). The progress of the reaction could be monitored by GC analysis and GC-MS analysis.

The reaction mixture was diluted with brine (10 mL) and extracted with EtOAc (3 x 10 mL) The combined organic layers were dried with Na_2SO_4, filtered and the solvent was removed under reduced pressure. Evaporation of volatiles led to the crude product. Purification was performed by automated flash-column chromatography (PE/EtOAc) yielding the corresponding pure product **3**.

((2,5-Dimethylphenyl)imino)diphenyl-λ^6-sulfanone (3a)
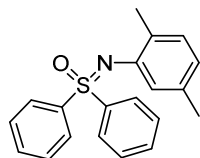
19.6 mg (61%), yellow solid

^{1}H NMR (300 MHz, CDCl$_3$) δ 8.09 – 8.02 (m, 4H), 7.51 – 7.41 (m, 6H), 7.03 (d, *J* = 7.6 Hz, 1H), 6.94 (d, *J* = 2.1 Hz, 1H), 6.64 (d, *J* = 7.6 Hz, 1H), 2.50 (s, 3H), 2.12 (s, 3H).

^{13}C NMR (75 MHz, CDCl$_3$) δ 142.9, 141.4, 135.9, 132.6, 130.1, 129.3, 128.5, 122.9, 122.6, 21.1, 18.6.

HRMS (ESI) (m/z): [M + H]$^+$ (C$_{20}$H$_{19}$NOS) calc.: 321.126, found: 321.1265.

((3,4-Dimethylphenyl)imino)diphenyl-λ^6-sulfanone (3b$_A$) and ((2,3-dimethyl-phenyl)imino)diphenyl-λ^6-sulfanone (3b$_B$)
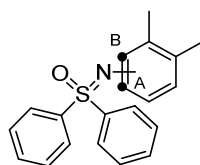
13.5 mg (42%; 2.6:1 C$_A$:C$_B$), yellow crystals

^{1}H NMR (300 MHz, CDCl$_3$) δ 8.09 – 8.02 (m, 5.11H), 7.50 – 7.42 (m, 7.61H), 6.98 (s, 1H), 6.96 (s, 0.22H), 6.89 (s, 1H), 6.88 (s, 1H), 6.79 (t, *J* = 7.6 Hz, 0.28H), 6.72 (d, *J* = 7.2 Hz, 0.28H), 2.48 (s, 0.83H), 2.28 (s, 0.83H), 2.14 (s, 3H), 2.12 (s, 3H).

^{13}C NMR (75 MHz, CDCl$_3$) δ 142.9, 142.1, 141.5, 141.1, 137.4, 137.2, 132.7, 132.6, 131.0, 130.1, 129.9, 129.4, 129.3, 128.7, 128.5, 125.5, 125.2, 123.6, 121.0, 120.0, 20.8, 20.0, 19.1, 14.6.

HRMS (ESI) (m/z): [M + H]$^+$ (C$_{20}$H$_{19}$NOS) calc.: 322.126, found: 322.1263.

((2,4-Dimethylphenyl)imino)diphenyl-λ^6-sulfanone (3c$_A$) and **((2,6-dimethylphenyl)imino)diphenyl-λ^6-sulfanone (3c$_B$)**
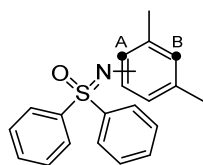
12.5 mg (39%; 6.5:1 C$_A$:C$_B$), yellow solid

^{1}H NMR (400 MHz, CDCl$_3$) δ 8.10 – 7.90 (m, 4.67H), 7.55 – 7.41 (m, 6.96H), 7.01 – 6.90 (m, 2.27H), 6.85 – 6.77 (m, 0.17H), 6.70 (dd, *J* = 8.1, 2.1 Hz, 1H), 2.50 (s, 3H), 2.28 (s, 0.46H), 2.19 (s, 3.45H).

^{13}C NMR (101 MHz, CDCl$_3$) δ 142.1, 141.4, 140.4, 138.5, 134.1, 132.7, 132.6, 132.5, 132.2, 131.2, 131.0, 129.3, 129.1, 128.7, 128.6, 128.3, 128.0, 126.9, 122.0, 121.6, 21.4, 20.8, 20.6, 19.0.

HRMS (ESI) (m/z): [M + H]$^+$ (C$_{20}$H$_{19}$NOS) calc.: 322.126, found: 322.1262.

((5-(*Tert*-butyl)-2-methylphenyl)imino)diphenyl-λ^6-sulfanone (3d)
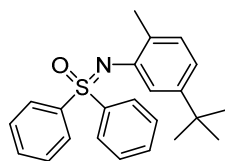
34.5 mg (95%), yellow solid

^{1}H NMR (300 MHz, CDCl$_3$) δ 8.11 – 8.01 (m, 4H), 7.53 – 7.42 (m, 6H), 7.08 – 7.03 (m, 2H), 6.82 (dd, *J* = 7.8, 2.0 Hz, 1H), 2.48 (s, 3H), 1.10 (s, 9H).

^{13}C NMR (75 MHz, CDCl$_3$) δ 149.2, 141.2, 132.6, 129.8, 129.6, 129.3, 128.7, 119.8, 118.5, 34.3, 31.3, 18.5.

HRMS (ESI) (m/z): [M + H]$^+$ (C$_{23}$H$_{25}$NOS) calc.: 364.173, found: 364.1738.

(Mesitylimino)diphenyl-λ⁶-sulfanone (3e)
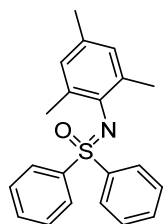
14.8 mg (44%), colorless oil

¹H NMR (400 MHz, CDCl₃) δ 7.97 – 7.90 (m, 4H), 7.56 – 7.38 (m, 6H), 6.75 (s, 2H), 2.24 (s, 6H), 2.18 (s, 3H).

¹³C NMR (101 MHz, CDCl₃) δ 142.3, 137.8, 133.7, 132.4, 132.1, 129.1, 129.0, 128.1, 20.8, 20.5.

HRMS (ESI) (m/z): $[M + H]^+$ ($C_{21}H_{21}NOS$) calc.: 336.1417, found: 336.1422.

((3-Bromo-2,4-dimethylphenyl)imino)diphenyl-λ⁶-sulfanone (3f$_A$) and ((4-bromo-3,5-dimethylphenyl)imino)diphenyl-λ⁶-sulfanone (3f$_A$)
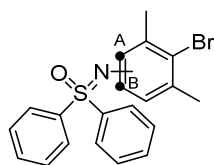
4.8 mg (12%; 2.6:1 C_A:C_B), yellow crystals

¹H NMR (300 MHz, CDCl₃) δ 8.06 – 7.98 (m, 5.53H), 7.55 – 7.43 (m, 8.38H), 6.98 (d, *J* = 8.0 Hz, 1H), 6.89 (s, 0.75H), 6.76 (d, *J* = 8.1 Hz, 1H), 2.66 (s, 2.35H), 2.27 (s, 6H).

¹³C NMR (75 MHz, CDCl₃) δ 143.3, 141.8, 141.1, 140.9, 138.6, 132.9, 132.8, 132.5, 131.5, 129.5, 129.4, 129.1, 128.6, 128.5, 128.5, 128.1, 127.7, 123.6, 120.8, 24.0, 23.7, 19.4.

HRMS (ESI) (m/z): $[M + H]^+$ ($C_{20}H_{18}BrNOS$) calc.: 400.0365, found: 400.0371.

([1,1'-Biphenyl]-4-ylimino)diphenyl-λ⁶-sulfanone (3g)
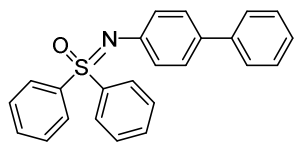
15.5 mg (42%), white solid

¹H NMR (300 MHz, DMSO-d_6) δ 8.12 – 8.03 (m, 4H), 7.68 – 7.52 (m, 8H), 7.51 – 7.44 (m, 2H), 7.42 – 7.34 (m, 2H), 7.32 – 7.23 (m, 1H), 7.18 – 7.09 (m, 2H).

¹³C NMR (75 MHz, DMSO-d_6) δ 144.3, 140.2, 139.8, 133.3, 133.2, 129.8, 128.8, 128.2, 127.3, 126.7, 126.0, 123.7.

HRMS (ESI) (m/z): $[M + H]^+$ ($C_{24}H_{19}NOS$) calc.: 370.126, found: 370.1261.

((9,9-Dimethyl-9*H*-fluoren-3-yl)imino)diphenyl-λ^6-sulfanone (3h)
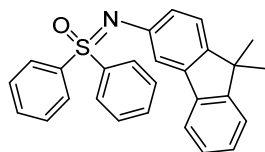
2.0 mg (5%), yellow crystals

^{1}H NMR (300 MHz, CDCl$_3$) δ 8.12 – 8.05 (m, 4H), 7.58 – 7.53 (m, 1H), 7.52 – 7.43 (m, 7H), 7.37 – 7.32 (m, 1H), 7.29 – 7.16 (m, 3H), 7.10 (dd, *J* = 8.1, 2.1 Hz, 1H), 1.37 (s, 6H).

^{13}C NMR (75 MHz, CDCl$_3$) δ 154.9, 153.4, 144.2, 140.8, 139.5, 133.2, 132.8, 129.4, 128.8, 126.9, 126.2, 122.5, 120.5, 119.3, 118.4, 46.8, 27.3.

HRMS (ESI) (m/z): [M + H]$^+$ (C$_{27}$H$_{23}$NOS) calc.: 410.1573, found: 410.1583.

((3-Bromo-2,4,6-trimethylphenyl)imino)diphenyl-λ^6-sulfanone (3i)
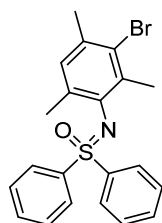
33.1 mg (80%), yellow viscos oil

^{1}H NMR (400 MHz, CDCl$_3$) δ 7.92 – 7.86 (m, 4H), 7.57 – 7.44 (m, 6H), 6.84 (s, 1H), 2.32 (s, 3H), 2.29 (s, 3H), 2.17 (s, 3H).

^{13}C NMR (75 MHz, CDCl$_3$) δ 141.6, 138.9, 134.1, 132.9, 132.6, 132.6, 129.8, 129.1, 127.9, 125.3, 23.7, 21.1, 20.2.

HRMS (ESI) (m/z): [M + H]$^+$ (C$_{21}$H$_{20}$BrNOS) calc.: 414.0522, found: 414.0526.

((3-Iodo-2,4,6-trimethylphenyl)imino)diphenyl-λ^6-sulfanone (3j)
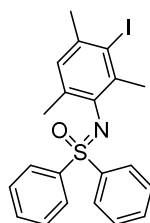
4.6 mg (10%), yellow crystals

^{1}H NMR (300 MHz, CDCl$_3$) δ 7.94 – 7.83 (m, 4H), 7.61 – 7.40 (m, 6H), 6.86 (s, 1H), 2.39 (s, 3H), 2.35 (s, 3H), 2.17 (s, 3H).

¹³C NMR (75 MHz, CDCl₃) δ 141.6, 137.6, 137.5, 136.6, 134.0, 132.7, 129.1, 128.0, 106.1, 29.5, 27.3, 20.2.

HRMS (ESI) (m/z): [M + H]⁺ (C₂₁H₂₀INOS) calc.: 462.0383, found: 462.0388.

Methyl(phenyl)((2,4,6-triethylphenyl)imino)-λ⁶-sulfanone (3l)
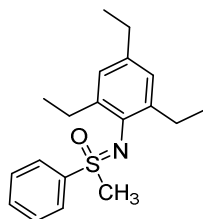
27.4 mg (87%), yellow oil

¹H NMR (400 MHz, CDCl₃) δ 8.21 – 8.12 (m, 2H), 7.69 – 7.53 (m, 3H), 6.91 (s, 2H), 3.04 (s, 3H), 2.78 (ddt, *J* = 17.3, 14.5, 7.2 Hz, 4H), 2.60 (q, *J* = 7.6 Hz, 2H), 1.24 (td, *J* = 7.6, 3.4 Hz, 9H).

¹³C NMR (101 MHz, CDCl₃) δ 141.6, 139.8, 139.3, 136.7, 133.1, 129.4, 128.0, 125.9, 43.1, 28.5, 25.7, 15.7, 14.8.

HRMS (ESI) (m/z): [M + H]⁺ (C₁₉H₂₅NOS) calc.: 316.173, found: 316.1734.

1-((2,4,6-Triethylphenyl)imino)tetrahydro-1*H*-1λ⁶-thiophene 1-oxide (3m)
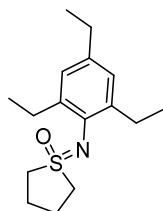
15.9 mg (57%), orange oil

¹H NMR (300 MHz, CDCl₃) δ 6.89 (s, 2H), 3.42 – 3.26 (m, 2H), 3.13 – 2.98 (m, 2H), 2.72 (q, *J* = 7.5 Hz, 4H), 2.58 (q, *J* = 7.6 Hz, 2H), 2.34 – 2.26 (m, 4H), 1.24 – 1.18 (m, 9H).

¹³C NMR (75 MHz, CDCl₃) δ 139.6, 125.8, 53.2, 28.6, 25.5, 24.0, 15.7, 14.7.

HRMS (ESI) (m/z): [M + H]⁺ (C₁₆H₂₅rNOS) calc.: 280.173, found: 280.1734.

Benzyl((2,5-dimethylphenyl)imino)(phenyl)-λ⁶-sulfanone (3n)
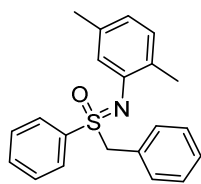
19.5 mg (58%), off-white solid

¹H NMR (400 MHz, CDCl₃) δ 8.05 – 7.98 (m, 2H), 7.95 – 7.86 (m, 1H), 7.81 – 7.72 (m, 2H), 7.69 – 7.60 (m, 1H), 7.60 – 7.51 (m, 2H), 7.41 – 7.26 (m, 4H), 7.06 – 6.98 (m, 1H), 5.01 (d, *J* = 13.6 Hz, 1H), 4.80 (d, *J* = 13.6 Hz, 1H), 2.64 (s, 3H), 2.54 (s, 3H).

¹³C NMR (101 MHz, CDCl₃) δ 143.5, 137.1, 136.0, 133.2, 131.4, 130.2, 129.7, 129.3, 129.0, 129.0, 128.6, 128.3, 122.5, 122.5, 63.0, 21.2, 18.5.

HRMS (ESI) (m/z): [M + H]⁺ (C₂₁H₂₁NOS) calc.: 336.1417, found: 336.1425.

Benzyl((3-bromo-2,4,6-trimethylphenyl)imino)(phenyl)-λ⁶-sulfanone (3o)
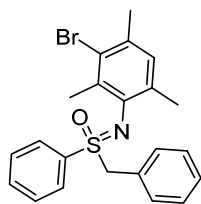
33.8 mg (79%), colorless oil

¹H NMR (400 MHz, CDCl₃) δ 8.22 – 8.14 (m, 2H), 7.96 (td, *J* = 7.3, 1.2 Hz, 1H), 7.83 (t, *J* = 7.8 Hz, 2H), 7.68 – 7.58 (m, 1H), 7.55 (t, *J* = 7.2 Hz, 2H), 7.34 – 7.25 (m, 3H), 4.85 (d, *J* = 13.5 Hz, 1H), 4.55 (d, *J* = 13.5 Hz, 1H), 2.91 (s, 3H), 2.73 (s, 3H), 2.71 (s, 3H).

¹³C NMR (101 MHz, CDCl₃) δ 139.4, 138.1, 134.1, 133.3, 133.0, 132.8, 131.1, 130.0, 129.3, 129.2, 129.0, 128.5, 128.3, 125.6, 62.7, 23.7, 21.2, 20.7.

HRMS (ESI) (m/z): [M + H]⁺ (C₂₂H₂₂BrNOS) calc.: 428.0678, found: 428.0679.

((3-Bromo-2,4,6-trimethylphenyl)imino)(methyl)(phenyl)-λ⁶-sulfanone (3p)
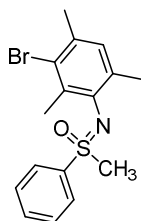
29.9 mg (85%), yellowish oil

¹H NMR (300 MHz, CDCl₃) δ 8.18 – 8.09 (m, 2H), 7.69 – 7.53 (m, 3H), 6.98 – 6.91 (m, 1H), 3.04 (s, 3H), 2.49 (s, 3H), 2.34 (s, 3H), 2.31 (s, 3H).

¹³C NMR (75 MHz, CDCl₃) δ 140.9, 139.2, 134.1, 133.3, 133.1, 132.9, 129.9, 129.4, 127.8, 125.5, 43.3, 23.7, 21.0, 19.9.

HRMS (ESI) (m/z): [M + H]⁺ (C₁₆H₁₈BrNOS) calc.: 352.0365, found: 352.0368.

((3-Bromo-2,4,6-trimethylphenyl)imino)(methyl)(phenyl)-λ⁶-sulfanone (3q)
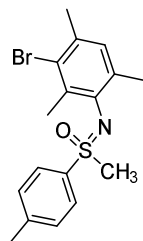
30.8 mg (84%), yellow crystals

¹H NMR (300 MHz, CDCl₃) δ 8.05 – 7.95 (m, 2H), 7.42 – 7.31 (m, 2H), 6.94 (s, 1H), 3.01 (s, 3H), 2.49 (s, 3H), 2.45 (s, 3H), 2.33 (s, 3H), 2.31 (s, 3H).

¹³C NMR (75 MHz, CDCl₃) δ 144.2, 139.4, 137.9, 134.1, 133.1, 132.8, 130.0, 129.9, 127.9, 125.5, 43.4, 23.7, 21.7, 21.0, 19.9.

HRMS (ESI) (m/z): [M + H]⁺ (C₁₇H₂₀BrNOS) calc.: 366.0522, found: 366.0526.

((3-Bromo-2,4,6-trimethylphenyl)imino)(4-methoxyphenyl)(methyl)-λ⁶-sulfanone (3r)
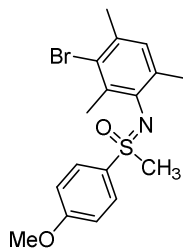
34.0 mg (89%), orange oil

¹H NMR (300 MHz, CDCl₃) δ 8.11 – 7.99 (m, 2H), 7.09 – 6.97 (m, 2H), 6.94 (s, 1H), 3.87 (s, 3H), 2.98 (s, 3H), 2.49 (s, 3H), 2.33 (s, 3H), 2.31 (s, 3H).

¹³C NMR (75 MHz, CDCl₃) δ 163.5, 139.5, 134.1, 133.1, 132.8, 132.2, 130.1, 129.9, 125.5, 114.5, 55.8, 43.5, 23.6, 21.0 , 19.9.

HRMS (ESI) (m/z): [M + H]⁺ (C₁₇H₂₀BrNO₂S) calc.: 382.0471, found: 382.0472.

((3-Bromo-2,4,6-trimethylphenyl)imino)(4-fluorophenyl)(methyl)-λ⁶-sulfanone (3s)
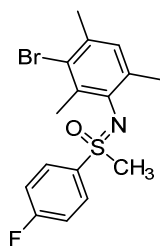
31.1 mg (84%), white solid

¹H NMR (400 MHz, CDCl₃) δ 8.17 – 8.12 (m, 2H), 7.31 – 7.20 (m, 2H), 6.94 (s, 1H), 3.03 (s, 3H), 2.47 (s, 3H), 2.33 (s, 3H), 2.29 (s, 3H).

¹³C NMR (101 MHz, CDCl₃) δ 165.6 (d, J = 255.7 Hz), 139.0, 136.8 (d, J = 3.2 Hz), 134.0, 133.1 (d, J = 12.3 Hz), 130.8 (d, J = 9.4 Hz), 130.0, 125.6, 116.6 (d, J = 22.6 Hz), 43.6, 23.7, 21.0, 19.9.

HRMS (ESI) (m/z): [M + H]⁺ (C₁₆H₁₇BrFNOS) calc.: 370.0271, found: 370.0278.

(4-Chlorophenyl)((2,5-dimethylphenyl)imino)(methyl)-λ⁶-sulfanone (3t)
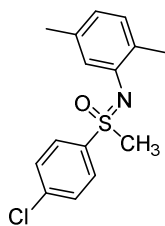
18.5 mg (63%), colorless oil

¹H NMR (400 MHz, CDCl₃) δ 7.93 – 7.89 (m, 2H), 7.52 – 7.47 (m, 2H), 7.01 (d, J = 7.6 Hz, 1H), 6.85 (s, 1H), 6.66 (d, J = 7.5 Hz, 1H), 3.21 (s, 3H), 2.31 (s, 3H), 2.16 (s, 3H).

¹³C NMR (101 MHz, CDCl₃) δ 142.9, 139.9, 138.6, 136.0, 130.3, 130.0, 129.8, 129.1, 122.9, 122.7, 45.7, 21.1, 18.3.

HRMS (ESI) (m/z): [M + H]⁺ (C₁₅H₁₆ClNOS) calc.: 294.0714, found: 294.0715.

((3-Bromo-2,4,6-trimethylphenyl)imino)(4-chlorophenyl)(methyl)-λ⁶-sulfanone (3u)
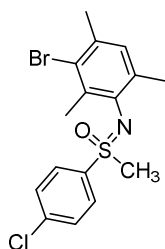
30.2 mg (78%), off-white solid

¹H NMR (400 MHz, CDCl₃) δ 8.10 – 8.01 (m, 2H), 7.59 – 7.51 (m, 2H), 6.94 (s, 1H), 3.05 (s, 3H), 2.46 (s, 3H), 2.34 (s, 3H), 2.28 (s, 3H).

¹³C NMR (101 MHz, CDCl₃) δ 140.0, 139.5, 138.9, 134.0, 133.2, 133.0, 130.0, 129.7, 129.4, 125.6, 43.6, 23.7, 21.0, 19.9.

HRMS (ESI) (m/z): [M + H]⁺ (C₁₆H₁₇BrClNOS) calc.: 385.9976, found: 285.9978.

4-(*N*-(3-bromo-2,4,6-trimethylphenyl)-*S*-methylsulfonimidoyl)benzonitrile (3v)
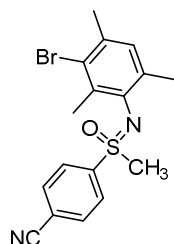
35.1 mg (93%), orange oil

¹H NMR (400 MHz, CDCl₃) δ 8.24 – 8.19 (m, 2H), 7.89 – 7.81 (m, 2H), 6.93 (s, 1H), 3.10 (s, 3H), 2.42 (s, 3H), 2.33 (s, 3H), 2.25 (s, 3H).

¹³C NMR (101 MHz, CDCl₃) δ 145.3, 138.3, 133.8, 133.4, 133.2, 132.8, 130.0, 128.5, 125.6, 117.3, 117.0, 43.5, 23.6, 21.0 , 19.9.

HRMS (ESI) (m/z): [M + H]⁺ (C₁₇H₁₇BrN₂OS) calc.: 377.0318, found: 377.0317.

((3-Bromo-2,4,6-trimethylphenyl)imino)(cyclopropyl)(phenyl)-λ⁶-sulfanone (3w)
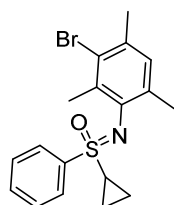
35.9 mg (95%), yellowish oil

¹H NMR (400 MHz, CDCl₃) δ 8.09 – 8.01 (m, 2H), 7.65 – 7.49 (m, 3H), 6.90 (s, 1H), 2.48 (s, 3H), 2.44 (td, *J* = 7.8, 3.9 Hz, 1H), 2.33 (s, 3H), 2.29 (s, 3H), 1.27 (ddt, *J* = 9.7, 6.7, 4.8 Hz, 1H), 1.11 – 1.04 (m, 1H), 0.91 (dddd, *J* = 9.1, 8.1, 6.8, 4.9 Hz, 1H), 0.83 (tdd, *J* = 9.1, 7.1, 4.7 Hz, 1H).

¹³C NMR (101 MHz, CDCl₃) δ 141.3, 139.5, 133.9, 132.8, 132.4, 129.7, 129.2, 127.7, 125.3, 32.5, 23.7, 21.0, 20.0, 5.7, 5.7.

HRMS (ESI) (m/z): [M + H]⁺ (C₁₈H₂₀BrNOS) calc.: 378.0522, found: 378.0525.

40

((3-Bromo-2,4,6-trimethylphenyl)imino)(2-hydroxyethyl)(phenyl)-λ⁶-sulfanone (3x)
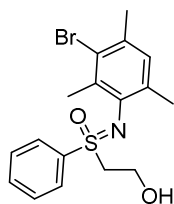

22.6 mg (59%), yellow oil

¹H NMR (300 MHz, CDCl₃) δ 8.08 – 7.97 (m, 2H), 7.69 – 7.52 (m, 3H), 6.91 (s, 1H), 4.06 (ddd, *J* = 12.7, 8.8, 2.7 Hz, 1H), 3.91 (ddd, *J* = 12.8, 5.5, 3.6 Hz, 1H), 3.69 (ddd, *J* = 14.3, 8.8, 3.6 Hz, 1H), 3.30 (s, 1H), 3.21 (ddd, *J* = 14.3, 5.6, 2.7 Hz, 1H), 2.45 (s, 3H), 2.32 (s, 3H), 2.28 (s, 3H).

¹³C NMR (75 MHz, CDCl₃) δ 139.1, 138.4, 134.0, 133.7, 133.3, 132.9, 130.0, 129.6, 128.3, 125.6, 57.1, 57.4, 23.7, 21.1, 20.1.

HRMS (ESI) (m/z): [M + H]⁺ (C₁₇H₂₀BrNO₂S) calc.: 382.0471, found: 382.0475.

1-((3-Bromo-2,4,6-trimethylphenyl)imino)tetrahydro-1*H*-1-λ⁶-thiophene 1-oxide (3z)
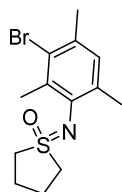
21.8 mg (69%), green crystals

¹H NMR (400 MHz, CDCl₃) δ 6.94 (s, 1H), 3.32 – 3.23 (m, 2H), 3.09 – 3.00 (m, 2H), 2.45 (s, 3H), 2.33 (s, 3H), 2.34 – 2.23 (m, 7H).

¹³C NMR (101 MHz, CDCl₃) δ 140.3, 133.8, 132.9, 132.9, 129.9, 125.5, 53.2, 23.9, 23.6, 20.8, 19.7.

HRMS (ESI) (m/z): [M + H]⁺ (C₁₃H₁₈BrNOS) calc.: 316.0365, found: 316.0371.

((3-Bromo-2,4,6-trimethylphenyl)imino)dibutyl-l-λ⁶-sulfanone (3aa)
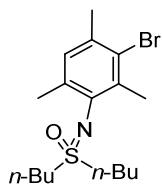
31.4 mg (84%), yellowish oil

¹H NMR (300 MHz, CDCl₃) δ 6.94 – 6.87 (m, 1H), 3.14 – 2.92 (m, 4H), 2.43 (s, 3H), 2.32 (s, 3H), 2.26 (s, 3H), 1.94 – 1.69 (m, 4H), 1.49 – 1.36 (m, 4H), 0.94 (t, *J* = 7.3 Hz, 6H).

^{13}C NMR (75 MHz, CDCl$_3$) δ 139.7, 133.9, 133.0, 132.5, 129.7, 125.4, 52.8, 25.5, 23.6, 22.0, 20.9, 19.8, 13.8.

HRMS (ESI) (m/z): [M + H]$^+$ (C$_{17}$H$_{28}$BrNOS) calc.: 374.1148, found: 374.1150.

Dibutyl((2,4,6-triethylphenyl)imino)-λ^6-sulfanone (3ab)
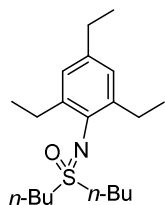
17.6 mg (52%), orange oil

^{1}H NMR (300 MHz, CDCl$_3$) δ 6.87 (s, 2H), 3.14 – 2.96 (m, 4H), 2.73 (q, *J* = 7.5 Hz, 4H), 2.57 (q, *J* = 7.6 Hz, 2H), 1.94 – 1.69 (m, 4H), 1.52 – 1.32 (m, 4H), 1.27 – 1.14 (m, 9H), 0.93 (t, *J* = 7.4 Hz, 6H).

^{13}C NMR (75 MHz, CDCl$_3$) δ 139.4, 138.8, 137.2, 125.6, 52.6, 28.5, 25.6, 25.5, 22.0, 15.8, 14.7, 13.8.

HRMS (ESI) (m/z): [M + H]$^+$ (C$_{20}$H$_{35}$NOS) calc.: 338.2512, found: 338.2520.

Dibutyl((3,5-di-tert-butylphenyl)imino)-λ^6-sulfanone (3ac)
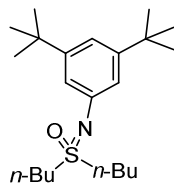
24.1 mg (66%), white crystals

^{1}H NMR (300 MHz, CDCl$_3$) δ 7.02 (t, *J* = 1.7 Hz, 1H), 6.95 (d, *J* = 1.7 Hz, 2H), 3.30 – 3.04 (m, 4H), 1.92 – 1.75 (m, 4H), 1.48 – 1.39 (m, 4H), 1.29 (s, 18H), 0.93 (t, *J* = 7.3 Hz, 6H).

^{13}C NMR (75 MHz, CDCl$_3$) δ 151.6, 144.4, 118.1, 116.1, 51.8, 34.9, 31.6, 25.3, 21.9, 13.7.

HRMS (ESI) (m/z): [M + H]$^+$ (C$_{22}$H$_{39}$NOS) calc.: 366.2825, found: 366.2832.

((3-Bromo-2,4,6-trimethylphenyl)imino)(1-methyl-1*H*-indol-2-yl)(thiophen-2-yl)-λ⁶-sulfanone (3ad)
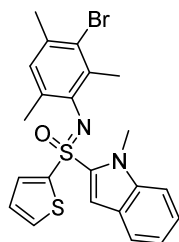
4.7 mg (10%), greenish oil

¹H NMR (400 MHz, CDCl₃) δ 7.90 (d, *J* = 8.4 Hz, 2H), 7.45 (ddd, *J* = 7.8, 4.4, 1.2 Hz, 2H), 7.38 (d, *J* = 8.2 Hz, 1H), 7.36 – 7.31 (m, 1H), 7.27 – 7.22 (m, 1H), 6.95 (dd, *J* = 4.9, 3.9 Hz, 1H), 6.88 (s, 1H), 3.87 (s, 3H), 2.43 (s, 3H), 2.31 (s, 3H), 2.29 (s, 3H).

¹³C NMR (75 MHz, CDCl₃) δ 145.2, 137.5, 134.7, 133.6, 133.2, 131.9, 131.6, 129.8, 127.7, 125.5, 124.9, 123.8, 122.6, 120.3, 110.5, 34.0, 23.8, 21.3, 20.4.

HRMS (ESI) (m/z): [M + H]⁺ (C₂₂H₂₁BrN₂OS₂) calc.: 473.0351, found: 473.0363.

1.8.2.2   General Procedure for the Preparation of NH-Sulfoximines

NH-sulfoximines were prepared from the respective sulfides according to published procedures, if not stated differently.[3]

Iminodiphenyl-λ[6]-sulfanone (1a)

Compound was prepared from the respective sulfoxide according to reported literature procedure and ^{1}H-NMR data are matching with the literature known spectra[4]
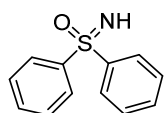
1H NMR (300 MHz, CDCl$_3$) δ 8.10 – 8.01 (m, 4H), 7.56 – 7.45 (m, 6H), 3.11 (s, 1H).

Imino(methyl)(phenyl)-λ[6]-sulfanone (1l)

Compound was prepared according to reported literature procedure and ^{1}H-NMR data are matching with the literature known spectra[3a]
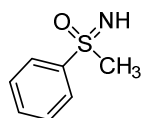
^{1}H NMR (400 MHz, CDCl$_3$) δ 7.99 – 7.94 (m, 2H), 7.62 – 7.55 (m, 1H), 7.55 – 7.47 (m, 2H), 3.07 (s, 3H), 2.64 (s, 1H).

1-Iminotetrahydro-1*H*-1λ[6]-thiophene 1-oxide (1m)

Compound was prepared according to reported literature procedure and ^{1}H-NMR data are matching with the literature known spectra[3a]

^{1}H NMR (400 MHz, CDCl$_3$) δ 3.03 – 2.96 (m, 5H), 2.11 (td, *J* = 6.8, 3.7 Hz, 4H).

Benzyl(imino)(phenyl)-λ^6-sulfanone (1n)

Compound was prepared according to reported literature procedure and ^{1}H-NMR data are matching with the literature known spectra[3a]

^{1}H NMR (300 MHz, CDCl$_3$) δ 7.80 – 7.73 (m, 2H), 7.62 – 7.53 (m, 1H), 7.50 – 7.40 (m, 2H), 7.34 – 7.23 (m, 3H), 7.14 – 7.07 (m, 2H), 4.36 (q, *J* = 13.4 Hz, 2H), 2.84 (s, 1H).

Imino(methyl)(*p*-tolyl)-λ^6-sulfanone (1p)

Compound was prepared according to reported literature procedure and ^{1}H-NMR data are matching with the literature known spectra[3b]

^{1}H NMR (400 MHz, CDCl$_3$) δ 7.89 – 7.80 (m, 2H), 7.34 – 7.28 (m, 2H), 3.05 (s, 3H), 2.57 (s, 1H), 2.40 (s, 3H).

Imino(4-methoxyphenyl)(methyl)-λ^6-sulfanone (1r)

Compound was prepared according to reported literature procedure and ^{1}H-NMR data are matching with the literature known spectra[3b]

^{1}H NMR (300 MHz, CDCl$_3$) δ 8.05 – 7.79 (m, 2H), 7.06 – 6.86 (m, 2H), 3.82 (s, 3H), 3.03 (s, 1H), 2.75 (s, 3H).

(4-Fluorophenyl)(imino)(methyl)-λ^6-sulfanone (1s)

Compound was prepared according to reported literature procedure and ^{1}H-NMR data are matching with the literature known spectra[3a]

^{1}H NMR (300 MHz, CDCl$_3$) δ 8.07 – 7.95 (m, 2H), 7.25 – 7.15 (m, 2H), 3.09 (s, 3H), 2.77 (s, 1H).

(4-Chlorophenyl)(imino)(methyl)-λ[6]-sulfanone (1t)

Compound was prepared according to reported literature procedure and ^{1}H-NMR data are matching with the literature known spectra[3a]

^{1}H NMR (400 MHz, CDCl$_3$) δ 8.00 – 7.87 (m, 2H), 7.57 – 7.48 (m, 2H), 3.11 (s, 3H), 2.59 (s, 1H).

4-(*S*-Methylsulfonimidoyl)benzonitrile (1v)

Compound was prepared according to reported literature procedure and ^{1}H-NMR data are matching with the literature known spectra[3b]

^{1}H NMR (300 MHz, CDCl$_3$) δ 8.14 – 8.08 (m, 2H), 7.86 – 7.81 (m, 2H), 3.10 (s, 3H), 2.83 (s, 1H).

Cyclopropyl(imino)(phenyl)-λ[6]-sulfanone (1w)

Compound was prepared according to reported literature procedure and ^{1}H-NMR data are matching with the literature known spectra[3c]

^{1}H NMR (300 MHz, CDCl$_3$) δ 7.99 – 7.87 (m, 2H), 7.63 – 7.43 (m, 3H), 2.69 (s, 1H), 2.50 (tt, *J* = 7.9, 4.8 Hz, 1H), 1.34 (ddt, *J* = 10.2, 7.0, 4.7 Hz, 1H), 1.24 – 1.07 (m, 1H), 1.01 (dddd, *J* = 9.0, 8.0, 6.8, 4.8 Hz, 1H), 0.87 (dddd, *J* = 9.0, 7.9, 6.9, 4.9 Hz, 1H).

(2-Hydroxyethyl)(imino)(phenyl)-λ[6]-sulfanone (1x)

Compound was prepared according to reported literature procedure and ^{1}H-NMR data are matching with the literature known spectra[3c]
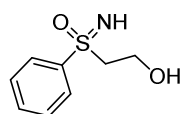
^{1}H NMR (300 MHz, CDCl$_3$) δ 8.04 – 7.91 (m, 2H), 7.72 – 7.49 (m, 3H), 4.12 – 4.00 (m, 1H), 3.89 – 3.78 (m, 1H), 3.71 – 3.60 (m, 2H), 3.34 – 3.28 (m, 2H).

Dibutyl(imino)-λ⁶-sulfanone (1aa)

Compound was prepared according to reported literature procedure and ¹H-NMR data are matching with the literature known spectra[3a]
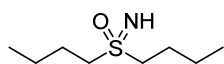
¹H NMR (400 MHz, CDCl₃) δ 3.01 – 2.88 (m, 4H), 2.72 (s, 1H), 1.82 – 1.69 (m, 4H), 1.41 (h, *J* = 7.4 Hz, 4H), 0.91 (t, *J* = 7.4 Hz, 6H).

Imino(1-methyl-1*H*-indol-2-yl)(thiophen-2-yl)-λ⁶-sulfanone (1ad)

Compound **1ad** was prepared as following:

539 mg of the respective sulfoxide (prepared according to reported literature[5]) (2.1 mmol, 1 equiv.), diacetoxyiodobenzene (6.2 mmol, 3 equiv., 1991 mg), ammonium carbamate (8.2 mmol, 4 equiv., 643 mg) and a magnetic stirring bar were added to a round-bottomed flask. MeOH (0.5 M) was added and the solution was stirred for 2h at room temperature. The progress of the reaction was monitored by TLC. The reaction mixture was diluted with brine (50 mL) and extracted with EtOAc (3 x 50 mL). The combined organic layers were dried with Na₂SO₄, filtered and the solvent was removed under reduced pressure. Evaporation of volatiles led to the crude product. Purification was performed by automated flash-column chromatography (PE/EtOAc, 50 – 100% EtOAc) yielding 69.0 mg (12%) of the corresponding *NH*-sulfoximine **1ad** as a brown solid.
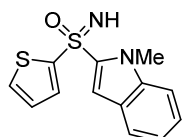
¹H NMR (300 MHz, CDCl₃) δ 8.12 – 8.01 (m, 1H), 7.74 (s, 1H), 7.65 (dd, *J* = 3.8, 1.4 Hz, 1H), 7.41 (dd, *J* = 5.0, 1.4 Hz, 1H), 7.32 – 7.17 (m, 3H), 6.91 (dd, *J* = 5.0, 3.8 Hz, 1H), 3.74 (s, 3H), 3.37 (s, 1H).

**¹³C NMR** (75 MHz, CDCl₃) δ 147.8, 137.5, 134.0, 132.2, 131.8, 127.6, 124.3, 123.5, 122.3, 120.2, 116.4, 110.4, 33.7.

HRMS (ESI) (m/z): [M + H]⁺ (C₁₃H₁₂N₂OS₂) calc.: 277.0464, found: 277.0468.

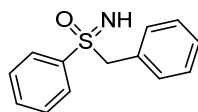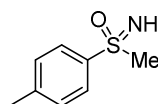**Benzo[*d*]thiazol-2-yl(imino)(4-(trifluoromethyl)benzyl)-λ⁶-sulfanone (1ae)**
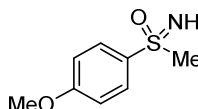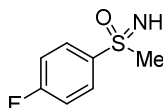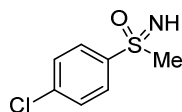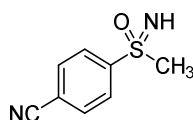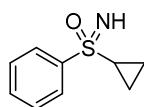
Compound was prepared according to reported literature procedure and ¹H-NMR data are matching with the literature known spectra[3a]
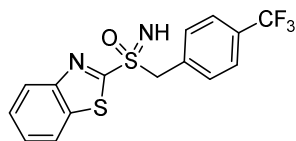
¹H NMR (300 MHz, CDCl₃) δ 8.29 – 8.17 (m, 1H), 8.02 – 7.85 (m, 1H), 7.70 – 7.58 (m, 1H), 7.64 – 7.50 (m, 3H), 7.48 – 7.36 (m, 2H), 5.03 – 4.59 (m, 2H), 3.43 (s, 1H).

1.8.3 Procedure for the Photoredox-Catalyzed *N*-Arylation Reaction of *NH*-Sulfoximines in Preparative-Scale

1.8.3.1 *Procedure in the Custom-Built Large-Scale Batch Reactor*

The reactor consists of two compartments: The outer vessel can be charged with a stirring bar and all substrates and reagents needed in the reaction. The inner vessel is cooled with running water. A thin film of reaction medium is created between the two compartments, enabling efficient illumination of the reaction mixture (**Figure 5**).

1.00 g of *NH*-sulfoximine **1a** (4.60 mmol, 1.0 equiv.), 379 mg 9-mesityl-10-methylacridinium perchlorate (**A**) (0.92 mmol, 20 mol%) as organic photocatalyst, 186 mg Co(dmgH)₂PyCl (**D**) (0.46 mmol, 10 mol%) as co-catalyst and a magnetic stirring bar were added to the reactor. Nitrogen atmosphere was introduced *via* five cycles vacuum/nitrogen (2 min at 7 mbar/2 min nitrogen atmosphere). 46 mL degassed MeCN (0.1 M) and 3.52 mL arene **2a** (23.0 mmol, 5.0 equiv.) were added *via* syringe under nitrogen atmosphere. The reaction mixture was stirred and irradiated using blue LEDs (455 nm) for 24 hours at 25 °C under nitrogen atmosphere.

The reaction mixture was diluted with brine (100 mL) and extracted with EtOAc (3 x 100 mL) The combined organic layers were dried with Na₂SO₄, filtered and the solvent was removed under reduced pressure. Evaporation of volatiles led to the crude product. Purification was performed by automated flash-column chromatography (PE/EtOAc) yielding 1.50 g (79%) of the corresponding pure product **3a**.

1.8.3.2   *Procedure of the Continuous Photo-Flow Approach*

A 5 mL gas-tight reaction vessel was charged with *NH*-sulfoximine **1l** (1.0 equiv.), 9-mesityl-10-methylacridinium tetrafluoroborate (**B**) (20 mol%) as organic photocatalyst, Co(dmgH)$_2$PyCl (**D**) (10 mol%) as co-catalyst and a magnetic stirring bar. Nitrogen atmosphere was introduced by bubbling nitrogen over 10 minutes. Degassed MeCN (0.1 M, 0.2 M or 0.25 M) and liquid arene **2i** (5.3 equiv.) were added *via* syringe, ending up with a total reaction volume of 2.0 mL. The reaction mixture was stirred for 5 minutes, sonicated for 15 minutes and quickly transferred into the sonicated 2.0 mL sample loop *via* syringe. Finally, the reaction mixture was pumped through the illuminated reactor-coil at given flowrates and residence times.

The processed crude product was collected, diluted with brine (10 mL) and extracted with EtOAc (3 x 10 mL). The combined organic layers were dried with MgSO$_4$, filtered and the solvent was removed under reduced pressure. Evaporation of volatiles led to the crude product. Purification was performed by flash-column chromatography (PE/acetone) yielding the corresponding pure product **3p**.

1.8.4   TEMPO Trapping of Radical Reaction Intermediates

A 5 mL crimp cap vial was equipped with solid *NH*-sulfoximine **1a** (21.7 mg, 0.10 mmol, 1.0 equiv.), 9-mesityl-10-methylacridinium perchlorate (**A**) (8.2 mg, 0.02 mmol, 20 mol%), Co(dmgH)$_2$PyCl (**D**) (4.0 mg, 0.01 mmol, 10 mol%), TEMPO (15.6 mg, 0.1 mmol, 1 equiv.) and a magnetic stirring bar and was capped with a septum. Nitrogen atmosphere was introduced *via* three cycles vacuum/nitrogen (2 min at 7 mbar/2 min nitrogen atmosphere). Degassed MeCN (0.1 M, 1 mL) and **2a** (123.23 µL, 1.00 mmol, 10 equiv.) were added *via* syringe under nitrogen atmosphere. The reaction mixture was stirred and irradiated using a blue LED (455 nm) for 20 hours at 25 °C under nitrogen atmosphere. After irradiation the reaction mixture was submitted to mass spectrometry (LC-MS) without further work-up.
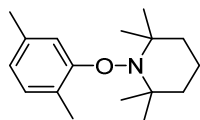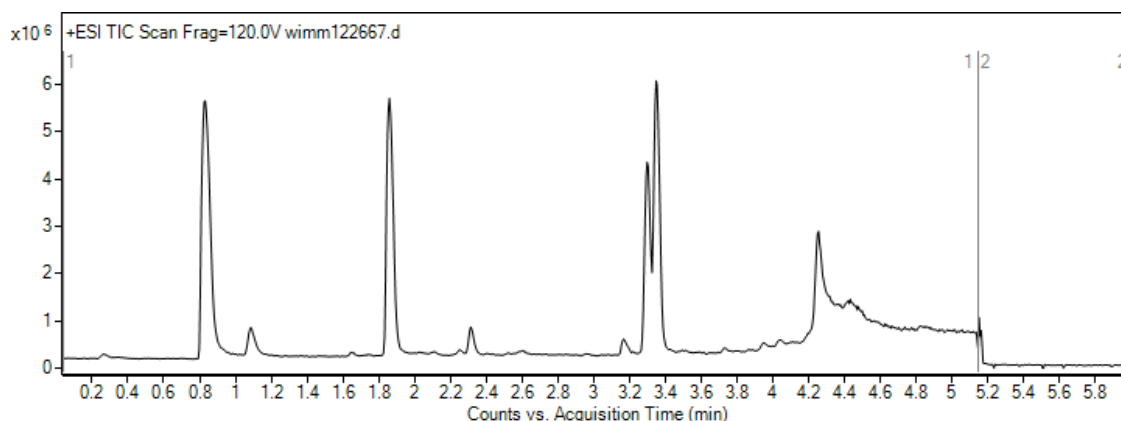
MS (ESI) (m/z): [M + H]$^+$ (C$_{17}$H$_{27}$NO) calc.: 262.2165, found: 262.2175.
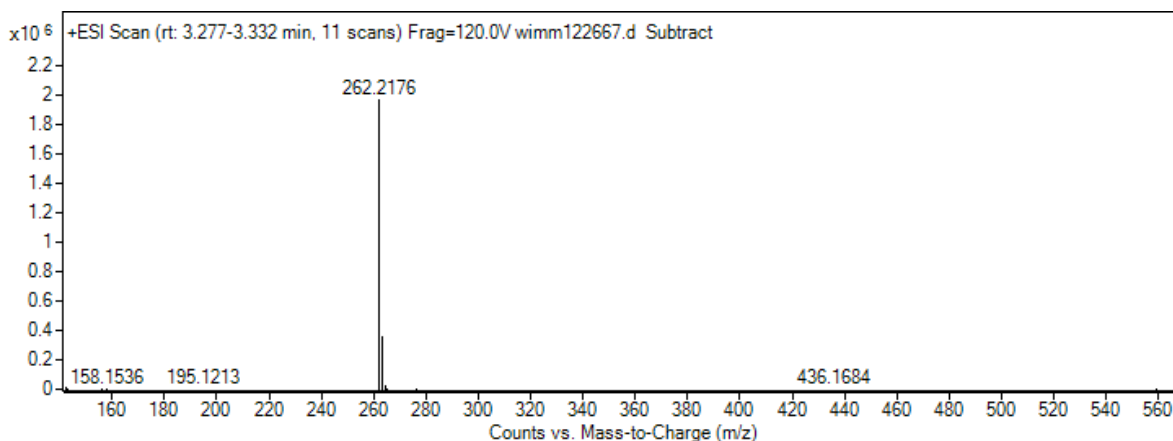
1.8.5 Cyclic Voltammetry Measurements

As the *NH*-sulfoximines did react with ferrocene at high oxidation potentials the measurement was carried out as following: First, the potential of the pure *NH*-sulfoximine was measured. After returning to 0 V, ferrocene was added to the solution and only the region of the ferrocene oxidation and reduction was measured.
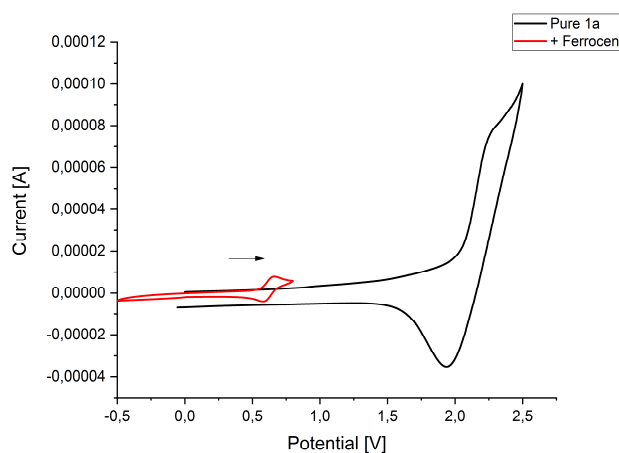
Figure 9. Representative cyclic voltammogram of **1a** in MeCN (scan direction is indicated by black arrow). The irreversible peak at +2.24 V is the oxidation of **1a**, which corresponds to an oxidation potential of +2.00 V vs. SCE.

Table 5. Oxidation potentials of *NH*-sulfoximines measured by cyclic voltammetry.

Entry	Substrate	E_{Ox} [V vs. SCE]
1	**1a**	+2.00
2	**1l**	+1.92
3	**1r**	+1.82
4	**1aa**	+1.97

1.8.6 Spectroscopic Investigation of the Mechanism

1.8.6.1 UV/Vis Spectroscopy
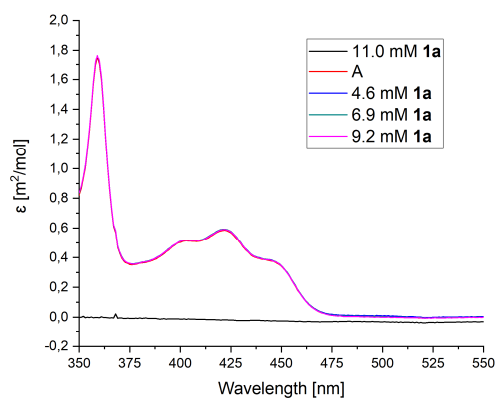
Figure 10. UV/Vis absorption spectra of *NH*-sulfoximine **1a** (11 mM in MeCN), **A** (50 µM in MeCN) and upon titration with **1a**.

1.8.7 NMR Spectra

All NMR spectra can be found in the appendix in the section 6.2.1.

1.8.8 References

[1]   R. K. Harris, E. D. Becker, S. M. Cabral de Menezes, R. Goodfellow, P. Granger, Magn. Reson. Chem., 2002, 40, 489-505.

[2]   a) H. E. Gottlieb, V. Kotlyar, A. Nudelman, J. Org. Chem., 1997, 62, 7512-7515; b) G. R. Fulmer, A. J. M. Miller, N. H. Sherden, H. E. Gottlieb, A. Nudelman, B. M. Stoltz, J. E. Bercaw, K. I. Goldberg, Organometallics, 2010, 29, 2176-2179.

[3]   a) A. Tota, M. Zenzola, S. J. Chawner, S. S. John-Campbell, C. Carlucci, G. Romanazzi, L. Degennaro, J. A. Bull, R. Luisi, Chemical Communications, 2017, 53, 348-351; b) J. Wang, J. Zhang, K. Miao, H. Yun, H. C. Shen, W. Zhao, C. Liang, Tetrahedron Lett., 2017, 58, 333-337; c) J.-F. Lohier, T. Glachet, H. Marzag, A.-C. Gaumont, V. Reboul, Chem. Commun., 2017, 53, 2064-2067.

[4]   M. Zenzola, R. Doran, L. Degennaro, R. Luisi, J. A. Bull, Angew. Chem. Int. Ed., 2016, 55, 7203-7207.

[5]   A. U. Meyer, A. Wimmer, B. König, Angew. Chem. Int. Ed., 2017, 56, 409-412.

2. *N*-Arylation of *NH*-Sulfoximines *via* dual Nickel Photocatalysis
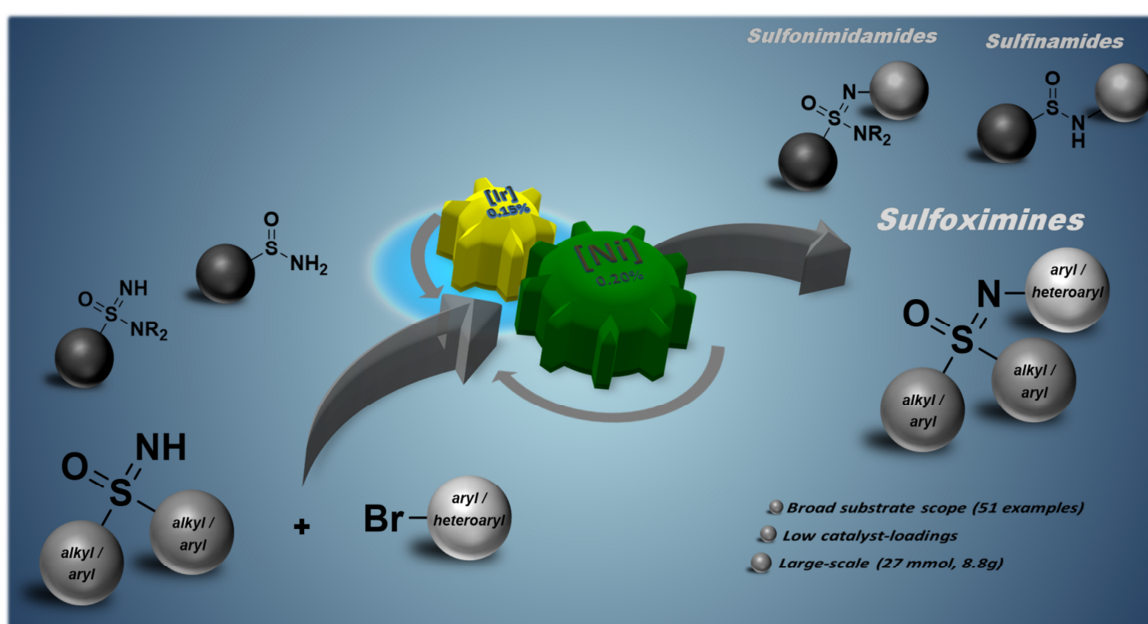
CHAPTER 2

2.1 Abstract

The pharmaceutically underexplored sulfoximine-moiety emerges as potential active pharmaceutical ingredient. We developed a scalable synthetic route to *N*-arylated sulfoximines from the respective "free" *NH*-sulfoximines and bromo arenes. Our strategy is based on a dual nickel photocatalytic approach, is applicable for a broad scope of substrates and exhibits a high functional group tolerance. In addition, we could demonstrate that other sulfoximidoyl derivatives like sulfonimidamides and sulfinamides proceed smoothly under the developed reaction conditions.

This Chapter has been published in:

A. Wimmer, B. König, *Org. Lett.* **2019**, *21*, 2740–2744.

Reprinted (adapted) with permission from A. Wimmer, B. König, *Org. Lett.* **2019**, *21*, 2740–2744. Copyright 2019 American Chemical Society.

https://pubs.acs.org/doi/10.1021/acs.orglett.9b00698

Author contributions:

AW developed the reaction, carried out the experiments and wrote the manuscript. BK supervised the project and is the corresponding author.

2.2   Introduction

Most organic chemists consider sulfoximines mainly as chiral auxiliaries or ligands, being applied in asymmetric reactions or catalysis.[1] However, recently sulfoximines emerged as potential active pharmaceutical ingredients (APIs) in medicinal and agricultural research.[2] Although their bioactivity is already long known, their exploration as APIs was scarce. Recently, it was found that the sulfoximines' mode of binding to biological receptors can be very different compared to established ligands. For example, the sulfoximine-based insecticide Sulfoxaflor is capable of by-passing many cross-resistances of pest species, because of its differing mechanism of binding.[3] Discoveries as such call for efficient synthetic routes to sulfoximines. Especially *N*-arylated sulfoximines are of interest for medicinal chemists, as they could serve as potent drug analogues.[4]

A) Transition-metal catalyzed *N*-arylation of *NH*-sulfoximines

R = aryl, alkyl
LG = Hal, OTf, $OS(O)_2(CF_2)_3CF_3$, OTs, $B(OH)_2$, IAr,
    $Si(OR)_3$, SO_2Na, $C(O)O_2C(O)Ar$

- High catalyst-loadings
- Elevated temperatures
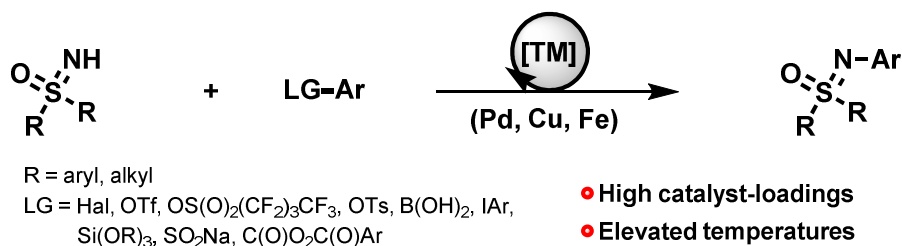
B) *This Work:*
Dual nickel photo-catalyzed *N*-arylation of *NH*-sulfoximines

R = (hetero)aryl, alkyl
X = C, N, O or S

- Low catalyst-loading: 0.15 mol% [Ir] & 0.20 mol% [Ni]
- 51 Examples, up to 99% yield
- Preparative scale: 8.8g
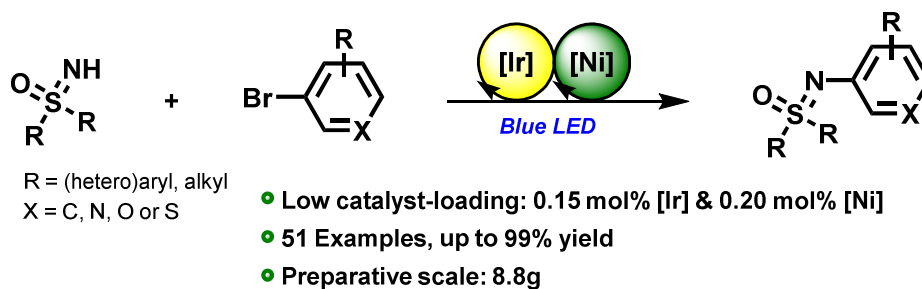
Scheme 6. A) Classic transition-metal catalyzed *N*-arylations of *NH*-sulfoximines. B) Dual nickel photo-catalyzed approach.

Various Pd-, Cu- or Fe-catalyzed *N*-arylations of *NH*-sulfoximines with different types of electrophiles were developed by Bolm, Harmata and others since the late 1990s (Scheme 6, A)).[1i, 1n, 5] However, demanding reaction conditions such as high catalyst-loadings, specialized ligands, elevated reaction temperatures and long reaction times often limit the practicability or the scope of substrates. This set of limitations already indicates that *NH*-sulfoximines often behave as a rather special and challenging class of *N*-nucleophiles for transition-metal catalyzed *N*-arylations.

In particular, the coupling of pharmaceutically relevant heteroaromatic scaffolds to *NH*-sulfoximines is rather unexplored. Consequently, there is still a great demand for general, mild and efficient synthetic solutions towards *N*-functionalized aliphatic, aromatic and heteroaromatic sulfoximines. Very recently, we reported the first photocatalytic approach for the *N*-arylation of *NH*-sulfoximines.[6] At the same time, Meier at al. published a similar method, showing that the mildness of the photocatalytic reaction also allows late-stage sulfoximination of complex molecules in the industrial context.[7]

Stimulated by the continuous interest on sulfoximines we wondered whether the *N*-arylation of *NH*-sulfoximines could be realized by the combination of classic transition-metal catalysis with visible-light photocatalysis (metallaphotocatalysis) (Scheme 6, B)). Dual nickel photocatalysis has emerged as a powerful strategy and a remarkably efficient tool for organic cross-coupling reactions in the last years.[8] Exemplary, *N*-arylation was reported for anilines, aliphatic amines and also sulfonamides.[9] We considered that *NH*-sulfoximines might be suitable substrates for such a strategy keeping in mind that a practicable synthetic method should work not only on milligram lab-scale, but also on preparative multi-gram scale.

2.3 Results and Discussion

2.3.1 Optimization of the Reaction Conditions

We started our investigations using similar reaction conditions as reported by MacMillan et al..[9c] *NH*-sulfoximine **1a** (1.5 equiv.) and bromo arene **2a** (1.0 equiv.) as model substrates were reacted with 1.0 mol% **[Ir]-Cat** ([Ir(ppy)$_2$(dtbbpy)]PF$_6$) as photocatalyst, 5.0 mol% **[Ni-1]-Cat** (NiBr$_2$ and dtbbpy as ligand (1.0 : 0.2 equiv.) added separately) and TMG (1,1,3,3-tetramethylguanidine, 1.5 equiv.) as base in dry and degassed DMSO (0.25 M, 1.0 mL) under nitrogen atmosphere. Irradiation with blue light of 455 nm for 3 hours at 25 °C yielded the desired *N*-arylated sulfoximine **3a** in an excellent yield of 94% (Table 6, entry 1).[10]

Table 6. Optimization of the reaction conditions.[a)]

Entry	1a : 2a (equiv.)	[Ir]-Cat [mol%]	[Ni]-Cat [mol%]	TMG (equiv.)	Yield[b)] [%]
1	1.5 : 1.0	1.0	5.0 **[Ni-1]-Cat**	1.5	94
2	1.5 : 1.0	0.15	5.0 **[Ni-1]-Cat**	1.5	96
3	1.5 : 1.0	0.15	1.0 **[Ni-1]-Cat**	1.5	95
4	1.5 : 1.0	0.15	0.2 **[Ni-2]-Cat**	1.5	76
5	1.0 : 1.1	0.15	0.2 **[Ni-2]-Cat**	1.5	99
6	1.0 : 1.1	0.15	0.2 **[Ni-2]-Cat**	1.2	99
7	1.0 : 1.1	0.15	0.2 **[Ni-2]-Cat**	1.2	99[c)]

[Ir]-Cat = [Ir(ppy)$_2$(dtbbpy)]PF$_6$, **[Ni-1]-Cat** = NiBr$_2$ + dtbbpy (1.0 : 0.20 equiv.) added separately, **[Ni-2]-Cat** = pre-formed [Ni(dtbbpy)]Br$_2$, TMG = 1,1,3,3-tetramethylguanidine, [a]Reaction conditions: **1a** (0.25 mmol, 1.0 equiv.), **2a** (0.28 mmol, 1.1 equiv.), **[Ir]-Cat** (0.15mol%), **[Ni-2]-Cat** (0.20 mol%), TMG (0.30 mmol, 1.2 equiv.), dry and degassed DMSO (0.25 M, 1.0 mL), irradiation at 455 nm for 3 h. [b]Yields were determined by GC analysis with naphthalene as internal standard. [c]Reaction was up-concentrated to 0.75 M, run for 17 h and yield is reported after purification *via* automated flash-column chromatography.

Further optimization significantly decreased the amount of substrates and catalysts for the transformation. Only 0.15 mol% of **[Ir]-Cat** were found to be sufficient for the reaction (Table 6, entry 2) and by using already pre-formed **[Ni-2]-Cat**, its amount could be decreased to only 0.20 mol% (Table 6, entries 3 – 5).

Finally, the amount of *NH*-sulfoximine **1a**, bromo arene **2a** and TMG could be optimized, reaching an atom-economic ratio of 1.0 : 1.1 : 1.2 equivalents, respectively (Table 6, entries 5 and 6). In addition, we found, that the overall substrate concentration could be increased from 0.25 M to 0.75 M.

Further studies revealed that also other common organic solvents like MeCN, DMF, DMAc or THF can be used without any decrease in yield and quinuclidine, DABCO or KOAc could be used as alternative bases, affording moderate yields (see section 2.7.2, Table 7 – Table 9).

Interestingly, a moderate yield of the product was obtained in the absence of photocatalyst when light of 390nm was used for irradiation.[11] This results indicates, that the reaction might proceed *via* photosensitization processes (Scheme 7).[9c] Control experiments showed that photocatalyst, nickel catalyst, base and the irradiation with light are all crucial for the reaction (see section 2.7.2, Table 10).

2.3.2 Mechanistic Proposal

Our mechanistic proposal is based on reported literature for similar type of compounds (Scheme 7).[9c] A photo-sensitized reaction pathway is suggested, where the *N*-arylated sulfoximine is produced *via* the reductive elimination from an excited-state nickel species (**A3***). Although the photosensitization mechanism is underlined by the fact that the reaction can proceed in the absence of **[Ir]-Cat** *via* direct excitation with light of 390 nm, photo-electron-transfer processes between **[Ir]-Cat** and any nickel species cannot be ruled out.
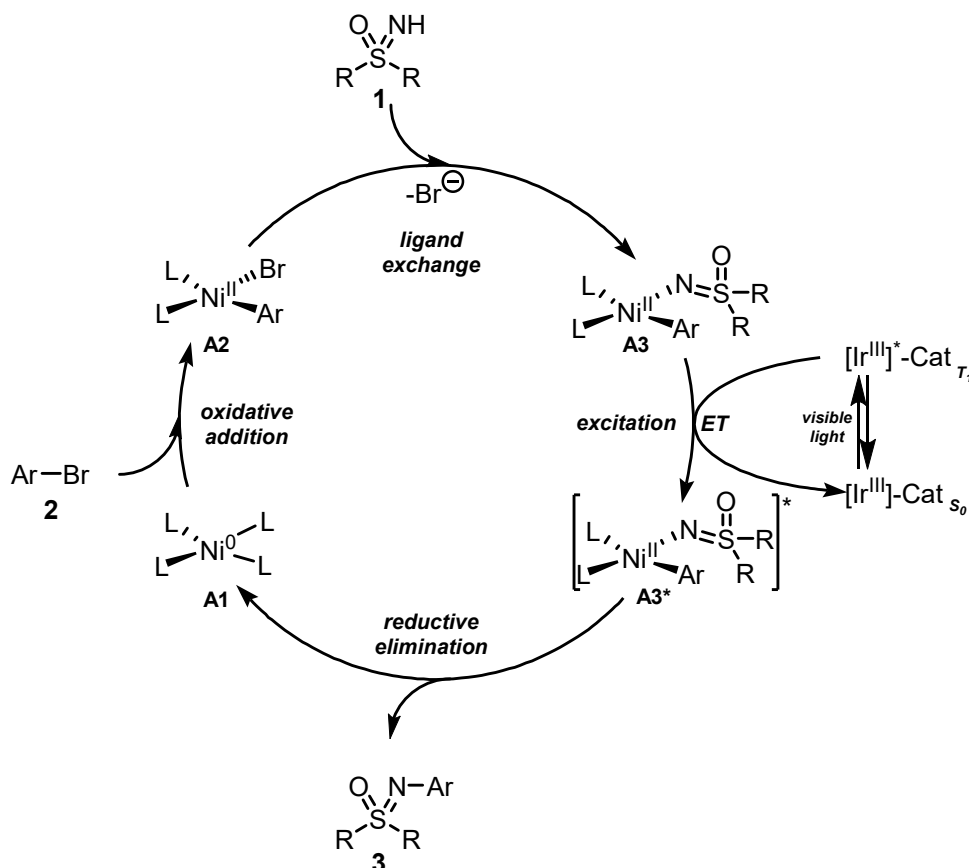
Scheme 7. Mechanistic proposal for the dual-catalytic *N*-arylation of *NH*-sulfoximines.

In a first step, oxidative addition of the nickel(0)-complex **A1** into the aryl bromide bond furnishes nickel(II)-species **A2**. *NH*-Sulfoximine **1** can act as ligand and substitutes the bromine, giving in nickel(II)-species **A3**. Upon excitation of the photosensitizer **[Ir^III]-Cat** to its excited-state, energy-transfer (ET) can occur between **[Ir(III)]*-Cat** and nickel(II)-species **A2**, resulting in excited-state nickel(II)-species **A3*** and the regenerated ground-state of the photosensitizer. Reductive elimination is facilitated from excited-state **A3*** and furnishes the desired *N*-arylated product **3** and nickel(0)-species **A1**.

2.3.3 Scope of the Reaction

With the optimized reaction conditions in hand (Table 6, entry 6), we started to explore the scope of the reaction. First, we focused on the scope of brominated arenes and hetero arenes (Figure 11 and Figure 12).

Both electron-rich and electron-deficient brominated arenes were reacting smoothly with *NH*-sulfoximine **1a**, giving the respective *N*-arylated sulfoximines **3a – 3r** in high to excellent yields (Figure 11). For this type of brominated substrates, we selected MeCN as solvent as it is easily removed under reduced pressure. Many functional groups, including thioethers (**3c**), cyanides (**3f**), ethers (**3h** and **3j**), amides (**3k**) or carbamates (**3r**), were tolerated under the reaction conditions, Interestingly, the reaction of 1,3-dibromobenzene stopped after onefold substitution, yielding mono-brominated **3l** as product. This observation could give the opportunity for further functionalizations in other cross-coupling reactions.

In particular, the compatibility of pharmaceutically relevant substrate classes like sulfoxides (**3m**) or sulfones (**3n**) and bioisosteric scaffolds like the -OCF_3 (**3o**), -SCF_3 (**3p**) or -SF_5 (**3q**) was investigated. Gratifyingly, all these moieties were found to be tolerated under the reaction conditions and afforded the respective sulfoximines in moderate to excellent yields. It has to be mentioned, that the lower yield of SF_5-containing sulfoximine **3q** is due to decomposition of the brominated arene during the reaction.

In addition, we conducted a large-scale version of the reaction in a custom-made reactor commonly used in our laboratories (see sections 2.7.1 and 2.7.4). The reaction was carried out on a 27 mmol scale, affording 8.8 grams (99%) of product, using only 37mg of **[Ir]-Cat** (0.15 mol%) and 26mg of **[Ni-2]-Cat** (0.20 mol%).[12]

Scope of brominated arenes:

3a: R = CF₃; 88%• [a]
Scale-up:
27 mmol; 8.8g; 99%

3b: R = *t*-Bu; 99%•
3c: R = SCH₃; 92%• [b]
3d: R = F; 99%• [b]
3e: R = Cl; 90%• [c]
3f: R = CN; 98%•

3g: R = CF₃; 96%• [b]
3h: R = OCH₃; 78%•

3i: R = H; 59%#
3j: R = OCH₃; 99%•
3k: R = NHCH₃; 95%•

3l: 66%• [d]

3m: 89%•, dr = 1:1

3n: 99%•

3o: 98%•

3p: 84%•

3q: 30%• [e]

3r: 98%• [b]
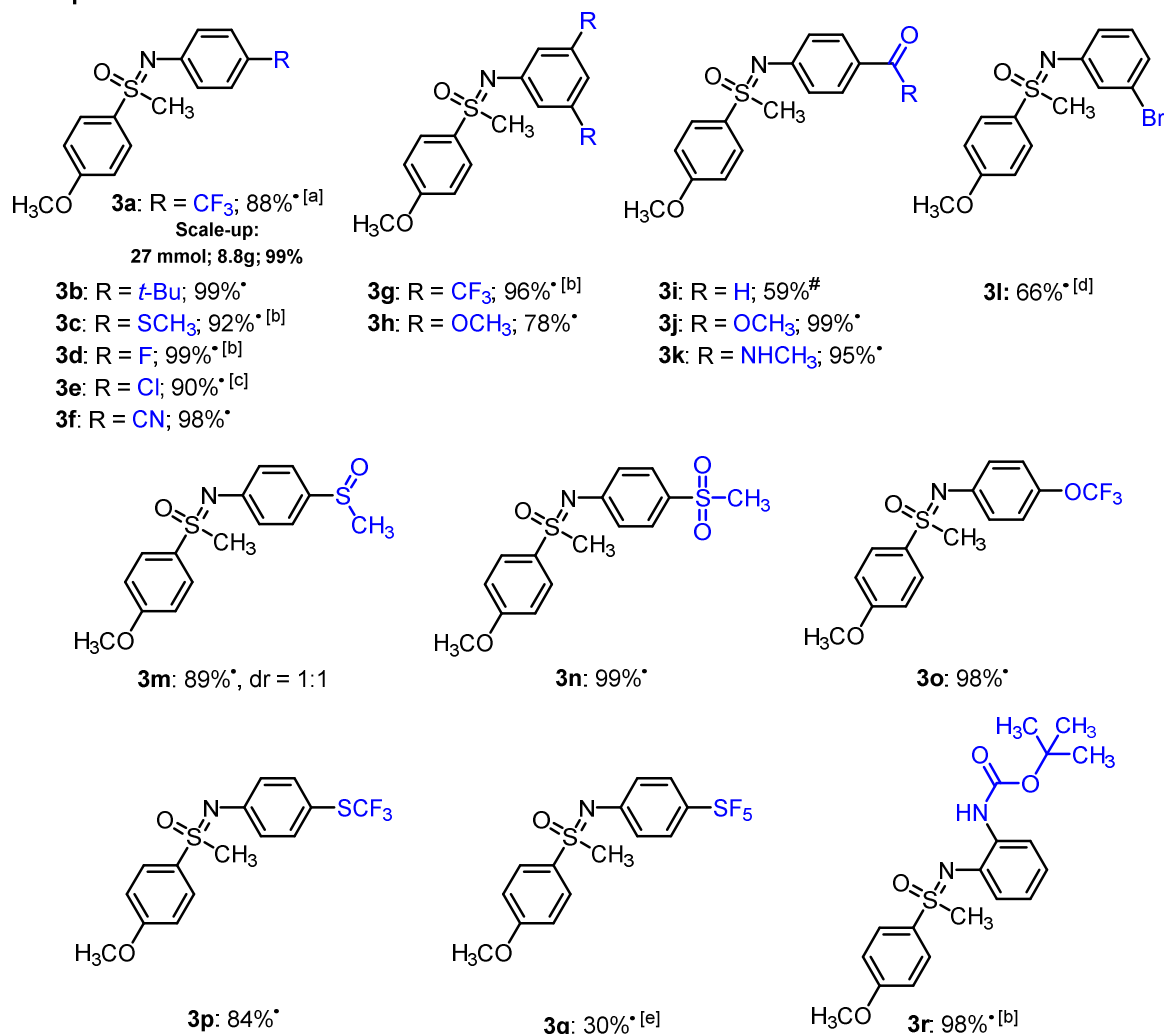
Figure 11. Substrate scope of bromo arenes. Reaction conditions: **1a** (0.25 mmol, 1.0 equiv.), bromo arene (**2**) (0.275 mmol, 1.1 equiv.), **[Ir]-Cat** (0.15 mol%), **[Ni-2]-Cat** (0.20 mol%), TMG (1.2 equiv.), dry and degassed MeCN (•) or DMA (#) (0.25 M), irradiation at 455 nm for 17 h. [a]3.5 h; 17 h for the large-scale reaction. [b]0.5 mol% **[Ir]-Cat**, 1.0 mol% **[Ni-2]-Cat**. [c]0.2 mol% **[Ir]-Cat**, 1.0 mol% **[Ni-2]-Cat**. [d]1,3-dibromo benzene (0.24 mmol, 1 equiv.) as limiting reagent. [e]0.5 mol% **[Ni-2]-Cat**.

The scope of brominated hetero arenes was explored with common hetero aromatic scaffolds, occurring in pharmaceutical agents or natural products (Figure 12). Introducing the sulfoximine moiety to established bioactive cores like indoles, pyridines, quinolines, pyrimidines, pyrazines, quinoxalines, benzofuranes, oxadiazoles or benzothiazoles might be of use for pharmaceutical or agricultural research.

Scope of brominated hetero arenes:
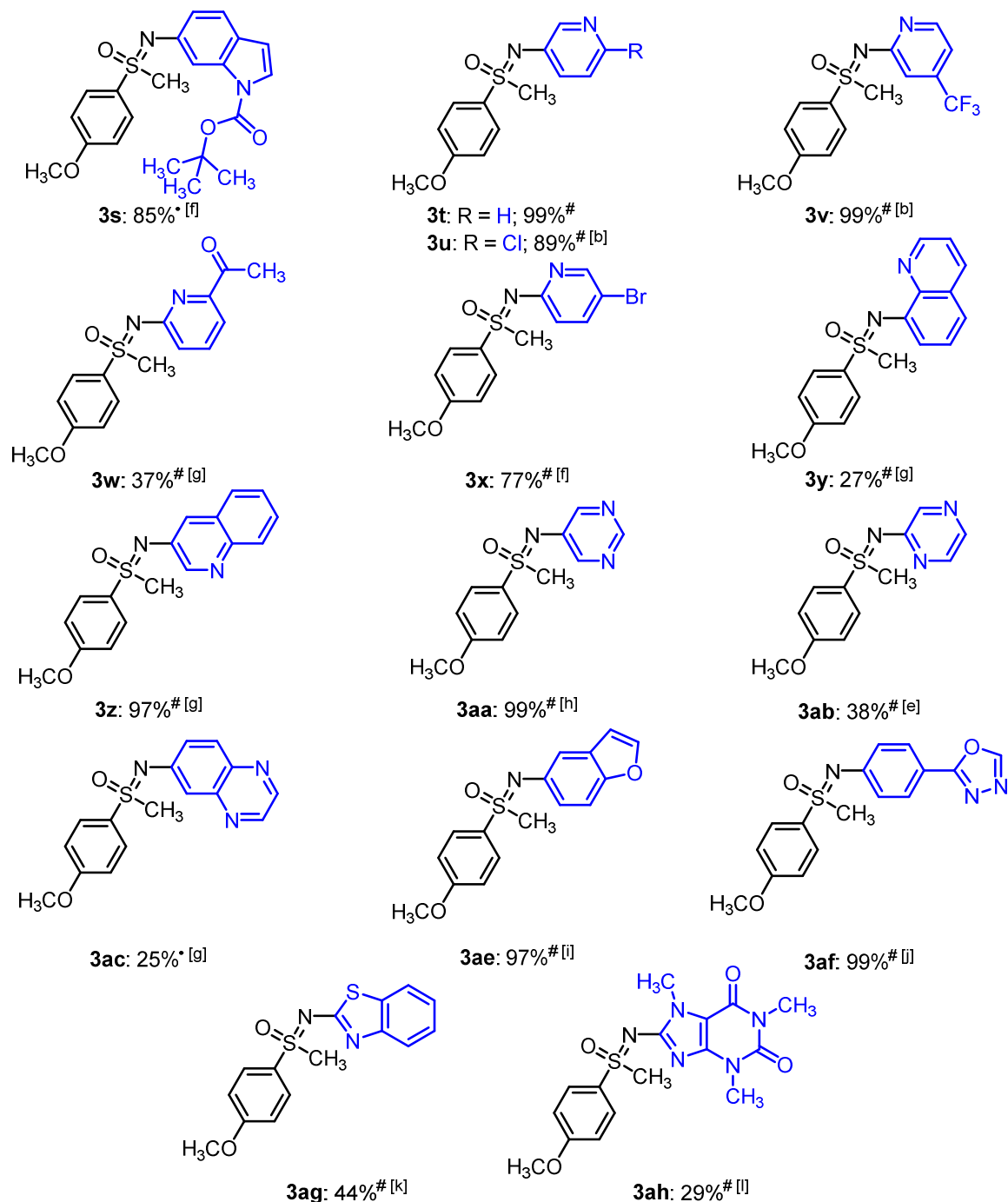
Figure 12. Substrate scope of brominated hetero arenes. Reaction conditions: **1a** (0.25 mmol, 1.0 equiv.), bromo arene (**2**) (0.275 mmol, 1.1 equiv.), **[Ir]-Cat** (0.15 mol%), **[Ni-2]-Cat** (0.20 mol%), TMG (1.2 equiv.), dry and degassed MeCN (*) or DMA (#) (0.25 M), irradiation at 455 nm for 17 h. [a]3.5 h; 17 h for the large-scale reaction. [b]0.5 mol% **[Ir]-Cat**, 1.0 mol% **[Ni-2]-Cat**. [c]0.2 mol% **[Ir]-Cat**, 1.0 mol% **[Ni-2]-Cat**. [d]1,3-dibromo benzene (0.24 mmol, 1 equiv.) as limiting reagent. [e]0.5 mol% **[Ni-2]-Cat**. [f]0.5 mol% **[Ir]-Cat**, 5.0 mol% **[Ni-2]-Cat**. [g]1.0 mol% **[Ir]-Cat**, 5.0 mol% **[Ni-2]-Cat**. [h]1.0 mol% **[Ni-2]-Cat**. [i]0.5 mol% **[Ir]-Cat**, 3.0 mol% **[Ni-2]-Cat**. [j]0.5 mol% **[Ir]-Cat**, 2.0 mol% **[Ni-2]-Cat**. [k]2.0 mol% **[Ni-2]-Cat**. [l]0.15 mol% **[Ir]-Cat**, 2.0 mol% **[Ni-2]-Cat**, 0.04 M.

66

All of the applied brominated substrates could be coupled with *NH*-sulfoximine **1a**, affording yields up to of 99%.[13] However, it has to be noted that these scaffolds showed lower reactivity in the *N*-arylation reaction, compared to brominated benzene derivatives. Nevertheless, when the conversion to the respective products was incomplete after 17 hours and starting substrates were remaining, careful adjustments of the loading of catalysts had beneficial effects on the yield of the reactions.[14]

Brominated *N*-Boc-protected indole did react smoothly under the reaction conditions, affording the desired product **3s** in 90% yield. The reactions with differently substituted pyridines did generally lead to high product yields, except for acetylated pyridine, where decomposition of the brominated pyridine diminished the outcome of the reaction (**3w**). Similar to 1,3-dibromobenzene, the reaction with 2,4-dibromopyridine stopped after onefold substitution, affording the mono-brominated sulfoximine derivative **3x** in high yield. Brominated quinolines, pyrimidines, pyrazines and quinoxalines reacted well under the reaction conditions and afforded the respective *N*-arylated sulfoximines in moderate to excellent yields. Again excellent yields were obtained applying 5-bromobenzofuran (**3ae**, 97%) and 2-(4-bromophenyl)-1,3,4-oxadiazole (**3af**, 99%) and the reaction with 2-bromobenzothiazole afforded sulfoximine **3ag** in moderate yield of 44%. Furthermore, methylxanthine alkaloid caffeine was tested as substrate. The reaction of brominated caffeine afforded the respective *N*-arylated sulfoximine **3ah** in an isolated yield of 29%.

Next, we focused on the scope of different *NH*-sulfoximines and conducted the reactions using methyl 4-bromobenzoate (**2j**) as model substrate (Figure 13, **A)**). Electron-rich as well as electron-deficient alkyl and aryl substituted *NH*-sulfoximines were suitable for the *N*-arylation reaction and afforded good to excellent yields of the desired products. Cyclopropyl moieties (**3ai**), benzylic positions (**3ak**), and heterocyclic scaffolds (**3ap and 3aq**) were well tolerated and yielded the respective products in moderate to excellent yields.

To further demonstrate the practicability of our method we investigated, whether the chiral information of an enantiopure *NH*-sulfoximine is conserved throughout the reaction to yield the respective enantiopure *N*-arylated sulfoximine. This allows the rapid generation of enantiopure substrate-libraries. We investigated the reaction of an enantiopure *NH*-sulfoximine with various brominated arenes and heteroarenes (Figure 13, **B)**) and verified the optical purity of the products by chiral HPLC analysis. To our delight, the reaction of enantiopure *NH*-sulfoximine yielded the respective chiral cross-coupling products ((*S*)-**3at** – (*S*)-**3ax**) and no racemization was observed.[15]

Finally, we decided to also test other sulfoximidoyl derivatives under the *N*-arylation conditions, optimized for *NH*-sulfoximines (Figure 13, **C)**). NH_2-sulfinamide **4** was reacted with methyl 4-bromobenzoate (**2j**) and afforded the respective product **5** in an excellent yield of 93%. Furthermore, applying *NH*-sulfonimidamide **6** yielded the respective *N*-arylated sulfonimidamide **7** in a yield of 96%.

A) Scope of *NH*-sulfoximines:

3ai: R = cyclopropyl; 98%·
3aj: R = C$_6$H$_5$; 97%·
3ak: R = CH$_2$C$_6$H$_5$; 88%·

3al: R = CH$_3$; 99%·
3am: R = F; 99%·
3an: R = Cl; 99%·
3ao: R = CN; 91%·

3ap: 61%·

3aq: 47%# [a]

3ar: 99%·

3as: 96%·
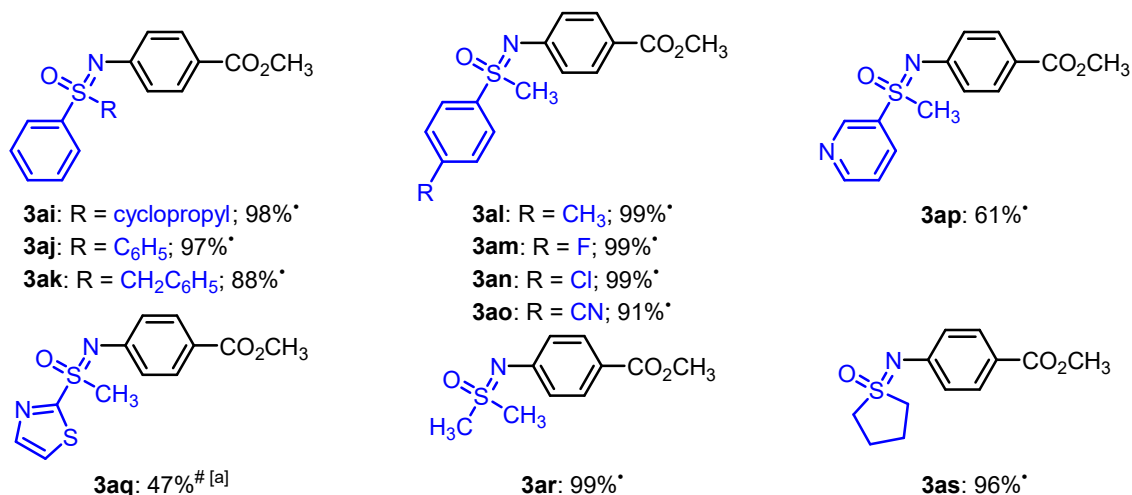
B) Scope of chiral sulfoximines:

(*S*)-3at: 80%·

(*S*)-3au: 77%# [b]

(*S*)-3av: 99%# [c]

(*S*)-3aw: 57%# [a]

(*S*)-3ax: 99%# [d]

C) Scope of other sulfoximidoyl derivatives:

4 → *Sulfinamides* → **5**: 93%· [d]

6 → *Sulfonimidamides* → **7**: 96%· [a]
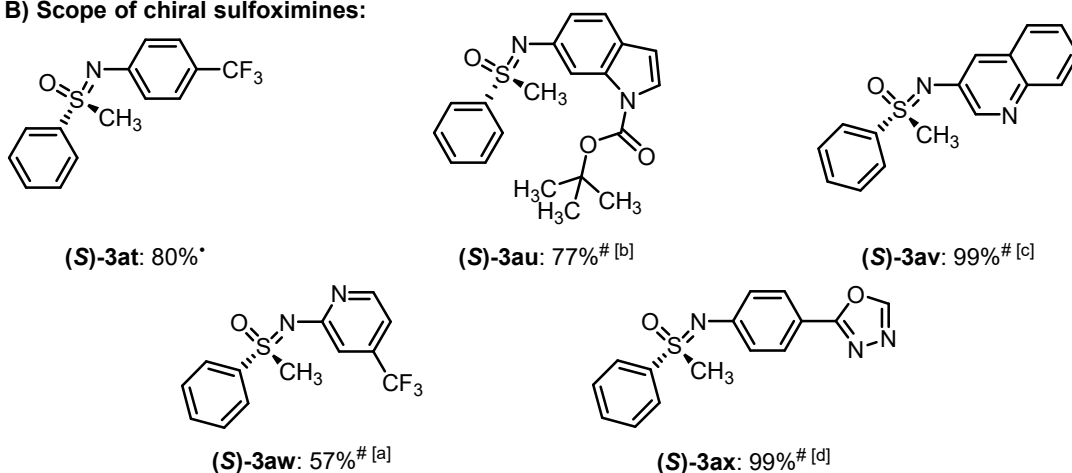
Figure 13. A) Scope of *NH*-sulfoximines. **B)** Scope of enantiopure substrates. **C)** Scope of other sulfoximidoyl derivatives. Reaction conditions: *NH*-sulfoximine (**1**) (0.25 mmol, 1.0 equiv.), methyl 4-bromobenzoate (**2j**) (0.275 mmol, 1.1 equiv.), **[Ir]-Cat** (0.15 mol%), **[Ni-2]-Cat** (0.20 mol%), TMG (1.2 equiv.), dry and degassed MeCN (·) or DMA (#) (0.25 M), irradiation at 455 nm for 17 h. [a]0.5 mol% **[Ir]-Cat**, 1.0 mol% **[Ni-2]-Cat**. [b]0.5 mol% **[Ir]-Cat**, 5.0 mol% **[Ni-2]-Cat**. [c]1.0 mol% **[Ir]-Cat**, 5.0 mol% **[Ni-2]-Cat**. [d]0.5 mol% **[Ir]-Cat**, 2.0 mol% **[Ni-2]-Cat**.

2.4   Conclusion

In conclusion, we demonstrated that *NH*-sulfoximines can be *N*-arylated with brominated arenes and hetero arenes as coupling partners, by using a dual nickel photo-catalyzed strategy. For the conversion of most of the benzene-based *NH*-sulfoximines and brominated arenes, catalyst loadings of only 0.15 mol% **[Ir]-Cat** and 0.20 mol% **[Ni-2]-Cat** were sufficient and afforded up to 99% yield of the desired products. In addition, by careful adjustment of the catalyst loadings a diverse range of hetero aromatic substrates could be applied, including a series of relevant scaffolds occurring in natural products and bioactive compounds. Additionally, the reaction was carried out on a preparative scale of 27 mmol (8.8g product) without any decrease in yield. Furthermore, it was shown that enantiopure products can be obtained by using enantiopure *NH*-sulfoximines as starting materials. Finally, we demonstrated that the same reaction conditions are suitable for structurally related sulfoximidoyl derivatives, like *NH$_2$*-sulfinamides and *NH*-sulfonimidamides. The method extends the synthetic toolbox for the synthesis of sulfoximidoyl derivatives and applications in the development of molecules for use in pharmaceutical industry or crop protection can be readily envisaged.

2.5   Acknowledgements

2.6 References

[1]   a) S. Otocka, M. Kwiatkowska, L. Madalinska, P. Kielbasinski, Chem. Rev., 2017, 117, 4147-4181; b) X. Shen, Q. Liu, W. Zhang, J. Hu, Eur. J. Org. Chem., 2016, 906-909; c) X. Shen, W. Miao, C. Ni, J. Hu, Angew. Chem. Int. Ed., 2014, 53, 775-779; d) D. Craig, F. Grellepois, A. J. White, J. Org. Chem., 2005, 70, 6827-6832; e) M. Langner, P. Remy, C. Bolm, Chem. Eur. J., 2005, 11, 6254-6265; f) M. T. Reetz, O. G. Bondarev, H. J. Gais, C. Bolm, Tetrahedron Lett., 2005, 46, 5643-5646; g) H. J. Gais, G. S. Babu, M. Gunter, P. Das, Eur. J. Org. Chem., 2004, 2004, 1464-1473; h) M. Langner, C. Bolm, Angew. Chem. Int. Ed., 2004, 43, 5984-5987; i) M. Harmata, X. Hong, J. Am. Chem. Soc., 2003, 125, 5754-5756; j) S. Koep, H. J. Gais, G. Raabe, J. Am. Chem. Soc., 2003, 125, 13243-13251; k) C. Bolm, M. Martin, O. Simic, M. Verrucci, Org. Lett., 2003, 5, 427-429; l) C. Bolm, M. Verrucci, O. Simic, P. G. Cozzi, G. Raabe, H. Okamura, Chem. Commun., 2003, 2826-2827; m) C. Bolm, O. Simić, J. Am. Chem. Soc., 2001, 123, 3830-3831; n) M. Harmata, S. K. Ghosh, Org. Lett., 2001, 3, 3321-3323; o) M. Reggelin, C. Zur, Synthesis, 2000, 1-64; p) C. Bolm, M. Felder, J. Müller, Synlett, 1992, 439-441; q) C. R. Johnson, Acc. Chem. Res., 1973, 6, 341-347.

[2]   U. Lucking, Angew. Chem. Int. Ed., 2013, 52, 9399-9408.

[3]   a) J. M. Babcock, C. B. Gerwick, J. X. Huang, M. R. Loso, G. Nakamura, S. P. Nolting, R. B. Rogers, T. C. Sparks, J. Thomas, G. B. Watson, Y. Zhu, Pest Management Science, 2011, 67, 328-334; b) Y. Zhu, M. R. Loso, G. B. Watson, T. C. Sparks, R. B. Rogers, J. X. Huang, B. C. Gerwick, J. M. Babcock, D. Kelley, V. B. Hegde, B. M. Nugent, J. M. Renga, I. Denholm, K. Gorman, G. J. DeBoer, J. Hasler, T. Meade, J. D. Thomas, J. Agric. Food. Chem., 2011, 59, 2950-2957; c) L. Bacci, S. Convertini, B. Rossaro, Journal of Entomological and Acarological Research, 2018, 50, 51 - 71.

[4]   a) M. Frings, C. Bolm, A. Blum, C. Gnamm, Eur. J. Med. Chem., 2017, 126, 225-245; b) J. A. Sirvent, U. Lucking, ChemMedChem, 2017, 12, 487-501.

[5]   a) C. Bolm, J. P. Hildebrand, Tetrahedron Lett., 1998, 39, 5731-5734; b) M. Harmata, N. Pavri, Angew. Chem. Int. Ed., 1999, 38, 2419-2421; c) C. Bolm, J. P. Hildebrand, J. Org. Chem., 2000, 65, 169-175; d) C. Bolm, J. P. Hildebrand, J. Rudolph, Synthesis, 2000, 911-913; e) C. Bolm, M. Martin, L. Gibson, Synlett, 2002, 832-834; f) M. Harmata, X. Hong, S. K. Ghosh, Tetrahedron Lett., 2004, 45, 5233-5236; g) N. Yongpruksa, N. L. Calkins, M. Harmata, Chem. Commun., 2011, 47, 7665-7667; h) H. Zhou, W. Chen, Z. Chen, Org. Lett., 2018, 20, 2590-2594; i) Q. Yang, P. Y. Choy, Q. Zhao, M. P. Leung, H. S. Chan, C. M. So, W.-T. Wong, F. Y. Kwong, J. Org. Chem., 2018, 83, 11369-11376; j) G. Y. Cho, P. Remy, J. Jansson, C. Moessner, C. Bolm, Org. Lett., 2004, 6, 3293-3296; k) J. Sedelmeier, C. Bolm, J. Org. Chem., 2005, 70, 6904-6906; l) A. Correa, C. Bolm, Adv. Synth. Catal., 2007, 349, 2673-2676; m) Y. Macé, B. Pégot, R. Guillot, C. Bournaud, M. Toffano, G. Vo-Thanh, E. Magnier, Tetrahedron, 2011, 67, 7575-7580; n) Z. J. Liu, J. P. Vors, E. R. F. Gesing, C. Bolm, Green Chem., 2011, 13, 42-45; o) C. Moessner, C. Bolm, Org. Lett., 2005, 7, 2667-

2669; p) B. Vaddula, J. Leazer, R. S. Varma, Adv. Synth. Catal., 2012, 354, 986-990; q) J. Kim, J. Ok, S. Kim, W. Choi, P. H. Lee, Org. Lett., 2014, 16, 4602-4605; r) H. Zhu, F. Teng, C. Pan, J. Cheng, J.-T. Yu, Tetrahedron Lett., 2016, 57, 2372-2374; s) Y. Jiang, Y. You, W. Dong, Z. Peng, Y. Zhang, D. An, J. Org. Chem., 2017, 82, 5810-5818; t) A. Correa, C. Bolm, Adv. Synth. Catal., 2008, 350, 391-394.

[6]   A. Wimmer, B. König, Adv. Synth. Catal., 2018, 360, 3277-3285.

[7]   H. Lämmermann, A. Sudau, D. Rackl, H. Weinmann, K. Collins, L. Wortmann, L. Candish, D. T. Hog, R. Meier, Synlett, 2018, 29, 2679-2684.

[8]   a) J. Twilton, C. Le, P. Zhang, M. H. Shaw, R. W. Evans, D. W. C. MacMillan, Nature Reviews Chemistry, 2017, 1, 0052; b) J. A. Terrett, J. D. Cuthbertson, V. W. Shurtleff, D. W. C. MacMillan, Nature, 2015, 524, 330-334; c) J. C. Tellis, D. N. Primer, G. A. Molander, Science, 2014, 345, 433-436; d) Z. Zuo, D. T. Ahneman, L. Chu, J. A. Terrett, A. G. Doyle, D. W. C. MacMillan, Science, 2014, 345, 437-440.

[9]   a) M. S. Oderinde, N. H. Jones, A. Juneau, M. Frenette, B. Aquila, S. Tentarelli, D. W. Robbins, J. W. Johannes, Angew. Chem. Int. Ed., 2016, 55, 13219-13223; b) E. B. Corcoran, M. T. Pirnot, S. Lin, S. D. Dreher, D. A. DiRocco, I. W. Davies, S. L. Buchwald, D. W. C. MacMillan, Science, 2016, 353, 279-283; c) T. Kim, S. J. McCarver, C. Lee, D. W. C. MacMillan, Angew. Chem. Int. Ed., 2018, 57, 3488-3492.

[10]   A comprehensive version of the optimization of the reaction conditions and all the control reactions is displayed in the experimental section.

[11]   For further experimental details see experimental section.

[12]   For further experimental details see experimental section.

[13]   Due to higher solubility of the brominated heteroarenes, mainly DMAc was used as solvent in this part of the substrate scope.

[14]   The amounts of [Ir]-Cat and [Ni-2]-Cat used in these cases vary between 0.15 − 1.0 mol% and 0.20 − 5.0 mol%, respectively, and are displayed for every single substrate in the table's description below the table.

[15]   For further experimental details see experimental section.

2.7 Experimental Part

2.7.1 Materials and Methods

Starting materials and reagents were purchased from commercial suppliers (Sigma Aldrich, Alfa Aesar, Acros, Fluka or TCI) and were used without further purification. Unless otherwise stated, all reactions were performed in dried and degassed solvents. Solvents were dried over molecular sieve (3Å or 4Å) and degassed by bubbling nitrogen for 15 minutes before used. Unless otherwise stated, yields are generally isolated amounts of products, obtained after automated flash-column chromatography on flash-silica gel, using HPLC-grade petrolether or hexane and ethylacetate as eluents. All reactions with oxygen- or moisture-sensitive reagents were carried out in glassware, which was dried before use by heating under vacuum. Dry nitrogen was used as inert gas. Liquid reagents and solvents were transferred *via* syringe, needle and septum technique. All NMR spectra were measured at room temperature, using a Bruker Avance 300 (300 MHz for ^{1}H, 75 MHz for ^{13}C and 282 MHz for ^{19}F) or a Bruker Avance 400 (400 MHz for ^{1}H, 101 MHz for ^{13}C and 376 MHz for ^{19}F) NMR spectrometer. All chemical shifts are reported in δ-scale as parts per million [ppm] (multiplicity, coupling constants *J*, number of protons) relative to the solvent residual peaks as the internal standard.[1] Coupling constants *J* are given in Hertz [Hz]. Abbreviations used for signal multiplicity: ^{1}H-, ^{13}C-NMR: b = broad, s = singlet, d = doublet, t = triplet, q = quartet, quint. = quintet, sept. = septet, dd = doublet of doublets, dt = doublet of triplets, dq = doublet of quartets, and m = multiplet. ^{13}C NMR: (+) = primary/tertiary, (-) = secondary, (C_q) = quaternary. The mass spectrometrical measurements were performed at the Central Analytical Laboratory of the University of Regensburg. All mass spectra were recorded on a Finnigan MAT 95, ThermoQuest Finnigan TSQ 7000, Finnigan MAT SSQ 710 A or an Agilent Q-TOF 6540 UHD instrument. GC measurements were performed on a GC 7890 from Agilent Technologies. Data acquisition and evaluation was done with Agilent ChemStation Rev.C.01.04.. GC measurements were made and analyzed *via* integration of the signal obtained with respect to the calibration with a suitable internal standard. Analytical TLC was performed on silica gel coated alumina. Visualization was done by UV light (254 or 366 nm). If necessary, potassium permanganate was used for chemical staining. Enantiomeric purity was determined by NP chiral HPLC (Varian 920-LC) analysis with either Daicel Chiralpak AS-H (5 μm, 4.6 x 250 mm) or Phenomenex Lux Cellulose-1 (5 μm, 4.6 x 250 mm) columns, using *n*-heptane and *iso*-propanol as eluents. Melting points were determined of purified solid products, using a MPA100 OptiMelt – automated melting point

system – from SRS: Starting operating temperature: 50 °C; Ending operating temperature: 300 °C; Heating gradient: 1 °C/min. The standard photochemical setup for experiments in regular scale consists of 455 nm LEDs (OSRAM Oslon SSL 80 royal-blue, 455 nm (±15 nm), radiant power 500 mW, 2.9 V, 350 mA) which illuminate from the bottom and a custom made aluminum cooling block connected to a thermostat which cools from the side (Figure 14). Large-scale reactions were performed in a self-designed batch-reactor which consists of the following three compartments: **1** A round-bottomed glass cylinder as vessel for the reaction mixture. **2** A second, slightly smaller glass cylinder with connection to cooling water, in order to cool the reaction mixture. By connecting the two glass cylinders a thin film of the reaction mixture is created and facilitates both, illumination and cooling of the reaction mixture. **3** 455 nm LEDs (OSRAM Oslon SSL 80 royal-blue, 455 nm (±15 nm), 500 mW, 2.9 V, 350 mA), generating a total radiant power of 12 W, are placed on the inside of a custom made aluminum cooling-block which surrounds the reaction vessel (Figure 15).
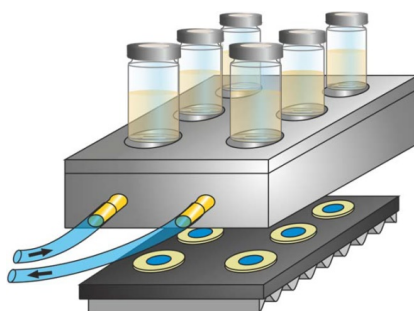

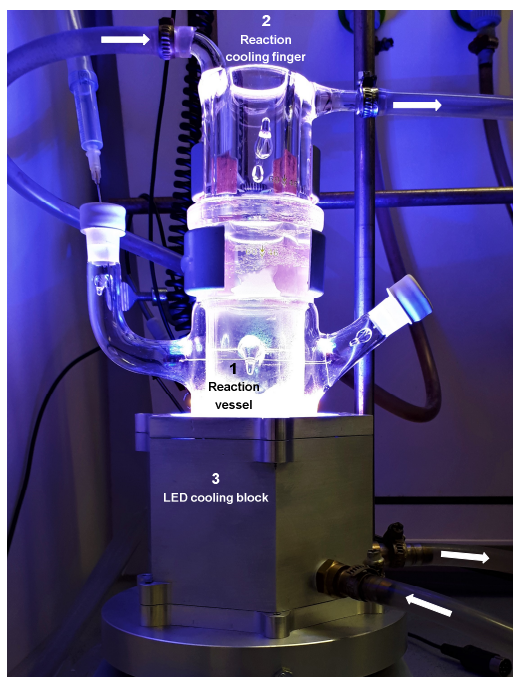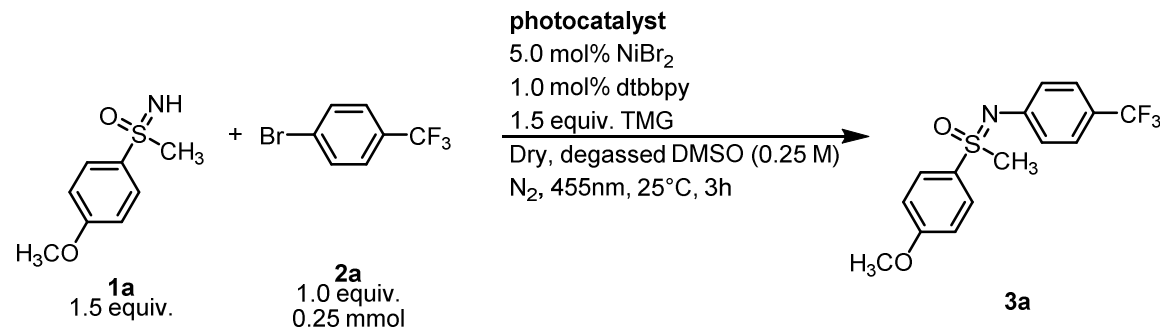**Figure 14.** Standard photochemical setup for small-scale reactions.

Figure 15. Custom-built reactor for large-scale photoreactions.

2.7.2   Additional Screening for Optimized Reaction Conditions

A 5 mL crimp vial was equipped with 46.3 mg of **1a** (0.25 mmol, 1.0 equiv.) and a magnetic stirring bar and was capped with a septum. Nitrogen atmosphere was introduced *via* three cycles of vacuum/nitrogen (2 min. at 7 mbar/2 min. flush with nitrogen atmosphere). 39 µL of **2a** (0.275 mmol, 1.1 equiv.), 50 µL of a 7.5 mM stock solution of $[Ir(ppy)_2(dtbbpy)]PF_6$ (1.125 µmol, 0.15 mol%) in dry and degassed DMSO and 50 µL of a 10 mM stock solution of $[Ni(dtbbpy)]Br_2$ (3.75 µmol, 0.20 mol%) in dry and degassed DMSO were added *via* Hamilton syringes under nitrogen atmosphere. Then, 38 µL tetramethylguanidine (TMG) (0.275 mmol, 1.2 equiv.) was added *via* Hamilton syringe under nitrogen atmosphere. Finally, 1 mL of dry and degassed DMSO (0.25 M) was added *via* syringe under nitrogen atmosphere. The reaction mixture was stirred and irradiated, using a blue LED (455 nm) for 3 hours at 25 °C in a typical irradiation setup used in our laboratories.
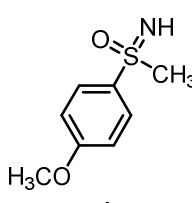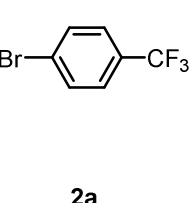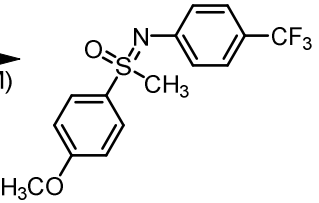
After 3 hours the reaction mixture was diluted in a 1:1 ratio with a stock solution of naphthalene in DMSO as internal standard and the reaction mixture was analyzed *via* calibrated gas chromatography.

Table 7. Screening of different photocatalyst.

Entry	Type of Photocatalyst	Yield[a] (%)
1	1.0 mol% $[Ir(dF(CF_3)ppy)_2(dtbbpy)]PF_6$	17
2	0.15 mol% $[Ir(dF(CF_3)ppy)_2(dtbbpy)]PF_6$	33
3	1.0 mol% $[Ir(dFppy)_3]$	49
4	0.15 mol% $[Ir(dFppy)_3]$	29
5	1.0 mol% $[Ru(bpy)_3]Cl_2$	51
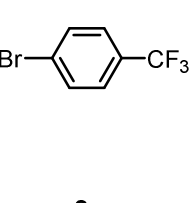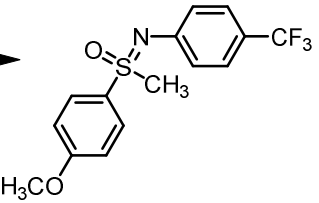
[a]Yields were determined by GC analysis with naphthalene as internal standard.

Table 8. Screening of different solvents.

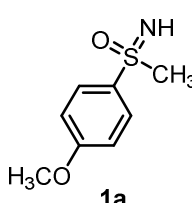| Entry	Type of Solvent	Yield[a] (%)
1	MeCN	99
2	DMF	99
3	DMAc	97
4	THF	99
4	DCM	4
5	DMSO (not dried)	91
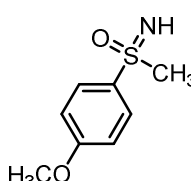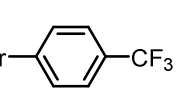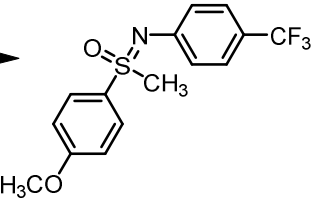
[a]Yields were determined by GC analysis with naphthalene as internal standard.

Table 9. Screening of different bases.

Entry	Type of Base	Yield[a] (%)
1	1.5 equiv. DBU	0
2	1.5 equiv. quinuclidine	80
3	1.5 equiv. DABCO	60
4	1.5 equiv. DIPEA	0
4	1.5 equiv. KOAc	27
5	1.5 equiv. Cs$_2$CO$_3$	0

[a]Yields were determined by GC analysis with naphthalene as internal standard.

Table 10. Control reactions.

Entry	Condition	Yield[a] (%)
1	No [Ir(ppy)$_2$(dtbbpy)]PF$_6$	1
2	No [Ir(ppy)$_2$(dtbbpy)]PF$_6$, but irradiation at 390nm	46[b]
3	No [Ni(dtbbpy)]Br$_2$	0
4	No TMG	0
4	No light, reaction in the dark	0
5	No degassing, O$_2$ atmosphere	14

[a]Yields were determined by GC analysis with naphthalene as internal standard. [b]Isolated yield after purification *via* automated flash-column chromatography.

2.7.3 General Procedures

2.7.3.1 Preparation of metal catalysts – [Ir(ppy)₂(dtbbpy)]PF₆ and [Ni(dtbbpy)]Br₂

The used $[Ir(ppy)_2(dtbbpy)]PF_6$[2] (**[Ir]-Cat**) and $[Ni(dtbbpy)]Br_2$[3] (**[Ni-2]-Cat**) catalysts were prepared according to literature known procedures.

2.7.3.2 Preparation of **NH-Sulfoximines**

NH-Sulfoximines **1ar** and ***S*-1at** were purchased from commercial suppliers and used without further purification.

Compound was prepared according to reported literature procedure and ¹H-NMR data are matching with the literature known spectra.[4]
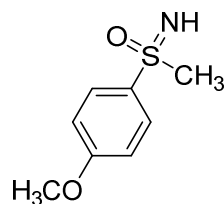
¹H NMR (300 MHz, CDCl₃) δ = 8.05 – 7.79 (m, 2H), 7.06 – 6.86 (m, 2H), 3.82 (s, 3H), 3.03 (s, 1H), 2.75 (s, 3H).

Cyclopropyl(imino)(phenyl)-λ⁶-sulfanone (1ai)

Compound was prepared according to reported literature procedure and ¹H-NMR data are matching with the literature known spectra.[5]

¹H NMR (300 MHz, CDCl₃) δ = 7.99 – 7.87 (m, 2H), 7.63 – 7.43 (m, 3H), 2.69 (s, 1H), 2.50 (tt, *J* = 7.9, 4.8 Hz, 1H), 1.34 (ddt, *J* = 10.2, 7.0, 4.7 Hz, 1H), 1.24 – 1.07 (m, 1H), 1.01 (dddd, *J* = 9.0, 8.0, 6.8, 4.8 Hz, 1H), 0.87 (dddd, *J* = 9.0, 7.9, 6.9, 4.9 Hz, 1H).

Iminodiphenyl-λ^6-sulfanone (1aj)

Compound was prepared from the respective sulfoxide according to reported literature procedure and ^{1}H-NMR data are matching with the literature known spectra.[6]

[1]**H NMR** (300 MHz, CDCl$_3$) δ = 8.10 – 8.01 (m, 4H), 7.56 – 7.45 (m, 6H), 3.11 (s, 1H).

Benzyl(imino)(phenyl)-λ^6-sulfanone (1ak)

Compound was prepared according to reported literature procedure and ^{1}H-NMR data are matching with the literature known spectra.[7]

[1]**H NMR** (300 MHz, CDCl$_3$) δ = 7.80 – 7.73 (m, 2H), 7.62 – 7.53 (m, 1H), 7.50 – 7.40 (m, 2H), 7.34 – 7.23 (m, 3H), 7.14 – 7.07 (m, 2H), 4.36 (q, *J* = 13.4 Hz, 2H), 2.84 (s, 1H).

Imino(methyl)(*p*-tolyl)-λ^6-sulfanone (1al)

Compound was prepared according to reported literature procedure and ^{1}H-NMR data are matching with the literature known spectra.[4]

[1]**H NMR** (400 MHz, CDCl$_3$) δ = 7.89 – 7.80 (m, 2H), 7.34 – 7.28 (m, 2H), 3.05 (s, 3H), 2.57 (s, 1H), 2.40 (s, 3H).

(4-Fluorophenyl)(imino)(methyl)-λ⁶-sulfanone (1am)

Compound was prepared according to reported literature procedure and ^{1}H-NMR data are matching with the literature known spectra.[7]

^{1}H NMR (300 MHz, CDCl₃) δ = 8.07 – 7.95 (m, 2H), 7.25 – 7.15 (m, 2H), 3.09 (s, 3H), 2.77 (s, 1H).

(4-Chlorophenyl)(imino)(methyl)-λ⁶-sulfanone (1an)

Compound was prepared according to reported literature procedure and ^{1}H-NMR data are matching with the literature known spectra.[7]

^{1}H NMR (400 MHz, CDCl₃) δ = 8.00 – 7.87 (m, 2H), 7.57 – 7.48 (m, 2H), 3.11 (s, 3H), 2.59 (s, 1H).

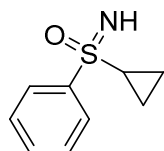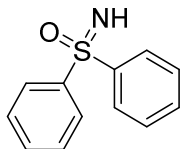## 4-(*S*-Methylsulfonimidoyl)benzonitrile (1ao)

Compound was prepared according to reported literature procedure and ^{1}H-NMR data are matching with the literature known spectra.[4]
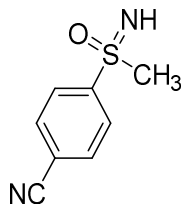
^{1}H NMR (300 MHz, CDCl₃) δ = 8.14 – 8.08 (m, 2H), 7.86 – 7.81 (m, 2H), 3.10 (s, 3H), 2.83 (s, 1H).

Imino(methyl)(pyridin-3-yl)- λ⁶-sulfanone (1ap)

Compound was prepared according to reported literature procedure for similar *NH*-sulfoximines.[7]
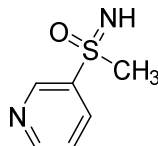
Yellowish oil, 140 mg, 24% yield.

Purified *via* automated flash-column chromatography on flash-silica gel (petrolether/ethylacetate, 90% ethylacetate).

¹H NMR (300 MHz, DMSO-d_6) δ = 8.73 – 8.70 (m, 1H), 8.15 – 8.03 (m, 2H), 7.68 – 7.61 (m, 1H), 4.44 (s, 1H), 3.16 (s, 3H).

¹³C NMR (75 MHz, DMSO-d_6) δ = 161.1 (C_q), 149.5 (+), 138.7 (+), 126.7 (+), 120.2 (+), 41.6 (+).

HRMS (ESI) (m/z): [M + H]⁺ ($C_6H_8N_2OS$) calc.: 157.0430, found: 157.0433.

Imino(methyl)(thiazol-2-yl)- λ⁶-sulfanone (1aq)

Compound was prepared according to reported literature procedure for similar *NH*-sulfoximines.[7]
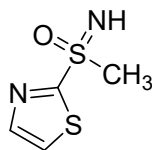
Yellowish oil, 259 mg, 21% yield.

Purified *via* automated flash-column chromatography on flash-silica gel (petrolether/ethylacetate, 60% ethylacetate).

¹H NMR (400 MHz, DMSO-d_6) δ = 8.12 (d, *J* = 3.1 Hz, 1H), 8.06 (d, *J* = 3.1 Hz, 1H), 5.08 (s, 1H), 3.26 (d, *J* = 1.2 Hz, 3H).

¹³C NMR (75 MHz, DMSO-d_6) δ = 170.8 (C_q), 144.4 (+), 127.1 (+), 44.3 (+).

HRMS (ESI) (m/z): [M + H]$^+$ (C$_4$H$_6$N$_2$OS$_2$) calc.: 162.9994, found: 162.9997.

1-Iminotetrahydro-1*H*-1λ^6-thiophene 1-oxide (1as)

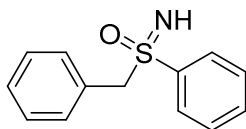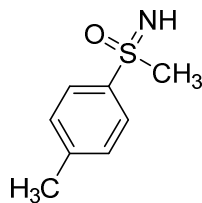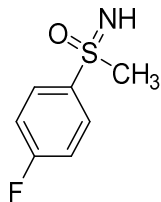Compound was prepared according to reported literature procedure and ^{1}H-NMR data are matching with the literature known spectra.[7]
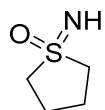
^{1}H NMR (400 MHz, CDCl$_3$) δ = 3.03 – 2.96 (m, 5H), 2.11 (td, *J* = 6.8, 3.7 Hz, 4H).

Imino(methyl)(phenyl)-λ^6-sulfanone (1at)

Compound was prepared according to reported literature procedure.[5]
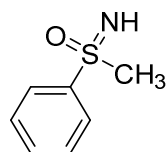
^{1}H NMR (300 MHz, DMSO-*d$_6$*) δ = 7.98 – 7.90 (m, 2H), 7.66 – 7.54 (m, 3H), 4.22 (s, 1H), 3.06 (s, 3H).

2.7.3.3 Preparation of Other Sulfoximidoyl Derivatives

4-Methylbenzenesulfinamide (4)

p-Toluenesulfinamide was purchased from commercial suppliers and used without further purification.
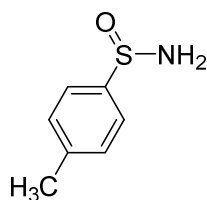
1-(S-Phenylsulfonimidoyl)piperidine (6)
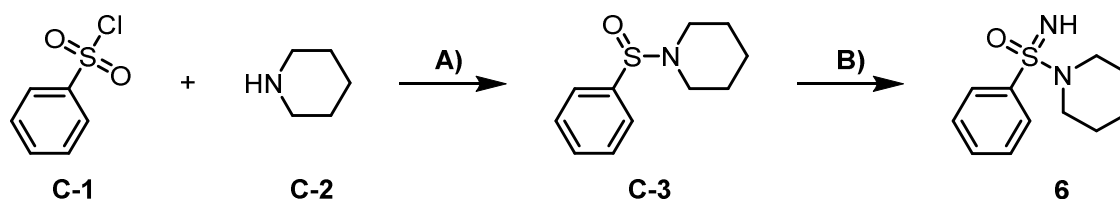
Scheme 8. A) Preparation of the sulfinamide **C-3** from the respective sulfonyl chloride (**C-1**) and piperidine (**C-2**). B) Preparation of the *NH*-sulfonimidamide **6**.

1-(Phenylsulfinyl)piperidine (C-3)

The sulfinamide derivative **C-3** was prepared according to literature known procedure for similar sulfinamides (**A)**[8]) and ^{1}H-NMR data are matching with the literature known spectra.[9]
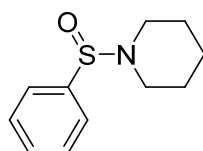
Procedure **A)**:

To a 0.3 M solution of phenyl sulfonyl chloride (1.45 mL, 11.3 mmol, 1.0 equiv.) and triethylamine (3.14 mL, 22.6 mmol, 2.0 equiv.) in anhydrous CH_2Cl_2 at 0 °C under nitrogen atmosphere, was added slowly a 0.3 M solution of piperidine (1.12 mL, 11.3 mmol, 1.0 equiv.) and triphenylphosphine (2.97 g, 11.3 mmol, 1.0 equiv.) in anhydrous CH_2Cl_2 *via* a dropping funnel. The reaction mixture was stirred for 18 hours, concentrated under reduced pressure and the crude mixture was purified by automated flash-column chromatography on flash-silica gel (petrolether/ethylacetate, 30% ethylacetate), affording 655 mg of sulfinamide **C-3** (28%) as a light yellow oil.

^{1}H NMR (300 MHz, $CDCl_3$) δ = 7.69 – 7.59 (m, 2H), 7.54 – 7.44 (m, 3H), 3.17 – 3.04 (m, 2H), 2.94 (m, 2H), 1.72 – 1.44 (m, 6H).

1-(*S*-Phenylsulfonimidoyl)piperidine (6)

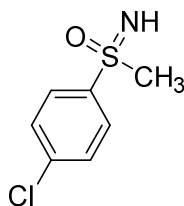The sulfonimidamide **6** was prepared according to reported literature procedure (**B)**) and ^{1}H-NMR data are matching with the literature known spectra.[9]
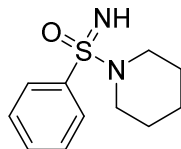
Yellow-orange solid, 264 mg, 38% yield.

Purified *via* automated flash-column chromatography on flash-silica gel (petrolether/ethylacetate, 30% ethylacetate).

**^{1}H NMR** (400 MHz, DMSO-d_6) δ = 7.81 – 7.71 (m, 2H), 7.68 – 7.51 (m, 3H), 4.28 (s, 1H), 2.87 – 2.78 (m, 4H), 1.60 – 1.42 (m, 4H), 1.29 (m, 2H).

2.7.3.4 General Procedure for the N-Arylation of NH-Sulfoximines with Bromo Arenes
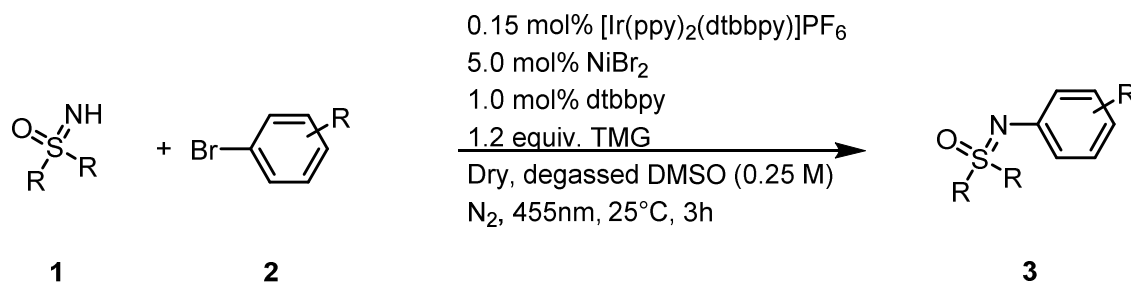
Scheme 9. *N*-Arylation of *NH*-sulfoximines.

A 5 mL crimp vial was equipped with solid *NH*-sulfoximine (**1**) (0.25 mmol, 1.0 equiv.), solid bromo arene (**2**) (0.275 mmol, 1.1 equiv.) and a magnetic stirring bar and was capped with a septum. All liquid substrates were added *via* syringe after degassing. Nitrogen atmosphere was introduced *via* three cycles of vacuum/nitrogen (2 min. at 7 mbar/2 min. flush with nitrogen atmosphere). 50 μL of a 7.5 mM stock solution of $[Ir(ppy)_2(dtbbpy)]PF_6$ (1.125 μmol, 0.15 mol%) in dry and degassed DMSO and 50 μL of a 10 mM stock solution of $[Ni(dtbbpy)]Br_2$ (3.75 μmol, 0.20 mol%) in dry and degassed DMSO were added *via* Hamilton syringes under nitrogen atmosphere. Then, 38 μL tetramethylguanidine (TMG) (0.275 mmol, 1.2 equiv.) was added *via* Hamilton syringe under nitrogen atmosphere. Finally, 1 mL of dry and degassed solvent (0.25 M) was added *via* syringe under nitrogen atmosphere. The reaction mixture was stirred and irradiated, using a blue LED (455 nm) for 3 – 17 hours at 25 °C in a typical irradiation setup used in our laboratories. The progress of the reaction could be monitored by GC analysis, GC-MS analysis or TLC analysis.

When the reaction was over, the reaction mixture was diluted with brine (10 mL) and extracted three times with ethylacetate (3 x 10 mL). The combined organic layers were dried with Na_2SO_4, filtered and the solvent was removed under reduced pressure. Evaporation of volatiles led to the crude product. Purification was performed *via* automated flash-column chromatography on flash-silica gel (petrolether/ethylacetate/methanol), affording the corresponding *N*-arylated sulfoximine (**3**) as pure product.

The color, shape and yield of the product, the type of used solvent, any deviations from the general reaction procedure and detailed information about purification *via* column chromatography are given for every compound in the respective section.

(4-Methoxyphenyl)(methyl)((4-(trifluoromethyl)phenyl)imino)-λ⁶-sulfanone (3a)
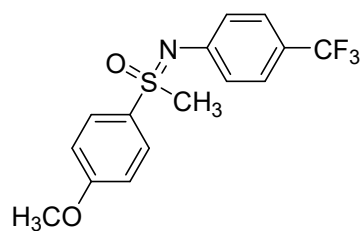
White oil, 72.5 mg, 88% yield.

Solvent: 1 mL dry and degassed acetonitrile (0.25 M); reaction time: 3.5 h; Purified *via* automated flash-column chromatography on flash-silica gel (petrolether/ethylacetate, 30% ethylacetate).

¹H NMR (400 MHz, CDCl₃) δ = 7.92 – 7.76 (m, 2H), 7.33 (d, *J* = 8.4 Hz, 2H), 7.03 (d, *J* = 8.4 Hz, 2H), 7.01 – 6.92 (m, 2H), 3.81 (s, 3H), 3.23 (s, 3H).

¹³C NMR (101 MHz, CDCl₃) δ = 163.8 (C$_q$), 149.1 (C$_q$), 130.7 (+), 129.7 (C$_q$), 126.2 (+, q, *J*=3.7), 124.7 (C$_q$, q, *J*=271.0), 123.0 (C$_q$, q, *J*=32.3), 122.8 (+), 115.0 (+), 55.6 (+), 46.7 (+).

¹⁹F NMR (376 MHz, CDCl₃) δ = -62.2 (s).

HRMS (ESI) (m/z): [M + H]⁺ (C₁₅H₁₄F₃NO₂S) calc.: 330.0770, found: 330.0776.

((4-(*tert*-Butyl)phenyl)imino)(4-methoxyphenyl)(methyl)-λ⁶-sulfanone (3b)
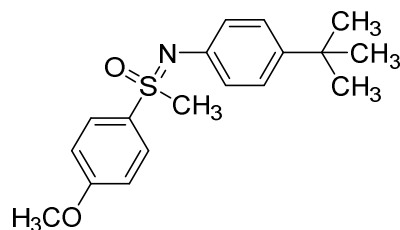
White oil, 78.6 mg, 99% yield.

Solvent: 1 mL dry and degassed acetonitrile (0.25 M); reaction time: 17 h; Purified *via* automated flash-column chromatography on flash-silica gel (petrolether/ethylacetate, 25% ethylacetate).

¹H NMR (400 MHz, CDCl₃) δ = 7.93 – 7.88 (m, 2H), 7.17 – 7.10 (m, 2H), 7.01 – 6.96 (m, 2H), 6.95 – 6.89 (m, 2H), 3.85 (s, 3H), 3.20 (s, 3H), 1.23 (s, 9H).

^{13}**C NMR** (75 MHz, CDCl$_3$) δ = 163.5 (C$_q$), 144.3 (C$_q$), 142.1 (C$_q$), 130.9 (+), 125.9 (+), 122.8 (+), 114.9 (+), 55.8 (+), 46.5 (+), 34.2 (C$_q$), 31.5 (+).

HRMS (ESI) (m/z): [M + H]$^+$ (C$_{18}$H$_{23}$NO$_2$S) calc.: 318.1522, found: 318.1527.

(4-Methoxyphenyl)(methyl)((4-(methylthio)phenyl)imino)-λ^6-sulfanone (3c)

White oil, 70.1 mg, 92% yield.

0.5 mol% [Ir(ppy)$_2$(dtbbpy)]PF$_6$; 1.0 mol% [Ni(dtbbpy)]Br$_2$; Solvent: 1 mL dry and degassed acetonitrile (0.25 M); reaction time: 17 h; Purified *via* automated flash-column chromatography on flash-silica gel (hexane/ethylacetate, 40% ethylacetate).

^{1}**H NMR** (400 MHz, CDCl$_3$) δ = 7.88 – 7.79 (m, 2H), 7.08 – 7.00 (m, 2H), 6.99 – 6.88 (m, 4H), 3.80 (s, 3H), 3.19 (s, 3H), 2.35 (s, 3H).

^{13}**C NMR** (101 MHz, CDCl$_3$) δ = 163.5 (C$_q$), 143.4 (C$_q$), 130.8 (+), 130.3 (C$_q$), 129.8 (C$_q$), 128.9 (+) 123.8 (+), 114.8 (+), 55.7 (+), 46.4 (+), 17.3 (+).

HRMS (ESI) (m/z): [M + H]$^+$ (C$_{15}$H$_{17}$NO$_2$S$_2$) calc.: 308.0773, found: 308.0779.

((4-Fluorophenyl)imino)(4-methoxyphenyl)(methyl)-λ^6-sulfanone (3d)

^{1}H-NMR data are matching with the literature known spectra.[10]
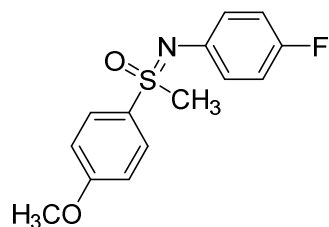
White oil, 69.1 mg, 99% yield.

0.5 mol% [Ir(ppy)$_2$(dtbbpy)]PF$_6$; 1.0 mol% [Ni(dtbbpy)]Br$_2$; Solvent: 1 mL dry and degassed acetonitrile (0.25 M); reaction time: 17 h; Purified *via* automated flash-column chromatography on flash-silica gel (petrolether/ethylacetate, 30% ethylacetate).

^{1}H NMR (400 MHz, CDCl$_3$) δ = 7.88 – 7.79 (m, 2H), 6.99 – 6.88 (m, 4H), 6.84 – 6.72 (m, 2H), 3.81 (s, 3H), 3.18 (s, 3H).

((4-Chlorophenyl)imino)(4-methoxyphenyl)(methyl)-λ^6-sulfanone (3e)

^{1}H-NMR data are matching with the literature known spectra.[10]
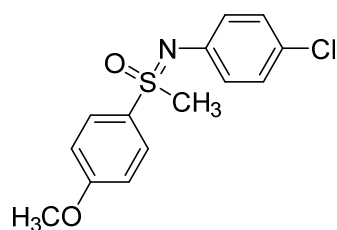
White oil, 66.6 mg, 90% yield.

0.2 mol% [Ir(ppy)$_2$(dtbbpy)]PF$_6$; 1.0 mol% [Ni(dtbbpy)]Br$_2$; Solvent: 1 mL dry and degassed acetonitrile (0.25 M); reaction time: 17 h; Purified *via* automated flash-column chromatography on flash-silica gel (petrolether/ethylacetate, 35% ethylacetate).

^{1}H NMR (400 MHz, CDCl$_3$) δ = 7.87 – 7.78 (m, 2H), 7.08 – 6.99 (m, 2H), 6.99 – 6.86 (m, 4H), 3.81 (s, 3H), 3.19 (s, 3H).

4-(((4-Methoxyphenyl)(methyl)(oxo)-λ^6-sulfaneylidene)amino)benzonitrile (3f)
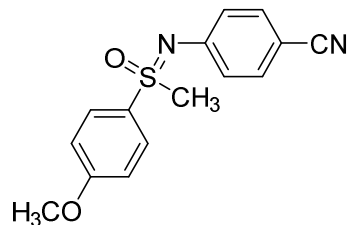
White oil, 70.2 mg, 98% yield.

Solvent: 1 mL dry and degassed acetonitrile (0.25 M); reaction time: 17 h; Purified *via* automated flash-column chromatography on flash-silica gel (hexane/ethylacetate, 50% ethylacetate).

¹H NMR (400 MHz, CDCl₃) δ = 7.88 – 7.79 (m, 2H), 7.41 – 7.32 (m, 2H), 7.05 – 6.93 (m, 4H), 3.86 (s, 3H), 3.26 (s, 3H).

¹³C NMR (101 MHz, CDCl₃) δ = 164.0 (C$_q$), 150.6 (C$_q$), 133.3 (+), 130.7 (+), 129.4 (C$_q$), 123.2 (+), 119.8 (C$_q$), 115.2 (+), 103.9 (C$_q$), 55.9 (+), 47.1 (+).

HRMS (ESI) (m/z): [M + H]⁺ (C₁₅H₁₄N₂O₂S) calc.: 287.0849, found: 287.0851.

((3,5-Bis(trifluoromethyl)phenyl)imino)(4-methoxyphenyl)(methyl)-λ⁶-sulfanone (3g)

White oil, 95.4 mg, 96% yield.

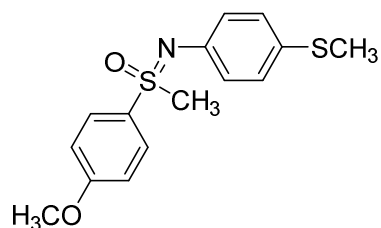0.5 mol% [Ir(ppy)₂(dtbbpy)]PF₆; 1.0 mol% [Ni(dtbbpy)]Br₂; Solvent: 1 mL dry and degassed acetonitrile (0.25 M); reaction time: 17 h; Purified *via* automated flash-column chromatography on flash-silica gel (petrolether/ethylacetate, 20% ethylacetate).

¹H NMR (300 MHz, CDCl₃) δ = 7.90 – 7.80 (m, 2H), 7.38 (s, 2H), 7.29 (s, 1H), 7.04 – 6.94 (m, 2H), 3.81 (s, 3H), 3.26 (s, 3H).

¹³C NMR (75 MHz, CDCl₃) δ = 164.0 (C$_q$), 147.4 (C$_q$), 132.0 (C$_q$, q, *J* = 32.8 Hz), 130.7 (+), 129.0 (C$_q$), 123.5 (C$_q$, q, *J* = 272.7 Hz), 122.8 (+, d, *J* = 4.0 Hz), 115.1 (+), 114.5 (+, sept., *J* = 4.1 Hz), 55.7 (+), 46.6 (+).

¹⁹F NMR (377 MHz, CDCl₃) δ = -63.6.

HRMS (ESI) (m/z): [M + H]⁺ (C₁₆H₁₃F₆NO₂S) calc.: 398.0644, found: 398.0652.

((3,5-Dimethoxyphenyl)imino)(4-methoxyphenyl)(methyl)-λ⁶-sulfanone (3h)
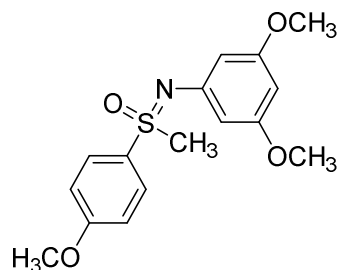
White oil, 62.7 mg, 78% yield.

Solvent: 1 mL dry and degassed acetonitrile (0.25 M); reaction time: 17 h; Purified *via* automated flash-column chromatography on flash-silica gel (petrolether/ethylacetate, 40% ethylacetate).

¹H NMR (400 MHz, CDCl₃) δ = 7.88 – 7.81 (m, 2H), 6.97 – 6.89 (m, 2H), 6.22 – 6.18 (m, 2H), 6.02 – 5.99 (m, 1H), 3.80 (s, 3H), 3.65 (s, 6H), 3.18 (s, 3H).

¹³C NMR (101 MHz, CDCl₃) δ = 163.5 (C_q), 161.0 (C_q), 147.2 (C_q), 130.7 (+), 130.4 (C_q), 114.8 (+), 101.6 (+), 94.5 (+), 55.7 (+), 55.2 (+), 46.4 (+).

HRMS (ESI) (m/z): [M + H]⁺ (C₁₆H₁₉NO₄S) calc.: 322.1108, found: 322.1110.

4-(((4-Methoxyphenyl)(methyl)(oxo)-λ⁶-sulfaneylidene)amino)benzaldehyde (3i)
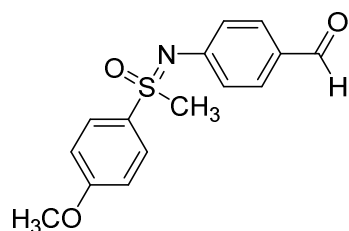
White oil, 42.6 mg, 59% yield.

Solvent: 1 mL dry and degassed dimethylacetamide (0.25 M); reaction time: 17 h; Purified *via* automated flash-column chromatography on flash-silica gel (hexane/ethylacetate, 30% ethylacetate).

¹H NMR (400 MHz, CDCl₃) δ = 9.76 (s, 1H), 7.89 – 7.79 (m, 2H), 7.67 – 7.55 (m, 2H), 7.09 – 7.00 (m, 2H), 7.02 – 6.93 (m, 2H), 3.83 (s, 3H), 3.26 (s, 3H).

¹³C NMR (101 MHz, CDCl₃) δ = 191.1 (+), 163.9 (C_q), 152.5 (C_q), 131.3 (+), 130.7 (+), 130.0 (C_q), 129.6 (C_q), 122.9 (+), 115.1 (+), 55.8 (+), 47.0 (+).

HRMS (ESI) (m/z): [M + H]⁺ (C₁₅H₁₅NO₃S) calc.: 290.0845, found: 290.0853.

Methyl 4-(((4-methoxyphenyl)(methyl)(oxo)-λ⁶-sulfaneylidene)amino)benzoate (3j)

White solid, 79.0 mg, 99% yield.

Melting point: 95 °C

Solvent: 1 mL dry and degassed acetonitrile (0.25 M); reaction time: 17 h; Purified *via* automated flash-column chromatography on flash-silica gel (petrolether/ethylacetate, 30% ethylacetate).

¹H NMR (400 MHz, CDCl₃) δ = 7.85 – 7.79 (m, 2H), 7.78 – 7.72 (m, 2H), 7.00 – 6.89 (m, 4H), 3.78 (s, 3H), 3.78 (s, 3H), 3.22 (s, 3H).

¹³C NMR (101 MHz, CDCl₃) δ = 167.10 (C_q), 163.66 (C_q), 150.61 (C_q), 130.78 (+), 130.64 (+), 129.66 (C_q), 122.67 (C_q), 122.42 (+), 114.93 (+), 55.68 (+), 51.70 (+), 46.75 (+).

HRMS (ESI) (m/z): [M + H]⁺ (C₁₆H₁₇NO₄S) calc.: 320.0951, found: 320.0952.

4-(((4-Methoxyphenyl)(methyl)(oxo)-λ⁶-sulfaneylidene)amino)-N-methylbenzamide (3k)

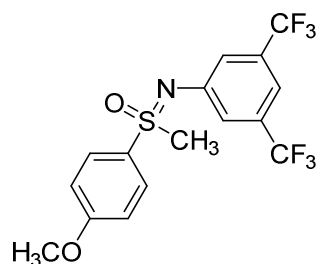White viscous oil, 75.6 mg, 95% yield.

Solvent: 1 mL dry and degassed acetonitrile (0.25 M); reaction time: 17 h; Purified *via* automated flash-column chromatography on flash-silica gel (hexane/ethylacetate, 80% ethylacetate).

¹H NMR (400 MHz, DMSO-*d₆*) δ = 8.10 (q, *J* = 4.5 Hz, 1H), 7.88 – 7.80 (m, 2H), 7.60 – 7.51 (m, 2H), 7.19 – 7.05 (m, 2H), 6.90 – 6.75 (m, 2H), 3.82 (s, 3H), 3.38 (s, 3H), 2.70 (d, *J* = 4.5 Hz, 3H).

¹³C NMR (101 MHz, DMSO-*d₆*) δ = 166.4 (C_q), 163.0 (C_q), 148.9 (C_q), 130.5 (+), 129.8 (C_q), 128.0 (+), 126.6 (C_q), 121.7 (+), 114.8 (+), 55.7 (+), 45.7 (+), 26.1 (+).

HRMS (ESI) (m/z): [M + H]⁺ ($C_{16}H_{18}N_2O_3S$) calc.: 319.1111, found: 319.1110.

((3-Bromophenyl)imino)(4-methoxyphenyl)(methyl)-λ⁶-sulfanone (3l)

White oil, 53.9 mg, 66% yield with respect to 1,3-dibromobenzene as limiting reagent.

92.6 mg of the *NH*-sulfoximine (0.5 mmol, 2.1 equiv.) was reacted with 30.0 μL of 1,3-dibromobenzene (58.4 mg, 0.24 mmol, 1 equiv.); 0.5 mol% [Ir(ppy)₂(dtbbpy)]PF₆; 2.0 mol% [Ni(dtbbpy)]Br₂; Solvent: 2 mL dry and degassed acetonitrile (0.12 M); reaction time: 17 h; Purified *via* automated flash-column chromatography on flash-silica gel (hexane/ethylacetate, 30% ethylacetate).

**¹H NMR** (400 MHz, CDCl₃) δ = 7.89 – 7.78 (m, 2H), 7.20 – 7.13 (m, 1H), 7.01 – 6.85 (m, 5H), 3.82 (s, 3H), 3.20 (s, 3H).

¹³C NMR (101 MHz, CDCl₃) δ = 163.6 (C_q), 147.0 (C_q), 130.7 (+), 130.1 (+), 129.9 (C_q), 126.2 (+), 124.4 (+), 122.5 (C_q), 121.7 (+), 114.9 (+), 55.7 (+), 46.6 (+).

HRMS (ESI) (m/z): [M + H]⁺ ($C_{14}H_{14}BrNO_2S$) calc.: 340.0001, found: 340.0002.

(4-Methoxyphenyl)(methyl)((4-(methylsulfinyl)phenyl)imino)-λ⁶-sulfanone (3m)
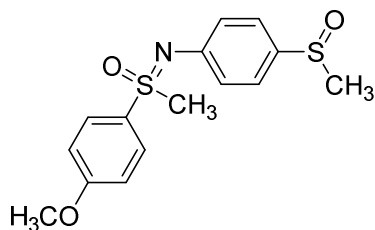
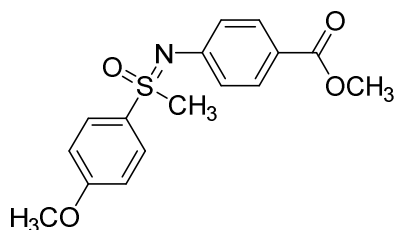
Yellow oil, 72.0 mg, 89% yield, diastereomeric ration of 1:1.

Solvent: 1 mL dry and degassed acetonitrile (0.25 M); reaction time: 17 h; Purified *via* automated flash-column chromatography on flash-silica gel (ethylacetate/methanol, 5% methanol).

¹H NMR (300 MHz, CDCl₃) δ = 7.90 – 7.82 (m, 2H), 7.43 – 7.37 (m, 2H), 7.16 – 7.08 (m, 2H), 7.03 – 6.94 (m, 2H), 3.85 (s, 3H), 3.30 (d, J = 1.9 Hz, 3H), 2.65 (d, J = 1.7 Hz, 3H).

¹³C NMR (101 MHz, CDCl₃) δ = 164.0 (C_q, d, J = 2.1 Hz), 148.3 (C_q, d, J = 3.9 Hz), 137.3 (C_q), 130.9 (+), 129.3 (C_q, d, J = 10.0 Hz), 125.1 (+), 123.7 (+, d, J = 7.8 Hz), 115.2 (+, d, J = 1.7 Hz), 55.9 (+), 46.7 (+), 43.8 (+, d, J = 5.4 Hz).

HRMS (ESI) (m/z): [M + H]⁺ ($C_{15}H_{17}NO_3S_2$) calc.: 324.0723, found: 324.0726.

(4-Methoxyphenyl)(methyl)((4-(methylsulfonyl)phenyl)imino)-λ⁶-sulfanone (3n)
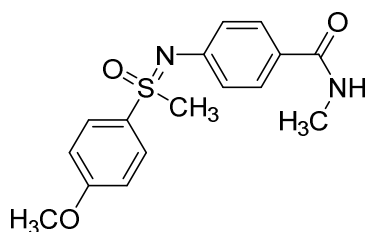

Yellow oil, 84.0 mg, 99% yield.

Solvent: 1 mL dry and degassed acetonitrile (0.25 M); reaction time: 17 h; Purified *via* automated flash-column chromatography on flash-silica gel (petrolether/ethylacetate, 70% ethylacetate).

¹H NMR (300 MHz, CDCl₃) δ = 7.87 – 7.80 (m, 2H), 7.67 – 7.59 (m, 2H), 7.09 – 7.02 (m, 2H), 7.03 – 6.95 (m, 2H), 3.85 (s, 3H), 3.27 (s, 3H), 2.96 (s, 3H).

¹³C NMR (75 MHz, CDCl$_3$) δ = 164.0 (C$_q$), 151.4 (C$_q$), 132.2 (C$_q$), 130.7 (+), 129.2 (C$_q$), 128.7 (+), 123.0 (+), 115.2 (+), 55.9 (+), 47.0 (+), 44.8 (+).

HRMS (ESI) (m/z): [M + H]$^+$ (C$_{15}$H$_{17}$NO$_4$S$_2$) calc.: 340.0672, found: 340.0676.

(4-Methoxyphenyl)(methyl)((4-(trifluoromethoxy)phenyl)imino)-λ^6-sulfanone (3o)
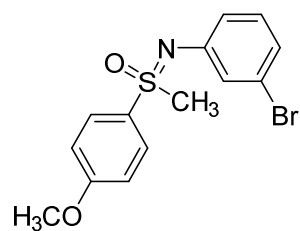

Yellow oil, 84.6 mg, 98% yield.

Solvent: 1 mL dry and degassed acetonitrile (0.25 M); reaction time: 17 h; Purified *via* automated flash-column chromatography on flash-silica gel (hexane/ethylacetate, 25% ethylacetate).

¹H NMR (400 MHz, CDCl$_3$) δ = 7.90 – 7.80 (m, 2H), 7.02 – 6.89 (m, 6H), 3.83 (s, 3H), 3.21 (s, 3H).

¹³C NMR (101 MHz, CDCl$_3$) δ = 163.6 (C$_q$), 144.1 (C$_q$), 143.6 (C$_q$, q, *J* = 1.9 Hz), 130.7 (+), 130.0 (C$_q$), 123.9 (+), 121.7 (+), 120.5 (C$_q$, q, *J* = 255.9 Hz), 114.9 (+), 55.6 (+), 46.5 (+).

¹⁹F NMR (377 MHz, CDCl$_3$) δ = -58.7.

HRMS (ESI) (m/z): [M + H]$^+$ (C$_{15}$H$_{14}$NO$_3$S) calc.: 346.0719, found: 346.0722.

(4-Methoxyphenyl)(methyl)((4-((trifluoromethyl)thio)phenyl)imino)-λ⁶-sulfanone (3p)
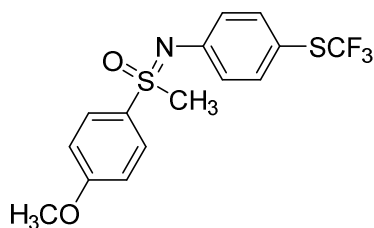
Yellow oil, 75.9 mg, 84% yield.

Solvent: 1 mL dry and degassed acetonitrile (0.25 M); reaction time: 17 h; Purified *via* automated flash-column chromatography on flash-silica gel (hexane/ethylacetate, 35% ethylacetate).

¹H NMR (400 MHz, CDCl$_3$) δ = 7.90 – 7.79 (m, 2H), 7.41 – 7.31 (m, 2H), 7.03 – 6.91 (m, 4H), 3.84 (s, 3H), 3.23 (s, 3H).

¹³C NMR (101 MHz, CDCl$_3$) δ = 163.8 (C$_q$), 148.7 (C$_q$), 137.7 (C$_q$), 130.7 (+), 129.9 (C$_q$), 129.8 (C$_q$, q, *J* = 308.2 Hz), 123.8 (+), 115.2 (C$_q$, q, *J* = 1.8 Hz), 115.1 (+), 55.8 (+), 46.9 (+).

¹⁹F NMR (282 MHz, CDCl$_3$) δ = -44.2.

HRMS (ESI) (m/z): [M + H]$^+$ (C$_{15}$H$_{14}$F$_3$NO$_2$S$_2$) calc.: 362.0491, found: 362.0494.

(4-Methoxyphenyl)(methyl)((4-(pentafluoro-λ⁶-sulfaneyl)phenyl)imino)-λ⁶-sulfanone (3q)
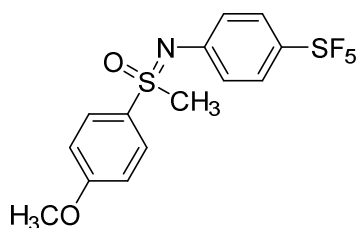
Colorless oil, 29.1 mg, 30% yield.

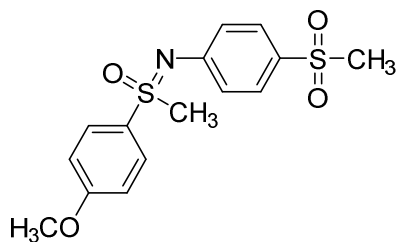0.5 mol% [Ni(dtbbpy)]Br$_2$; Solvent: 1 mL dry and degassed acetonitrile (0.25 M); reaction time: 17 h; Purified *via* automated-flash column chromatography on flash-silica gel (hexane/ethylacetate, 15% ethylacetate).

¹H NMR (400 MHz, CDCl₃) δ = 7.90 – 7.81 (m, 2H), 7.51 – 7.42 (m, 2H), 7.05 – 6.93 (m, 4H), 3.87 (s, 3H), 3.25 (s, 3H).

¹³C NMR (101 MHz, CDCl₃) δ = 163.9 (C$_q$), 148.9 (C$_q$), 147.1 (C$_q$), 130.8 (+), 129.7 (C$_q$), 126.9 (+, p, *J* = 4.4 Hz), 122.3 (+), 115.2 (+), 55.9 (+), 47.0 (+).

¹⁹F NMR (376 MHz, CDCl₃) δ = -90.5.

HRMS (ESI) (m/z): [M + H]$^+$ (C$_{14}$H$_{14}$F$_5$NO$_2$S$_2$) calc.: 388.0459, found: 388.0466.

tert-Butyl-(2-(((4-methoxyphenyl)(methyl)(oxo)-λ^6-sulfaneylidene)amino)phenyl) carbamate (3r)
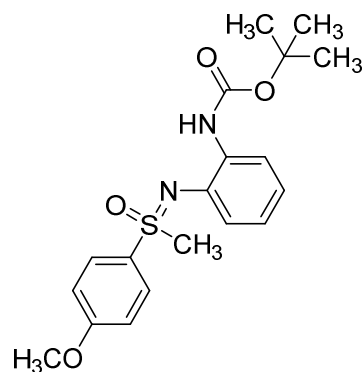
White oil, 92.2 mg, 98% yield.
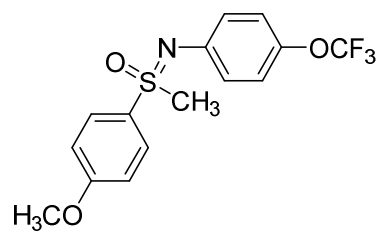
0.5 mol% [Ir(ppy)₂(dtbbpy)]PF₆; 1.0 mol% [Ni(dtbbpy)]Br₂; Solvent: 1 mL dry and degassed acetonitrile (0.25 M); reaction time: 17 h; Purified *via* automated flash-column chromatography on flash-silica gel (hexane/ethylacetate, 25% ethylacetate).

¹H NMR (400 MHz, DMSO-d_6) δ = 8.00 (s, 1H), 7.91 – 7.80 (m, 3H), 7.18 – 7.07 (m, 2H), 6.80 – 6.69 (m, 2H), 6.63 (td, *J* = 7.6, 1.6 Hz, 1H), 3.81 (s, 3H), 3.47 (s, 3H), 1.51 (s, 9H).

¹³C NMR (101 MHz, DMSO-d_6) δ = 163.0 (C$_q$), 152.4 (C$_q$), 134.4 (C$_q$), 131.7 (C$_q$), 130.5 (+), 129.4 (C$_q$), 122.0 (+), 120.7 (+), 119.9 (+), 117.9 (+), 114.8 (+), 79.4 (C$_q$), 55.7 (+), 45.7 (+), 28.1 (+).

HRMS (ESI) (m/z): [M + H]$^+$ (C$_{19}$H$_{24}$N$_2$O$_4$S) calc.: 377.1530, found: 377.1534.

tert-Butyl-6-(((4-methoxyphenyl)(methyl)(oxo)-λ^6-sulfaneylidene)amino)-1H-indole-1-carboxylate (3s)
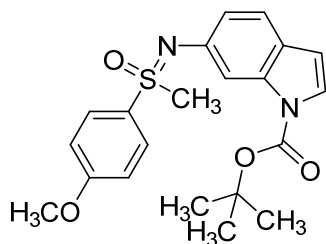
Yellowish viscous oil, 85.1 mg, 85% yield.

0.5 mol% [Ir(ppy)$_2$(dtbbpy)]PF$_6$; 5.0 mol% [Ni(dtbbpy)]Br$_2$; Solvent: 1 mL dry and degassed acetonitrile (0.25 M); reaction time: 17 h; Purified *via* automated flash-column chromatography on flash-silica gel (petrolether/ethylacetate, 30% ethylacetate).

^{1}H NMR (400 MHz, CDCl$_3$) δ = 7.96 – 7.87 (m, 2H), 7.84 (s, 1H), 7.44 (d, *J* = 3.6 Hz, 1H), 7.29 (d, *J* = 8.3 Hz, 1H), 7.01 – 6.90 (m, 3H), 6.41 (d, *J* = 3.6 Hz, 1H), 3.81 (s, 3H), 3.22 (s, 3H), 1.65 (s, 9H).

^{13}C NMR (101 MHz, CDCl$_3$) δ = 163.4 (C$_q$), 150.0 (C$_q$), 142.4 (C$_q$), 136.0 (C$_q$), 131.0 (+), 130.7 (C$_q$), 125.5 (C$_q$), 124.8 (+), 121.0 (+), 119.8 (+), 114.7 (+), 110.0 (+), 107.2 (+), 83.5 (C$_q$), 55.7 (+), 46.3 (+), 28.4 (+).

HRMS (ESI) (m/z): [M + H]$^+$ (C$_{21}$H$_{24}$N$_2$O$_4$S) calc.: 401.1530, found: 401.1538.

(4-Methoxyphenyl)(methyl)(pyridin-3-ylimino)-λ^6-sulfanone (3t)
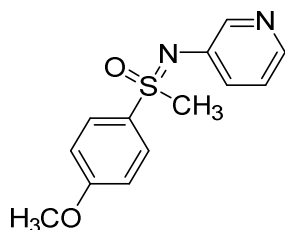
Dark oil, 64.9 mg, 99% yield.

1.0 mol% [Ni(dtbbpy)]Br$_2$; Solvent: 1 mL dry and degassed dimethylacetamide (0.25 M); reaction time: 17 h; Purified *via* automated flash-column chromatography on flash-silica gel (petrolether/ethylacetate, 90 % ethylacetate).

¹H NMR (400 MHz, DMSO-d_6) δ = 8.11 (d, J = 2.6 Hz, 1H), 7.98 (dd, J = 4.6, 1.6 Hz, 1H), 7.89 – 7.82 (m, 2H), 7.18 – 7.11 (m, 3H), 7.08 (dd, J = 8.2, 4.6 Hz, 1H), 3.82 (s, 3H), 3.41 (s, 3H).

¹³C NMR (101 MHz, DMSO-d_6) δ = 163.0 (C_q), 144.2 (+), 142.5 (C_q), 141.5 (+), 130.5 (+), 129.5 (C_q), 128.5 (+), 123.6 (+), 114.9 (+), 55.8 (+), 45.5 (+).

HRMS (ESI) (m/z): [M + H]⁺ ($C_{13}H_{14}N_2O_2S$) calc.: 263.0849, found: 263.0849.

((6-Chloropyridin-3-yl)imino)(4-methoxyphenyl)(methyl)-λ⁶-sulfanone (3u)

White oil, 66.0 mg, 89% yield.

0.5 mol% [Ir(ppy)$_2$(dtbbpy)]PF$_6$; 1.0 mol% [Ni(dtbbpy)]Br$_2$; Solvent: 1 mL dry and degassed dimethylacetamide (0.25 M); reaction time: 17 h; Purified *via* automated flash-column chromatography on flash-silica gel (petrolether/ethylacetate, 45% ethylacetate).

¹H NMR (400 MHz, CDCl$_3$) δ = 8.02 (d, J = 2.5 Hz, 1H), 7.85 – 7.76 (m, 2H), 7.22 (dd, J = 8.5, 2.9 Hz, 1H), 7.03 – 6.93 (m, 3H), 3.84 (s, 3H), 3.25 (s, 3H).

¹³C NMR (101 MHz, CDCl$_3$) δ = 163.3 (C_q), 144.4 (+), 143.2 (C_q), 141.4 (C_q), 132.5 (+), 130.8 (+), 129.1 (C_q), 124.0 (+), 115.2 (+), 55.8 (+), 46.7 (+).

HRMS (ESI) (m/z): [M + H]⁺ ($C_{13}H_{13}ClN_2O_2S$) calc.: 297.0459, found: 297.0463.

(4-Methoxyphenyl)(methyl)((4-(trifluoromethyl)pyridin-2-yl)imino)-λ⁶-sulfanone (3v)

White oil, 81.8 mg, 99% yield.

0.5 mol% [Ir(ppy)$_2$(dtbbpy)]PF$_6$; 1.0 mol% [Ni(dtbbpy)]Br$_2$; Solvent: 1 mL dry and degassed dimethylacetamide (0.25 M); reaction time: 17 h; Purified *via* automated flash-column chromatography on flash-silica gel (petrolether/ethylacetate, 30% ethylacetate).

¹H NMR (400 MHz, DMSO-d_6) δ = 8.20 (d, J = 5.2 Hz, 1H), 7.93 – 7.87 (m, 2H), 7.17 – 7.12 (m, 2H), 7.04 (d, J = 5.3 Hz, 1H), 7.01 (s, 1H), 3.84 (s, 3H), 3.46 (s, 3H).

¹³C NMR (101 MHz, DMSO-d_6) δ = 162.9 (C$_q$), 160.1 (C$_q$), 149.2 (+), 138.3 (C$_q$, q, J = 32.8 Hz), 130.7 (C$_q$), 129.7 (+), 123.0 (C$_q$, q, J = 273.1 Hz), 114.7 (+), 111.7 (+, q, J = 3.8 Hz), 110.4 (+, q, J = 3.0 Hz), 55.8 (+), 44.9 (+).

¹⁹F NMR (376 MHz, DMSO-d_6) δ = -63.3.

HRMS (ESI) (m/z): [M + H]$^+$ (C$_{14}$H$_{13}$F$_3$N$_2$O$_2$S) calc.: 331.0723, found: 331.0724.

((6-Acetylpyridin-2-yl)imino)(4-methoxyphenyl)(methyl)-λ⁶-sulfanone (3w)
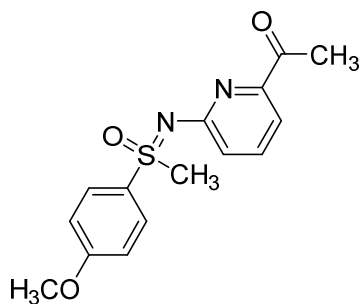
White viscous oil, 28.2 mg, 37% yield.

1.0 mol% [Ir(ppy)$_2$(dtbbpy)]PF$_6$; 5.0 mol% [Ni(dtbbpy)]Br$_2$; Solvent: 1 mL dry and degassed dimethylacetamide (0.25 M); reaction time: 17 h; Purified *via* automated flash-column chromatography on flash-silica gel (petrolether/ethylacetate, 60% ethylacetate).

¹H NMR (400 MHz, CDCl₃) δ = 7.95 – 7.86 (m, 2H), 7.61 – 7.54 (m, 1H), 7.44 (dd, *J* = 7.5, 0.9 Hz, 1H), 7.04 – 6.96 (m, 3H), 3.86 (s, 3H), 3.32 (s, 3H), 2.27 (s, 3H).

¹³C NMR (101 MHz, CDCl₃) δ = 200.6 (C_q), 163.3 (C_q), 158.3 (C_q), 151.4 (C_q), 138.4 (+), 131.2 (C_q), 129.9 (+), 120.7 (+), 114.8 (+), 114.0 (+), 55.8 (+), 46.3 (+), 26.0 (+).

HRMS (ESI) (m/z): [M + H]⁺ (C₁₅H₁₆N₂O₃S) calc.: 305.0954, found: 305.0958.

((6-Bromopyridin-3-yl)imino)(4-methoxyphenyl)(methyl)-λ⁶-sulfanone (3x)
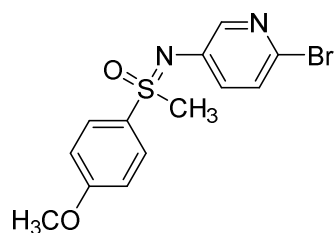
White solid, 65.7 mg, 77% yield.
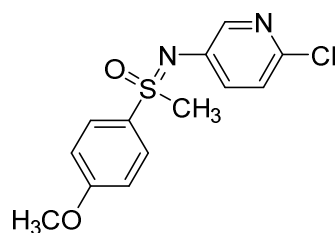
Melting point: 147 °C.

0.5 mol% [Ir(ppy)₂(dtbbpy)]PF₆; 5.0 mol% [Ni(dtbbpy)]Br₂; Solvent: 1 mL dry and degassed dimethylacetamide (0.25 M); reaction time: 17 h; Purified *via* automated flash-column chromatography on flash-silica gel (hexane/ethylacetate, 30% ethylacetate).

¹H NMR (400 MHz, CDCl₃) δ = 8.12 (d, *J* = 2.4 Hz, 1H), 7.95 – 7.86 (m, 2H), 7.53 (dd, *J* = 8.7, 2.6 Hz, 1H), 7.04 – 6.95 (m, 2H), 6.75 (d, *J* = 8.7 Hz, 1H), 3.87 (s, 3H), 3.33 (s, 3H).

¹³C NMR (101 MHz, CDCl₃) δ = 163.6 (C_q), 158.0 (C_q), 148.7 (+), 140.2 (+), 130.9 (C_q), 130.1 (+), 118.4 (+), 114.9 (+), 111.7 (C_q), 55.8 (+), 46.1 (+).

HRMS (ESI) (m/z): [M + H]⁺ (C₁₃H₁₃BrN₂O₂S) calc.: 340.9954, found: 340.9959.

(4-Methoxyphenyl)(methyl)(quinolin-8-ylimino)-λ^6-sulfanone (3y)
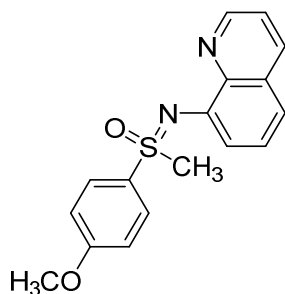
Orange solid, 21.1 mg, 27% yield.
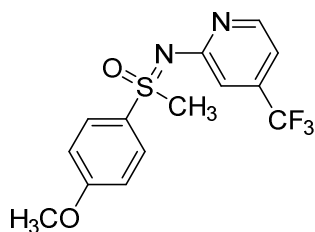
Melting point: 121 °C.

1.0 mol% [Ir(ppy)$_2$(dtbbpy)]PF$_6$; 5.0 mol% [Ni(dtbbpy)]Br$_2$; Solvent: 1 mL dry and degassed dimethylacetamide (0.25 M); reaction time: 17 h; Purified *via* automated flash-column chromatography on flash-silica gel (petrolether/ethylacetate, 70% ethylacetate).

^{1}H NMR (400 MHz, DMSO-d_6) δ = 8.87 – 8.82 (m, 2H), 7.90 – 7.84 (m, 2H), 7.49 (dd, *J* = 8.1, 4.5 Hz, 1H), 7.47 – 7.43 (m, 1H), 7.38 (dd, *J* = 8.5, 7.4 Hz, 1H), 7.12 – 7.06 (m, 2H), 6.94 (dd, *J* = 7.4, 1.2 Hz, 1H), 3.79 (s, 3H), 3.52 (s, 3H).

^{13}C NMR (101 MHz, DMSO-d_6) δ = 163.0 (C$_q$), 150.2 (+), 148.8 (C$_q$), 142.8 (C$_q$), 132.4 (+), 130.3 (+), 129.7 (C$_q$), 129.4 (+), 124.6 (C$_q$), 121.2 (+), 120.3 (+), 115.3 (+), 114.8 (+), 55.7 (+), 45.6 (+).

HRMS (ESI) (m/z): [M + H]$^+$ (C$_{17}$H$_{16}$N$_2$O$_2$S) calc.: 313.1005, found: 313.1005.

(4-Methoxyphenyl)(methyl)(quinolin-3-ylimino)-λ^6-sulfanone (3z)

Orange oil, 75.8 mg, 97% yield.

1.0 mol% [Ir(ppy)$_2$(dtbbpy)]PF$_6$; 5.0 mol% [Ni(dtbbpy)]Br$_2$; Solvent: 1 mL dry and degassed dimethylacetamide (0.25 M); reaction time: 17 h; Purified *via* automated flash-column chromatography on flash-silica gel (hexane/ethylacetate, 70% ethylacetate).

**¹H NMR** (400 MHz, CDCl₃) δ = 8.69 (d, *J* = 2.6 Hz, 1H), 7.94 – 7.82 (m, 3H), 7.57 (d, *J* = 2.5 Hz, 1H), 7.53 (dd, *J* = 8.1, 1.1 Hz, 1H), 7.45 (ddd, *J* = 8.4, 6.9, 1.5 Hz, 1H), 7.36 (ddd, *J* = 8.0, 6.9, 1.1 Hz, 1H), 6.97 – 6.89 (m, 2H), 3.78 (s, 3H), 3.30 (s, 3H).

¹³C NMR (101 MHz, CDCl₃) δ = 163.8 (C$_q$), 149.8 (+), 143.9 (C$_q$), 139.5 (C$_q$), 130.9 (+), 129.3 (C$_q$), 129.0 (C$_q$), 128.8 (+), 126.8 (+), 126.8 (+), 126.6 (+), 124.2 (+), 115.1 (+), 55.7 (+), 46.7 (+).

HRMS (ESI) (m/z): [M + H]⁺ (C$_{17}$H$_{16}$N$_2$O$_2$S) calc.: 313.1005, found: 313.1009.

(4-Methoxyphenyl)(methyl)(pyrimidin-5-ylimino)-λ⁶-sulfanone (3aa)

Yellowish oil, 65.2 mg, 99% yield.

1.0 mol% [Ni(dtbbpy)]Br₂; Solvent: 1 mL dry and degassed dimethylacetamide (0.25 M); reaction time: 17 h; Purified *via* automated flash-column chromatography on flash-silica gel (petrolether/ethylacetate, 80% ethylacetate).

¹H NMR (400 MHz, DMSO-*d₆*) δ = 8.60 (s, 1H), 8.25 (s, 2H), 7.92 – 7.86 (m, 2H), 7.21 – 7.11 (m, 2H), 3.83 (s, 3H), 3.50 (s, 3H).

¹³C NMR (101 MHz, DMSO-*d₆*) δ = 163.3 (C$_q$), 150.6 (+), 149.5 (+), 141.2 (C$_q$), 130.5 (+), 128.7 (C$_q$), 115.1 (+), 55.8 (+), 45.3 (+).

HRMS (ESI) (m/z): [M + H]⁺ (C$_{12}$H$_{13}$N$_3$O$_2$S) calc.: 264.0801, found: 264.0805.

(4-Methoxyphenyl)(methyl)(pyrazin-2-ylimino)-λ⁶-sulfanone (3ab)

Yellowish oil, 25.0 mg, 38% yield.

0.5 mol% [Ni(dtbbpy)]Br$_2$; Solvent: 1 mL dry and degassed dimethylacetamide (0.25 M); reaction time: 17 h; Purified *via* automated flash-column chromatography on flash-silica gel (petrolether/ethylacetate, 40% ethylacetate).

^{1}H NMR (400 MHz, DMSO-d_6) δ = 8.13 (d, J = 1.0 Hz, 1H), 7.97 – 7.94 (m, 2H), 7.92 – 7.87 (m, 2H), 7.19 – 7.10 (m, 2H), 3.84 (s, 3H), 3.48 (s, 3H).

^{13}C NMR (101 MHz, DMSO-d_6) δ = 162.9 (C$_q$), 155.7 (C$_q$), 141.4 (+), 139.5 (+), 135.4 (+), 130.4 (C$_q$), 129.7 (+), 114.7 (+), 55.8 (+), 44.9 (+).

HRMS (ESI) (m/z): [M + H]$^+$ (C$_{12}$H$_{13}$N$_3$O$_2$S) calc.: 264.0801, found: 264.0802.

(4-Methoxyphenyl)(methyl)(quinoxalin-6-ylimino)-λ⁶-sulfanone (3ac)

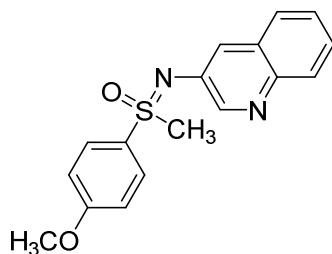

Yellowish oil, 19.6 mg, 25% yield.

1.0 mol% [Ir(ppy)$_2$(dtbbpy)]PF$_6$; 5.0 mol% [Ni(dtbbpy)]Br$_2$; Solvent: 1 mL dry and degassed acetonitrile (0.25 M); reaction time: 17 h; Purified *via* automated flash-column chromatography on flash-silica gel (petrolether/ethylacetate, 60% ethylacetate).

^{1}H NMR (400 MHz, DMSO-d_6) δ = 8.67 (dd, J = 25.4, 1.9 Hz, 2H), 7.95 – 7.88 (m, 2H), 7.84 (d, J = 9.0 Hz, 1H), 7.44 (dd, J = 9.0, 2.5 Hz, 1H), 7.27 (d, J = 2.4 Hz, 1H), 7.17 – 7.09 (m, 2H), 3.80 (s, 3H), 3.49 (s, 3H).

¹³C NMR (101 MHz, DMSO-d_6) δ = 163.1 (C_q), 148.1 (C_q), 145.3 (+), 143.4 (C_q), 142.5 (+), 138.3 (C_q), 130.5 (+), 129.5 (+), 129.2 (C_q), 129.0 (+), 116.5 (+), 115.0 (+), 55.7 (+), 45.7 (+).

HRMS (ESI) (m/z): [M + H]⁺ ($C_{16}H_{15}N_3O_2S$) calc.: 314.0958, found: 314.0960.

(Benzofuran-5-ylimino)(4-methoxyphenyl)(methyl)-λ⁶-sulfanone (3ae)
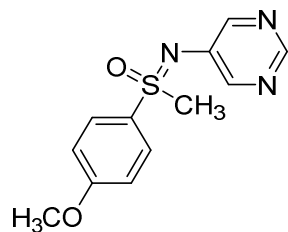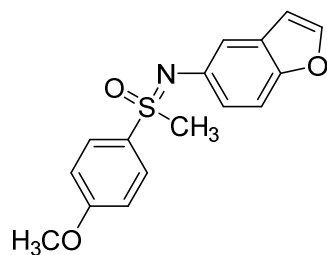

Orange oil, 73.1 mg, 97% yield.

0.5 mol% [Ir(ppy)₂(dtbbpy)]PF₆; 3.0 mol% [Ni(dtbbpy)]Br₂; Solvent: 1 mL dry and degassed dimethylacetamide (0.25 M); reaction time: 17 h; Purified *via* automated flash-column chromatography on flash-silica gel (hexane/ethylacetate, 30% ethylacetate).

¹H NMR (400 MHz, CDCl₃) δ = 7.94 – 7.85 (m, 2H), 7.48 (d, *J* = 2.2 Hz, 1H), 7.26 (d, *J* = 8.7 Hz, 1H), 7.23 (d, *J* = 2.1 Hz, 1H), 7.01 (dd, *J* = 8.7, 2.2 Hz, 1H), 6.99 – 6.91 (m, 2H), 6.58 (dd, *J* = 2.1, 0.9 Hz, 1H), 3.81 (s, 3H), 3.22 (s, 3H).

¹³C NMR (101 MHz, CDCl₃) δ = 163.4 (C_q), 151.1 (C_q), 145.2 (+), 140.5 (C_q), 131.0 (+), 130.6 (C_q), 128.0 (C_q), 121.3 (+), 114.8 (+), 111.5 (+), 106.7 (+), 55.7 (+), 46.3 (+).

HRMS (ESI) (m/z): [M + H]⁺ ($C_{16}H_{15}NO_3S$) calc.: 302.0845, found: 302.0848.

((4-(1,3,4-Oxadiazol-2-yl)phenyl)imino)(4-methoxyphenyl)(methyl)-λ^6-sulfanone (3af)
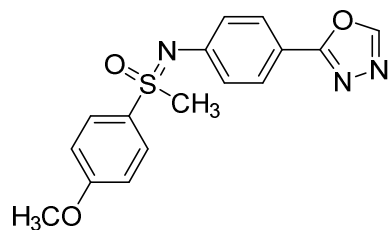
White solid, 81.5 mg, 99% yield.

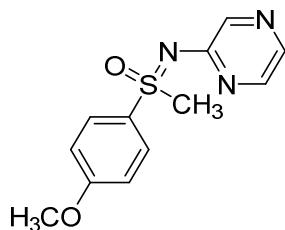Melting point: 133 °C

0.5 mol% [Ir(ppy)$_2$(dtbbpy)]PF$_6$; 2.0 mol% [Ni(dtbbpy)]Br$_2$; Solvent: 1 mL dry and degassed dimethylacetamide (0.25 M); reaction time: 17 h; Purified *via* automated flash-column chromatography on flash-silica gel (petrolether/ethylacetate, 60% ethylacetate).

^{1}H NMR (400 MHz, CDCl$_3$) δ = 8.34 (s, 1H), 7.88 – 7.82 (m, 2H), 7.81 – 7.76 (m, 2H), 7.10 – 7.04 (m, 2H), 6.99 – 6.94 (m, 2H), 3.82 (s, 3H), 3.25 (s, 3H).

^{13}C NMR (101 MHz, CDCl$_3$) δ = 165.0 (C$_q$), 163.8 (C$_q$), 152.1 (+), 149.8 (C$_q$), 130.7 (+), 129.7 (C$_q$), 128.2 (+), 123.3 (+), 116.1 (C$_q$), 115.0 (+), 55.8 (+), 46.9 (+).

HRMS (ESI) (m/z): [M + H]$^+$ (C$_{16}$H$_{15}$N$_3$O$_3$S) calc.: 330.0907, found: 330.0908.

(Benzo[*d*]thiazol-2-ylimino)(4-methoxyphenyl)(methyl)-λ^6-sulfanone (3ag)
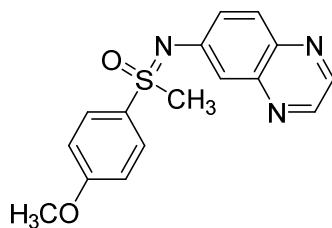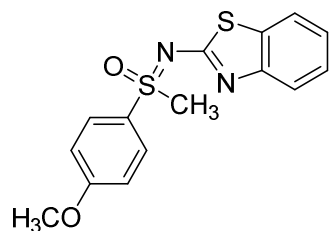

Yellowish oil, 35.0 mg, 44% yield.

2.0 mol% [Ni(dtbbpy)]Br$_2$; Solvent: 1 mL dry and degassed dimethylacetamide (0.25 M); reaction time: 17 h; Purified *via* automated flash-column chromatography on flash-silica gel (petrolether/ethylacetate, 40% ethylacetate).

^{1}H NMR (300 MHz, DMSO-d_6) δ = 7.74 (dd, *J* = 7.9, 0.9 Hz, 1H), 7.47 (dd, *J* = 7.9, 1.0 Hz, 1H), 7.26 (ddd, *J* = 8.2, 7.3, 1.3 Hz, 1H), 7.25 – 7.13 (m, 2H), 7.14 (ddd, *J* = 8.2, 7.4, 1.2 Hz, 1H), 3.85 (s, 3H), 3.63 (s, 3H).

13C NMR (75 MHz, DMSO-d_6) δ = 166.4 (C_q), 163.4 (C_q), 151.5 (C_q), 132.5 (C_q), 130.1 (+), 129.0 (C_q), 125.6 (+), 122.6 (+), 121.2 (+), 119.8 (+), 114.9 (+), 55.9 (+), 44.4 (+).

HRMS (ESI) (m/z): [M + H]$^+$ ($C_{15}H_{14}N_2O_2S_2$) calc.: 319.0569, found: 319.0574.

8-(((4-Methoxyphenyl)(methyl)(oxo)-λ^6-sulfaneylidene)amino)-1,3,7-trimethyl-3,7-dihydro-1*H*-purine-2,6-dione (3ah)
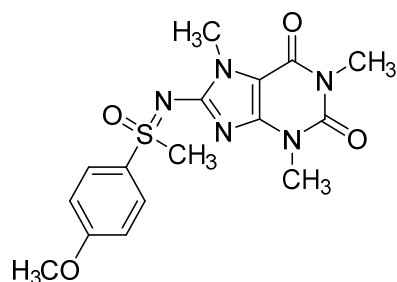
White solid, 27.4 mg, 29% yield.

Melting point: 235 °C

0.15 mol% [Ir(ppy)$_2$(dtbbpy)]PF$_6$; 2.0 mol% [Ni(dtbbpy)]Br$_2$; Solvent: 6 mL dry and degassed dimethylacetamide (0.04 M); reaction time: 17 h; Purified *via* automated flash-column chromatography on flash-silica gel (petrolether/ethylacetate, 60% ethylacetate) and subsequent recrystallization in ethanol.

1H NMR (400 MHz, acetone-d_6) δ = 8.09 – 8.02 (m, 2H), 7.23 – 7.17 (m, 2H), 3.94 (s, 3H), 3.71 (s, 3H), 3.65 (s, 3H), 3.33 (s, 3H), 3.24 (s, 3H).

13C NMR (101 MHz, DMSO-d_6) δ = 163.3 (C_q), 153.5 (C_q), 151.3 (C_q), 150.9 (C_q), 147.0 (C_q), 129.9 (+), 129.8 (C_q), 114.7 (+), 102.7 (C_q), 55.9 (+), 43.9 (+), 30.2 (+), 29.3 (+), 27.3 (+).

HRMS (ESI) (m/z): [M + H]$^+$ ($C_{16}H_{19}N_5O_4S$) calc.: 378.1231, found: 378.1236.

Methyl 4-((cyclopropyl(oxo)(phenyl)-λ⁶-sulfaneylidene)amino)benzoate (3ai)
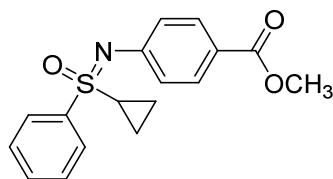
White solid, 77.3 mg, 98% yield.

Melting point: 158 °C

Solvent: 1 mL dry and degassed acetonitrile (0.25 M); reaction time: 17 h; Purified *via* automated flash-column chromatography on flash-silica gel (hexane/ethylacetate, 25% ethylacetate).

¹H NMR (400 MHz, CDCl₃) δ = 7.89 – 7.84 (m, 2H), 7.79 – 7.73 (m, 2H), 7.59 – 7.53 (m, 1H), 7.52 – 7.45 (m, 2H), 7.03 – 6.97 (m, 2H), 3.80 (s, 3H), 2.73 – 2.63 (m, 1H), 1.62 – 1.54 (m, 1H), 1.30 – 1.21 (m, 1H), 1.21 – 1.13 (m, 1H), 1.00 – 0.88 (m, 1H).

¹³C NMR (101 MHz, CDCl₃) δ = 167.2 (C_q), 150.4 (C_q), 139.2 (C_q), 133.3 (+), 130.8 (+), 129.6 (+), 128.7 (+), 122.8 (+), 122.7 (C_q), 51.7 (+), 34.6 (+), 6.8 (-), 5.3 (-).

HRMS (ESI) (m/z): [M + H]⁺ (C₁₇H₁₇NO₃S) calc.: 316.1002, found: 316.1002.

Methyl 4-((oxodiphenyl-λ⁶-sulfaneylidene)amino)benzoate (3aj)

White solid, 85.2 mg, 97% yield.

Melting point: 158 °C

Solvent: 1 mL dry and degassed acetonitrile (0.25 M); reaction time: 17 h; Purified *via* automated flash-column chromatography on flash-silica gel (hexane/ethylacetate, 15% ethylacetate).

¹H NMR (400 MHz, CDCl₃) δ = δ 8.06 – 8.01 (m, 4H), 7.85 – 7.80 (m, 2H), 7.55 – 7.43 (m, 6H), 7.18 – 7.12 (m, 2H), 3.82 (s, 3H).

^{13}C NMR (101 MHz, CDCl$_3$) δ = 167.2 (C$_q$), 150.0 (C$_q$), 140.5 (C$_q$), 133.1 (+), 130.9 (+), 129.5 (+), 128.5 (+), 123.2 (+), 123.2 (C$_q$) 51.8 (+).

HRMS (ESI) (m/z): [M + H]$^+$ (C$_{20}$H$_{17}$NO$_3$S) calc.: 352.1002, found: 352.1009.

Methyl 4-((benzyl(oxo)(phenyl)-λ^6-sulfaneylidene)amino)benzoate (3ak)

Yellowish solid, 80.4 mg, 88% yield.

Melting point: 133 °C

Solvent: 1 mL dry and degassed acetonitrile (0.25 M); reaction time: 17 h; Purified *via* automated flash-column chromatography on flash-silica gel (hexane/ethylacetate, 15% ethylacetate).

^{1}H NMR (400 MHz, CDCl$_3$) δ = 7.86 – 7.77 (m, 2H), 7.61 – 7.56 (m, 2H), 7.56 – 7.49 (m, 1H), 7.41 – 7.34 (m, 2H), 7.32 – 7.27 (m, 1H), 7.24 – 7.16 (m, 2H), 7.11 – 6.94 (m, 4H), 4.63 – 4.48 (m, 2H), 3.82 (s, 3H).

^{13}C NMR (101 MHz, CDCl$_3$) δ = 167.2 (C$_q$), 150.7 (C$_q$), 136.2 (C$_q$), 133.6 (+), 131.4 (+), 130.9 (+), 129.7 (+), 129.2 (+), 129.1 (+), 128.5 (+), 127.9 (C$_q$), 122.9 (C$_q$), 122.7 (+), 63.9 (-), 51.8 (+).

HRMS (ESI) (m/z): [M + H]$^+$ (C$_{21}$H$_{19}$NO$_3$S) calc.: 366.1158, found: 366.1160.

Methyl 4-((methyl(oxo)(*p*-tolyl)-λ⁶-sulfaneylidene)amino)benzoate (3al)

¹H-NMR data are matching with the literature known spectra.[11]
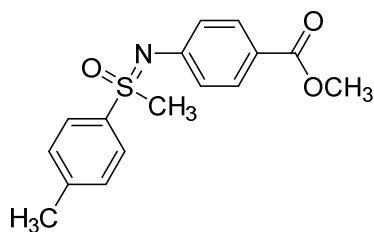
White solid, 75.1 mg, 99% yield.

Solvent: 1 mL dry and degassed acetonitrile (0.25 M); reaction time: 17 h; Purified *via* automated flash-column chromatography on flash-silica gel (petrolether/ethylacetate, 25% ethylacetate).

¹H NMR (400 MHz, CDCl₃) δ = 7.82 – 7.75 (m, 4H), 7.32 – 7.27 (m, 2H), 7.02 – 6.94 (m, 2H), 3.80 (s, 3H), 3.24 (s, 3H), 2.39 (s, 3H).

Methyl 4-(((4-fluorophenyl)(methyl)(oxo)-λ⁶-sulfaneylidene)amino)benzoate (3am)
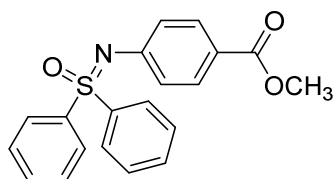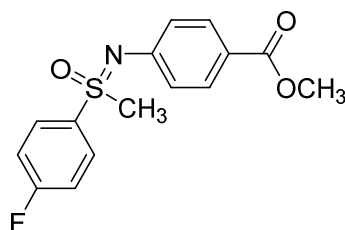

Yellowish oil, 76.1 mg, 99% yield.

Solvent: 1 mL dry and degassed acetonitrile (0.25 M); reaction time: 17 h; Purified *via* automated flash-column chromatography on flash-silica gel (petrolether/ethylacetate, 30% ethylacetate).

¹H NMR (300 MHz, CDCl₃) δ = 8.00 – 7.90 (m, 2H), 7.84 – 7.76 (m, 2H), 7.24 – 7.16 (m, 2H), 7.03 – 6.92 (m, 2H), 3.82 (s, 3H), 3.28 (s, 3H).

¹³C NMR (75 MHz, CDCl₃) δ = 167.1 (C$_q$), 165.9 (C$_q$, d, J = 256.5 Hz), 149.9 (C$_q$), 134.7 (C$_q$, d, J = 3.2 Hz), 131.5 (+), 131.4 (+), 131.0 (+), 123.3 (C$_q$), 122.6 (+), 117.3 (+), 117.0 (+), 51.9 (+), 46.6 (+).

¹⁹F NMR (282 MHz, CDCl₃) δ = -104.2.

HRMS (ESI) (m/z): [M + H]$^+$ (C$_{15}$H$_{14}$FNO$_3$S) calc.: 308.0751, found: 308.0756.

Methyl 4-(((4-chlorophenyl)(methyl)(oxo)-λ^6-sulfaneylidene)amino)benzoate (3an)
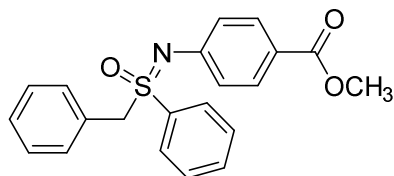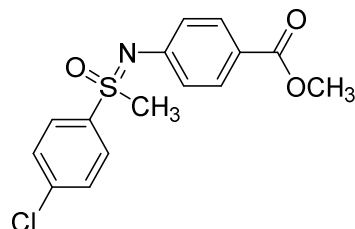

Yellowish oil, 80.1 mg, 99% yield.

Solvent: 1 mL dry and degassed acetonitrile (0.25 M); reaction time: 17 h; Purified *via* automated flash-column chromatography on flash-silica gel (petrolether/ethylacetate, 30% ethylacetate).

^{1}H NMR (300 MHz, CDCl$_3$) δ = 7.92 – 7.85 (m, 2H), 7.84 – 7.78 (m, 2H), 7.54 – 7.46 (m, 2H), 7.03 – 6.94 (m, 2H), 3.83 (s, 3H), 3.29 (s, 3H).

^{13}C NMR (75 MHz, CDCl$_3$) δ = 167.1 (C$_q$), 149.7 (C$_q$), 140.6 (C$_q$), 137.2 (C$_q$), 131.0 (+), 130.2 (+), 130.2 (+), 123.5 (C$_q$), 122.6 (+), 51.9 (+), 46.5 (+).

HRMS (ESI) (m/z): [M + H]$^+$ (C$_{15}$H$_{14}$ClNO$_3$S) calc.: 324.0456, found: 324.0459.

Methyl 4-(((4-cyanophenyl)(methyl)(oxo)-λ^6-sulfaneylidene)amino)benzoate (3ao)

Yellowish oil, 71.5 mg, 91% yield.

Solvent: 1 mL dry and degassed acetonitrile (0.25 M); reaction time: 17 h; Purified *via* automated flash-column chromatography on flash-silica gel (petrolether/ethylacetate, 45% ethylacetate).

^{1}H NMR (400 MHz, CDCl$_3$) δ = 8.08 – 8.00 (m, 2H), 7.85 – 7.73 (m, 4H), 7.00 – 6.92 (m, 2H), 3.81 (s, 3H), 3.29 (s, 3H).

¹³C NMR (101 MHz, CDCl₃) δ = 166.9 (C_q), 149.3 (C_q), 143.5 (C_q), 133.5 (+), 131.0 (+), 129.4 (+), 123.8 (C_q), 122.6 (+), 117.5 (C_q), 117.1 (C_q), 51.9 (+), 46.0 (+).

HRMS (ESI) (m/z): [M + H]⁺ ($C_{16}H_{14}N_2O_3S$) calc.: 315.0798, found: 315.0803.

Methyl 4-((methyl(oxo)(pyridin-3-yl)-λ⁶-sulfaneylidene)amino)benzoate (3ap)

Yellowish crystals, 44.3 mg, 61% yield.

Melting point: 144 °C

Solvent: 1 mL dry and degassed acetonitrile (0.25 M); reaction time: 17 h; Purified *via* automated flash-column chromatography on flash-silica gel (petrolether/ethylacetate, 60% ethylacetate).

¹H NMR (400 MHz, DMSO-d_6) δ = 8.76 (d, *J* = 4.3 Hz, 1H), 8.19 (dt, *J* = 7.9, 1.1 Hz, 1H), 8.14 (td, *J* = 7.7, 1.7 Hz, 1H), 7.73 – 7.65 (m, 3H), 6.97 – 6.90 (m, 2H), 3.75 (s, 3H), 3.52 (s, 3H).

¹³C NMR (101 MHz, DMSO-d_6) δ = 166.0 (C_q), 156.2 (C_q), 150.7 (C_q), 150.5 (+), 138.9 (+), 130.4 (+), 127.7 (+), 123.4 (+), 121.9 (+), 121.8 (C_q), 51.7 (+), 41.6 (+).

HRMS (ESI) (m/z): [M + H]⁺ ($C_{14}H_{14}N_2O_3S$) calc.: 291.0798, found: 291.0801

Methyl 4-((methyl(oxo)(thiazol-2-yl)-λ⁶-sulfaneylidene)amino)benzoate (3aq)

Yellowish crystals, 34.8 mg, 47% yield.

Melting point: 131 °C

0.5 mol% [Ir(ppy)$_2$(dtbbpy)]PF$_6$; 1.0 mol% [Ni(dtbbpy)]Br$_2$; Solvent: 1 mL dry and degassed dimethylacetamide (0.25 M); reaction time: 17 h; Purified *via* automated flash-column chromatography on flash-silica gel (petrolether/ethylacetate, 55% ethylacetate).

¹H NMR (400 MHz, CDCl$_3$) δ = 7.99 (d, *J* = 3.1 Hz, 1H), 7.86 – 7.82 (m, 2H), 7.68 (d, *J* = 3.0 Hz, 1H), 7.13 – 7.08 (m, 2H), 3.84 (s, 3H), 3.52 (s, 3H).

¹³C NMR (101 MHz, CDCl$_3$) δ = 167.1 (C$_q$), 165.6 (C$_q$), 148.7 (C$_q$), 145.2 (+), 131.0 (+), 126.8 (+), 124.5 (C$_q$), 123.3 (+), 52.0 (+), 44.8 (+).

HRMS (ESI) (m/z): [M + H]$^+$ (C$_{12}$H$_{12}$N$_2$O$_3$S$_2$) calc.: 297.0362, found: 297.0366.

Methyl 4-((dimethyl(oxo)-λ⁶-sulfaneylidene)amino)benzoate (3ar)
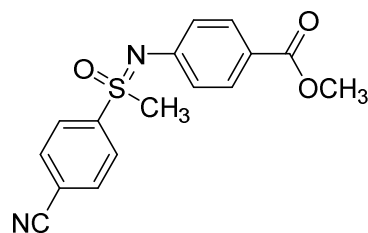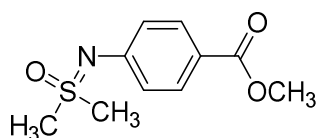

Colorless oil, 56.3 mg, 99% yield.

Solvent: 1 mL dry and degassed acetonitrile (0.25 M); reaction time: 17 h; Purified *via* automated flash-column chromatography on flash-silica gel (petrolether/ethylacetate, 60% ethylacetate).

¹H NMR (400 MHz, CDCl$_3$) δ = 7.94 – 7.87 (m, 2H), 7.12 – 7.06 (m, 2H), 3.87 (s, 3H), 3.20 (s, 6H).

¹³C NMR (101 MHz, CDCl$_3$) δ = 167.2 (C$_q$), 150.3 (C$_q$), 131.2 (+), 123.6 (C$_q$), 122.5 (+), 52.0 (+), 42.5 (+).

HRMS (ESI) (m/z): [M + H]$^+$ (C$_{10}$H$_{13}$NO$_3$S) calc.: 228.0689, found: 228.0688.

Methyl 4-((1-oxidotetrahydro-1λ^6-thiophen-1-ylidene)amino)benzoate (3as)
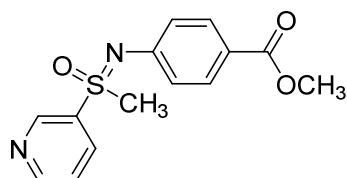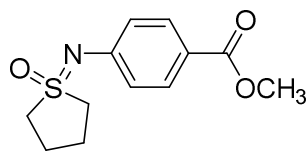

Yellowish oil, 60.8 mg, 96% yield.

Solvent: 1 mL dry and degassed acetonitrile (0.25 M); reaction time: 17 h; Purified *via* automated flash-column chromatography on flash-silica gel (hexane/ethylacetate, 30% ethylacetate).

^{1}H NMR (400 MHz, CDCl$_3$) δ = 7.94 – 7.87 (m, 2H), 7.08 – 7.01 (m, 2H), 3.87 (s, 3H), 3.48 – 3.38 (m, 2H), 3.28 – 3.15 (m, 2H), 2.42 – 2.17 (m, 4H).

^{13}C NMR (101 MHz, CDCl$_3$) δ = 167.2 (C$_q$), 151.2 (C$_q$), 131.2 (+), 123.1 (C$_q$), 121.9 (+), 53.1 (+), 51.9 (-), 24.0 (-).

HRMS (ESI) (m/z): [M + H]$^+$ (C$_{12}$H$_{15}$NO$_3$S) calc.: 254.0845, found: 254.0850.

Methyl(phenyl)((4-(trifluoromethyl)phenyl)imino)-λ⁶-sulfanone (3at)

¹H-NMR data are matching with the literature known spectra.[12]

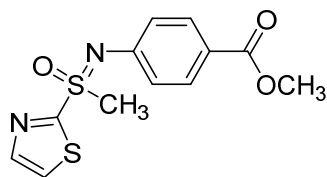Colorless oil, 67.3 mg, 90% yield.

Solvent: 1 mL dry and degassed acetonitrile (0.25 M); reaction time: 17 h; Purified *via* automated flash-column chromatography on flash-silica gel (petrolether/ethylacetate, 20% ethylacetate).

(Chiralpak AS-H, *n*-heptane/*iso*-propanol = 95/5, 1.0 mL/min, 254 nm): t_R = 12.00 min, 16.99 min.

For chiral HPLC trace see appendix section 6.3.1, Figure 26.

¹H NMR (400 MHz, CDCl₃) δ = 7.99 – 7.91 (m, 2H), 7.66 – 7.49 (m, 3H), 7.38 – 7.31 (m, 2H), 7.12 – 7.01 (m, 2H), 3.26 (s, 3H).

(*S*)-Methyl(phenyl)((4-(trifluoromethyl)phenyl)imino)-λ⁶-sulfanone ((*S*)-3at)

Colorless oil, 59.9 mg, 80% yield.

Solvent: 1 mL dry and degassed acetonitrile (0.25 M); reaction time: 17 h; Purified *via* automated flash-column chromatography on flash-silica gel (petrolether/ethylacetate, 20% ethylacetate).

(Chiralpak AS-H, *n*-heptane/*iso*-propanol = 95/5, 1.0 mL/min, 254 nm): t_R = 16.57 min.

For chiral HPLC trace see appendix section 6.3.1, Figure 27.

tert-Butyl 6-((methyl(oxo)(phenyl)-λ⁶-sulfaneylidene)amino)-1*H*-indole-1-carboxylate (3au)
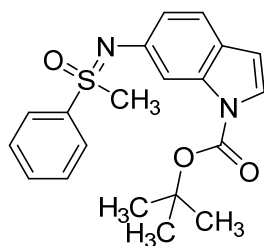

Colorless oil, 88.9 mg, 96% yield.

0.5 mol% [Ir(ppy)$_2$(dtbbpy)]PF$_6$; 5.0 mol% [Ni(dtbbpy)]Br$_2$. Solvent: 1 mL dry and degassed dimethylacetamide (0.25 M); reaction time: 17 h; Purified *via* automated flash-column chromatography on flash-silica gel (hexane/ethylacetate, 30% ethylacetate).

(Chiralpak AS-H, *n*-heptane/*iso*-propanol = 95/5, 1.0 mL/min, 215 nm): t_R = 16.87 min, 18.91 min.

For chiral HPLC trace see appendix section 6.3.1, Figure 28.

¹H NMR (400 MHz, CDCl$_3$) δ = 8.04 – 7.98 (m, 2H), 7.86 (s, 1H), 7.58 – 7.40 (m, 4H), 7.30 (d, *J* = 8.3 Hz, 1H), 6.98 (dd, *J* = 8.3, 2.0 Hz, 1H), 6.41 (dd, *J* = 3.7, 0.8 Hz, 1H), 3.24 (s, 3H), 1.65 (s, 9H).

¹³C NMR (101 MHz, CDCl$_3$) δ = 150.0 (C$_q$), 142.2 (C$_q$), 139.6 (C$_q$), 135.9 (C$_q$), 133.2 (+), 129.5 (+), 128.8 (+), 125.6 (C$_q$), 124.9 (+), 121.0 (+), 119.8 (+), 110.0 (+), 107.2 (+), 83.5 (C$_q$), 45.9 (+), 28.3 (+).

HRMS (ESI) (m/z): [M + H]$^+$ (C$_{20}$H$_{22}$N$_2$O$_3$S) calc.: 371.1424, found: 371.1429.

tert-**Butyl** **(*S*)-6-((methyl(oxo)(phenyl)-λ⁶-sulfaneylidene)amino)-1*H*-indole-1-carboxylate ((*S*)-3au)**
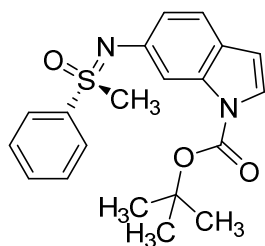
Colorless oil, 71.3 mg, 77% yield.

0.5 mol% [Ir(ppy)₂(dtbbpy)]PF₆; 5.0 mol% [Ni(dtbbpy)]Br₂. Solvent: 1 mL dry and degassed dimethylacetamide (0.25 M); reaction time: 17 h; Purified *via* automated flash-column chromatography on flash-silica gel (petrolether/ethylacetate, 30% ethylacetate).
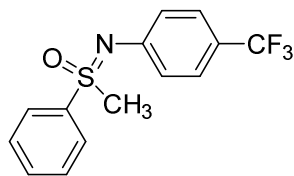
(Chiralpak AS-H, *n*-heptane/*iso*-propanol = 95/5, 1.0 mL/min, 215 nm): t$_R$ = 18.80 min.

For chiral HPLC trace see appendix section 6.3.1, Figure 29.

Methyl(phenyl)(quinolin-3-ylimino)-λ⁶-sulfanone (3av)
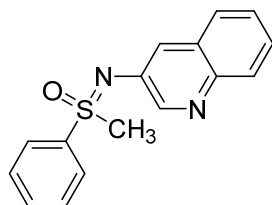
Orange oil, 69.2 mg, 98% yield.

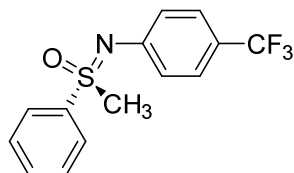1.0 mol% [Ir(ppy)₂(dtbbpy)]PF₆; 5.0 mol% [Ni(dtbbpy)]Br₂. Solvent: 1 mL dry and degassed dimethylacetamide (0.25 M); reaction time: 17 h; Purified *via* automated flash-column chromatography on flash-silica gel (hexane/ethylacetate, 70% ethylacetate).

(Chiralpak AS-H, *n*-heptane/*iso*-propanol = 70/30 + 0.5v% diethylamine, 0.5 mL/min, 254 nm): t$_R$ = 18.76 min, 22.32 min.

For chiral HPLC trace see appendix section 6.3.1, Figure 30.

¹H NMR (400 MHz, CDCl₃) δ = 8.71 (d, *J* = 2.6 Hz, 1H), 8.02 – 7.97 (m, 2H), 7.93 (d, *J* = 8.4 Hz, 1H), 7.61 – 7.50 (m, 5H), 7.49 – 7.44 (m, 1H), 7.42 – 7.35 (m, 1H), 3.33 (s, 3H).

¹³C NMR (101 MHz, CDCl₃) δ = 149.8 (+), 144.0 (C_q), 139.2 (C_q), 138.6 (C_q), 133.8 (+), 129.9 (+), 129.0 (+), 128.8 (C_q), 128.7 (+), 127.0 (+), 126.9 (+), 126.7 (+), 124.4 (+), 46.3 (+).

HRMS (ESI) (m/z): [M + H]⁺ ($C_{16}H_{14}N_2OS$) calc.: 283.0900, found: 283.0901.

(*S*)-Methyl(phenyl)(quinolin-3-ylimino)-λ⁶-sulfanone ((*S*)-3av)
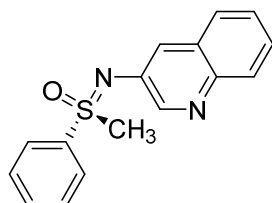
Orange oil, 69.7 mg, 99% yield.

1.0 mol% [Ir(ppy)₂(dtbbpy)]PF₆; 5.0 mol% [Ni(dtbbpy)]Br₂. Solvent: 1 mL dry and degassed dimethylacetamide (0.25 M); reaction time: 17 h; Purified *via* automated flash-column chromatography on flash-silica gel (petrolether/ethylacetate, 70% ethylacetate).

(Chiralpak AS-H, *n*-heptane/*iso*-propanol = 70/30 + 0.5v% diethylamine, 0.5 mL/min, 254 nm): t_R = 22.17 min.

For chiral HPLC trace see appendix section 6.3.1, Figure 31.

Methyl(phenyl)((4-(trifluoromethyl)pyridin-2-yl)imino)-λ⁶-sulfanone (3aw)

White solid, 29.3 mg, 39% yield.

Melting point: 98 °C

0.5 mol% [Ir(ppy)₂(dtbbpy)]PF₆; 1.0 mol% [Ni(dtbbpy)]Br₂. Solvent: 1 mL dry and degassed dimethylacetamide (0.25 M); reaction time: 17 h; Purified *via* automated flash-column chromatography on flash-silica gel (petrolether/ethylacetate, 25% ethylacetate).

(Chiralpak AS-H, *n*-heptane/*iso*-propanol = 95/5, 1.0 mL/min, 254 nm): t_R = 15.28 min, 20.47 min.

For chiral HPLC trace see appendix section 6.3.1, Figure 33.

¹H NMR (400 MHz, CDCl₃) δ = 8.18 (d, *J* = 5.3 Hz, 1H), 8.04 – 7.95 (m, 2H), 7.67 – 7.60 (m, 1H), 7.56 (ddt, *J* = 8.3, 6.3, 1.5 Hz, 2H), 7.08 (s, 1H), 6.94 – 6.86 (m, 2H), 3.38 (s, 3H).

¹³C NMR (101 MHz, CDCl₃) δ = 160.0 (C$_q$), 148.9 (+), 140.0 (C$_q$, q, *J* = 33.5 Hz), 139.8 (C$_q$), 133.4 (+), 129.7 (+), 127.8 (+), 123.1 (C$_q$, q, *J* = 273.2 Hz), 113.0 (+, q, *J* = 4.0 Hz), 111.4 (+, q, *J* = 3.4 Hz), 45.6 (+).

¹⁹F NMR (377 MHz, CDCl₃) δ = -65.6.

HRMS (ESI) (m/z): [M + H]⁺ (C$_{13}$H$_{11}$F$_3$N$_2$OS) calc.: 301.0617, found: 301.0621.

### (*S*)-Methyl(phenyl)((4-(trifluoromethyl)pyridin-2-yl)imino)-λ⁶-sulfanone ((*S*)-3aw)
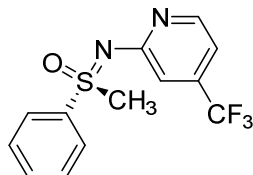
Orange oil, 42.8 mg, 57% yield.

0.5 mol% [Ir(ppy)₂(dtbbpy)]PF₆; 1.0 mol% [Ni(dtbbpy)]Br₂. Solvent: 1 mL dry and degassed dimethylacetamide (0.25 M); reaction time: 17 h; Purified *via* automated flash-column chromatography on flash-silica gel (petrolether/ethylacetate, 25% ethylacetate).

(Chiralpak AS-H, *n*-heptane/*iso*-propanol = 95/5, 1.0 mL/min, 254 nm): t$_R$ = 20.25 min.

For chiral HPLC trace see appendix section 6.3.1, Figure 33.

((4-(1,3,4-Oxadiazol-2-yl)phenyl)imino)(methyl)(phenyl)-λ⁶-sulfanone (3ax)
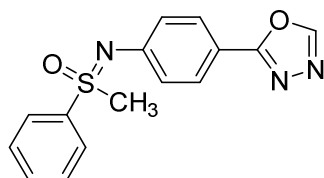
Orange oil, 72.6 mg, 97% yield.

0.5 mol% [Ir(ppy)₂(dtbbpy)]PF₆; 2.0 mol% [Ni(dtbbpy)]Br₂. Solvent: 1 mL dry and degassed dimethylacetamide (0.25 M); reaction time: 17 h; Purified *via* automated flash-column chromatography on flash-silica gel (hexane/ethylacetate, 50% ethylacetate).

(Lux Cellulose-1, *n*-heptane/ *iso*-propanol = 50/50 + 0.5vol% diethylamine, 0.5 mL/min, 254 nm): t_R = 16.46 min, 18.04 min.

For chiral HPLC trace see appendix section 6.3.1, Figure 34.

¹H NMR (400 MHz, CDCl₃) δ = 8.35 (s, 1H), 7.99 – 7.93 (m, 2H), 7.85 – 7.79 (m, 1H), 7.65 – 7.58 (m, 1H), 7.57 – 7.49 (m, 2H), 7.12 – 7.05 (m, 2H), 3.29 (s, 3H).

¹³C NMR (101 MHz, CDCl₃) δ = 165.0 (C$_q$), 152.1 (+), 149.5 (C$_q$), 138.8 (C$_q$), 133.8 (+), 129.9 (+), 128.6 (+), 128.3 (+), 123.4 (+), 116.4 (C$_q$), 46.5 (+).

HRMS (ESI) (m/z): [M + H]⁺ (C₁₅H₁₃N₃O₂S) calc.: 300.0801, found: 300.0810.

(*S*)-((4-(1,3,4-Oxadiazol-2-yl)phenyl)imino)(methyl)(phenyl)-λ⁶-sulfanone ((*S*)-3ax)
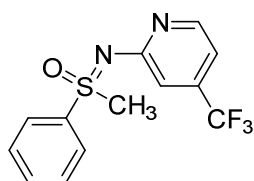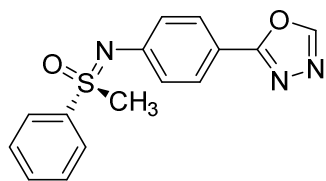

Orange oil, 73.9 mg, 99% yield.

0.5 mol% [Ir(ppy)₂(dtbbpy)]PF₆; 2.0 mol% [Ni(dtbbpy)]Br₂. Solvent: 1 mL dry and degassed dimethylacetamide (0.25 M); reaction time: 17 h; Purified *via* automated flash-column chromatography on flash-silica gel (petrolether/ethylacetate, 50% ethylacetate).

(Cellulose-1, *n*-heptane/*iso*-propanol = 50/50 + 0.5vol% diethylamine, 0.5 mL/min, 254 nm): t_R = 17.99 min.

For chiral HPLC trace see appendix section 6.3.1, Figure 35.

2.7.3.5   Procedure for the N-Arylation of Sulfoximidoyl Derivatives 4 and 6

Methyl-4-((*p*-tolylsulfinyl)amino)benzoate (5)

p-Toluenesulfinamide (**4**) (38.8 mg, 0.25 mmol, 1.0 equiv.) was used as sulfoximidoyl derivative instead of *NH*-sulfoximines and reacted as described in the general procedure for *NH*-sulfoximines.
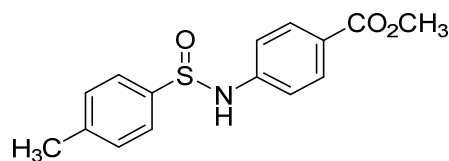
White crystals, 67.3 mg, 93% yield.

Melting point: 126 °C

0.5 mol% [Ir(ppy)$_2$(dtbbpy)]PF$_6$; 2.0 mol% [Ni(dtbbpy)]Br$_2$. Solvent: 1 mL dry and degassed acetonitrile (0.25 M); reaction time: 17 h; Purified *via* automated flash-column chromatography on flash-silica gel (petrolether/ethylacetate, 20% ethylacetate).

^{1}H NMR (300 MHz, DMSO-d_6) δ = 9.84 (s, 1H), 7.88 – 7.80 (m, 2H), 7.67 – 7.57 (m, 2H), 7.45 – 7.37 (m, 2H), 7.22 – 7.13 (m, 2H), 3.79 (s, 3H), 2.38 (s, 3H).

^{13}C NMR (75 MHz, DMSO-d_6) δ = 165.9 (C$_q$), 146.8 (C$_q$), 141.4 (C$_q$), 140.9 (C$_q$), 130.8 (+), 129.7 (+), 125.5 (+), 122.5 (C$_q$), 116.2 (+), 51.8 (+), 20.9 (+).

HRMS (ESI) (m/z): [M + H]$^+$ (C$_{15}$H$_{15}$NO$_3$S) calc.: 290.0845, found: 290.0848.

Methyl 4-((oxo(phenyl)(piperidin-1-yl)-λ^6-sulfaneylidene)amino)benzoate (7)

^{1}H-NMR data are matching with the literature known spectra.[13]

1-(Phenylsulfonimidoyl)piperidine (**C-3**) (56.1 mg, 0.25 mmol, 1.0 equiv.) was used as sulfoximidoyl derivative instead of *NH*-sulfoximines and reacted as described in the general procedure for *NH*-sulfoximines.
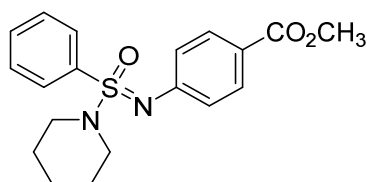
White solid, 86.0 mg, 96% yield.

0.5 mol% [Ir(ppy)$_2$(dtbbpy)]PF$_6$; 1.0 mol% [Ni(dtbbpy)]Br$_2$. Solvent: 1 mL dry and degassed acetonitrile (0.25 M); reaction time: 17 h; Purified *via* automated flash-column chromatography on flash-silica gel (petrolether/ethylacetate, 10% ethylacetate).

^{1}H NMR (400 MHz, CDCl$_3$) δ = 8.00 – 7.88 (m, 4H), 7.64 – 7.50 (m, 3H), 7.28 – 7.24 (m, 2H), 3.88 (s, 3H), 3.07 (ddd, J = 11.2, 7.0, 3.9 Hz, 2H), 2.98 (ddd, J = 11.4, 7.0, 3.9 Hz, 2H), 1.61 – 1.43 (m, 4H), 1.36 (quint., J = 5.7 Hz, 2H).

2.7.4 Procedure for the *N*-Arylation Reaction of *NH*-Sulfoximines in Preparative-Scale

(4-Methoxyphenyl)(methyl)((4-(trifluoromethyl)phenyl)imino)-λ^6-sulfanone (3a)
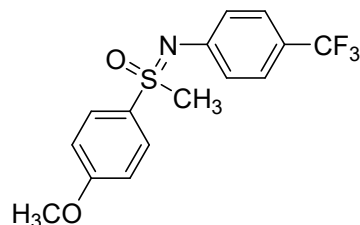
The large-scale synthesis of *N*-arylated sulfoximine **3a** was performed in the custom-built batch-reactor, which is depicted in section 2.7.1, Figure 15.

Compartment 1 was charged with 5.0 g of *NH*-sulfoximine **1a** (27.0 mmol, 1.0 equiv.), 37.0 mg of [Ir(ppy)$_2$(dtbbpy)]PF$_6$ (0.04 mmol, 0.15 mol%) and 26.3 mg [Ni(dtbbpy)]Br$_2$ (0.05 mmol, 0.20 mol%) and a magnetic stirring bar. The closed apparatus was degassed *via* three cycles of vacuum/nitrogen (2 min. at 7 mbar/2 min. flush with nitrogen atmosphere). After that, 4.2 mL bromo arene **2a** (29.7 mmol, 1.1 equiv.), 4.1 mL of tetramethylguanidine (32.4 mmol, 1.2 equiv.) and 108 mL dry and degassed acetonitrile were added *via* syringe under nitrogen atmosphere. The reaction mixture was stirred and irradiated, using blue LEDs (455 nm) for 17 hours at 25 °C. The reaction mixture was diluted with brine (250 mL) and extracted three times with ethylacetate (3 x 150 mL). The combined organic layers were dried with Na$_2$SO$_4$, filtered and the solvent was removed under reduced pressure. Evaporation of volatiles led to the crude product. Purification was performed *via* automated flash-column chromatography on flash-silica gel (petrolether/ethylacetate, 30% ethylacetate), affording 8.8 g of the corresponding *N*-arylated sulfoximine **3a** (99%).

2.7.5 NMR Spectra

All NMR spectra can be found in the appendix in the section 6.3.2.

2.7.6 References

[1]   a) R. K. Harris, E. D. Becker, S. M. Cabral de Menezes, R. Goodfellow, P. Granger, Magn. Reson. Chem., 2002, 40, 489-505; b) H. E. Gottlieb, V. Kotlyar, A. Nudelman, J. Org. Chem., 1997, 62, 7512-7515; c) G. R. Fulmer, A. J. M. Miller, N. H. Sherden, H. E. Gottlieb, A. Nudelman, B. M. Stoltz, J. E. Bercaw, K. I. Goldberg, Organometallics, 2010, 29, 2176-2179.

[2]   a) S. Sprouse, K. A. King, P. J. Spellane, R. J. Watts, J. Am. Chem. Soc., 1984, 106, 6647-6653; b) H. Ye, Q. Ye, D. Cheng, X. Li, X. Xu, Tetrahedron Lett., 2018, 59, 2046-2049.

[3]   K. Yahata, N. Ye, Y. Ai, K. Iso, Y. Kishi, Angew. Chem. Int. Ed., 2017, 56, 10796-10800.

[4]   J. Wang, J. Zhang, K. Miao, H. Yun, H. C. Shen, W. Zhao, C. Liang, Tetrahedron Lett., 2017, 58, 333-337.

[5]   J.-F. Lohier, T. Glachet, H. Marzag, A.-C. Gaumont, V. Reboul, Chem. Commun., 2017, 53, 2064-2067.

[6]   M. Zenzola, R. Doran, L. Degennaro, R. Luisi, J. A. Bull, Angew. Chem. Int. Ed., 2016, 55, 7203-7207.

[7]   A. Tota, M. Zenzola, S. J. Chawner, S. S. John-Campbell, C. Carlucci, G. Romanazzi, L. Degennaro, J. A. Bull, R. Luisi, Chemical Communications, 2017, 53, 348-351.

[8]   A. U. Meyer, A. Wimmer, B. König, Angew. Chem. Int. Ed., 2017, 56, 409-412.

[9]   F. Izzo, M. Schäfer, R. Stockman, U. Lücking, Chem. Eur. J., 2017, 23, 15189-15193.

[10] J. Kim, J. Ok, S. Kim, W. Choi, P. H. Lee, Org. Lett., 2014, 16, 4602-4605.

[11] C. Bolm, J. P. Hildebrand, J. Org. Chem., 2000, 65, 169-175.

[12] P. M. Matos, W. Lewis, J. C. Moore, R. A. Stockman, Org. Lett., 2018, 20, 3674-3677.

[13] F. Izzo, M. Schäfer, P. Lienau, U. Ganzer, R. Stockman, U. Lücking, Chem. Eur. J., 2018, 24, 9295-9304.

3. CO₂ or SO₂: Should It Stay, or Should It Go?

Two oxidative approaches to radical formation

$R-C(=O)OH \xrightarrow[-H^+]{-e^-} R-C(=O)O^\bullet \xrightarrow{-CO_2} R^\bullet$ general

$R-S(=O)OH \xrightarrow[-H^+]{-e^-} R-S(=O)O^\bullet \xrightarrow[-SO_2]{} $ depends on R

$CH_3 < CH_2F < CHF_2 < CF_3$

ΔG

$R\!\!-\!\!XO_2H$ vs $R\!\!-\!\!XO_2^\bullet$

$R = Ar, Alk, Alk_F$

X=C

X=S

<40

X=S

BDE drop, kcal/mol: >100

X=C

unfavorable

favorable
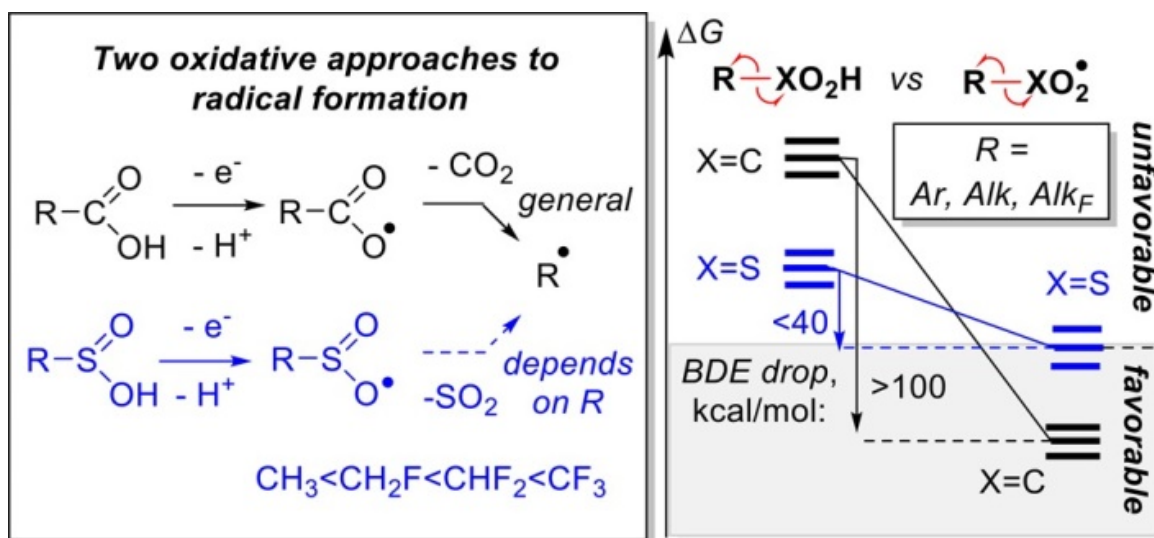
CHAPTER 3

3.1   Abstract

A broad computational analysis of carbon-centered radical formation *via* the loss of either CO_2 or SO_2 from the respective RXO_2 radical precursors (X = C or S) reveals dramatic differences between these two types of dissociative processes.

Whereas the C–C scission with the loss of CO_2 is usually exothermic, the C–S scission with loss of SO_2 is generally endothermic. However, two factors can make the C–S scission thermodynamically favorable: increased entropy, characteristic for the dissociative processes, and stereoelectronic influences of substituents. The threshold between endergonic and exergonic C–S fragmentations depends on subtle structural effects. In particular, the degree of fluorination in a radical precursor has notable impact on the reaction outcome.

In a synthetic section we try to validate the computational predictions for SO_2 retention or extrusion upon single-electron oxidation of various fluoroalkyl sulfinate anions.

The study aims to demystify the intricacies in reactivity regarding the generation of radicals from sulfinates and carboxylates as related to their role in radical cross-coupling.

Author contributions:

AW and GPG wrote the introduction (section 3.2). Collection of all computational data and its evaluation and discussion (section 3.3 and 3.4) was done by GPG under the supervision of JMS and IVA. Synthetic experimentation and discussion (section 3.5) was contributed by AW under the supervision of BK.

3.2   Introduction

In chemical synthesis, the ability to harness various functional handles for controlled and chemoselective transformations is of paramount importance.[1] In turn, making use of functional groups that are endogenous to cheap carbon feedstocks gives leverage to synthetic chemists for exploiting the most efficacious retrosynthetic disconnections.[2] This certainty allows practitioners to avoid functional group interconversion, protecting groups, and lengthy, circuitous assembly of carbogenic skeletons. To this end, the radical cross-coupling of both carboxylic acids and sulfinate[3] salts has emerged as a powerful tool for the concise synthesis of complex molecules both of historical and translational importance.[2c]
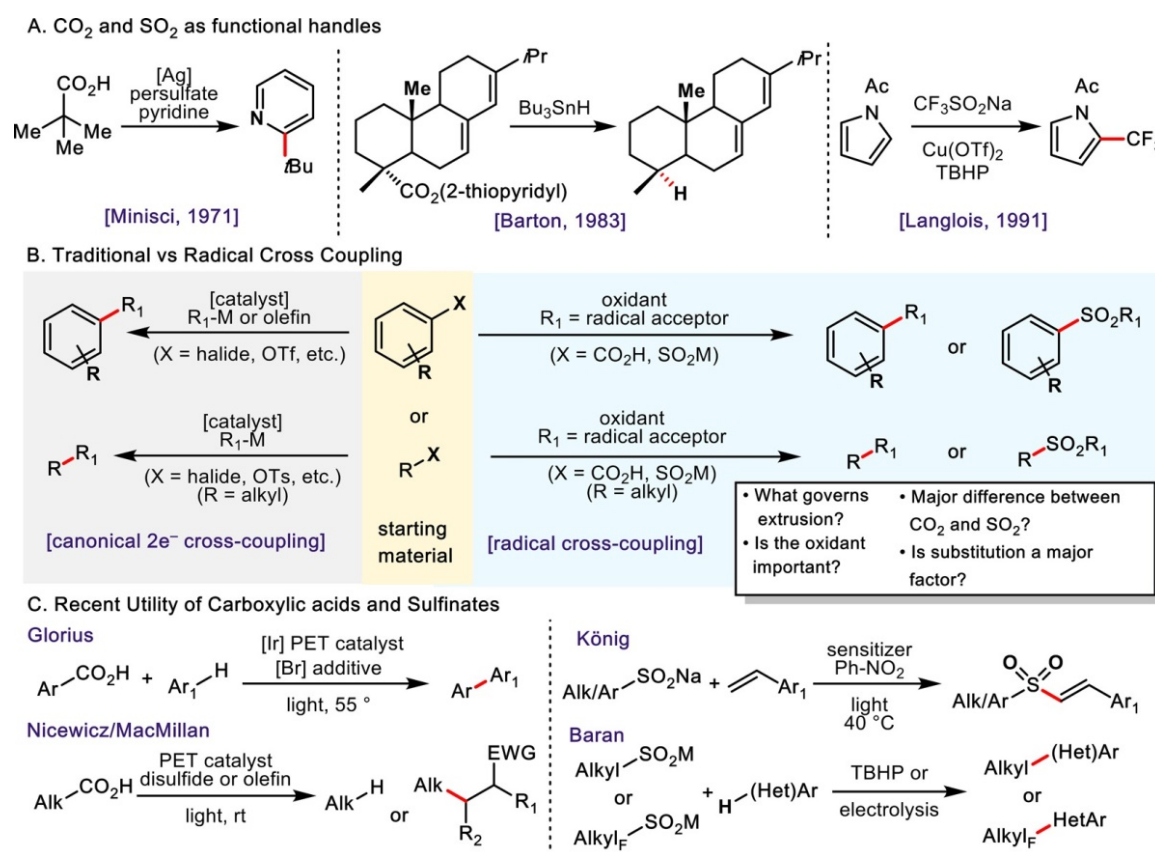
Scheme 10. (**A**) Historic examples of utilizing carboxylic acids and sulfinates as synthetic hands. (**B**) Traditional cross-coupling compared to decarboxylative and desulfonylative radical cross-coupling. (**C**) Selected literature reports of (photo)oxidative coupling reactions with aryl and alkyl carboxylates and sulfinate salts. Abbreviations: B = base; Ar = aryl; AlkylF = fluorinated alkyls; (Het)Ar = heteroarenes.

Since the mid-19th century, carboxylic acids have had a special role as abundant and ubiquitous starting materials for effective tactical and strategic synthesis.[4] With regard to carboxylic acids serving as progenitors for carbon-centered radicals, the work of Minisci pioneered their utilization in the functionalization of electron-poor arenes (Scheme 10A).[5] As this reaction was revolutionary for its day, radical decarboxylation has seen a resurgence in recent years, both from the direct oxidative decarboxylation of acids[6] and the reductive manipulation of redox-active esters akin to the pioneering Sn-mediated work of Barton in 1983.[7] As a parallel, a synthetic relative to the carboxylate is the sulfinate, which Langlois exploited in the early 1990s for the C–H trifluoromethylation of arenes.[8] This technology was later popularized and made broadly useful by Baran in recent years.[9] Principally, the utilization of both sulfinates and carboxylic acids in radical cross-coupling has shown important advantages over canonical cross-coupling tactics.

As traditional cross-coupling typically utilizes a starting halide or pseudohalide combined with an organometallic coupling partner, the radical cross-coupling of sulfinates and carboxylic acids most often employs a radical acceptor as the reactive partner (Scheme 10B).[10] Intriguingly, the nature of the arene or alkyl unit bearing the acid or sulfinate can have a drastic effect on the radical formation and downstream coupling event. This is most reflected in whether the CO_2 or SO_2 unit is retained in the coupled product or lost as a gaseous byproduct. For example, the work of Glorius and co-workers showed that a radical coupling of carboxylic acids proceeded through photoinduced electron transfer, but decarboxylation only occurred in the presence of a mild brominating agent such as NBS (Scheme 10C).[11] Typically, decarboxylation (either two-electron or radical) of benzoic acids require higher temperatures and/or stronger oxidants.[6a, 12] Similarly, photoinduced electron transfer (PET) has promoted the decarboxylation of alkyl carboxylic acids in the work of Nicewicz and MacMillan.[13] The resulting radical can either be trapped, for example, with a hydrogen atom[13a] or an electron-deficient alkene.[13b-d] With the case of sulfinates, König showed that the use of PET with alkyl and aryl sulfinates resulted in cross-coupling with styrenes, however with retention of the SO_2 group in both cases.[14] Baran's sulfinate chemistry, which mostly employs TBHP as a simple oxidant, generates (fluoro)alkyl radicals that are subsequently trapped by heteroaryl radical acceptors.[3, 9]

130

Given this mixture of outcomes, a deeper understanding of these phenomena would be ultimately beneficial toward the future utilization of these functionalities. Computational methods will probe the sensitivity of these homolytic C–C and C–S scissions to the nature of the departing carbon-centered radicals. By comparing and contrasting the two dissociative approaches to radical formation, we will establish general guidelines for the use of sulfinates as radical precursors. The dramatic electronic differences in the two types of fragmentations will be shown to be particularly important for the design of radical reactions mediated by the loss of SO_2. It is anticipated that the results should allow practitioners to predictably design radical cross-coupling events enabling exploration of the desired chemical space.

3.3 Computational Results

First, let us compare the trends for the C–C and C–S bond dissociation energies (BDEs) over the broad range of neutral carboxylic and sulfinic acids (Figure 16). As one would expect, the homolytic scission is much more energetically costly for the C–C bonds than for the C–S bonds. The differences are very large: the fragmentations of the C–C bond are 30-50 kcal/mol more endothermic at the M06-2X level.
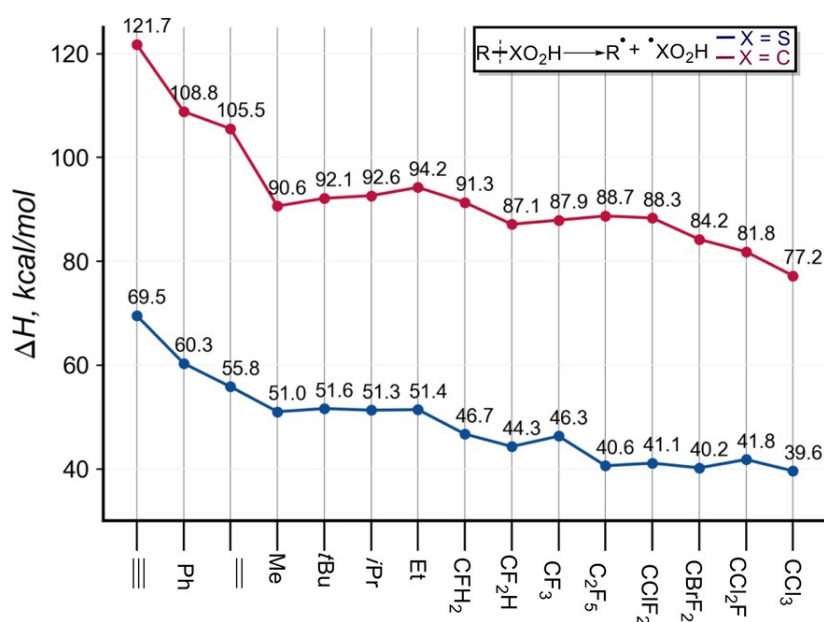
Figure 16. Bond dissociation energies (BDEs, as ΔH energies) for C–X (X = C or S) scission in neutral carboxylic and sulfinic acids.

In this context, it is especially remarkable how the situation dramatically changes for the fragmentation of the RXO_2 radicals produced by oxidation of the carboxylate and sulfinate anions. Counterintuitively at first, it is the C–S bond scission that now comes with a greater thermodynamic penalty. Furthermore, the difference in the BDEs for the C–C and the C–S scissions remain dramatic, even though the trend is inverted! Whereas most of the C–C scissions with the loss of CO_2 are exothermic, the C–S scissions with the loss of SO_2 are generally endothermic.

The thermodynamics of the two types of bond scission depends strongly on the nature of the forming radical. In particular, Figure 17 illustrates that the C–S scission is made much more favorable by acceptor substitution at the carbon atoms of the C–S bond. Furthermore, it is also greatly assisted by entropic factors. As is typical for dissociative processes, the entropic contribution is large and can render the overall process exothermic at the right temperature.[15] However, with the help of entropy, free energy for the C–S bond dissociation remains positive for many important systems (e.g., aryl and alkyl radicals).

Figure 17. Comparison of the enthalpies for the C–S and C–C bond scissions in the radicals formed from carboxylic and sulfinic acids. The data are organized by decreasing ΔH for the C–S scission.

These results provide a rational for the diverging reactivity of a non-aromatic sulfinate upon their oxidation into RSO_2 radicals. The fluorinated $AlkF_nSO_2$ systems reported by Baran underwent clean C–S scission with the formation of CF_3 and CF_2H radicals,[3, 9] but the $AlkSO_2$ radicals by König reacted further without SO_2 loss.[14] Whereas the loss of SO_2 is exergonic for CF_3 and CF_2H formation, the same process is uphill for each of the four alkyl radicals included in Figure 18. The monofluorinated CH_2 radical formation is a borderline case in terms of fragmentation thermodynamics. However, experimental data from Baran suggest that radical generation is facile under oxidation with TBHP.[3]
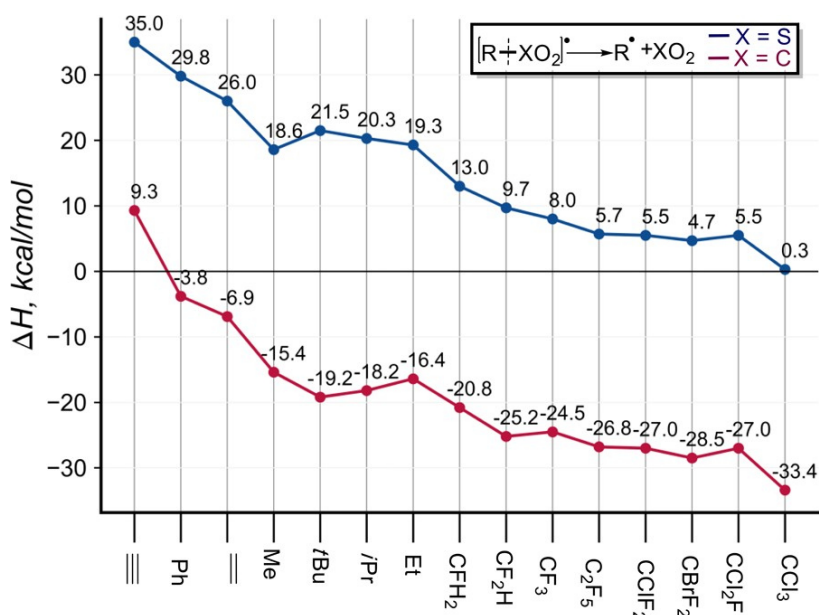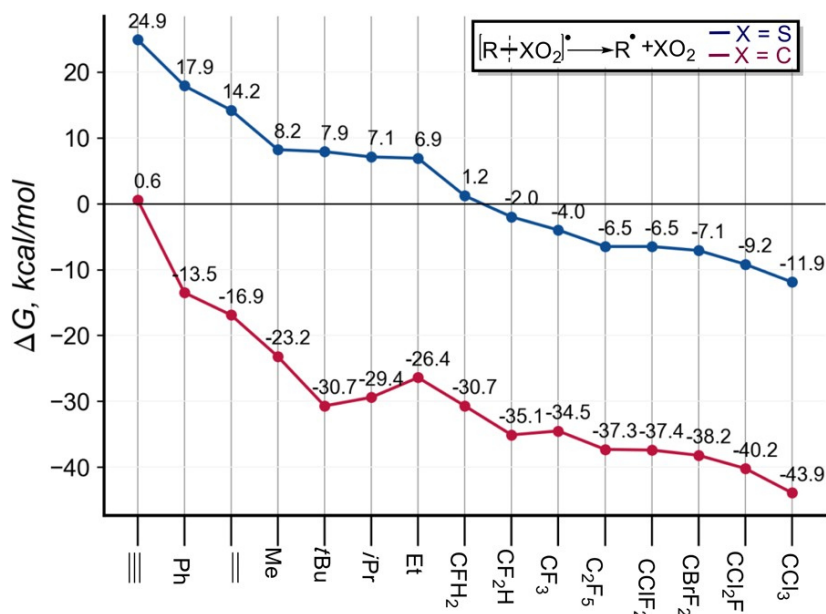
Figure 18. Comparison of the Gibbs free energies for the C–S and C–C bond scissions in the radicals formed from carboxylic and sulfinic acids. The data are organized by decreasing ΔG for the C–S scission.

It also must be noted that uphill fragmentations are not impossible. However, the endergonicity of such processes imposes an additional thermodynamic penalty on reaction efficiency. At equilibrium, if the SO_2 byproduct does not escape, the equilibrium constant is small, and the concentration of reactive intermediates (alkyl radicals) is low. For example, the 7 kcal/mol penalty for the formation of i-Pr radical from i-PrSO$_2$ radical would make the equilibrium constant lower than 10^{-5} M (<0.001% of the i-PrSO$_2$ radical will be dissociated). Of course, the equilibrium can be shifted by using Le Chatelier's principle, that is, by removal of SO_2 from the reaction sphere (either physically or chemically).

3.4 Discussion

So, what controls the observed BDE trends? There are two main questions that will be addressed. First, we will address the difference in BDE magnitudes in the RXO_2 radical systems relative to those in the parent acids. Second, we will discuss why fluorination decreases both the C–C and C–S BDEs to the extent where even the C–S scissions become thermodynamically favorable.

By definition, BDEs come from two sources: energy of the reactant and energy of the two bond-dissociation products. In this regard, considering only the product stability (i.e., stability of alkyl radical as a predictor of the C–H BDEs) can only predict the BDE trends when delocalization effects of substituents in the starting material are relatively small. Such approximation if often reasonable because delocalization effects are more important for species that lack a stable octet than they are for stable molecules.[16] This is why undergraduate students are taught that the C–H bonds at tertiary carbons are weaker "because tertiary radicals are more stable". However, predictions based on the product stability can fail for these cases where the starting materials are stabilized by delocalization more than the products, that is, the case of the C–F BDEs in alkyl fluorides (BDE (C–F): Me–F < *t*-Bu–F, Figure 19).[17][18]
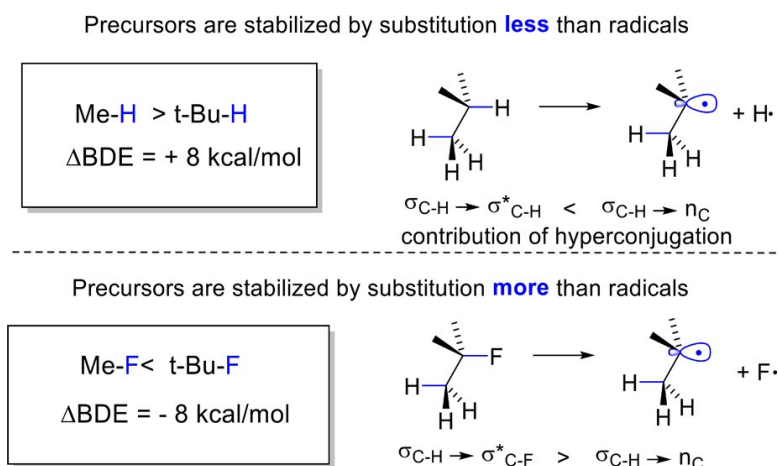

Figure 19. Contrasting effects of alkyl substitution on BDEs for C–H and C–F bonds. The BDEs increase in the more substituted alkyl fluorides but decrease in respective alkanes.

When both reactants and products are radicals, the balance of electronic effects can be quite delicate. For the systems studied herein, both reactants and products are odd-electron

species. Neither can satisfy the octet rule, and both have to rely strongly on delocalization interactions as a supplement source of stability. If delocalization effects between the radical center and the substituents in the reactant are stronger than they are in the product, then counterintuitive trends in the C–S BDEs that go against the *C*-centered product radical stability are possible.

As one can see, the trends in the BDEs can originate from a complicated combination of factors. Let us start our analysis with the reactants. There are two types of delocalizing interactions that will be considered: (i) radical delocalization and (ii) interaction of the π-system of XO_2 groups with the substituent R

3.4.1 Radical Stabilization in the RXO_2 Reactants

The carboxyl free radicals have been a topic of many investigations.[19] These species are quite complex from the electronic point of view due to the presence of several low-lying electronic states. Furthermore, the lowest $^2B_2$ state was suggested to distort from C_{2v} to C_S symmetry due to Jahn-Teller instability that localizes spin substantially at one of the oxygen atoms.[20] However, the analysis of McBride and Merrill demonstrated that the benzoyloxyl radical has a $^2B_2$ ground state with the symmetrical spin distribution.[21]

The in-depth discussion of the electronic structure of the RSO_2 radicals will be left for a future theoretical study and will limit our current work to the comparison of spin-density delocalization in two radicals, namely $MeCO_2$ and $MeSO_2$. In the carboxyl radical the unpaired electron is delocalized between the in-plane lone pairs of the two oxygen atoms. In this σ radical, the radical center is aligned perfectly at the C–C bond that needs to be broken in the decarboxylation process. Such kinetic stereoelectronic assistance is typical for radical β-scission reactions.[22] However, communication of the radical center with substituent R in the RCO_2 species is inefficient due to the lack of spin density at the central carbon.[23]
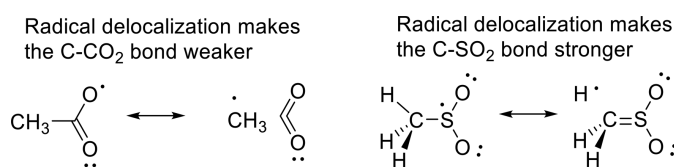
Scheme 11. Distribution of spin density in RCO_2 and RSO_2 radicals and resonance structures explaining the contrasting substituent effects at the RCO_2 and RSO_2 BDEs (only electrons directly participating in radical delocalization are shown in the resonance structures).

In contrast, the MeSO$_2$ radical is a p-type were the radical density is delocalized between a non-bonding orbital at sulfur and the two out-of-plane p orbitals of the two oxygen atoms. In this case, the sulfur-centered radical can communicate with the vicinal substituent orbitals *via* either conjugation or hyperconjugation (Scheme 11).[16]

Furthermore, the radical center in the RSO$_2$ radical is stabilized by conjugation (3c,5e) within the SO$_2$ moiety. The loss of such interaction in the product may also contribute to the counterintuitive greater thermodynamic penalty for the C–S bond scission relative to the C–C bond scission in the RCO$_2$ analog.

In the following discussion, we will show how the difference in the radical delocalization patterns can explain the contrasting trends in Me group substitution at the C–X BDEs for the RSO$_2$ and RCO$_2$ systems (Figure 20).
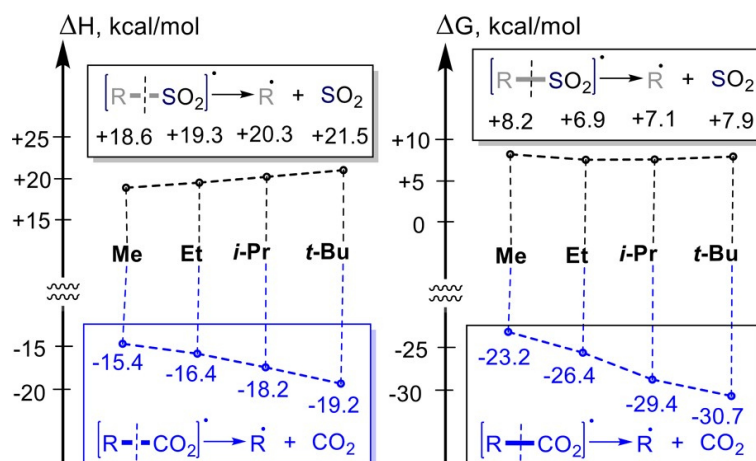

Figure 20. Enthalpies (left) and free energies (right) for the C–S bond fragmentations in the alkyl-SO$_2$ radicals are insensitive to the structure of the alkyl group, whereas the fragmentation of C–C bonds in alkyl-CO$_2$ radicals are more favorable for the formation of more substituted radical R.

The general trends in the stability of alkyl radicals (Me < Et < *i*-Pr < *t*-Bu) are of course, well understood, and BDEs for the C–C scission in radical decarboxylation do follow these expectations. In the RCO$_2$ species, C–C BDEs decrease as the forming radical becomes more substituted (~4 kcal/mol difference between Me and *t*-Bu). However, the C–S BDE for the loss of SO$_2$ follows the opposite trend. The C–S BDE is ~3 kcal/mol greater for the formation of *t*-Bu radical than for the formation of Me radicals. The striking feature of these C–S scissions is that the BDEs increase as the stability of forming radicals becomes greater!

Why do the two C–X bond scissions display such contrasting trends? The C–C BDE directly reflects the stability of forming radicals because the radical center in the RCO_2 radicals is stereoelectronically isolated from the substituent R as shown in Scheme 11. In contrast, the radical center in the RSO_2 species directly communicates with the substituent R. Increased BDE for the more substituted radicals for the C–S bond scission simply means that the stabilizing effects of Me groups in the RSO_2 reactant is greater than it is in the product.

The ΔG trends illustrate that entropic effects can either mask or amplify the enthalpy trends. When the free energy is used for the comparison, the increase in the alkyl radical stability has a small (~1 kcal/mol) and irregular effect at the free energy of the C–S bond scission (Me = t-Bu > Et = i-Pr). In contrast, the effect of Me substitution at the free energy of C–C bond becomes even larger (<7 kcal/mol).

3.4.2 Hybridization Effects

As expected scission of the stronger C(sp)–S and C(sp$_2$)–S bonds is more thermodynamically unfavorable than scission of the C(sp^3)–S bond. This finding agrees well with the known stability of the $ArCO_2$, alkynyl–CO_2 and vinyl–CO_2 radicals towards the loss of CO_2.[24] These hybridization effects[25][26] at bond stability continue to apply to the bond scission in the RSO_2 radicals, albeit to a slight different extent. For example, the differences for the alkyne–XO_2 and Ph–XO_2 bonds are noticeable larger for X = C (14 kcal/mol) than for X = S (7 kcal/mol). On the other hand, the differences for the Ph–XO_2 and Me–XO_2 BDEs are about the same (~10 kcal/mol) for both X = C and X = S.

Additional hybridization effects are associated with Bent's rule, a well-established connection between hybridization and electronegativity.[27] Thus rule states that "s-character concentrates in orbitals directed toward electropositive substituents" or alternatively, that "atoms direct hybrid orbitals with more p-character toward more electronegative elements". Bent's rule explains a variety of rehybridization effects [25, 28] in reactivity in organic[29] and main group[30] compounds.

Figure 8 illustrates the role of Bent's rule in contributing to the relative instability of fluorinated RSO_2 radicals. According to Bent's rule, the C–F bonds usually get an increased amount of p-character. The use of the higher energy p electrons by carbon facilitates polarization of the C–F bonds toward fluorine. This rehybridization is readily seen in the decreased FCF angle of fluoroform (~108°). At the same time, the HCF angle opens up

relative to the ideal tetrahedral geometry due to the allocation of additional s-character in the C–H bond. The electronic origin of these geometric changes can be tracked by analyzing variable fractional orbital hybridization of CF_3H with natural bond orbital (NBO) analysis. The carbon hybrid in the $C–SO_2$ bond of a $MeSO_2$ radical is even more p-rich ($sp^{4.5}$) than each of the carbon hybrids in the C–F bonds of CF_3H ($sp^{3.4}$). This p-character increase is consistent with the acceptor character of the SO_2 moiety and is amplified further by the large size of s orbitals.[30] Such rehybridization effects can make C–F and C–S bonds stronger and more polar. However, in the case of CF_3SO_2, rehybridization is difficult. Fluorine and sulfur compete for the p-character, and neither one is "happy" with the hybridization of carbon in their bonds (Figure 21). The C–S bond scission can partially alleviate this "hybridization frustration", explaining why such scission is assisted by the fluorine substitution.

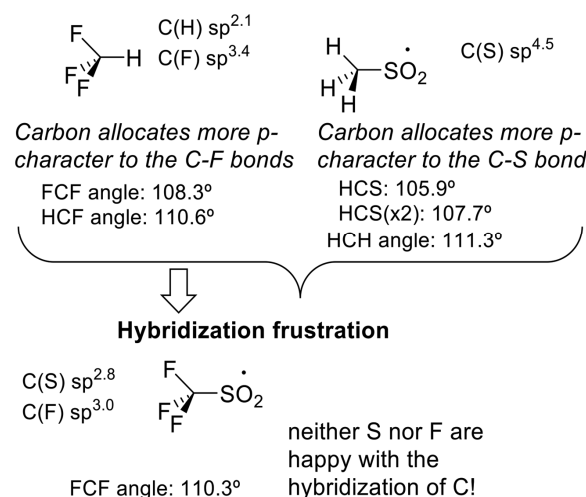**Bent's rule: increased p-character in C-F and C-S bonds**

Figure 21. Illustration of "hybridization frustration" in the CF_3SO_2 radical. Average NBO hybridization values from the *a*- and *β*-spin NBOs are given.

Although, the above effects are not negligible, they are not large enough to explain the dramatic differences between the C–C and C–S bond dissociation energies in the RXO_2H/RXO_2 systems. Hence, we need to look at the contribution of products to the observed BDE trends. There are two factors: the nature of the gaseous co-product (CO_2 vs SO_2 and the stability of radical R forming from RXO_2.

3.4.3 The Gaseous Co-Product Stability: CO_2 vs SO_2

The general strategy for making an unstable species (e.g., a radical) is to couple this process with the formation of a stable co-product. This strategy finds numerous applications in chemistry.[31] In this section, we will compare the two such "thermodynamic auxiliaries" (CO_2 and SO_2) and show that they are dramatically different.

In this regard, it is instructive to compare the BDEs or RXO_2H and RXO_2. The inversion of the relative BDE magnitudes for the C–C and C–S bond scissions in the radicals comes from the fact that BDE is lower by the introduction of the radical much more for the loss of CO_2 (~110 kcal/mol) than for the loss of SO_2 (~35-40 kcal/mol). The situation is summarized schematically in Figure 22. As discussed earlier, the BDEs reflect two components: stability of the reactants and stability of the products. The effect of product stability can be evaluated from the H-atom transfer equation shown in the figure. It illustrates that the product stability plays a major role in the observed trend (~55 kcal/mol). The largest part of this effect is likely to stem from the high thermodynamic stability of CO_2[32] as the result of the greater strength of the C=O bonds and the efficiency of the $n_{O1} \rightarrow \pi^*_{C2O3}$ resonance.[33] The rest should come from the intrinsic differences in the C–C and C–S bond strength in the reactants and, possibly from the difference in the radical stabilization discussed in the previous section.
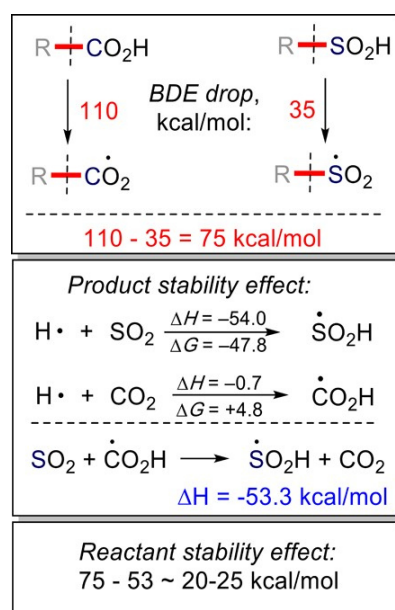

Figure 22. Dramatic difference in the radical effect at the C–C and C–S bond scissions in the RXO_2 systems.

3.4.4   Nature of the Departing Radical

Like true chameleons, radicals display a wide range of stabilities and reactivities as a function of many possible delocalization effects. In the following sections we will concentrate on several types of substrates with the goal of highlighting the underlying electronic factors that are responsible for the observed trends.

3.4.5   Effect of Acceptors

In order to evaluate the importance of donor/acceptor interactions of the substituent at the departing radical with the π system of CO_2 (and SO_2), we have calculated BDEs for a group of para-substituted aryl radical precursors (Figure 23). These systems are convenient since they help us to separate the effects of delocalization from the effects of hybridization.

Although it is natural to concentrate on delocalization interactions that involve the radical centers, one should not forget that other effects also contribute to the observed BDEs. In particular, both the CO_2R and SO_2R groups are strong π acceptors as illustrated by their relative large and positive Hammet σ_{para} values ($CO_2H = 0.45$, $CO_2Et = 0.45$, $SO_2Me = 0.72$)[34].

The calculated energies in Figure 23 include both the π effects and the effects of radical delocalization. The individual contributions from the two effects in the RCO_2 and RSO_2 systems should be quite different. Nevertheless, Figure 10 illustrates that the net substituent effects on the CO_2 and SO_2 loss are remarkably similar. For the loss of CO_2, the donor NH_2 group increases the BDE by 3.9 kcal/mol, whereas the acceptor NO_2 group decreases the BDE by (up to) 2.5 kcal/mol. The effects of the same groups (-3.5 kcal/mol and +2.1 kcal/mol) on the C–S BDE in the RSO_2 species are essentially the same.

Figure 23. Substituent effects on the BDEs for the group of para-substituted aryl radical precursors. Note that delocalization interactions that do not involve the radicals still have a large effect at the BDEs.

For comparison, we have included the C–H BDEs for the formation of the same radicals from the respective monosubstituted benzenes (Scheme 12). As one can see, the effects are much smaller because the σ_{C-H} bond is orthogonal to the aromatic π system and has to interact with the para substituents either through-space or through the σ framework.[35]
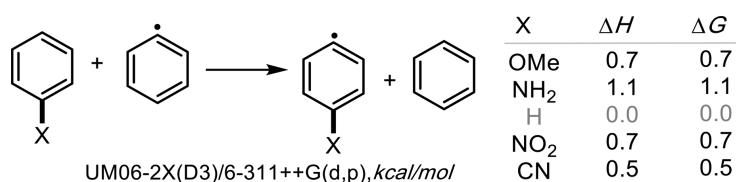
Scheme 12. Isodesmic equation evaluating the impact of para-substituted phenyl radicals. Both donor and acceptor groups offer little difference when compared to H.

An analogous set of systems was tested for the formation of substituted vinyl radicals (Scheme 13). The formation of the parent vinyl radicals is similar to the formation of the phenyl radical. Again, acceptor substitution decreases the C–S BDE. The effect is moderate for the formation of trifluorovinyl radicals where the π-donating properties of the fluorine

atoms partially compensate for their σ-accepting power. In agreement with the decrease in π-donation for Cl and Br[17], these substituents provide less stabilization to the starting RSO_2 species and render fragmentation less unfavorable. The greatest facilitating effect is observed in the presence of π acceptors. For example, the fragmentation of the tricyano precursor is predicted to be ~3 kcal/mol exergonic.
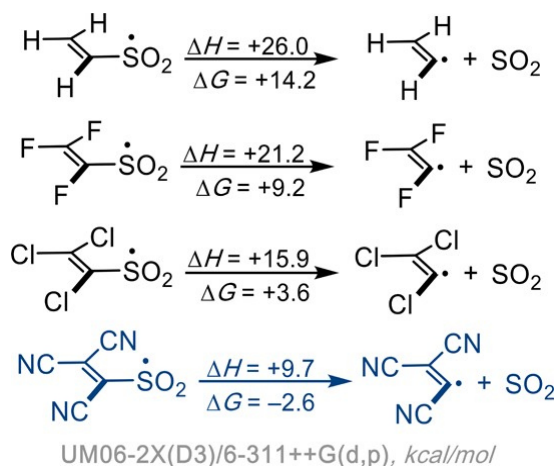
Scheme 13. Substituent effects on the BDEs of alkene sulfonyl precursors.

3.4.6   σ-Acceptors: Fluoroalkyls vs Alkyls

Our computations suggest that for all alkyl radical formations, the loss of SO_2 is uphill! This result agrees very well with the results of König et al. who observed the reactions of sulfinyl radicals not accompanied by the loss of SO_2.[14] On the other hand, they bring mechanistic questions about the chemically induced oxidation of sulfinate salts by Baran. An additional factor in these reactions may be a different oxidation mechanism for the sulfinate anion by hydroperoxides. So far, no detailed mechanistic studies have been reported for the chemical oxidation of sulfinate anions.

This situation changes when acceptor groups are introduced at the scissile bond (Figure 24). The formation of halogen-containing radicals is less endothermic than the formation of simple alkyl radicals. This finding is especially important for the $C–SO_2$ scissions where, with the help of entropic factors, fluorination allows the process to become thermodynamically favorable. For the loss of SO_2 at 298 K, the threshold occurs between CH_2F/CF_2CH_3 and CF_2H. Higher temperatures should help to shift the equilibrium further in favor of the dissociated products even for CH_2F.
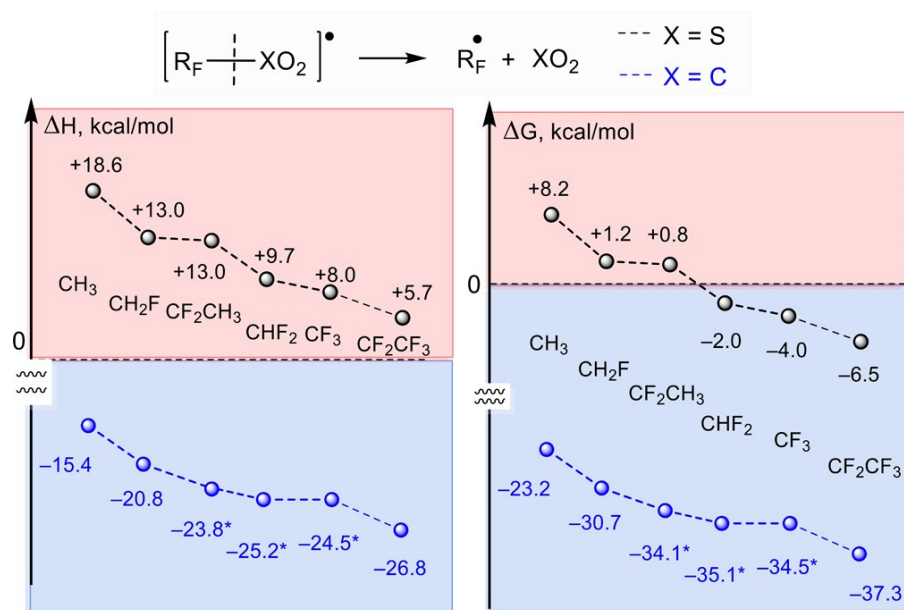
Figure 24. Enthalpies and free energies for the $R_F XO_2$ (X = S (top) or C (bottom)) bond fragmentations in the fluoroalkyl-XO_2 radicals.

Although the exact position of the threshold is affected by the computational uncertainty of the current methods, the M06-2X data do agree with the scarcity of the literature reports describing the formation of the CH_2F radical *via* this approach.

Stereoelectronic analysis can explain why the fragmentations of radical precursors with the σ-acceptors at the incipient radical centers (i.e., the C–F and C–Cl bonds) are more favorable than fragmentations that produce alkyl radicals. The origin of these effects lies in the chameleonic[36] behavior of *C*-halogen moieties (Figure 25). In contrast to the C–H and C–C bonds in the alkyl groups that serve as hyperconjugative donors in stabilizing interactions with the π* and σ* CO and CS orbitals in the reactants and with the carbon-centered radical in the dissociated product (Figure 25), the dominant electronic effect of halogen groups undergoes a reversal in the process of fragmentation. Although the C–F and C–Cl bonds are strong σ-acceptors[37] and do not stabilize the adjacent XO_2 groups, the same substituents act as donors (*via* the n(X) → n(C) interactions) toward the R-centered radicals formed after the fragmentations. In other words, the "chameleonic" properties of the halogen groups originate from the switch from being a σ-acceptor relative to a β-substituent to become a π-donor relative to an α-substituent.
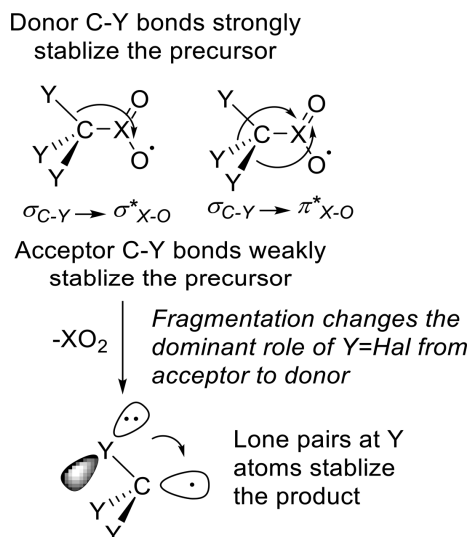
Figure 25. Chameleonic change of halogen substituents from σ_{C-Y} acceptors to n_Y donors in the process of C–X bond fragmentation.

3.4.7 Additional Substituent Effects

A similar effect was observed for the oxygen-containing substrates in Scheme 14. In ethers, the formation of anomeric radicals at the α-carbon is ~4-5 kcal/mol less endergonic (less unfavorable) than the formation of radicals at the β-carbon. This result illustrates that donation from the *S*-centered radical to the σ* (CO) is less important than the 2c,3e stabilization[38] by the interaction of the $MeOCH_2$ radical with the α-oxygen lone pair.
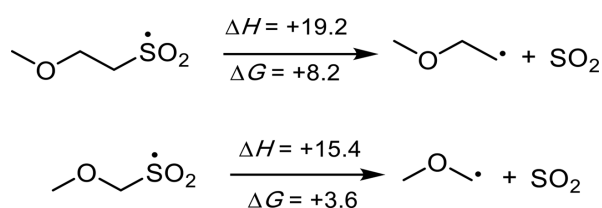
Scheme 14. Evaluation of systems that invoke anomeric stabilization.

Stabilization of the *C*-centered radical product by an adjacent π-system renders the SO_2 extrusion exergonic. In agreement with the greater stabilization of the radical center by an alkene,[39] the formation of the allyl radical is slightly more favorable than the formation of the benzylic radical (-6 vs -2 kcal/mol, Scheme 15).
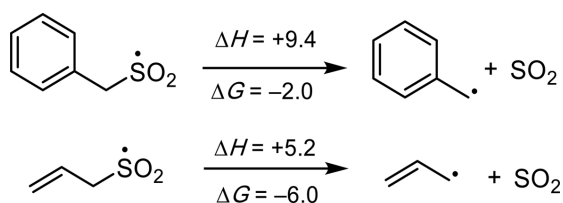
Scheme 15. Evaluation of systems that invoke benzylic and allylic stabilization.

3.4.8 Selected Barriers for the C–C Scission in the RXO$_2$ (X = C or S) Systems

Analysis of the activation barriers is more difficult in RXO$_2$ systems. Since our initial attempts using DFT methods were unsuccessful, we have chosen the UMP2(full)/cc-pVTZ method as an alternative approach. The barriers for the C–C and C–S bond scissions were found by performing a full relaxed scan for the interatomic distances corresponding to the breaking bonds. The results are presented in Scheme 16. Although the introduction of fluorine atoms significantly decreases the barrier for the C–S bond scission, the fluorine substitution only has a small (<1 kcal/mol) effect on the C–C scission. In RXO$_2$ species, the C–S scission barriers are higher than the C–C barriers and affected much more by the change in the nature of substitution in radical R.
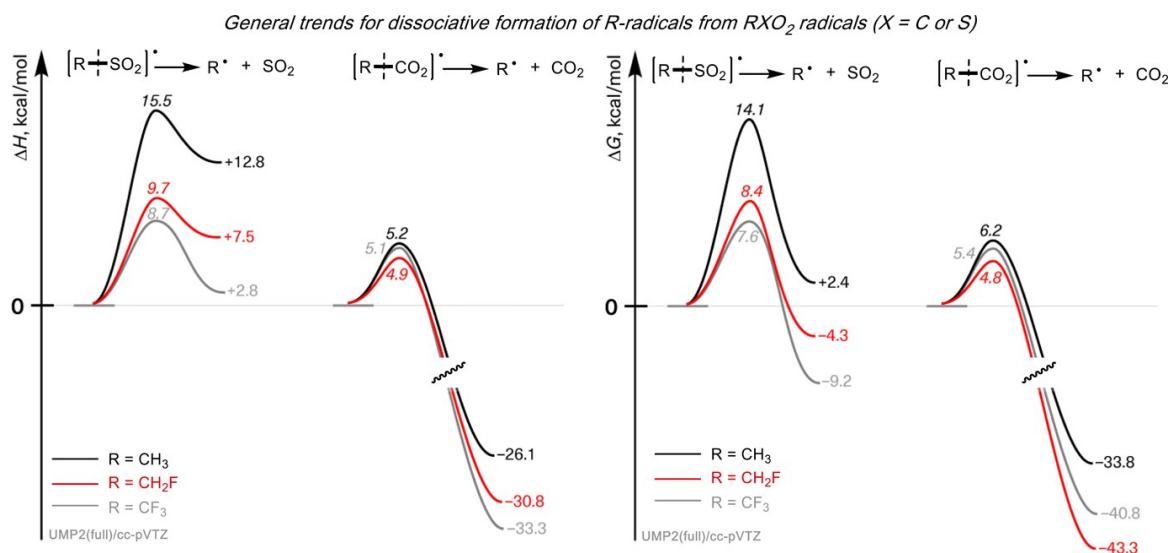

Scheme 16. Effect of fluorine substitution on kinetics and thermodynamics of XO$_2$ extrusion from RXO$_2$ Radicals (X = S or C).

3.4.9 General Trends for Radical Formation *via* the Extrusion of Triatomic Heterocumulenes: Comparison with the Literature Systems

It is interesting to compare the above trends with the alkoxycarbonyl and alkoxythiocarbonyl radicals reported by Coote and co-workers.[40] Although both of these earlier studied systems had similar fragmentation enthalpies and breaking the same type of bond (O–R), the alkoxycarbonyl precursors displayed higher activation barriers for the β-scission. The difference in the barriers has been attributed to the greater radical stabilization in the alkoxycarbonyl starting materials. As the C=O bond is shorter than the C=S bond, oxygen is more effective at engaging the radical center in a 2c,3e bond than its sulfur counterpart. Since this stabilization effect is weakened in the TS, this cost has to be paid as an increase in the activation barrier. From the point of view of the Marcus theory, the observed trends indicate that the intrinsic barriers for the fragmentation are different.[39]

In the present case, the types of the breaking bonds are different (C–C vs C–S), and the reaction enthalpy for the C–C scission is 30-40 kcal/mol more negative than it is for the C–S scission (Scheme 17). The relative activation barriers for the C–C and C–S scissions follow the same trend as thermodynamics. However, one should know that the barrier difference (3-10 kcal/mol) is much smaller than differences in the reaction energies. Analysis of these observations through the prism of the Marcus theory[39] suggests that although the intrinsic bond scission barrier is lower for the C–S bonds, the full barrier is lower for the C–C bond scission due to much more favorable thermodynamic contribution for the loss of CO_2.
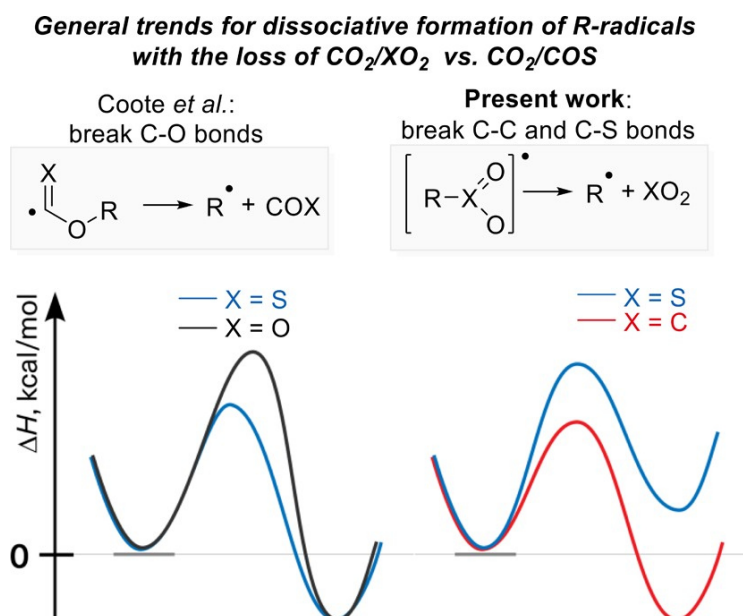

Scheme 17. Comparison of kinetic and thermodynamic trends in fragmentations producing an alkyl radical and a triatomic heterocumulene.

3.4.10 Implications for the Design of Isomerization Cascades

The difference in the relative exergonicities of alkyl and fluoroalkyl radical formation *via* the RXO$_2$ fragmentation may be possible to exploit for the design of isomerization cascades similar to those shown in Scheme 18.

The proposed cascades are based on relative favorability of the C–S scission for the formation of fluorinated radicals. In the first example, the radical can be trapped by alkene. Although one can suggest that RXO$_2$ precursor can be also trapped by a 6-exo cyclization before the SO$_2$ extrusion, this process is uphill and thus can be reversed *via* ring opening. The loss of SO$_2$ should lead to a fast and irreversible 5-exo cyclization. Because the cyclization step produces an alkyl radical, this product should be capable of recapturing SO$_2$ by forming a new C–S bond, thus completing the isomerization cascade.

The second example combines the C–S scission with a C–C fragmentation by involving a cyclopropyl radical clock. Again, ring opening transforms a fluorinated radical (poor trap for SO$_2$) into an alkyl radical (a good trap for SO$_2$), rendering the overall isomerization thermodynamically favorable. Interestingly, ring opening proceeds thermoneutral with a relatively high barrier. This finding suggests that, in the presence of more efficient traps, the intermediate cyclopropyl radical can be intercepted, suggesting a new strategy for the usually problematic installation of cyclopropyl-CF$_2$ groups.
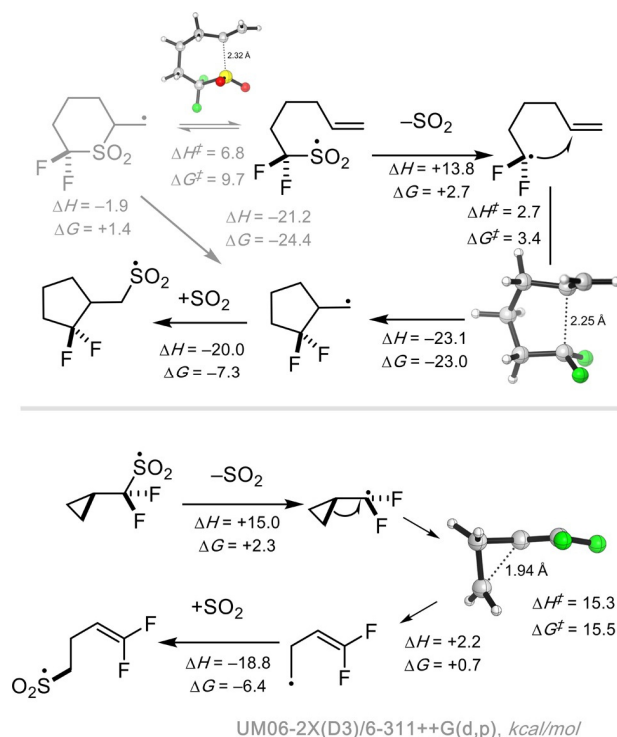
Scheme 18. Possible radical isomerization cascades in substituted RXO$_2$ systems.

3.5   Experimental Validation

In order to validate the computational prognosis for the bond fragmentations in the fluoroalkyl-SO_2 radicals (R_F-$SO_2\bullet$), we performed single-electron photo-oxidations on sodium sulfinate salts lying at the energetic borderline predicted in Figure 24. Chemical trapping of the generated radicals can occur before (highlighted in red) or after (highlighted in blue) extrusion of SO_2 (Table 11). In either scenario, it leads to stable cross-coupled products. We have chosen to employ two common types of radical traps: Olefinic substrates are known to efficiently trap both, *C*-centered radicals as well as *S*-centered radicals. Heteroaromatic scaffolds however are efficient *C*-centered radical traps often used in Minisci-type reactions.[41]

As already reported, **CH₃-SO₂Na** does not extrude SO_2 upon single-electron photo-oxidation. The respective sulfonyl radical is trapped and forms the respective sulfonylated adduct **1** (Entry 1, Table 11).[14] For the photo-oxidation of **CH₃CF₂-SO₂Na** only desulfinylated coupling products **2a** and **2b** were obtained for both, olefinic and heteroaromatic radical traps. (Entry 2, Table 11). The computational data suggest that the process of SO_2 extrusion should be slightly uphill (0.8 kcal/mol) for CH_3CF_2-SO_2Na. However, SO_2 extrusion is occurring under our reaction conditions. For this extreme borderline case two factors may be decisive: Considering that the thermodynamic equilibrium of the reaction lies on the sulfinylated side as suggested by the calculations (only small concentrations of $CH_3CF_2\bullet$ and SO_2 are present), extruded SO_2 still may escape into the headspace of the reaction vessel as a gas and therefore shift the overall equilibrium towards the desulfinylated alkyl radical. Alternatively, uncertainty of the used computational methods could be an explanation for the different theoretical and experimental outcomes. The **CF₂H-SO₂Na** is following the suggestions of the calculations. We found that extrusion of SO_2 takes place upon photo-oxidation and solely desulfinylated adducts **3a** and **3b** are formed with both, olefinic and heteroaromatic radical traps. (Entry 3, Table 11). The single-electron photo-oxidation of **CF₃-SO₂Na** was already reported earlier to lead to the respective desulfinylated coupling product **4** (Entry 4, Table 11).[42]

Table 11. Experimental validation of the computationally predicted energetic borderline cases of fluoroalkyl sulfinate salts for the retention or extrusion of SO_2 upon single-electron photo-oxidation.

Entry	R_F-SO_2Na	Product	
1	CH_3-SO_2Na	**1**	
2	CH_3CF_2-SO_2Na	**2a**	**2b**
3	CF_2H-SO_2Na	**3a**	**3b**
4	CF_3-SO_2Na	**4**	

As a conclusion, we could show that the energetic borderline for the extrusion of SO_2 lies between CH_3-SO_2Na and CH_3CF_2-SO_2Na. Although the computational data suggested that the extrusion of SO_2 should be slightly uphill for CH_3CF_2-SO_2Na, either the shift of the overall reaction equilibrium by removal of SO_2 or uncertainties of the computational methods can be decisive factors at this narrow borderline scenario.

3.6   Conclusion and Practical Implications

In summary, this study highlights the important differences between oxidative generation of *C*-centered radicals *via* the loss of CO_2 and SO_2 from the respective radical precursors. Whereas the loss of CO_2 is generally thermodynamically favorable, the loss of SO_2 does not enjoy the same thermodynamic assistance and, in many cases, is uphill. The paradoxical observation that the C–C bon is weaker than the C–S bond in these reactions is explained by the combination if conjugative and hybridization effects.

The differences in the spin density distribution illustrate that the radical centers in the RCO_2 radicals do not interact with the R group *via* conjugation. The lack of spin density at the central carbon is a stereoelectronic barricade that isolates the *O*-centered radicals from the rest of the molecule. In contrast, the sulfur atom in the RSO_2 radical has a significant amount of spin density and can interact directly with the appropriately aligned orbitals at the substituent R.

The C–C scission in radical decarboxylation does follow the usual trends defined by the stability of forming radicals. For example, the C–C BDEs decrease as the forming radical becomes more substituted (~4 kcal/mol difference between Me and *t*-Bu). However, the C–S BDE follows an opposite trend: it is ~3 kcal/mol greater for the formation of the *t*-Bu radical than for the formation of the Me radical.

Both RSO_2 and RCO_2 radicals are stabilized by donor substituents and destabilized by acceptor substituents in R. The stabilizing effects include both conjugation and hyperconjugation. In particular, a progressive increase in the number of fluorine atoms makes the fragmentations more favorable. The choice of conditions is crucial for radical fragmentation with SO_2 loss. One has to clearly distinguish between reactions that proceed *via* true "outer sphere" electron transfer, such as electrochemical oxidation and photoredox pathways, and chemical oxidation (e.g., by TBHP), which may proceed *via* mechanistically distinct scenario requiring a separate analysis in the future.

Thermodynamic limitations described in this work only apply to ground-state fragmentations of true radicals. For the SO_2-centered radicals that are immune to thermal loss of SO_2, additional photochemical activation of the RSO_2 precursor should be considered. It is possible, that the photochemical excitation of stable (or metastable) RSO_2 radicals can also assist to the loss of SO_2.

The differences in the two types of dissociative approaches to the formation of *C*-centered radicals are important for the design of radical reactions mediated by fragmentations. The loss of SO_2 can be a more selective process than the loss of CO_2. Due to applications of RSO_2 radicals in synthesis,[43] the search for new approaches to their generations continues.[44] In this context, the reverse process (i.e., the reactions of SO_2 and alkyl and aryl radicals) may be useful for the synthesis of RSO_2 radicals in the same way as the reaction of radicals with carbon monoxide can be a source of acyl radicals.[45]

3.7   Acknowledgements

3.8 References

[1] R. A. Shenvi, D. P. O'Malley, P. S. Baran, Acc. Chem. Res., 2009, 42, 530-541.

[2] a) E. J. Corey, X. M. Cheng, The Logic of Chemical Synthesis, 1989; b) T. Gaich, P. S. Baran, J. Org. Chem., 2010, 75, 4657-4673; c) J. M. Smith, S. J. Harwood, P. S. Baran, Acc. Chem. Res., 2018, 51, 1807-1817.

[3] Y. Fujiwara, J. A. Dixon, F. O'Hara, E. D. Funder, D. D. Dixon, R. A. Rodriguez, R. D. Baxter, B. Herlé, N. Sach, M. R. Collins, Y. Ishihara, P. S. Baran, Nature, 2012, 492, 95.

[4] H. Kolbe, Annal. Chem. Pharm., 1848, 64, 339.

[5] F. Minisci, R. Bernardi, F. Bertini, R. Galli, M. Perchinummo, Tetrahedron, 1971, 27, 3575-3579.

[6] a) N. Rodríguez, L. J. Goossen, Chem. Soc. Rev., 2011, 40, 5030-5048; b) M. A. J. Duncton, MedChemComm, 2011, 2, 1135-1161; c) A. Studer, D. P. Curran, Angew. Chem. Int. Ed., 2016, 55, 58-102.

[7] D. H. R. Barton, D. Crich, W. B. Motherwell, J. Chem. Soc., Chem. Commun., 1983, 0, 939.

[8] B. R. Langlois, E. Laurent, N. Roidot, Tetrahedron Lett., 1991, 32, 7525-7528.

[9] a) Y. Fujiwara, J. A. Dixon, R. A. Rodriguez, R. D. Baxter, D. D. Dixon, M. R. Collins, D. G. Blackmond, P. S. Baran, J. Am. Chem. Soc., 2012, 134, 1494-1497; b) Y. Ji, T. Brueckl, R. D. Baxter, Y. Fujiwara, I. B. Seiple, S. Su, D. G. Blackmond, P. S. Baran, Proceedings of the National Academy of Sciences, 2011, 108, 14411-14415; c) Q. Zhou, A. Ruffoni, R. Gianatassio, Y. Fujiwara, E. Sella, D. Shabat, P. S. Baran, Angew. Chem. Int. Ed., 2013, 52, 3949-3952; d) F. O'Hara, R. D. Baxter, A. G. O'Brien, M. R. Collins, J. A. Dixon, Y. Fujiwara, Y. Ishihara, P. S. Baran, Nature Protocols, 2013, 8, 1042; e) F. O'Hara, A. C. Burns, M. R. Collins, D. Dalvie, M. A. Ornelas, A. D. N. Vaz, Y. Fujiwara, P. S. Baran, J. Med. Chem., 2014, 57, 1616-1620; f) J. Gui, Q. Zhou, C.-M. Pan, Y. Yabe, A. C. Burns, M. R. Collins, M. A. Ornelas, Y. Ishihara, P. S. Baran, J. Am. Chem. Soc., 2014, 136, 4853-4856; g) F. O'Hara, D. G. Blackmond, P. S. Baran, J. Am. Chem. Soc., 2013, 135, 12122-12134; h) H. Yao, Y. Liu, S. Tyagarajan, E. Streckfuss, M. Reibarkh, K. Chen, I. Zamora, F. Fontaine, L. Goracci, R. Helmy, K. P. Bateman, S. W. Krska, Eur. J. Org. Chem., 2017, 2017, 7122-7126; i) A. O. Terent'ev, O. M. Mulina, D. A. Pirgach, D. V. Demchuk, M. A. Syroeshkin, G. I. Nikishin, RSC Adv., 2016, 6, 93476-93485; j) A. O. Terent'ev, O. M. Mulina, D. A. Pirgach, A. I. Ilovaisky, M. A. Syroeshkin, N. I. Kapustina, G. I. Nikishin, Tetrahedron, 2017, 73, 6871-6879.

[10] a) C. Punta, F. Minisci, Trends Heterocycl. Chem., 2008, 13, 1; b) F. Minisci, F. Fontana, E. Vismara, J. Heterocycl. Chem., 1990, 27, 79-96; c) F. Minisci, E. Vismara, F. Fontana, Heterocycles, 1989, 28, 489-519.

[11] L. Candish, M. Freitag, T. Gensch, F. Glorius, Chem. Sci., 2017, 8, 3618-3622.

[12]   J. Kan, S. Huang, J. Lin, M. Zhang, W. Su, Angew. Chem. Int. Ed., 2015, 54, 2199-2203.

[13]   a) J. D. Griffin, M. A. Zeller, D. A. Nicewicz, J. Am. Chem. Soc., 2015, 137, 11340-11348; b) S. Bloom, C. Liu, D. K. Kölmel, J. X. Qiao, Y. Zhang, M. A. Poss, W. R. Ewing, D. W. C. MacMillan, Nature Chemistry, 2018, 10, 205; c) S. J. McCarver, J. X. Qiao, J. Carpenter, R. M. Borzilleri, M. A. Poss, M. D. Eastgate, M. M. Miller, D. W. C. MacMillan, Angew. Chem. Int. Ed., 2017, 56, 728-732; d) L. Chu, C. Ohta, Z. Zuo, D. W. C. MacMillan, J. Am. Chem. Soc., 2014, 136, 10886-10889.

[14]   A. U. Meyer, K. Straková, T. Slanina, B. König, Chem. Eur. J., 2016, 22, 8694-8699.

[15]   For an intriguing temperature effect that leads to a switch from SO2 preservation to extrusion in photocatalytic reactions of sulfonyl chlorides, see: S. K. Pagire, A. Hossain, O. Reiser, Org. Lett., 2018, 20, 648-651.

[16]   I. V. Alabugin, G. dos Passos Gomes, M. A. Abdo, Wiley Interdisciplinary Reviews: Computational Molecular Science, 2019, 9, e1389.

[17]   a) E. I. Izgorodina, M. L. Coote, L. Radom, The Journal of Physical Chemistry A, 2005, 109, 7558-7566; b) I. V. Alabugin, Stereoelectronic Effects: the Bridge between Structure and Reactivity, 2016.

[18]   The CH/CF hyperconjugation explains other seeming paradoxes, such is why CF3 has a negative Radical Stabilization Energy (a) A. S. Menon, D. J. Henry, T. Bally, L. Radom, Org. Biomol. Chem., 2011, 9, 3636-3657; or why the C-H bond in H-C6F5 is stronger than C-H bond in benzene, whereas the C-F bond in F-C6F5 is weaker than F-C6H5 (b) O. Eisenstein, J. Milani, R. N. Perutz, Chem. Rev., 2017, 117, 8710-8753.

[19]   A. Rauk, D. Yu, D. A. Armstrong, J. Am. Chem. Soc., 1994, 116, 8222-8228.

[20]   M. B. Yim, O. Kikuchi, D. E. Wood, J. Am. Chem. Soc., 1978, 100, 1869-1872.

[21]   J. M. McBride, R. A. Merrill, J. Am. Chem. Soc., 1980, 102, 1723-1725.

[22]   a) A. Baroudi, J. Mauldin, I. V. Alabugin, J. Am. Chem. Soc., 2010, 132, 967-979; b) K. Pati, G. dos Passos Gomes, T. Harris, A. Hughes, H. Phan, T. Banerjee, K. Hanson, I. V. Alabugin, J. Am. Chem. Soc., 2015, 137, 1165-1180; c) T. Harris, G. d. P. Gomes, R. J. Clark, I. V. Alabugin, J. Org. Chem., 2016, 81, 6007-6017.

[23]   There is also an interesting symmetry problem because the radical center populates an MO with the nodal structure that renders its interaction with the scissile C-C bond symmetry forbidden. Although this feature is likely to be of significance, a more detailed discussion of its consequences goes beyond the scope of the present work.

[24]   a) J. Chateauneuf, J. Lusztyk, B. Maillard, K. U. Ingold, J. Am. Chem. Soc., 1988, 110, 6727-6731; b) H. G. Korth, J. Chateauneuf, J. Lusztyk, K. U. Ingold, J. Am. Chem. Soc., 1988, 110, 5929-5931; c) H. G. Korth, J. Chateauneuf, J. Lusztyk, K. U. Ingold, J. Org. Chem., 1991, 56, 2405-2410; d) J. Chateauneuf, J. Lusztyk, K. U. Ingold, J. Am. Chem. Soc., 1988, 110, 2877-2885; e) J. Chateauneuf, J. Lusztyk, K. U. Ingold, J. Am. Chem. Soc., 1988, 110, 2886-2893; f) H.-G. Korth, W. Müller, J.

Lusztyk, K. U. Ingold, Angew. Chem. Int. Ed., 1989, 28, 183-185; g) S. Yamauchi, N. Hirota, S. Takahara, H. Sakuragi, K. Tokumaru, J. Am. Chem. Soc., 1985, 107, 5021-5022.

[25]   a) I. V. Alabugin, S. Bresch, G. dos Passos Gomes, J. Phys. Org. Chem., 2015, 28, 147-162; b) K. Pati, G. dos Passos Gomes, I. V. Alabugin, Angew. Chem. Int. Ed., 2016, 55, 11633-11637.

[26]   Such effects can be useful in synthetic radical chemistry. For example, the greater strength of X-aryl bonds in comparison to that of X-alkyl bonds was used to redirect the classic Barton-McCombie decarboxylation: (a) D. H. R. Barton, S. W. McCombie, J. Chem. Soc., Perkin Trans. 1, 1975, 1574-1585; (b) S. Z. Zard, Aust. J. Chem., 2006, 59, 663-668; (c) A. Baroudi, J. Alicea, P. Flack, J. Kirincich, I. V. Alabugin, J. Org. Chem., 2011, 76, 1521-1537; (d) P. Poonpatana, G. dos Passos Gomes, T. Hurrle, K. Chardon, S. Bräse, K.-S. Masters, I. Alabugin, Chem. Eur. J., 2017, 23, 9091-9097.

[27]   H. A. Bent, Chem. Rev., 1961, 61, 275-311.

[28]   I. V. Alabugin, M. Manoharan, J. Comput. Chem., 2007, 28, 373-390.

[29]   a) M. Prall, A. Wittkopp, A. A. Fokin, P. R. Schreiner, J. Comput. Chem., 2001, 22, 1605-1614; b) H. H. Wenk, A. Balster, W. Sander, D. A. Hrovat, W. T. Borden, Angew. Chem. Int. Ed., 2001, 40, 2295-2298; c) G. W. Plourde, P. M. Warner, D. A. Parrish, G. B. Jones, J. Org. Chem., 2002, 67, 5369-5374; d) R. K. Mohamed, P. W. Peterson, I. V. Alabugin, Chem. Rev., 2013, 113, 7089-7129; e) J. A. Codelli, J. M. Baskin, N. J. Agard, C. R. Bertozzi, J. Am. Chem. Soc., 2008, 130, 11486-11493; f) B. Gold, N. E. Shevchenko, N. Bonus, G. B. Dudley, I. V. Alabugin, J. Org. Chem., 2012, 77, 75-89; g) D. O'Hagan, Chem. Soc. Rev., 2008, 37, 308-319.

[30]   I. V. Alabugin, S. Bresch, M. Manoharan, The Journal of Physical Chemistry A, 2014, 118, 3663-3677.

[31]   a) M. A. Syroeshkin, F. Kuriakose, E. A. Saverina, V. A. Timofeeva, M. P. Egorov, I. V. Alabugin, Angew. Chem. Int. Ed., 2019, 58, 2-21; b) R. E. Messersmith, S. Yadav, M. A. Siegler, H. Ottosson, J. D. Tovar, J. Org. Chem., 2017, 82, 13440-13448; c) R. Papadakis, H. Ottosson, Chem. Soc. Rev., 2015, 44, 6472-6493; d) S. Villaume, H. A. Fogarty, H. Ottosson, ChemPhysChem, 2008, 9, 257-264; e) P. W. Peterson, R. K. Mohamed, I. V. Alabugin, Eur. J. Org. Chem., 2013, 2013, 2505-2527; f) R. K. Mohamed, S. Mondal, K. Jorner, T. F. Delgado, V. V. Lobodin, H. Ottosson, I. V. Alabugin, J. Am. Chem. Soc., 2015, 137, 15441-15450; g) D. J. Babinski, X. Bao, M. El Arba, B. Chen, D. A. Hrovat, W. T. Borden, D. E. Frantz, J. Am. Chem. Soc., 2012, 134, 16139-16142.

[32]   I. Alabugin, R. K. Mohamed, Science, 2014, 344, 45-46.

[33]   This delocalization is a π-analogue of the n --> σ^*CO delocalization involved in the anomeric effect (a) J. Podlech, The Journal of Physical Chemistry A, 2010, 114, 8480-8487; (b) E. Juaristi, G. dos Passos Gomes, A. O. Terent'ev, R. Notario, I. V. Alabugin, J. Am. Chem. Soc., 2017, 139, 10799-10813.

[34]   J. E. Leffler, E. Grunwald, Rates and Equilibria of Organic Reactions, 1963.

[35]   For an example of substituent effects on σ radicals, see: Pickard, R. L. Shepherd, A. E. Gillis, M. E. Dunn, S. Feldgus, K. N. Kirschner, G. C. Shields, M. Manoharan, I. V. Alabugin, The Journal of Physical Chemistry A, 2006, 110, 2517-2526.

[36]   S. Z. Vatsadze, Y. D. Loginova, G. dos Passos Gomes, I. V. Alabugin, Chem. Eur. J., 2017, 23, 3225-3245.

[37]   I. V. Alabugin, T. A. Zeidan, J. Am. Chem. Soc., 2002, 124, 3175-3185.

[38]   For a dramatic effect of 2c,3e-stabilization on a radical fragmentation, see: (a) S. Mondal, B. Gold, R. K. Mohamed, I. V. Alabugin, Chem. Eur. J., 2014, 20, 8664-8669, (b) R. K. Mohamed, S. Mondal, B. Gold, C. J. Evoniuk, T. Banerjee, K. Hanson, I. V. Alabugin, J. Am. Chem. Soc., 2015, 137, 6335-6349.

[39]   a) I. V. Alabugin, M. Manoharan, J. Am. Chem. Soc., 2005, 127, 12583-12594; b) I. V. Alabugin, M. Manoharan, J. Am. Chem. Soc., 2005, 127, 9534-9545.

[40]   M. L. Coote, C. J. Easton, S. Z. Zard, J. Org. Chem., 2006, 71, 4996-4999.

[41]   R. S. J. Proctor, R. J. Phipps, Angew. Chem. Int. Ed., 0.

[42]   D. J. Wilger, N. J. Gesmundo, D. A. Nicewicz, Chem. Sci., 2013, 4, 3160-3165.

[43]   a) I. V. Alabugin, V. I. Timokhin, J. N. Abrams, M. Manoharan, R. Abrams, I. Ghiviriga, J. Am. Chem. Soc., 2008, 130, 10984-10995; b) Y. Ning, Q. Ji, P. Liao, E. A. Anderson, X. Bi, Angew. Chem. Int. Ed., 2017, 56, 13805-13808.

[44]   K. Gilmore, B. Gold, R. J. Clark, I. V. Alabugin, Aust. J. Chem., 2013, 66, 336-340.

[45]   a) C. Chatgilialoglu, D. Crich, M. Komatsu, I. Ryu, Chem. Rev., 1999, 99, 1991-2070; b) K. Zhou, M. Chen, L. Yao, J. Wu, Org. Chem. Front., 2018, 5, 371-375; c) G. Qiu, K. Zhou, J. Wu, Chem. Commun., 2018, 54, 12561-12569.

[46]   G. dos Passos Gomes, A. Wimmer, J. M. Smith, B. König, I. Alabugin, ChemRxiv, 2019, in press, DOI: 10.26434/chemrxiv.7464587.v7464582.

3.9   Experimental Part

3.9.1   Computational Methods

DFT calculations were carried with Gaussian 09 software package,[1] using the (U)M06-2X DFT functional[2] (with an ultrafine integration grid of 99,590 points) with the 6-311++G(d,p) basis set for all atoms. Grimme's D3 version (zero damping) for empirical dispersion[3] was also included. Frequency calculations were conducted for all structures to confirm them as either a minimum or a transition state (TS). Intrinsic reaction coordinates (IRCs)[4] were determined for the TSs of interest. Full (U)MP2[1] with cc-pVTZ basis set for all atoms was also employed in selected cases. Natural bon orbital (NBO)[5] analysis was performed on key intermediates and transition states. Spin density was evaluated from the NBO analysis data. The Gibbs free energy values are reported at 298 K, unless otherwise. For selected systems, DLPNO-CCSD(T)[6] calculations were performed with ORCA 4.0[7] (see sections 6.4.1 and 6.4.2 for details). Three-dimensional structures were produced with CYLView 1.0.1.[8]

3.9.2   Materials and Methods

Starting materials and reagents were purchased from commercial suppliers (Sigma Aldrich, Alfa Aesar, Acros, Fluka or TCI) and were used without further purification. Unless otherwise stated, yields are generally isolated amounts of products, obtained after automated flash-column chromatography on flash-silica gel, using HPLC-grade petrolether and ethylacetate as eluents or after Kugelrohr distillation. Liquid reagents and solvents were transferred *via* syringe, needle and septum technique. All NMR spectra were measured at room temperature, using a Bruker Avance 300 (300 MHz for ^{1}H, 75 MHz for ^{13}C and 282 MHz for ^{19}F) or a Bruker Avance 400 (400 MHz for ^{1}H, 101 MHz for ^{13}C and 376 MHz for ^{19}F) NMR spectrometer. All chemical shifts are reported in δ-scale as parts per million [ppm] (multiplicity, coupling constants *J*, number of protons) relative to the solvent residual peaks as the internal standard.[9] Coupling constants *J* are given in Hertz [Hz]. Abbreviations used for signal multiplicity: ^{1}H-, ^{13}C-NMR: b = broad, s = singlet, d = doublet, t = triplet, q = quartet, quint. = quintet, sept. = septet, dd = doublet of doublets, dt = doublet of triplets, dq = doublet of quartets, and m = multiplet. ^{13}C NMR: (+) = primary/tertiary, (-) = secondary, (C$_q$) = quaternary. The mass spectrometrical measurements were performed at the Central Analytical Laboratory of the University of Regensburg. All mass spectra were recorded on a

Finnigan MAT 95, ThermoQuest Finnigan TSQ 7000, Finnigan MAT SSQ 710 A or an Agilent Q-TOF 6540 UHD instrument. GC measurements were performed on a GC 7890 from Agilent Technologies. Data acquisition and evaluation was done with Agilent ChemStation Rev.C.01.04.. GC measurements were made and analyzed *via* integration of the signal obtained with respect to the calibration with a suitable internal standard. Analytical TLC was performed on silica gel coated alumina. Visualization was done by UV light (254 or 366 nm). If necessary, potassium permanganate was used for chemical staining. The standard photochemical setup for experiments in regular scale consists of 455 nm LEDs (OSRAM Oslon SSL 80 royal-blue, 455 nm (±15 nm), radiant power 500 mW, 2.9 V, 350 mA) which illuminate from the bottom and a custom made aluminum cooling block connected to a thermostat which cools from the side (Section 2.7.1, Figure 14).

3.9.3 Procedure for Single-Electron Photo-Oxidations on Fluoroalkyl Sulfinate Salts

A 5 mL crimp vial was equipped with the sodium sulfinate salt (0.48 mmol, 3 equiv.), $[Ir(ppy_2)(dtbbpy)]PF_6$ (7.3 mg, 0.008 mmol, 5 mol%), dihydronaphthalene (21.1 μL, 0.16 mmol, 1 equiv., added *via* Hamilton syringe) or caffeine (31.4 mg, 0.16 mmol, 1 equiv.) as the radical trapping reagents and a stirring bar. DMF/H_2O (2.0 mL, 0.08 M, 3:1) was added *via* syringe and the vessel was capped. To keep the reaction aerated, the septum of the vessel was pierced with two steel cannulas. The reaction mixture was stirred and irradiated using a blue LED (455 nm) for 18 hours at 25 °C. The outcome of the reaction was analyzed by GC and GC-MS analysis. Cross-coupling products with olefinic dihydronaphthalene were purified by automated flash-column chromatography (PE/EtOAc), followed by Kugelrohr distillation.

3-Methanesulfonyl-1,2-dihydronaphthalene (1)

^{1}H-NMR data are matching with the literature known spectra.[10]
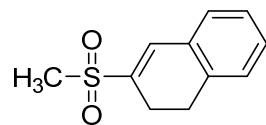
29.4 mg, 88% yield.

^{1}H NMR (400 MHz, DMSO-d_6): δ 7.45 – 7.36 (m, 2H), 7.38 – 7.29 (m, 1H), 7.27 (t, J = 6.7 Hz, 2H), 3.09 (s, 3H), 2.94 (t, J = 8.3 Hz, 2H), 2.64 (dt, J = 8.3, 1.4 Hz, 2H).

2-(1,1-Difluoroethyl)-1,2,3,4-tetrahydronaphthalene (2a)
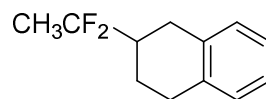
GC-MS verified that no sulfinylated cross-coupling product was formed. Major fractions of the Kugelrohr distillation were taken for NMR and HRMS analysis.

^{1}H NMR (300 MHz, CD_2Cl_2) δ 7.10 (s, 4H), 3.00 – 2.67 (m, 4H), 2.31 – 2.06 (m, 2H), 1.74 – 1.50 (m, 4H).

^{13}C NMR (101 MHz, CD_2Cl_2) δ 136.7 (C_q) , 135.6 (C_q), 129.7 (+), 129.2 (+), 126.4 (+), 126.3 (+), 126.2 (C_q, t, J = 239.6 Hz), 42.7 (+, t, J = 24.4 Hz), 29.8 (–, t, J = 4.9 Hz), 29.5 (–) , 23.6 (–, t, J = 4.5 Hz), 21.4 (+, t, J = 28.2 Hz).

^{19}F NMR (282 MHz, CD_2Cl_2) δ -95.9 – -98.0 (m).

HRMS (EI+) (m/z): [M]$^{•+}$ ($C_{12}H_{14}F_2$) calc.: 196.1058, found: 196.1060.

8-(1,1-Difluoroethyl)-1,3,7-trimethyl-3,7-dihydro-1*H*-purine-2,6-dione (2b)
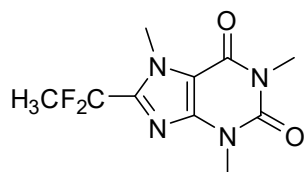

Due to low yield of the reaction only GC-MS analysis could be performed for the analysis of the cross-coupled product **2b**. Note: Big signal at 4.28 minutes can be attributed to DMF.

HRMS (EI+) (m/z): [M]$^{\bullet+}$ (C$_{10}$H$_{12}$F$_2$N$_4$O$_2$) calc.: 258.0923, found: 258.0928.
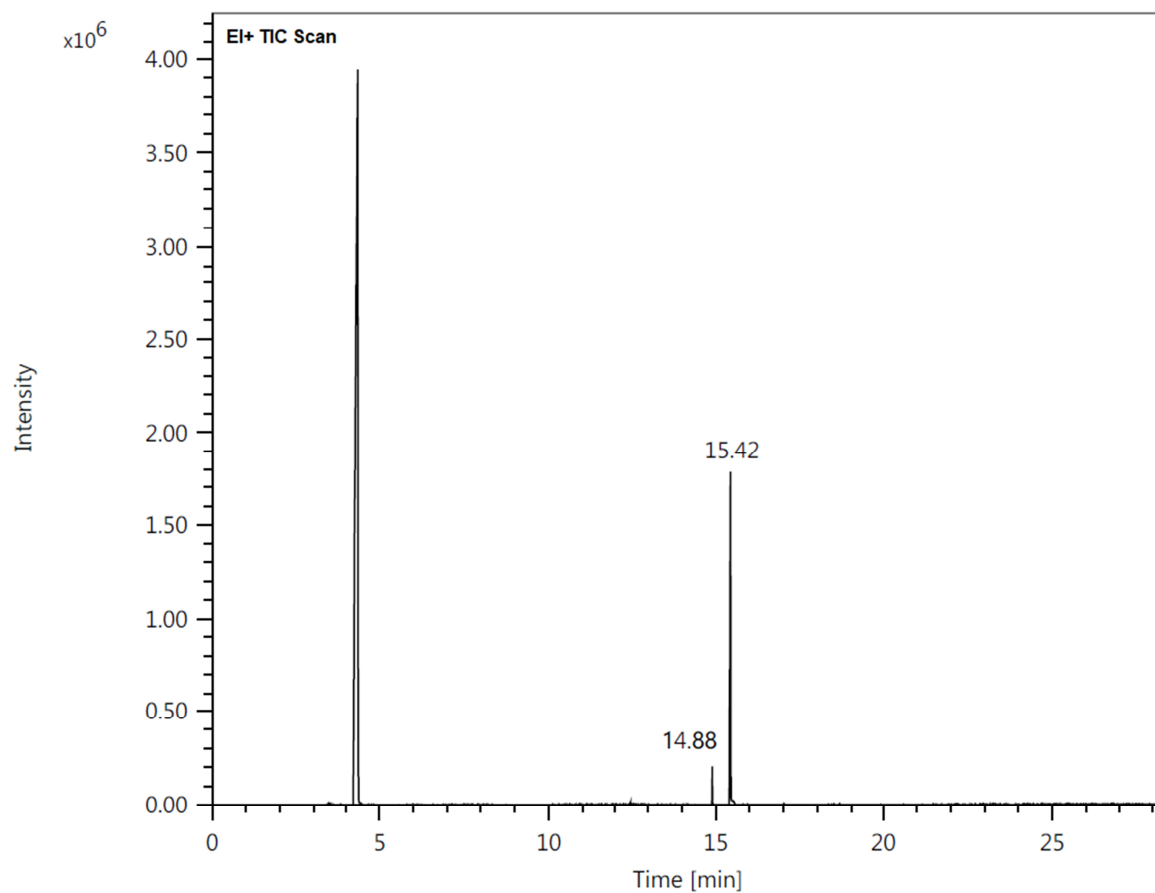
Adduct fragmentation:

Two important fragments of the CH_3CF_2-caffeine adduct **3b** could be identified. Cleavage of the CH_3CF_2 moiety (**C**) leads the respective mass peak of caffeine. Fragmentation assigned by **D** leaves back a CH_3CF_2-functionalized imidazolium core, verifying that the CH_3CF_2H moiety is attached to the caffeine molecule in the suggested way.
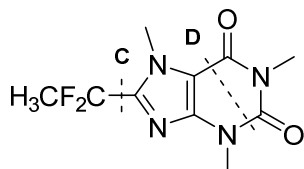
Fragment C: HRMS (EI+) (m/z): $[M - CH_3CF_2]^{\bullet+}$ ($C_8H_9N_4O_2$) calc.: 193.0720, found: 193.0724.

Fragment D: HRMS (EI+) (m/z): $[M - C_3H_3NO_2]^{\bullet+}$ ($C_7H_9F_2N_3$) calc.: 173.0760, found: 173.0763.
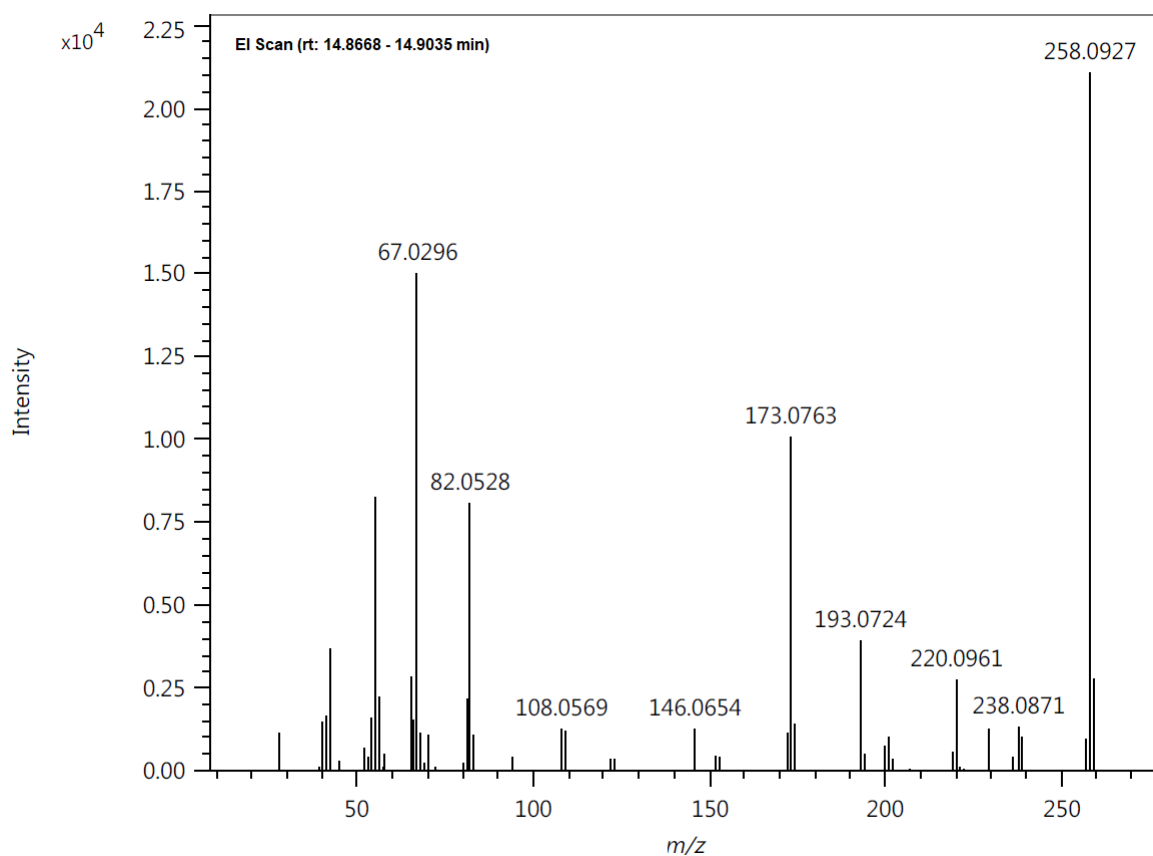
2-(Difluoromethyl)-1,2,3,4-tetrahydronaphthalene (3a)
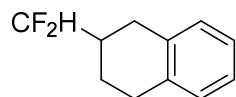
^{1}H NMR (400 MHz, CD$_2$Cl$_2$) δ 7.12 – 7.10 (s, 4H), 5.76 (td, J = 56.8, 4.7 Hz, 1H), 2.96 – 2.82 (m, 3H), 2.77 – 2.68 (m, 1H), 2.33 – 2.16 (m, 1H), 2.11 – 2.01 (m, 1H), 1.68 – 1.52 (m, 1H).

^{13}C NMR (101 MHz, CD$_2$Cl$_2$) δ 136.7 (C$_q$), 135.0 (C$_q$), 129.7 (+), 129.3 (+), 126.5 (+), 126.4 (+), 119.6 (+, t, J = 241.1 Hz), 39.2 (–, t, J = 19.8 Hz), 28.8 (–, t, J = 5.2 Hz), 28.7 , 22.9 (–, t, J = 4.9 Hz).

^{19}F NMR (376 MHz, CD$_2$Cl$_2$) δ -122.56 – -124.71 (m).

HRMS (EI+) (m/z): [M]$^{•+}$ (C$_{11}$H$_{12}$F$_2$) calc.: 182.0902, found: 182.0897.

8-(Difluoromethyl)-1,3,7-trimethyl-3,7-dihydro-1H-purine-2,6-dione (3b)
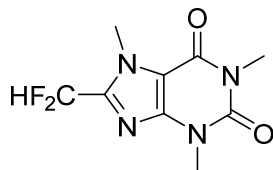
Due to low yield of the reaction only GC-MS analysis could be performed for the analysis of the cross-coupled product **3b**. Note: Nitrobenzene (16.4 μL, 0.16 mmol, 1 equiv.) was employed as terminal oxidant instead of O$_2$ and appears at 8.75 minutes in the gas chromatogram.

HRMS (EI+) (m/z): [M]$^{•+}$ (C$_9$H$_{10}$F$_2$N$_4$O$_2$) calc.: 244.0766, found: 244.0763.
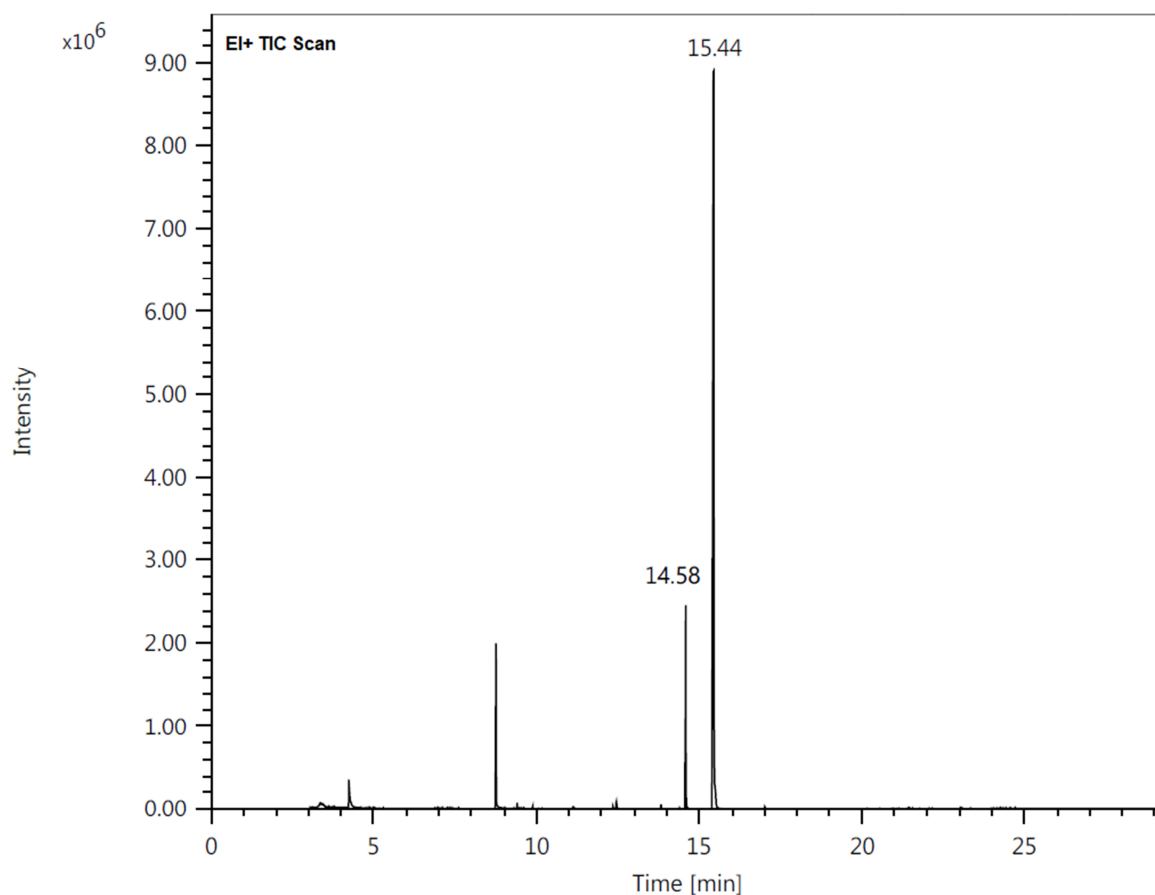
Adduct fragmentation:

Two important fragments of the CF_2H-caffeine **3b** adduct could be identified. Cleavage of the CF_2H moiety (**A**) leads the respective mass peak of caffeine. Fragmentation assigned by **B** leaves back a CF_2H-functionalized imidazolium core, verifying that the CF_2H moiety is attached to the caffeine molecule in the suggested way.
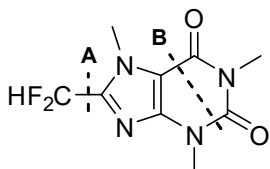
Fragment A: HRMS (EI+) (m/z): $[M - CF_2H]^{•+}$ ($C_8H_9N_4O_2$) calc.: 193.0720, found: 193.0723.

Fragment B: HRMS (EI+) (m/z): $[M - C_3H_3NO_2]^{\cdot+}$ $(C_6H_7F_2N_3)$ calc.: 159.0603, found: 159.0599.
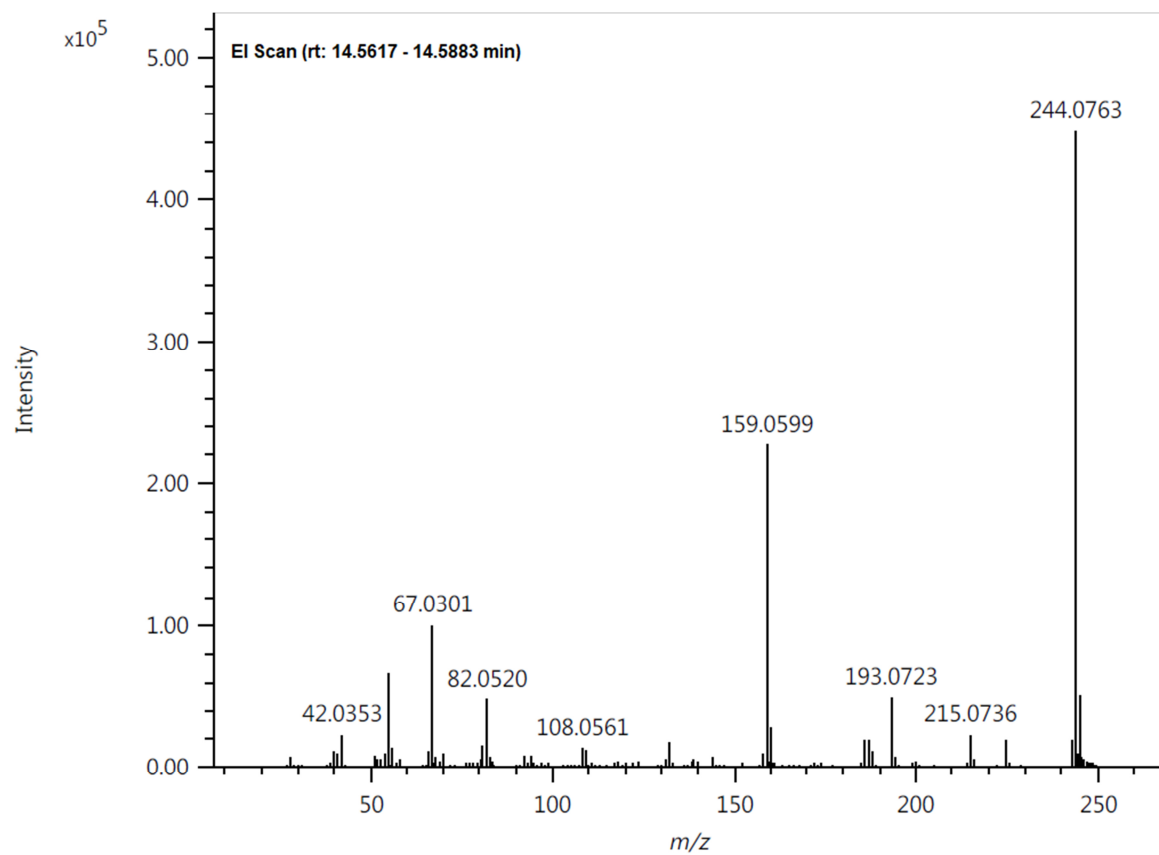
3.9.4 NMR Spectra

All NMR spectra can be found in the appendix in the section 6.4.3.

3.9.5 References

[1]   M. Head-Gordon, J. A. Pople, M. J. Frisch, Chem. Phys. Lett., 1988, 153, 503-506.

[2]   a) Y. Zhao, D. G. Truhlar, Theor. Chem. Acc., 2008, 120, 215-241; b) Y. Zhao, D. G. Truhlar, Acc. Chem. Res., 2008, 41, 157-167.

[3]   S. Grimme, J. Antony, S. Ehrlich, H. Krieg, The Journal of Chemical Physics, 2010, 132, 154104.

[4]   K. Fukui, Acc. Chem. Res., 1981, 14, 363-368.

[5]   a) L. Yuan, C. Han, M.-Q. Yang, Y.-J. Xu, Int. Rev. Phys. Chem., 2016, 35, 1-36; b) A. E. Reed, F. Weinhold, The Journal of Chemical Physics, 1985, 83, 1736-1740; c) A. E. Reed, F. Weinhold, Isr. J. Chem., 1991, 31, 277-285; d) A. E. Reed, L. A. Curtiss, F. Weinhold, Chem. Rev., 1988, 88, 899-926; e) J. Podlech, The Journal of Physical Chemistry A, 2010, 114, 8480-8487; f) M. P. Freitas, J. Org. Chem., 2012, 77, 7607-7611; g) K. T. Greenway, A. G. Bischoff, B. M. Pinto, J. Org. Chem., 2012, 77, 9221-9226; h) E. Juaristi, R. Notario, J. Org. Chem., 2015, 80, 2879-2883; i) G. d. P. Gomes, V. Vil, A. Terent'ev, I. V. Alabugin, Chem. Sci., 2015, 6, 6783-6791; j) D. V. Vidhani, M. E. Krafft, I. V. Alabugin, J. Am. Chem. Soc., 2016, 138, 2769-2779; k) V. A. Vil', G. dos Passos Gomes, O. V. Bityukov, K. A. Lyssenko, G. I. Nikishin, I. V. Alabugin, A. O. Terent'ev, Angew. Chem. Int. Ed., 2018, 57, 3372-3376.

[6]   C. Riplinger, F. Neese, The Journal of Chemical Physics, 2013, 138, 034106.

[7]   F. Neese, WIREs Comput. Mol. Sci., 2018, 8, e1327.

[8]   CYLview, 1.0b; Legault, C.Y., Université de Sherbrooke: 2009 (http://www.cylview.org).

[9]   a) R. K. Harris, E. D. Becker, S. M. Cabral de Menezes, R. Goodfellow, P. Granger, Magn. Reson. Chem., 2002, 40, 489-505; b) H. E. Gottlieb, V. Kotlyar, A. Nudelman, J. Org. Chem., 1997, 62, 7512-7515; c) G. R. Fulmer, A. J. M. Miller, N. H. Sherden, H. E. Gottlieb, A. Nudelman, B. M. Stoltz, J. E. Bercaw, K. I. Goldberg, Organometallics, 2010, 29, 2176-2179.

[10]   A. U. Meyer, K. Straková, T. Slanina, B. König, Chem. Eur. J., 2016, 22, 8694-8699.

4. Summary

This thesis presents various photocatalytic approaches towards the preparation of the pharmaceutically relevant substrate classes of *N*-functionalized sulfoximines and sulfoximidoyl derivatives (**Chapter 1 & 2**). Furthermore, a detailed theoretical and experimental study on the stability of *S*-centered sulfonyl radicals revealed a strong relation between the extrusion of SO_2 and the substitution pattern of the sulfonyl radical (**Chapter 3**).

A visible-light-mediated, photo-oxidative *N*-arylation of *NH*-sulfoximines is presented in **Chapter 1**. The highly oxidizing, organic dye 9-mesityl-10-methylacridinium perchlorate was used as photocatalyst and initiates the C-N cross-coupling reaction. A second, proton-reducing catalyst (Co(dmgH)$_2$PyCl) was employed to close the photocatalytic cycle and generate dihydrogen as only byproduct. The mechanism of the reaction was elucidated by steady-state and time-resolved UV/Vis and fluorescence spectroscopy and radical-radical cross-coupling was proposed as mechanistic key step for the C-N bond formation. In addition, the protocol was adapted to continuous flow, which resulted in significantly increased process productivity.

In **Chapter 2**, the preparation of *N*-functionalized sulfoximines was achieved by a combination of iridium photocatalysis and nickel catalysis, based on a photosensitization mechanism. Exceptionally low catalyst loadings were found to efficiently drive the cross-coupling reaction between brominated arenes and *NH*-sulfoximines, tolerating a broad range of functional moieties. The developed synthetic method was also suitable for other sulfoximidoyl derivatives like sulfinamides and sulfonimidamides and can be employed for the synthesis of enantiopure products. Furthermore, scale-up of the reaction was successfully conducted at multi gram scale in a custom-built photoreactor.

Chapter 3 presents a detailed study on the stability of *S*-centered sulfonyl radicals and their tendency to keep or extrude SO_2. Stereoelectronic influences of substituents like conjugation and hyperconjugation as well as entropic factors highly affect the thermodynamics of a C-S fragmentation process. Progressive fluorination of the *S*-adjacent

C-atom destabilizes the sulfonyl radical and renders the SO_2 extrusion thermodynamically favorable, which can be rationalized by the chameleonic electronic properties of halogen atoms. Furthermore, we performed several single-electron, photo-oxidation experiments on fluoroalkyl sulfinate salts in order to validate the computationally predicted thermodynamic borderline for the extrusion of SO_2.

5. Zusammenfassung

Im Zuge dieser Arbeit wurden neue, photokatalysierte Synthesemethoden zur Herstellung von pharmazeutisch wertvollen, *N*-funktionalisierten Sulfoximinen und strukturverwandten Derivaten entwickelt und vorgestellt (**Kapitel 1 & 2**). Außerdem wurde die chemische Stabilität von *S*-zentrierten Sulfonylradikalen im Detail untersucht und herausgefunden, dass die Abspaltung von SO_2 stark von Einflüssen benachbarter Substituenten abhängt (**Kapitel 3**).

In **Kapitel 1** wird eine durch sichtbares Licht vermittelte, oxidative *N*-Arylierung von *NH*-Sulfoximinen vorgestellt. Die C-N Bindungsknüpfung wird durch den Einsatz von 9-Mesityl-10-methylacridinium Perchlorat, einem stark oxidierenden organischen Photokatalysator, initiiert. Die Verwendung eines zweiten, protonen-reduzierenden Katalysators (Co(dmgH)$_2$PyCl) schließt den Photokatalysezyklus und generiert Wasserstoff als einziges Nebenprodukt der Reaktion. Mechanistische Untersuchungen mittels UV/Vis und Fluoreszenzspektroskopie deuten darauf hin, dass der Reaktion eine Radikal-Radikal Kreuzkupplung als Schlüsselschritt zu Grunde liegt. Außerdem konnte die Reaktion für den kontinuierlichen Betrieb in einem Durchflussreaktor optimiert werden, wodurch die Produktivität der Reaktion signifikant gesteigert wurde.

Die Funktionalisierung von *NH*-Sulfoximinen mittels einer Kombination aus Iridium und Nickel Photokatalyse wird in **Kapitel 2** vorgestellt und basiert auf einer Photosensibilisierung als grundlegendem Reaktionsmechanismus. Die Reaktion zwischen bromierten Aromaten und *NH*-Sulfoximinen verläuft bereits mit außerordentlich geringen Mengen an Katalysatoren und ist außerdem für eine weite Bandbreite an funktionellen Gruppen geeignet. Strukturelle Derivate der Sulfoximine wie Sulfinamide und Sulfonimidamide konnten unter unveränderten Reaktionsbedingungen funktionalisiert werden und die Synthese enantiomerenreiner Produkte wurde realisiert. Außerdem wurde die

entwickelte Reaktion in einem speziell angefertigten Reaktor im Multigramm-Maßstab erfolgreich durchgeführt.

Kapitel 3 ist eine Studie zur Stabilität von *S*-zentrierten Sulfonylradikalen und der spontanen Abspaltung von SO_2. Die Tendenz zur C-S Bindungsspaltung ist stark von stereoelektronischen Einflüssen wie Konjugation und Hyperkonjugation durch benachbarte Substituenten und entropischen Faktoren abhängig. Die Studie zeigt, dass mit der Anzahl an Fluoratomen am benachbarten C-Atom zum *S*-Radikal die Destabilisierung ansteigt, was auf die chamäleonartigen elektronischen Eigenschaften von Halogenen zurückgeführt werden kann. Um die theoretischen Berechnungen experimentell zu validieren, wurden mit entsprechenden fluorierten Alkylsulfinaten Photooxidationsreaktionen durchgeführt und die Produkte auf eine eventuelle SO_2 Abspaltung untersucht.

6. Appendix

6.1 Abbreviations

°C	degrees Celsius
µM	micro molar
Å	Ångström (10^{-10} m)
acetone-d_6	deuterated acetone
API	active pharmaceutical ingredient
Ar	aryl
BDE	bonding dissociation energy
Bu	Butyl
c	concentration
calc.	calculated
CD_2Cl_2	deuterated dichloromethane
$CDCl_3$	deuterated chloroform
CV	cyclic voltammetry
DABCO	1,4-diazabicyclo(2.2.2)octan
DCE	1,2-dichloroethane
DCM	1,1-dichloromethane
deg.	degassed
DIPEA	diisopropylethylamine
DMAc	dimethylacetamide
DMF	dimethylformamide
dmgH	dimethylglyoximate
DMSO	dimethylsulfoxide
DMSO-d_6	deuterated dimethylsulfoxide
dtbbpy	4,4'-di-*tert*-butyl-2,2'-dipyridyl
EI	electron ionization
equiv.	equivalent
E_{Red}	reduction potential
ESI	electrospray ionization
Et	ethyl
EtOAc	ethylacetate
EtOH	ethanol

g	gram
GC	gas chromatography
h	hour
Hal	halogen
HPLC	high-performance/pressure liquid chromatography
HRMS	high resolution mass spectrometry
hν	incident photon energy
I	intensity
kcal	kilogram calorie
KOAc	potassium acetate
l	length
L	liter
LED	light emitting diode
M	molarity = mol/L
Me	methyl
MeCN	acetonitrile
MeOH	methanol
Mes-Acr-Me$^+$	9-mesityl-10-methylacridinium
mg	milligram
MgSO$_4$	magnesium sulfate
MHz	mega hertz
min	minute
mL	milli liter
mM	milli molar
mm	milli meter
mmol	milli mole
mol%	mole percent
MS	mass spectrometry
Na$_2$SO$_4$	sodium sulfate
nm	nano meter
NMR	nuclear magnetic resonance
NP	normal phase
OTf	triflates
OTs	tosylate
PE	petrol ether
Ph	phenyl
Ph-NO$_2$	nitrobenzene
ppm	parts per million
ppy	2-phenylpyridine
psi	pounds per square inch
Py	pyridine
r.t.	room temperature
s	seconds

SCE	saturated calomel electrode
T	transmission
T	temperature
TBHP	*tert*-butyl hydroperoxide
TEMPO	(2,2,6,6-tetramethylpiperidinyl)oxyl
THF	tetrahydrofuran
TIC	total ion current
TLC	thin layer chromatography
TM	transition metal
TMG	1,1,3,3-tetramethylguanidine
t_R	retention time
UV	ultraviolet
V	volt
Vis	visible
W	watt
ΔG	Gibbs free energy
ΔH	enthalpy
ε	molar extinction coefficient
λ	wavelength
ν	flowrate

6.2 Appendix Chapter 1

6.2.1 NMR Spectra

Compound **3a**, [^1]H- and [^13]C-NMR:

Compound **3b**, ^{1}H- and ^{13}C-NMR:

1H NMR (300 MHz, CDCl$_3$)

13C NMR (75 MHz, CDCl$_3$)

Compound **3c**, ^{1}H- and ^{13}C-NMR:

1H NMR (400 MHz, CDCl$_3$)

13C NMR (101 MHz, CDCl$_3$)
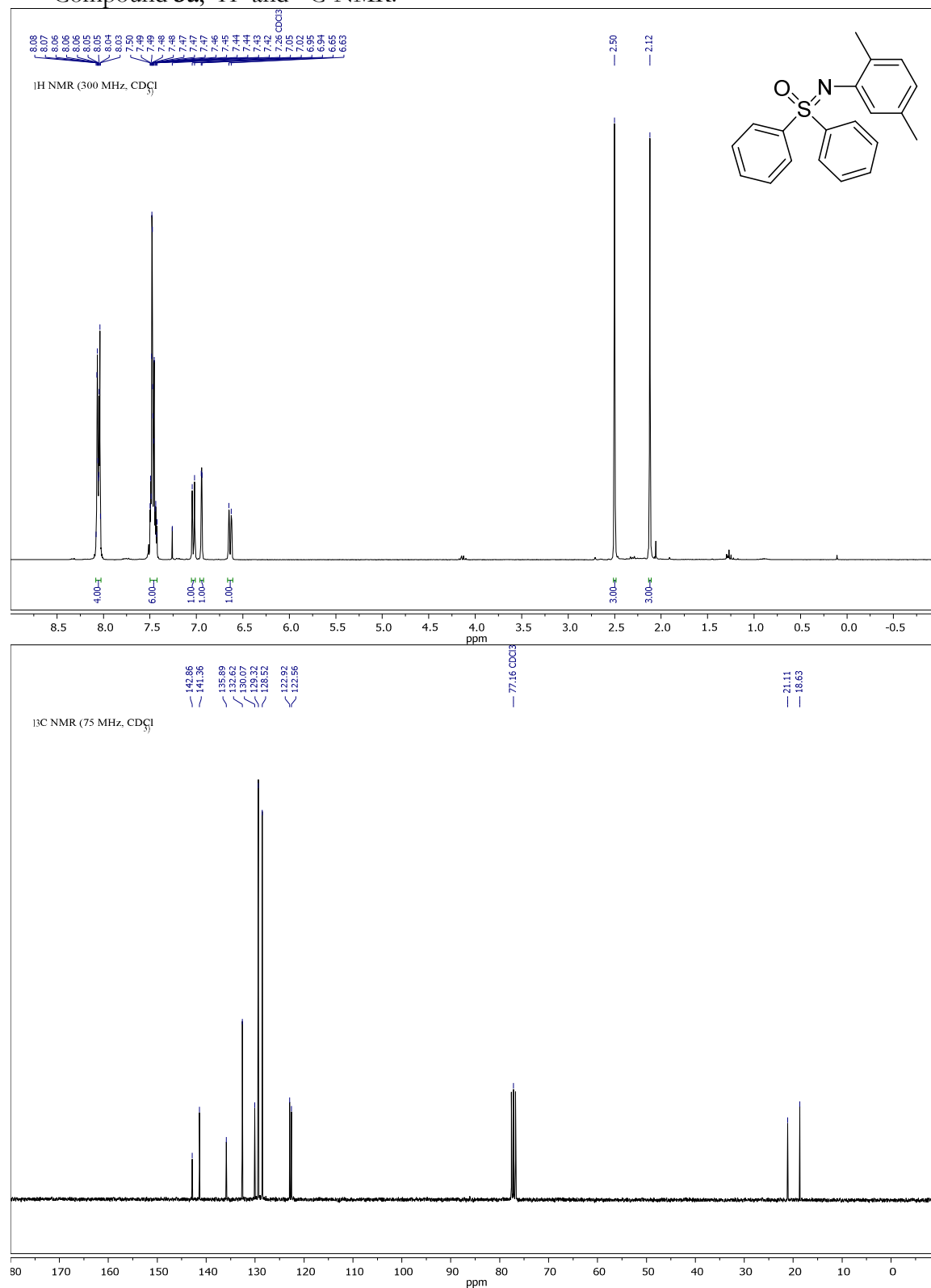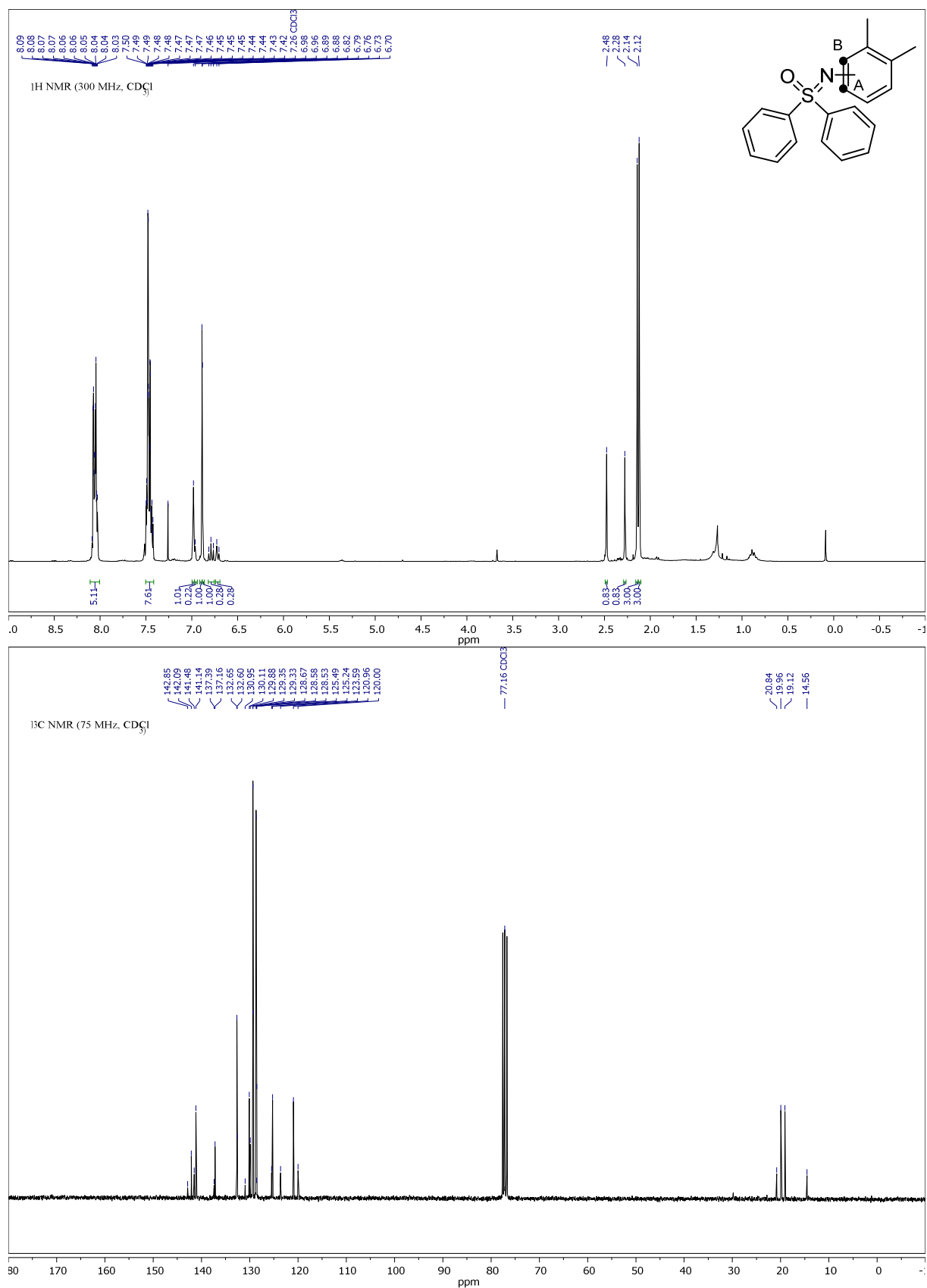
Compound **3d**, ^{1}H- and ^{13}C-NMR:

1H NMR (300 MHz, CDCl₃)

8.08, 8.07, 8.07, 8.06, 8.06, 8.05, 8.05, 8.04, 8.04, 8.03, 7.53, 7.52, 7.51, 7.50, 7.50, 7.49, 7.49, 7.48, 7.48, 7.48, 7.47, 7.46, 7.46, 7.46, 7.45, 7.45, 7.44, 7.44, 7.43, 7.26 CDCl3, 7.08, 7.07, 7.05, 7.04, 7.03, 6.84, 6.83, 6.81, 6.80

2.48

1.10

4.00, 6.00, 2.00, 1.00, 3.00, 9.00

8.5 8.0 7.5 7.0 6.5 6.0 5.5 5.0 4.5 4.0 3.5 3.0 2.5 2.0 1.5 1.0 0.5 0.0 -0.5
ppm

13C NMR (75 MHz, CDCl₃)

149.22, 142.62, 141.19, 132.60, 129.77, 129.57, 129.31, 128.67, 119.79, 118.50, 77.16 CDCl3, 34.26, 31.31, 18.47

180 170 160 150 140 130 120 110 100 90 80 70 60 50 40 30 20 10 0
ppm

Compound **3e**, ^{1}H- and ^{13}C-NMR:

1H NMR (400 MHz, CDCl$_3$)

13C NMR (101 MHz, CDCl$_3$)
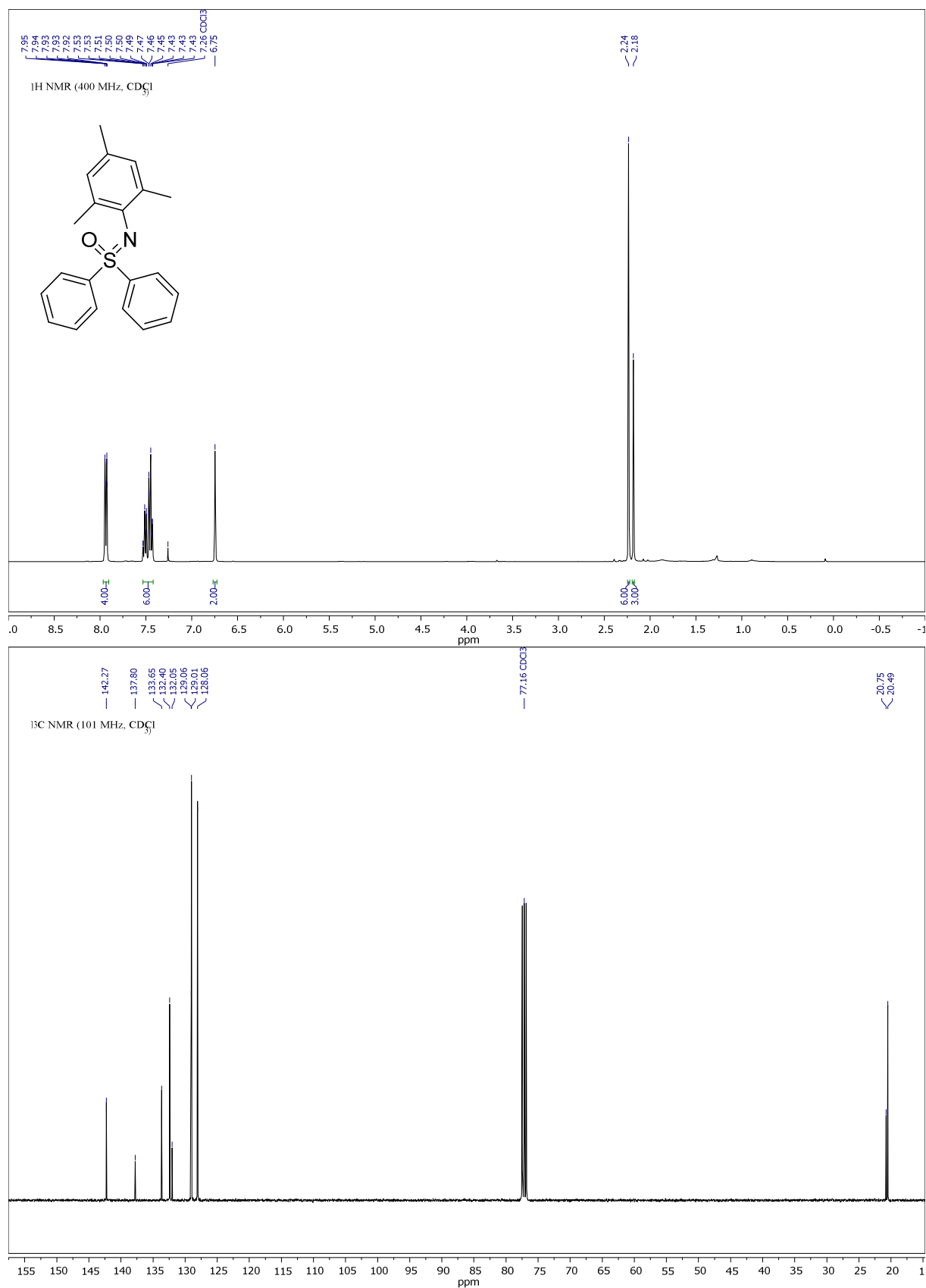
Compound **3f**, ¹H- and ¹³C-NMR:
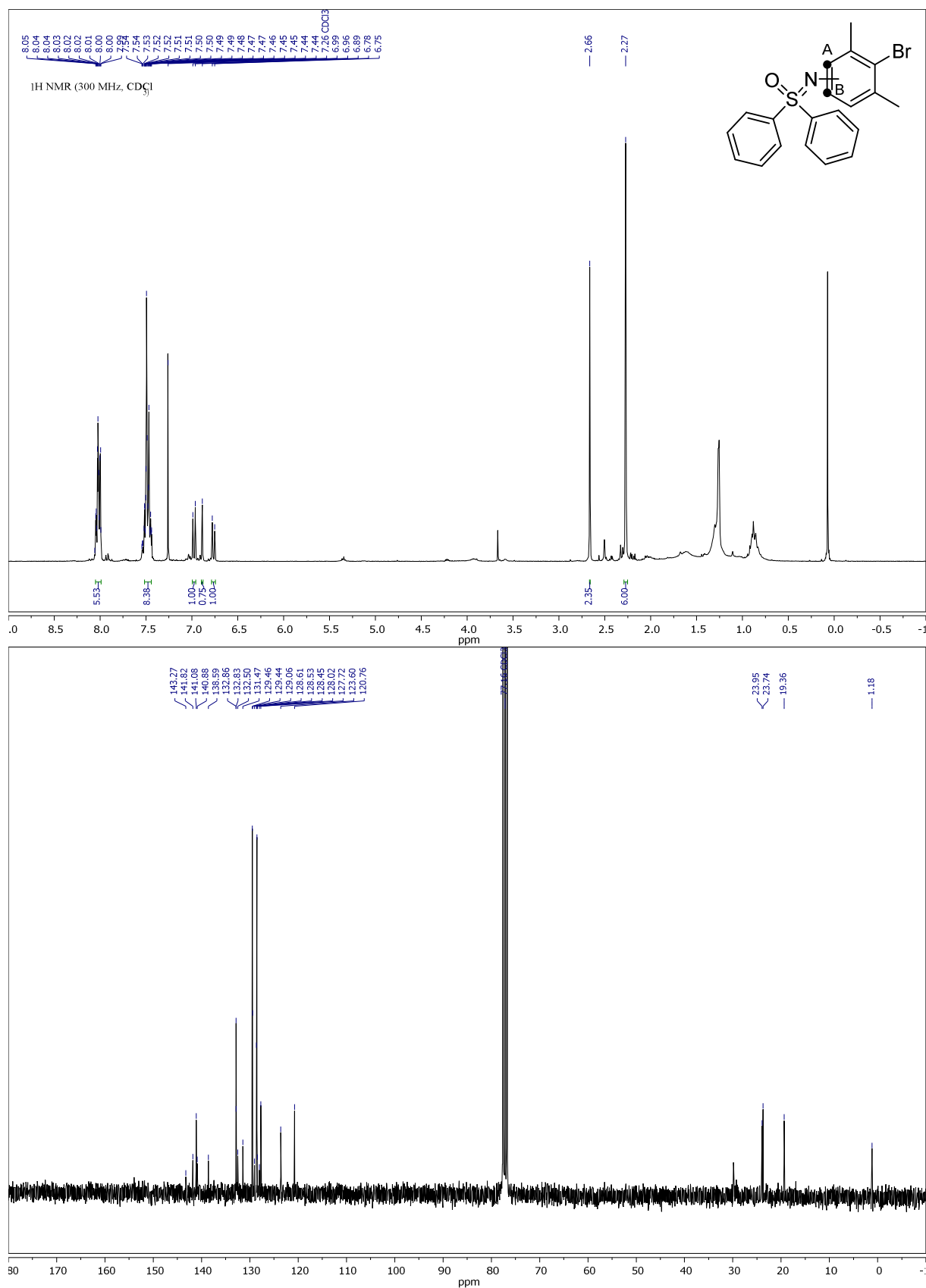
Compound **3g**, ^{1}H- and ^{13}C-NMR:

Compound **3h**, ^{1}H- and ^{13}C-NMR:

1H NMR (300 MHz, CDCl3)

13C NMR (75 MHz, CDCl3)

Compound **3i**, ^{1}H- and ^{13}C-NMR:

1H NMR (400 MHz, CDCl3)

13C NMR (75 MHz, CDCl3)
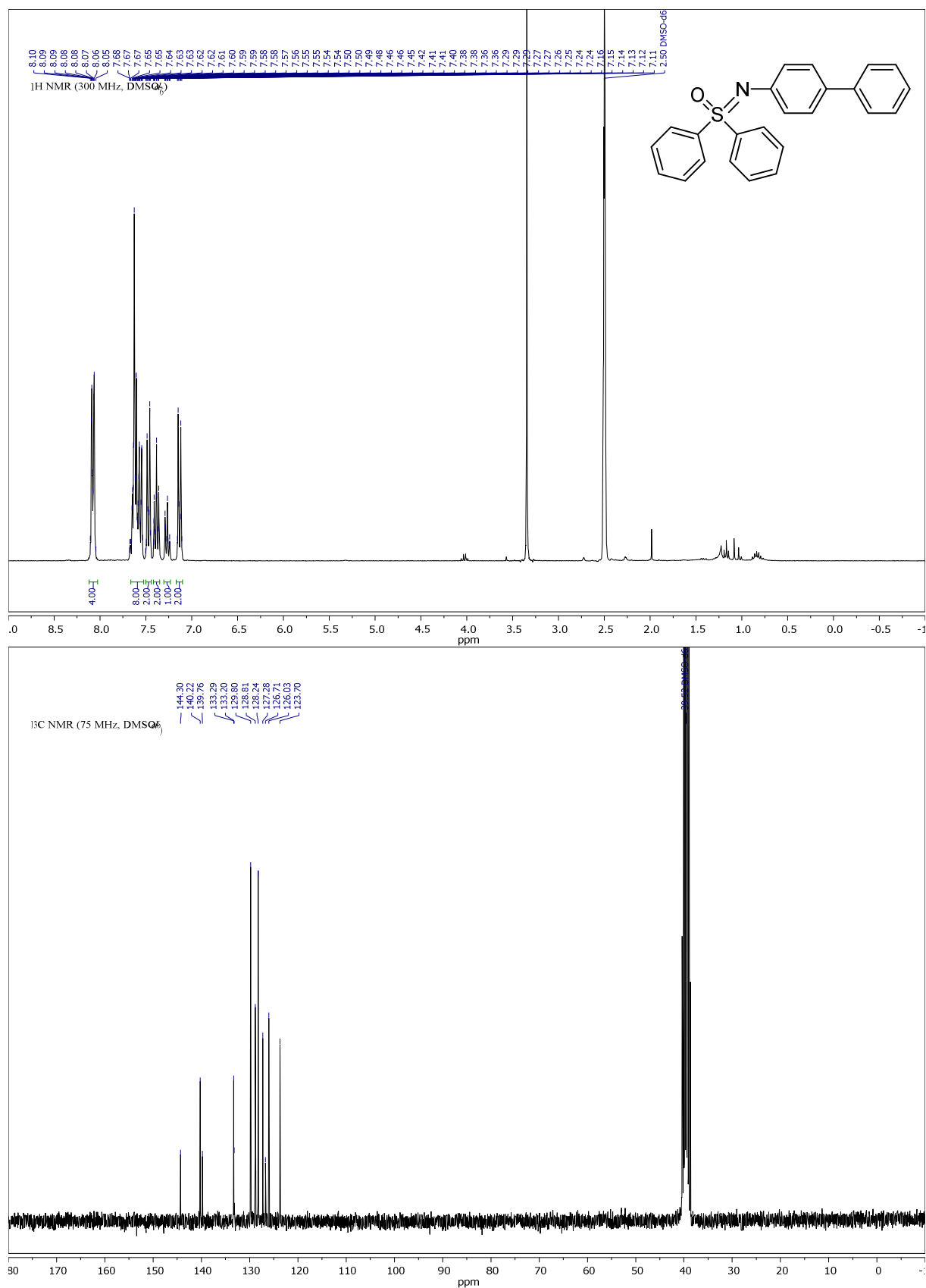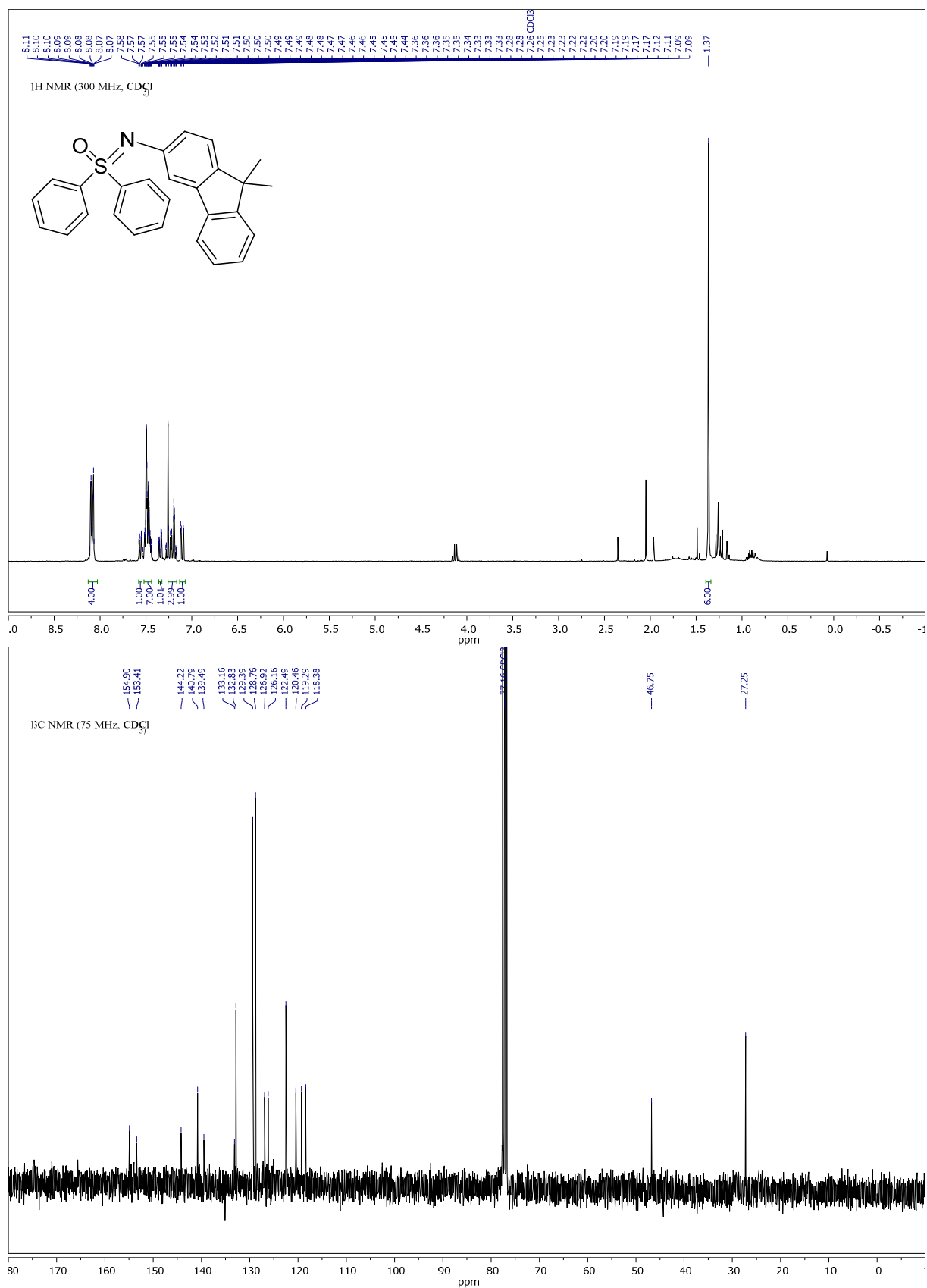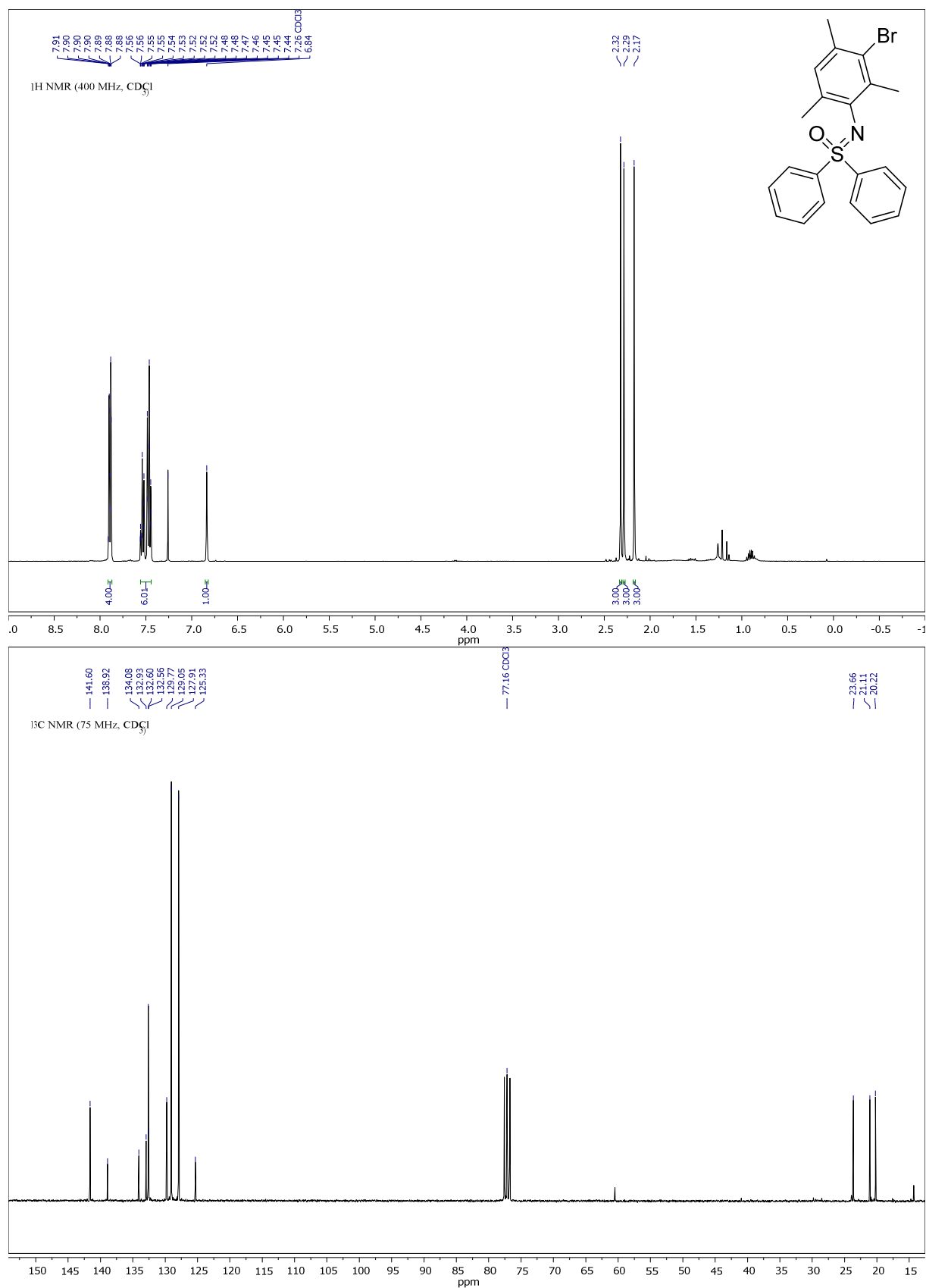
Compound **3j,** ^{1}H- and ^{13}C-NMR:
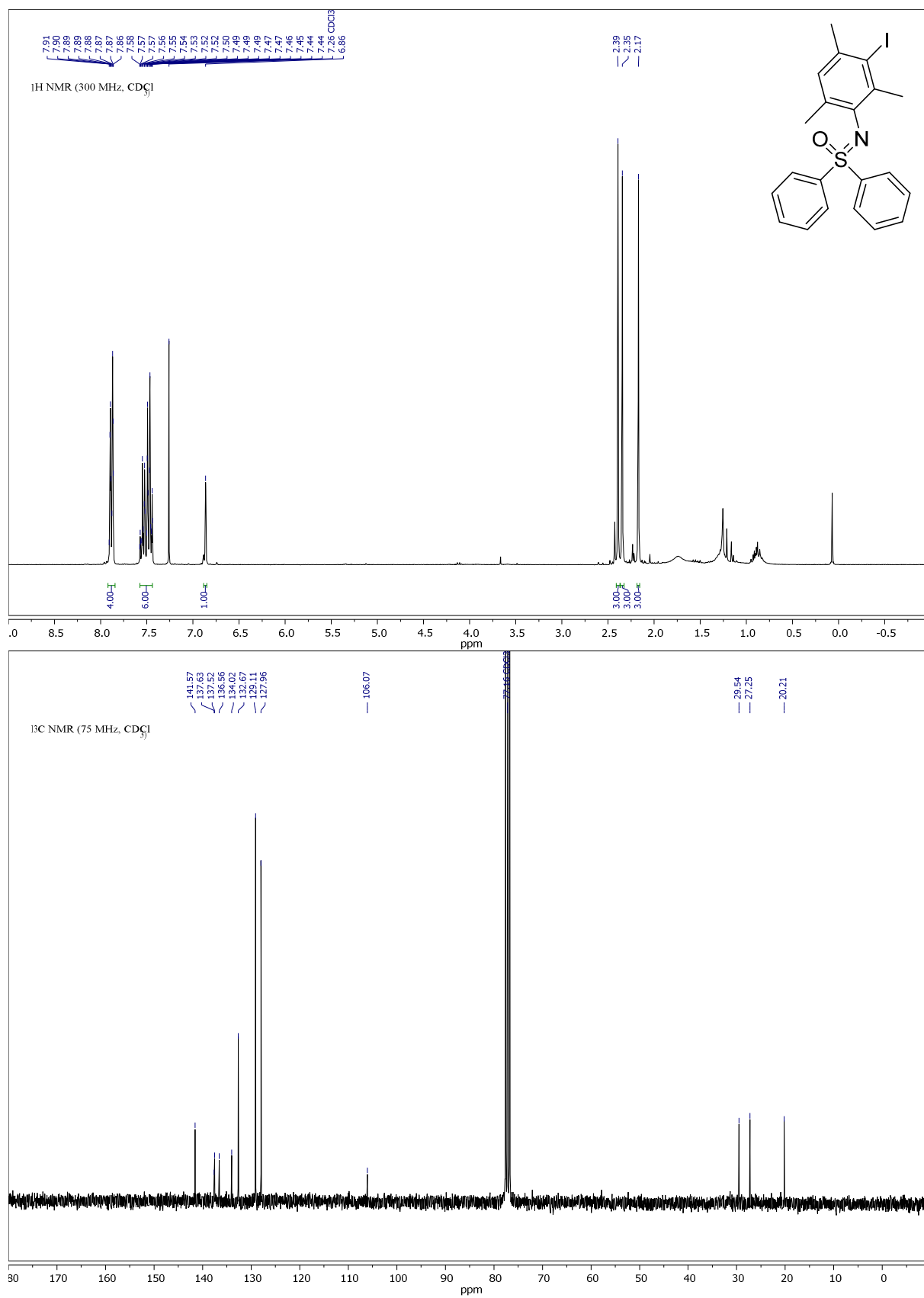
Compound **3l**, ^{1}H- and ^{13}C-NMR:

Compound **3m**, ^{1}H- and ^{13}C-NMR:

1H NMR (300 MHz, CDCl$_3$)

13C NMR (75 MHz, CDCl$_3$)

Compound **3n**, ^{1}H- and ^{13}C-NMR:

1H NMR (400 MHz, CDCl$_3$)

13C NMR (101 MHz, CDCl$_3$)

Compound **3o**, ^{1}H- and ^{13}C-NMR:

1H NMR (400 MHz, CDCl$_3$)

13C NMR (101 MHz, CDCl$_3$)

Compound **3p**, ^{1}H- and ^{13}C-NMR:

1H NMR (300 MHz, CDCl$_3$)

13C NMR (75 MHz, CDCl$_3$)
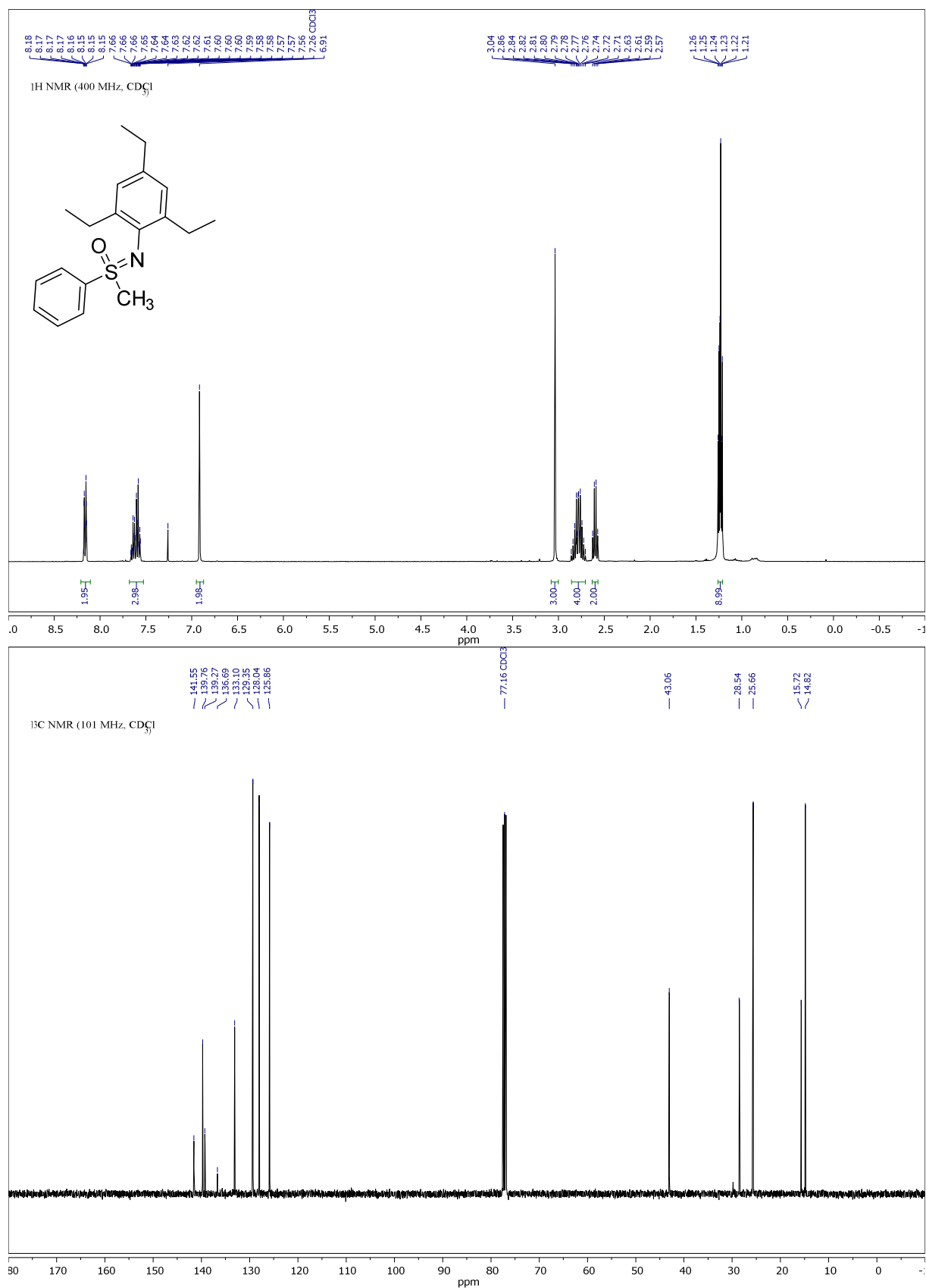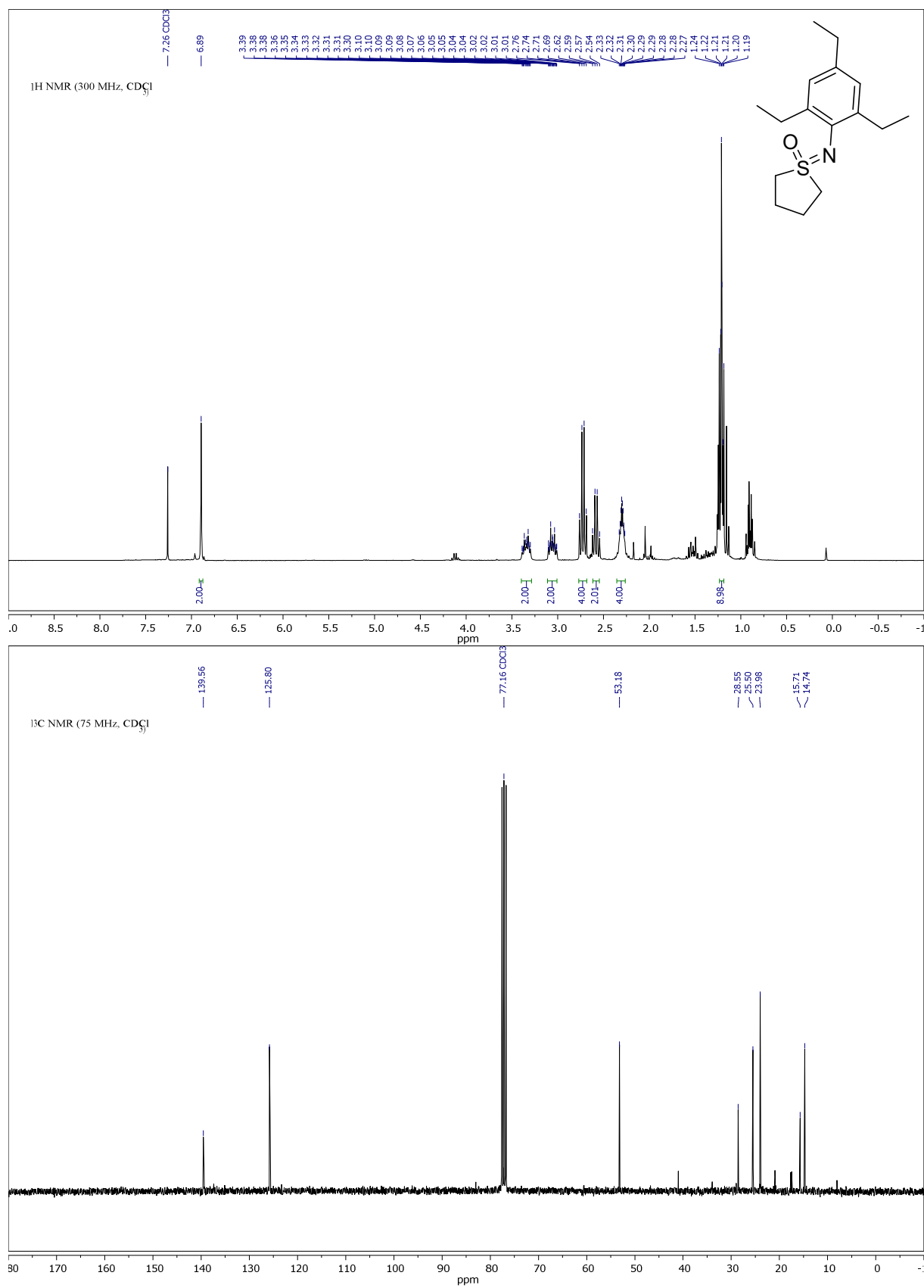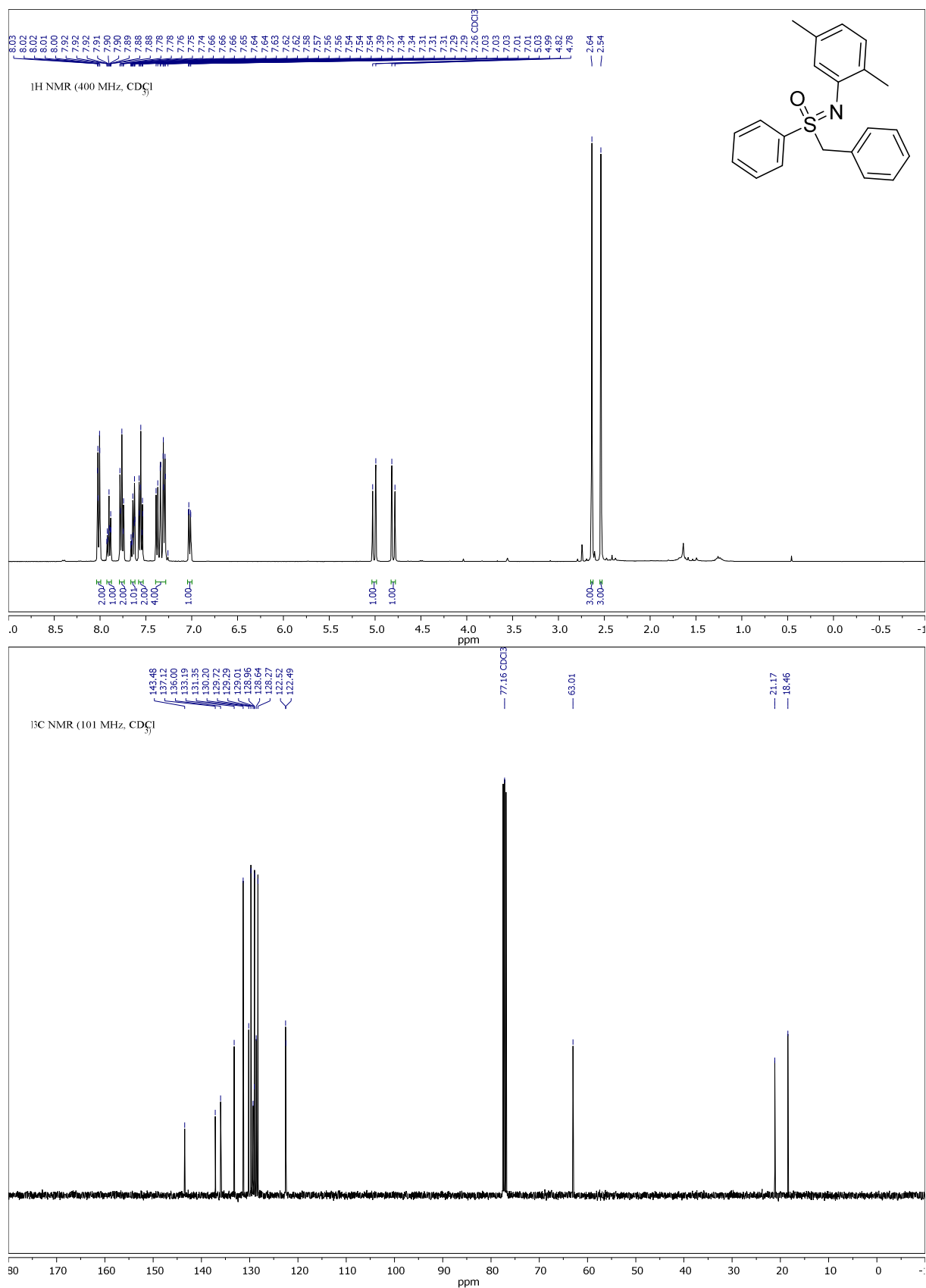
Compound **3q**, ^{1}H- and ^{13}C-NMR:
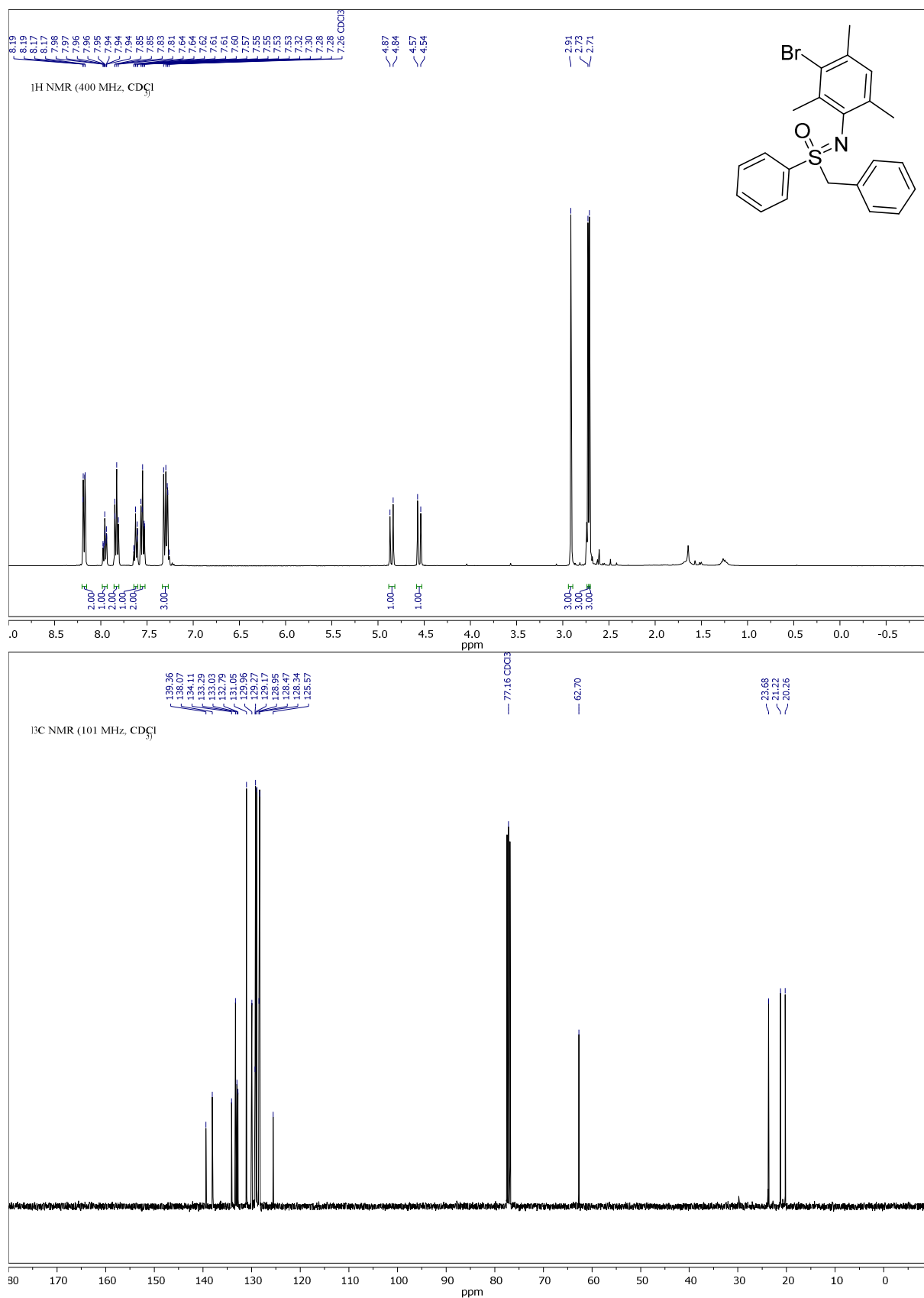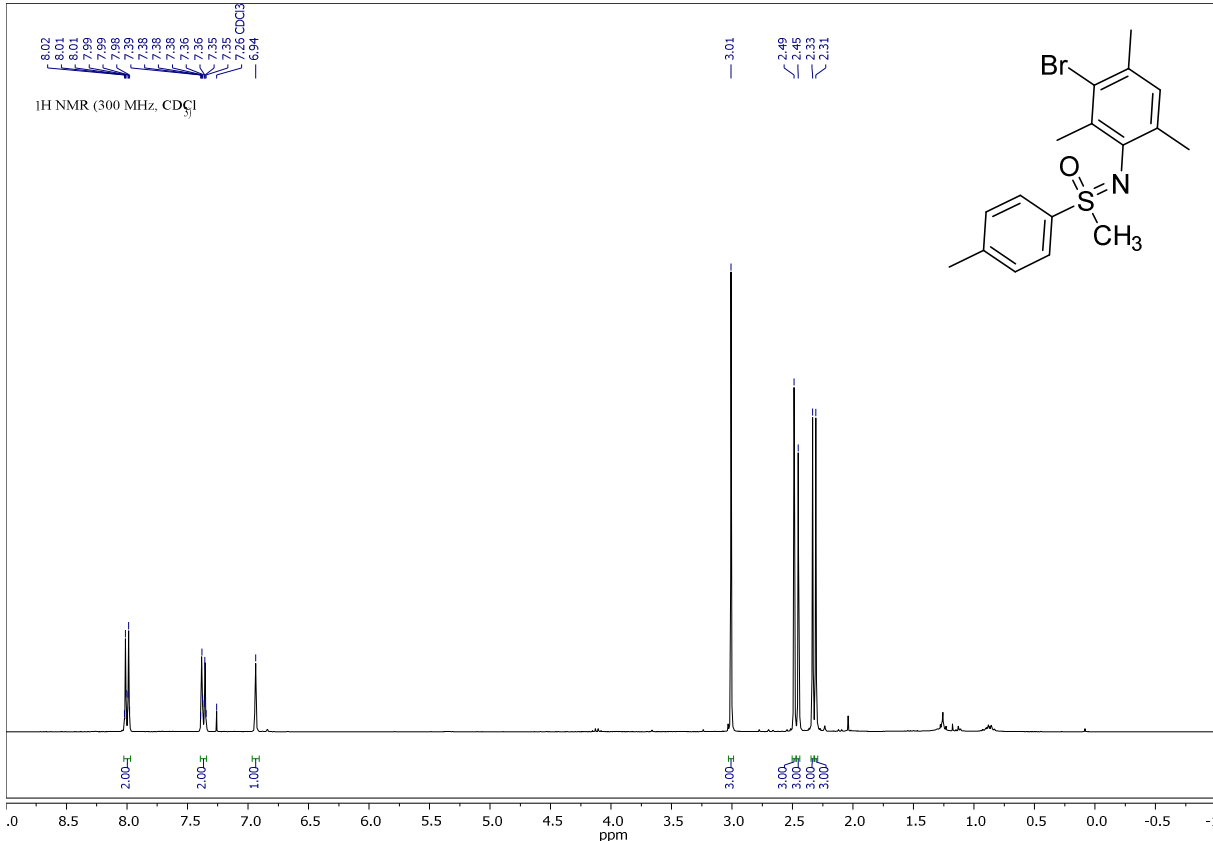
Compound **3r**, ^{1}H- and ^{13}C-NMR:
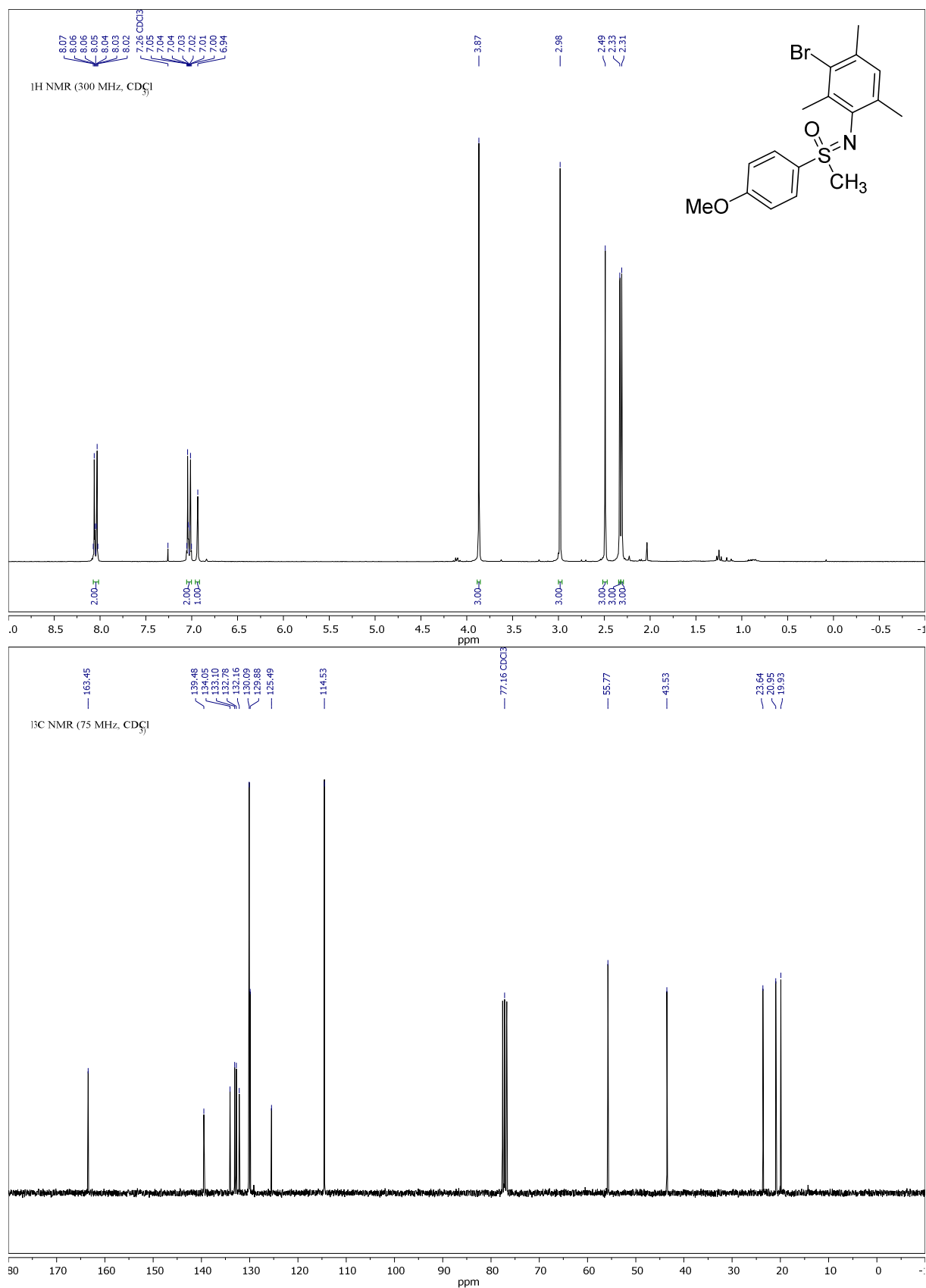
Compound **3s**, ^{1}H- and ^{13}C-NMR:

1H NMR (400 MHz, CDCl$_3$)

13C NMR (101 MHz, CDCl$_3$)

Compound **3t**, ¹H- and ¹³C-NMR:

1H NMR (400 MHz, CDCl₃)

13C NMR (101 MHz, CDCl₃)

Compound **3u**, ^{1}H- and ^{13}C-NMR:

1H NMR (400 MHz, CDCl$_3$)

8.07, 8.07, 8.06, 8.05, 8.04, 7.57, 7.56, 7.56, 7.55, 7.54, 7.53, 7.26 CDCl3, 6.94, 3.05, 2.46, 2.34, 2.28

13C NMR (101 MHz, CDCl$_3$)

140.03, 139.45, 138.86, 133.98, 133.18, 132.97, 129.99, 129.70, 129.43, 125.58, 77.16 CDCl3, 43.61, 23.67, 20.98, 19.93
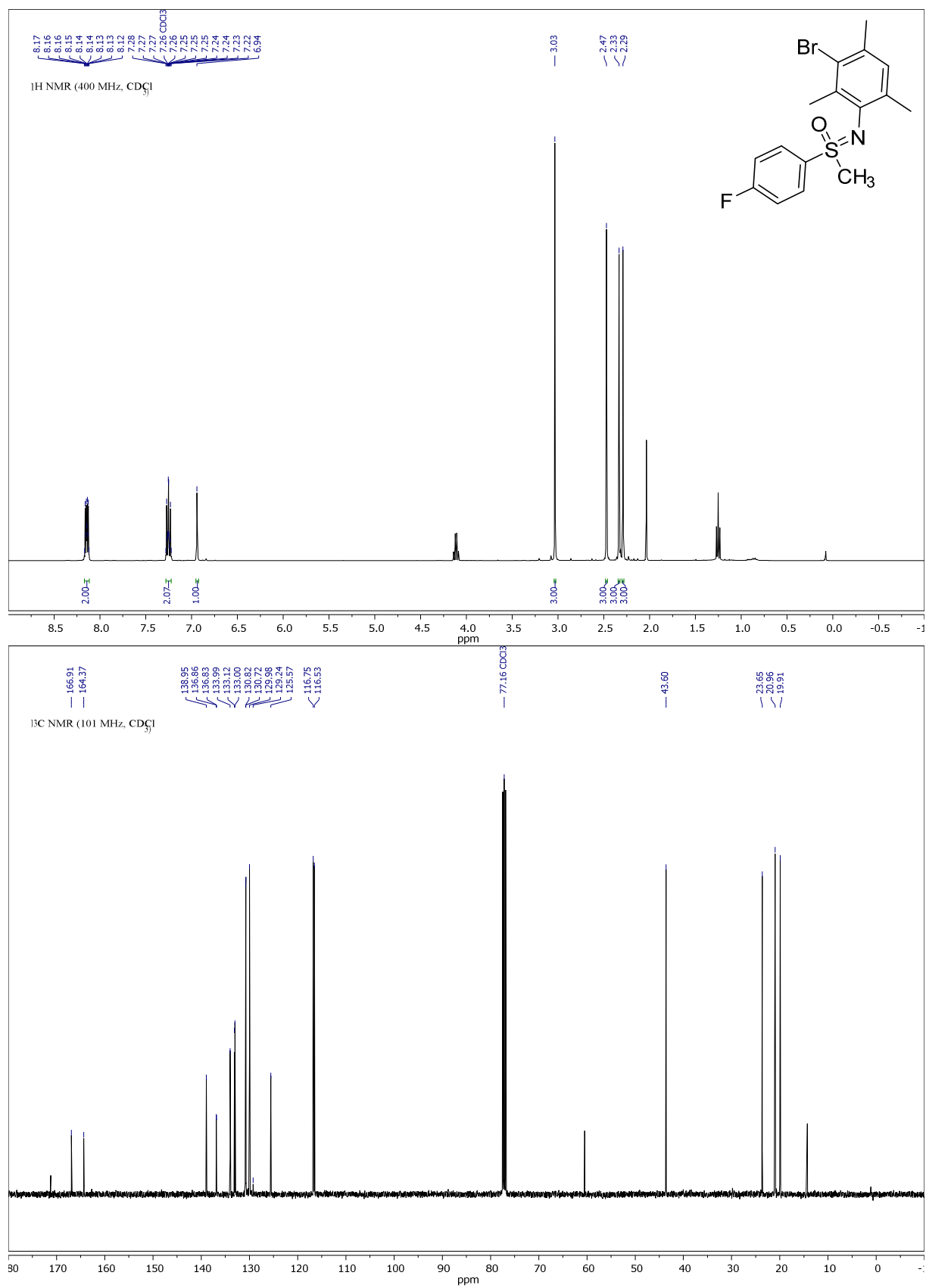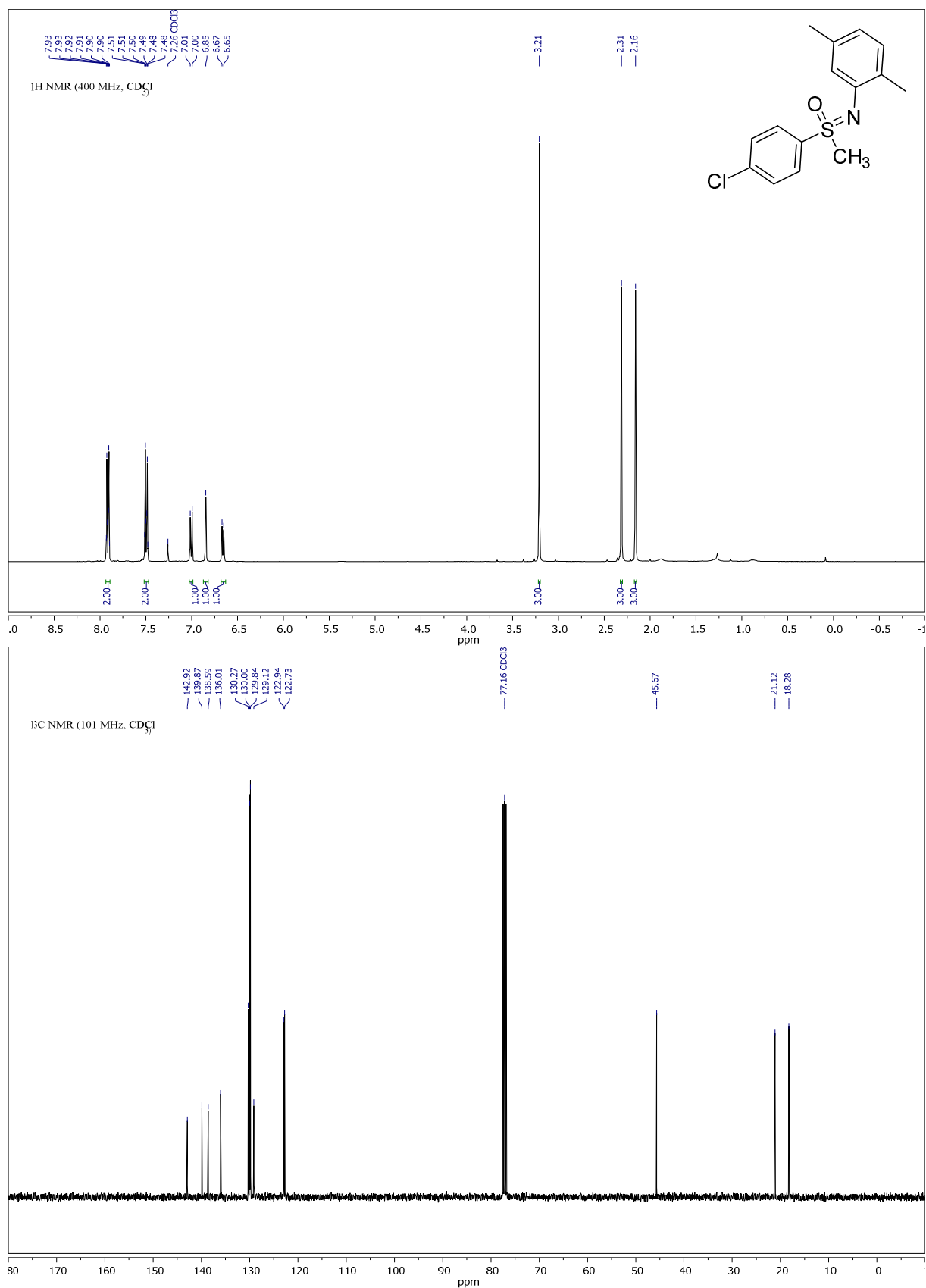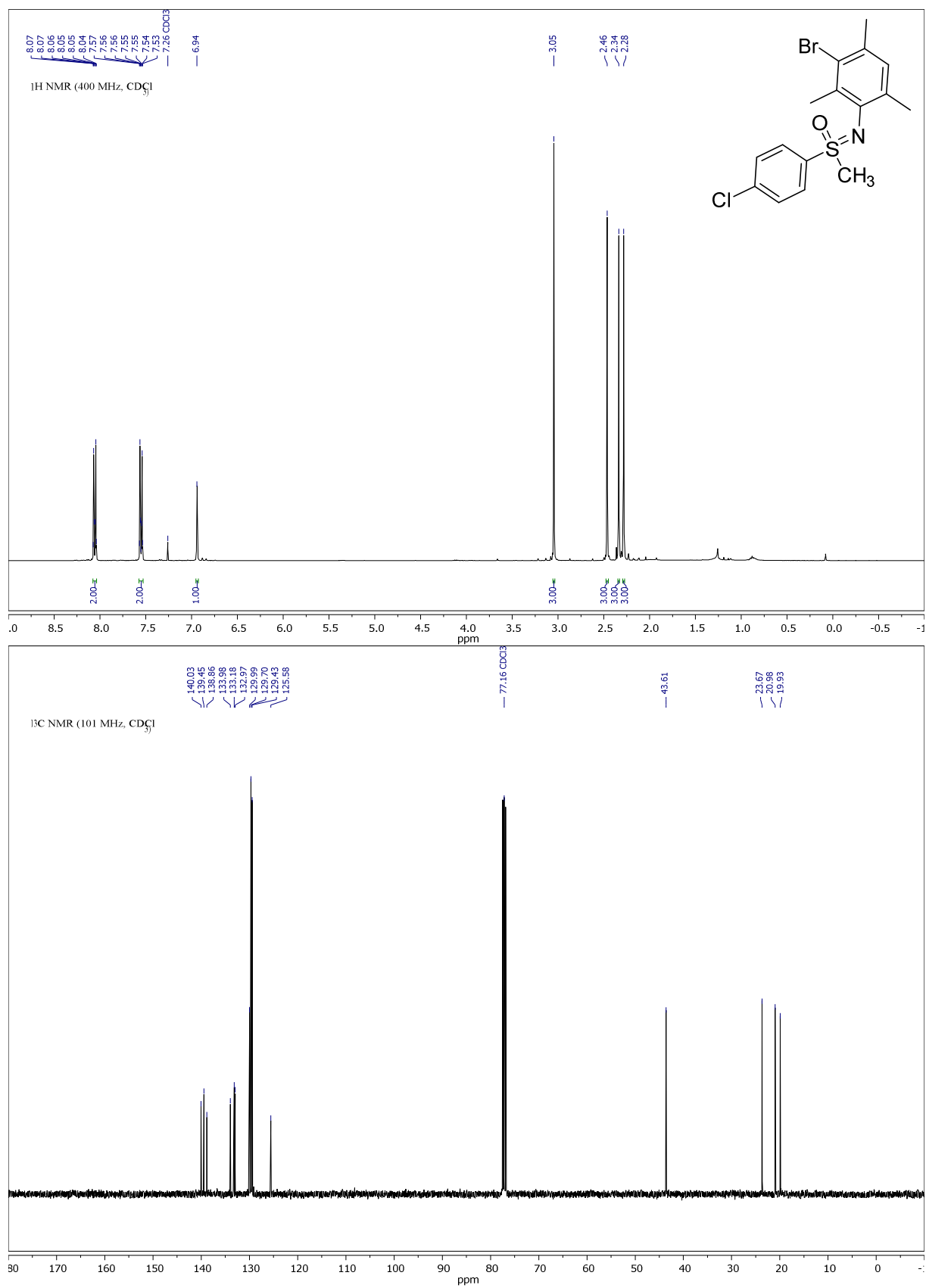
Compound **3v**, ^{1}H- and ^{13}C-NMR:
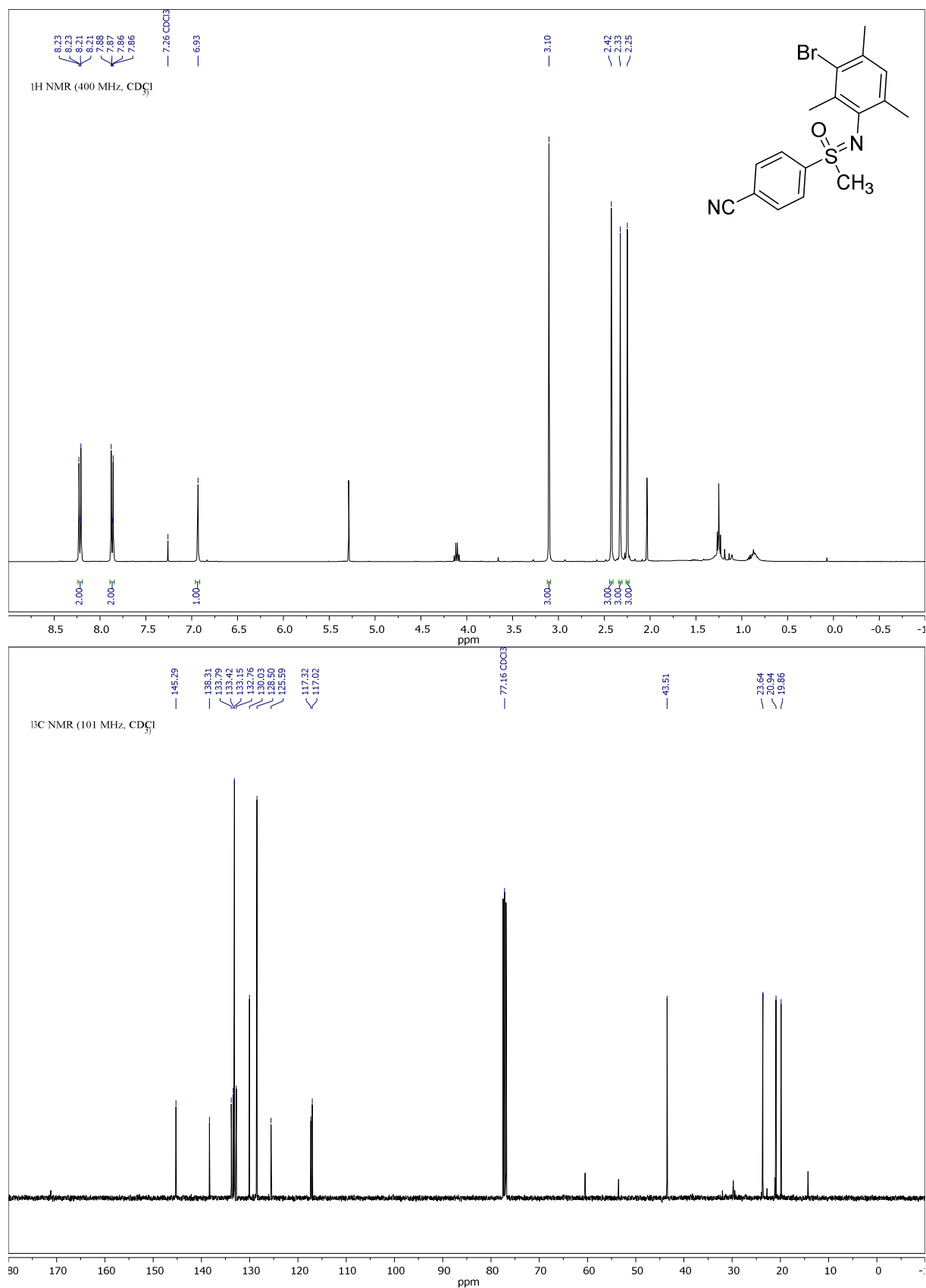
Compound **3w**, ^{1}H- and ^{13}C-NMR:
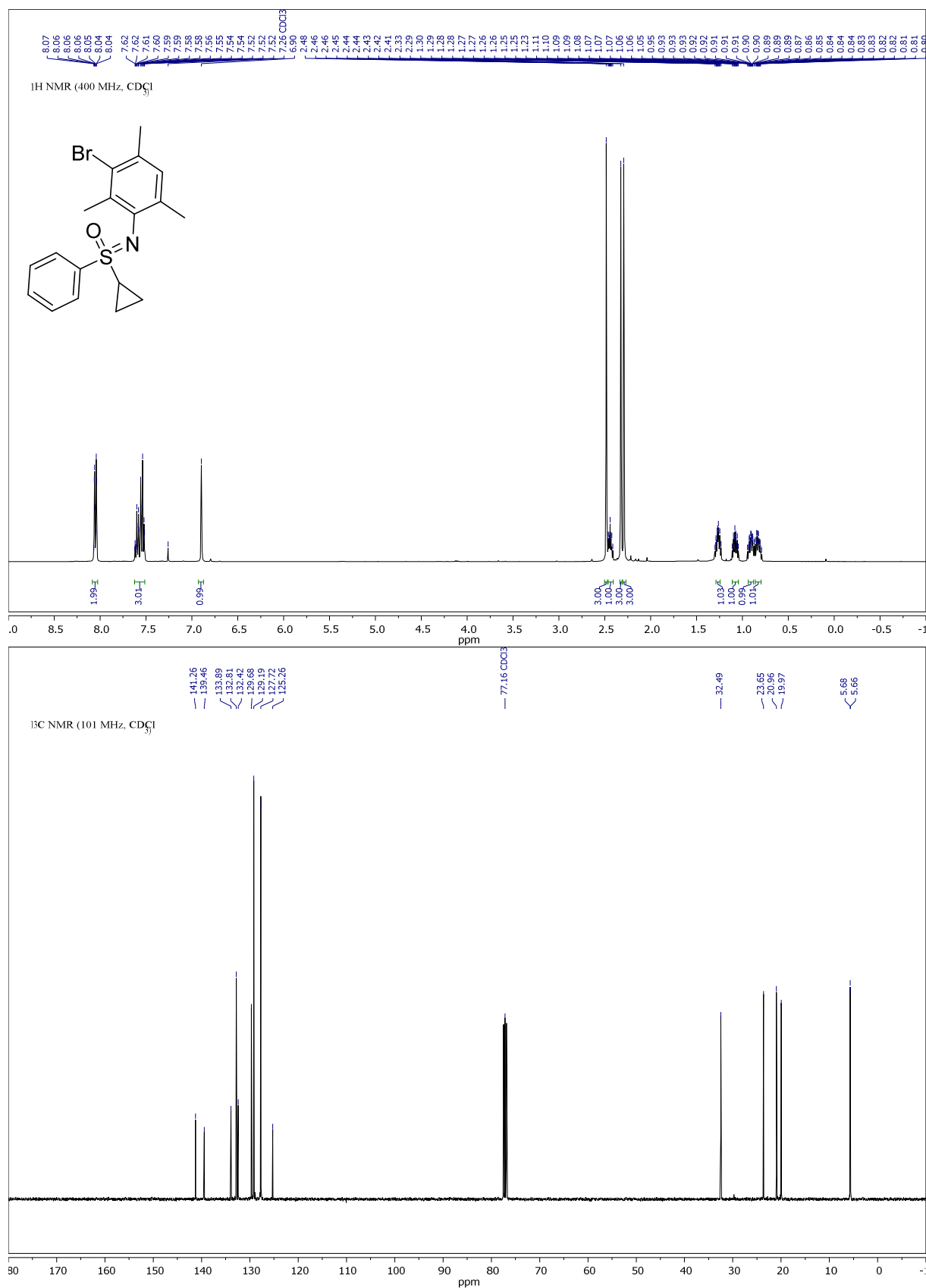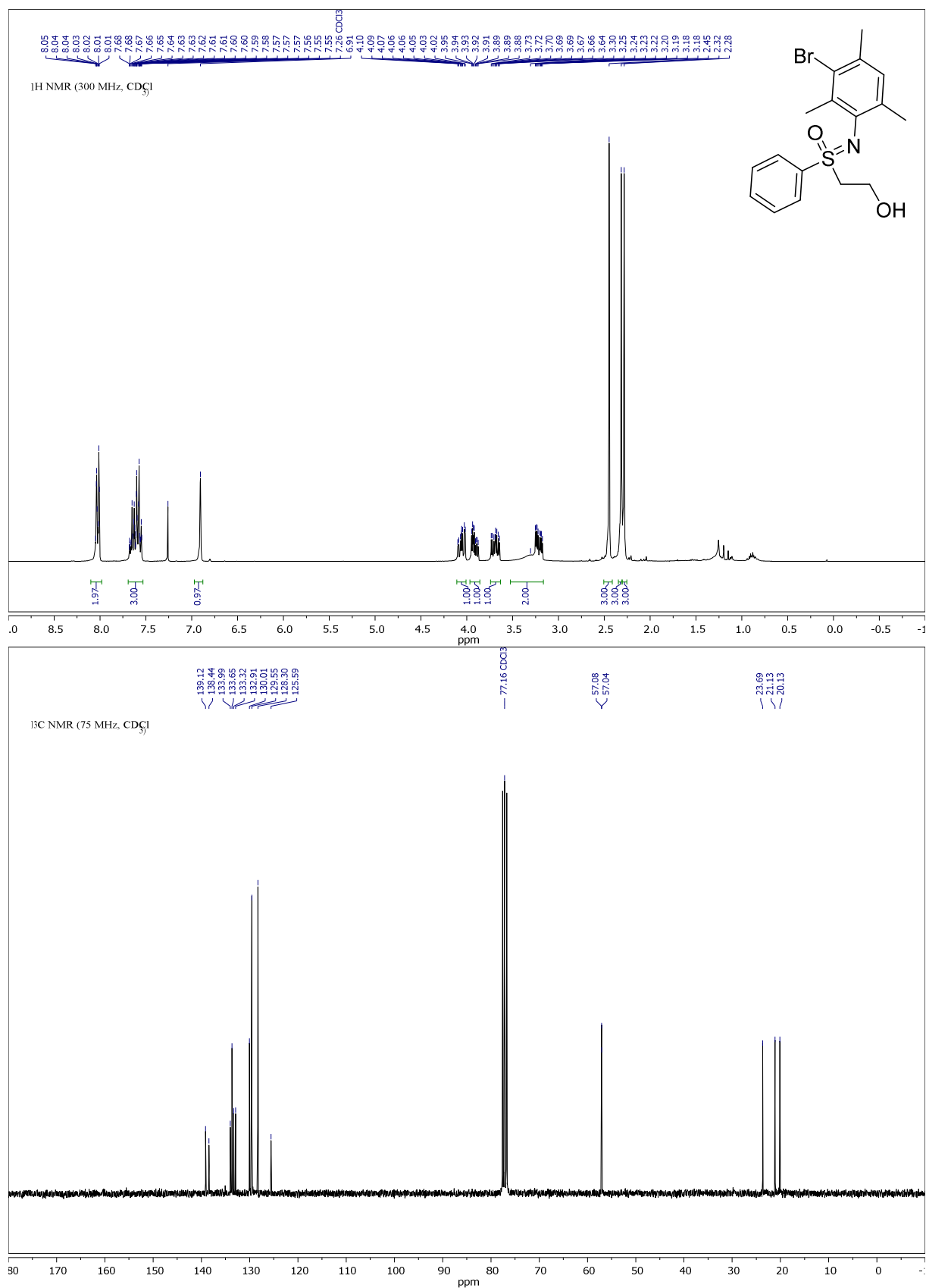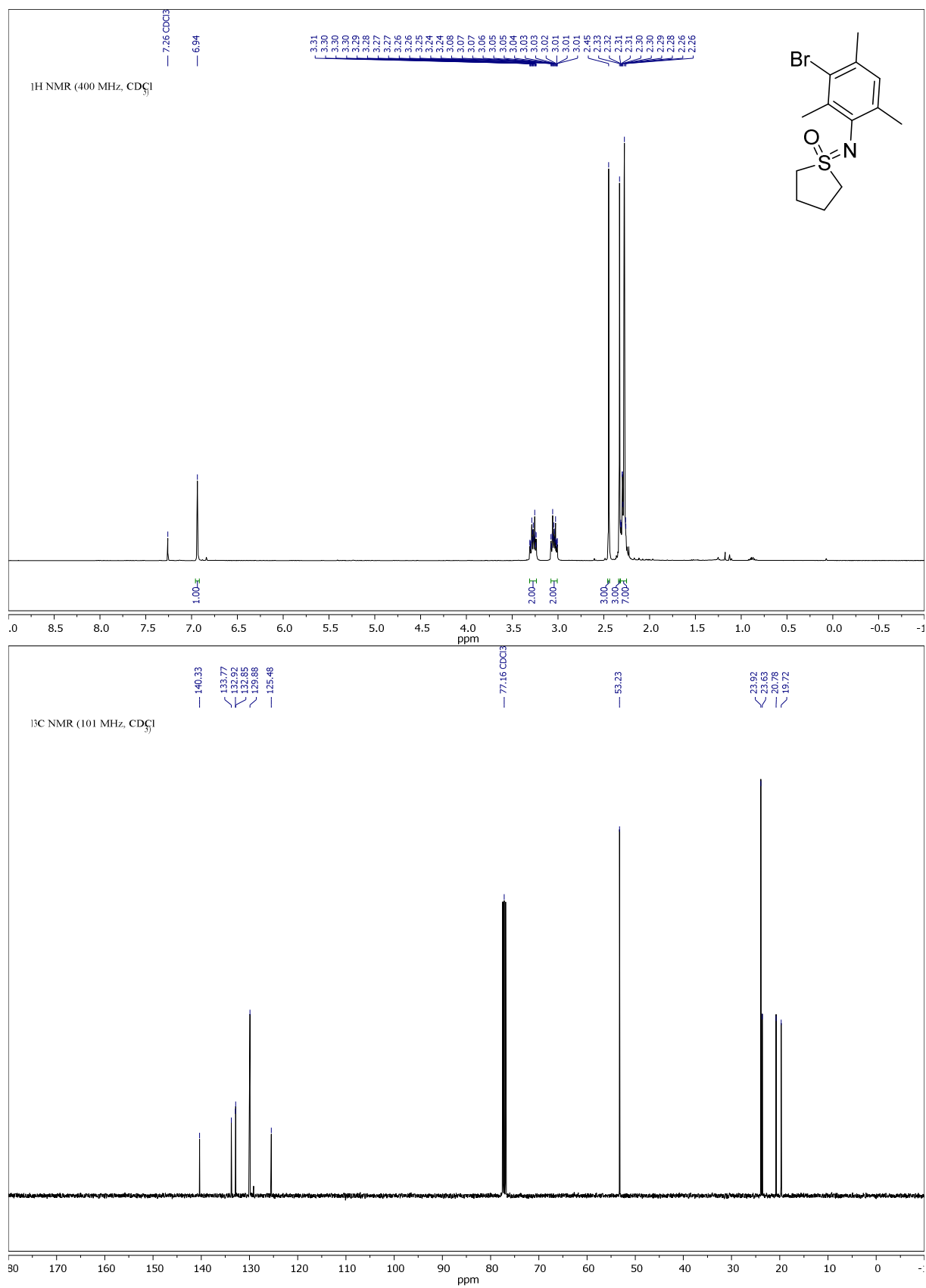
1H NMR (400 MHz, CDCl$_3$)

13C NMR (101 MHz, CDCl$_3$)

Compound **3x**, ¹H- and ¹³C-NMR:

1H NMR (300 MHz, CDCl₃)

13C NMR (75 MHz, CDCl₃)

Compound **3z**, ¹H- and ¹³C-NMR:

1H NMR (400 MHz, CDCl₃)

13C NMR (101 MHz, CDCl₃)

Compound **3aa**, ^{1}H- and ^{13}C-NMR:

1H NMR (300 MHz, CDCl$_3$)

13C NMR (75 MHz, CDCl$_3$)

Compound **3ab**, ^{1}H- and ^{13}C-NMR:

1H NMR (300 MHz, CDCl$_3$)

13C NMR (75 MHz, CDCl$_3$)

Compound **3ac**, ^{1}H- and ^{13}C-NMR:

1H NMR (300 MHz, CDCl₃)

13C NMR (75 MHz, CDCl₃)
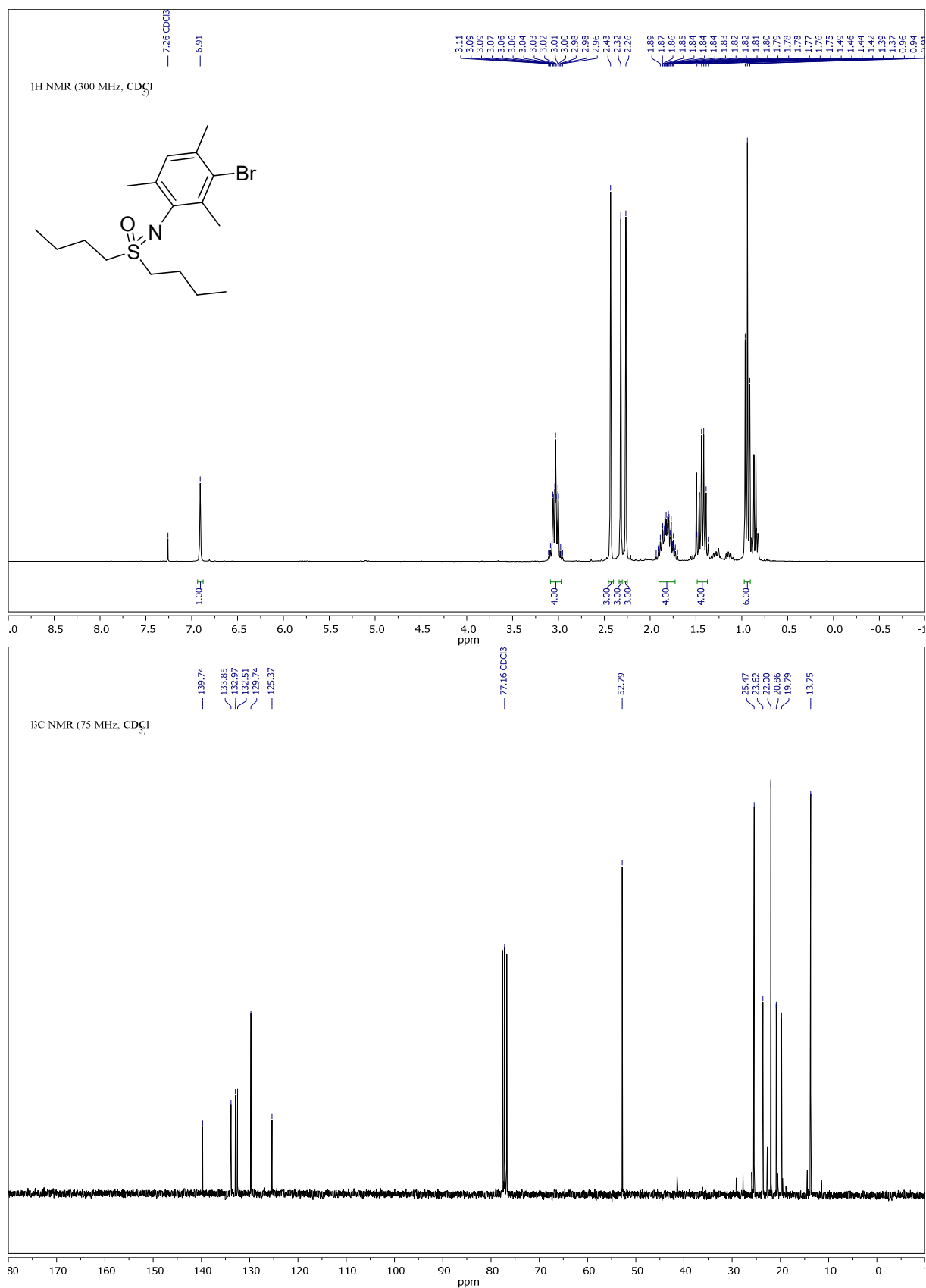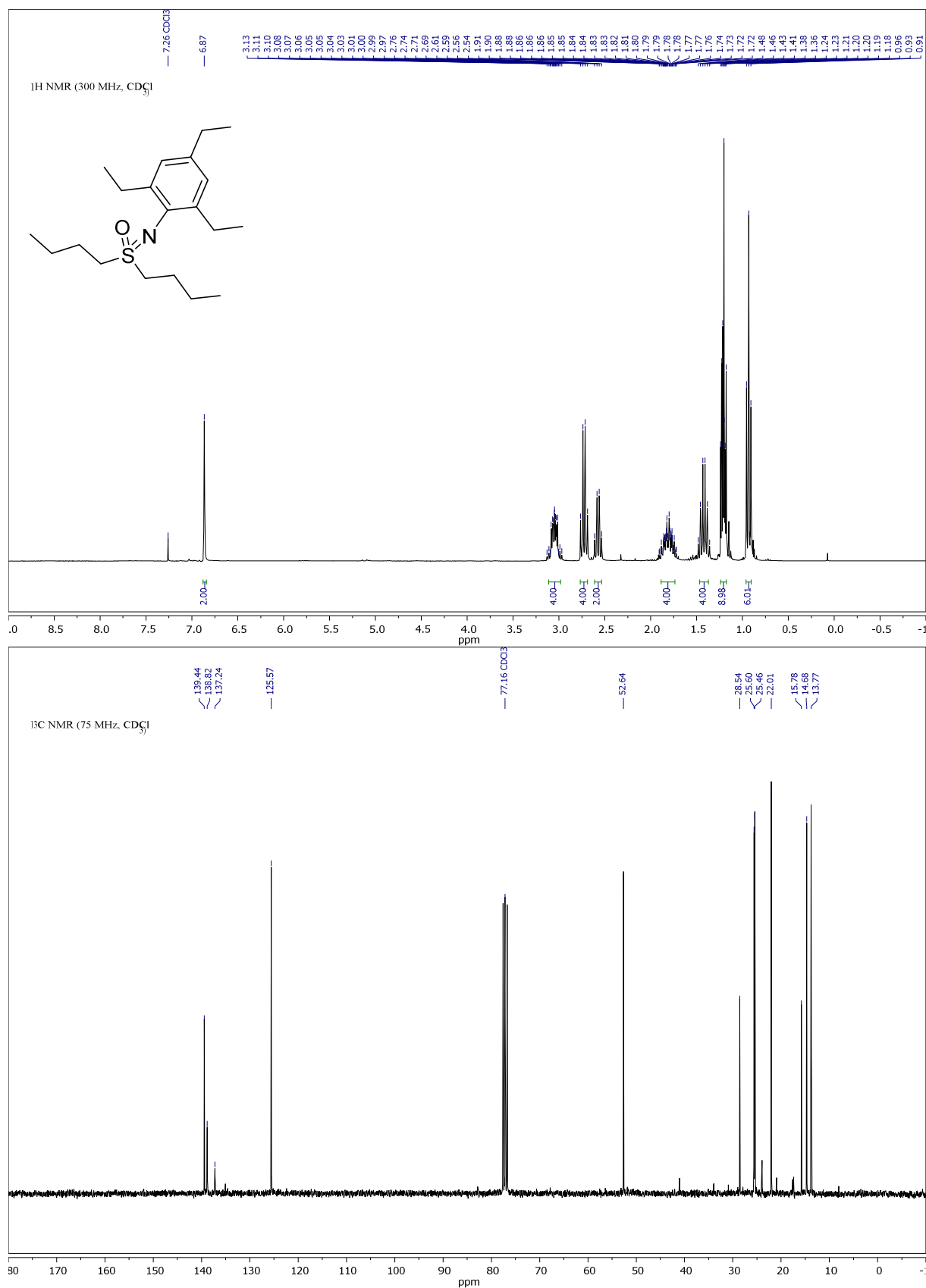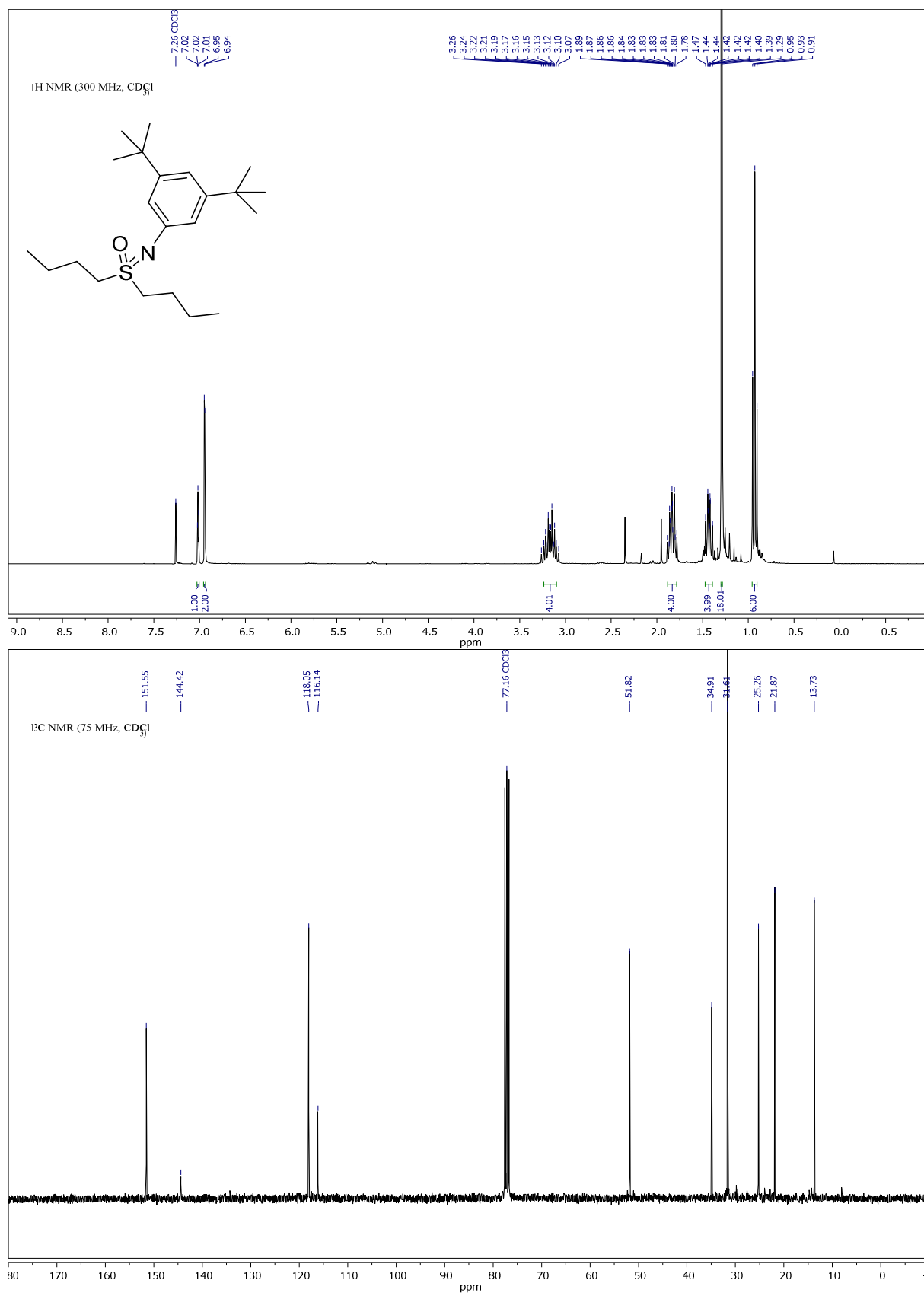
Compound **3ad**, ^{1}H- and ^{13}C-NMR:

1H NMR (400 MHz, CDCl$_3$)

13C NMR (75 MHz, CDCl$_3$)
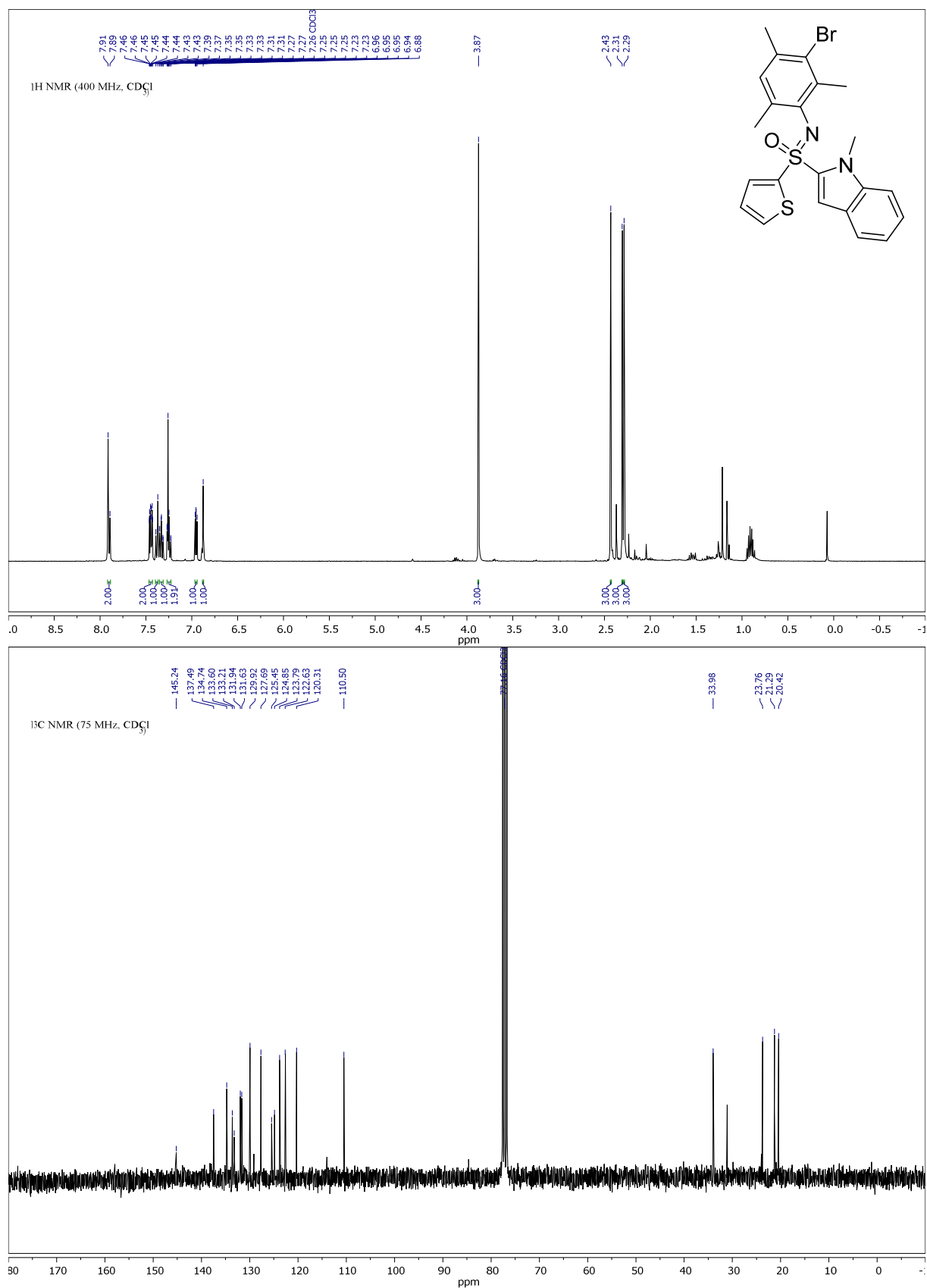
Compound **1ad**, ^{1}H- and ^{13}C-NMR:

1H NMR (300 MHz, CDCl[3])

13C NMR (75 MHz, CDCl[3])
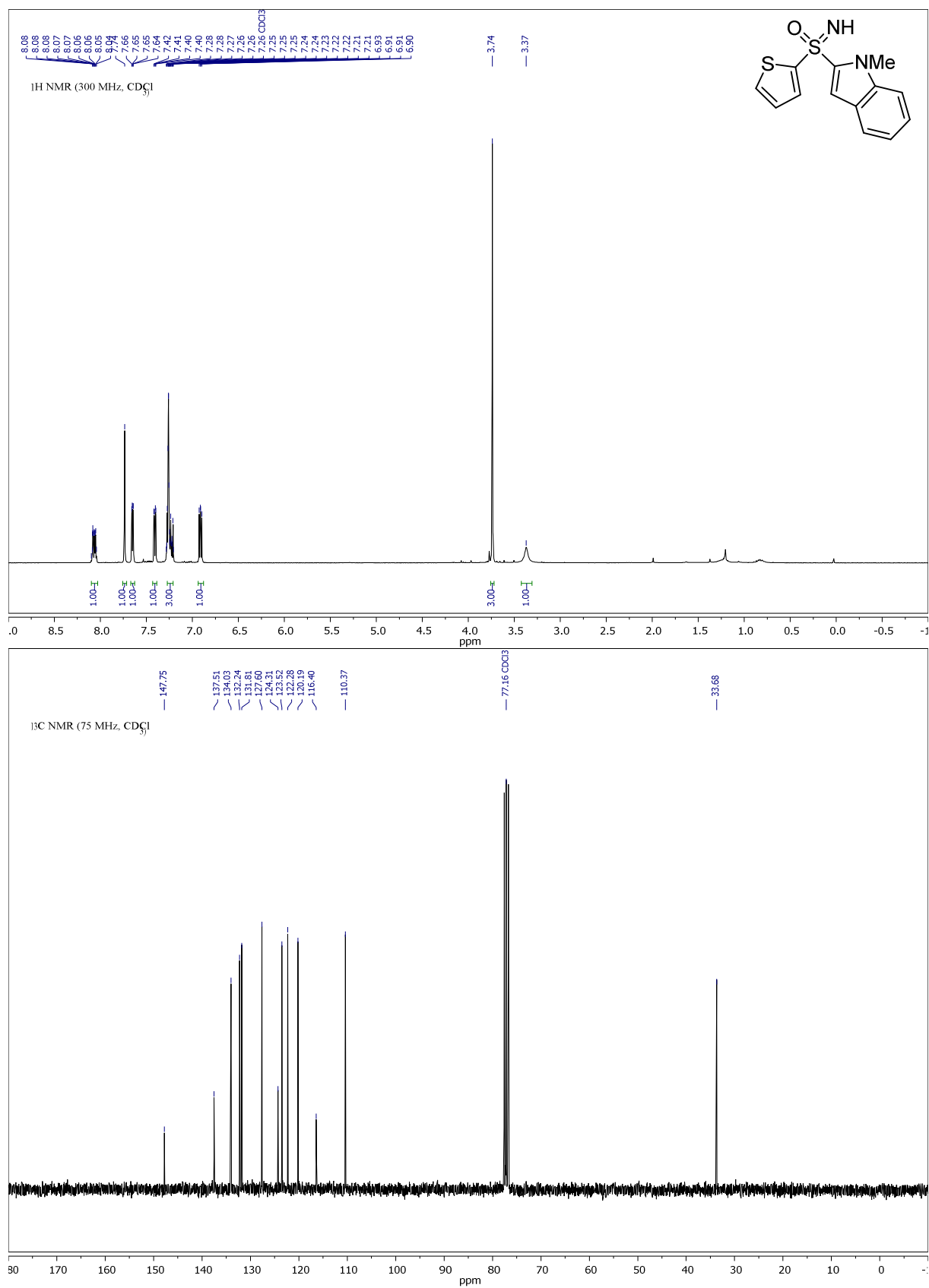
6.3 Appendix Chapter 2

6.3.1 Experimental Details of the Analysis of Enantiopure Sulfoximines by NP chiral HPLC

Methyl(phenyl)((4-(trifluoromethyl)phenyl)imino)-λ^6-sulfanone (3at)
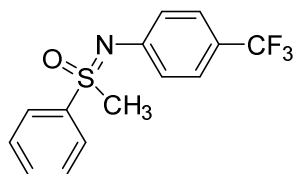
Table 12. Chiral HPLC Data of Compound **3at**.

Peak	Retention Time	Height	Area	Area%
#	[min]	[mAU]	[mAU * min]	[%]
1	12.00	471.1	189.0	49
2	16.99	373.0	199.4	51
Total		844.1	388.4	100
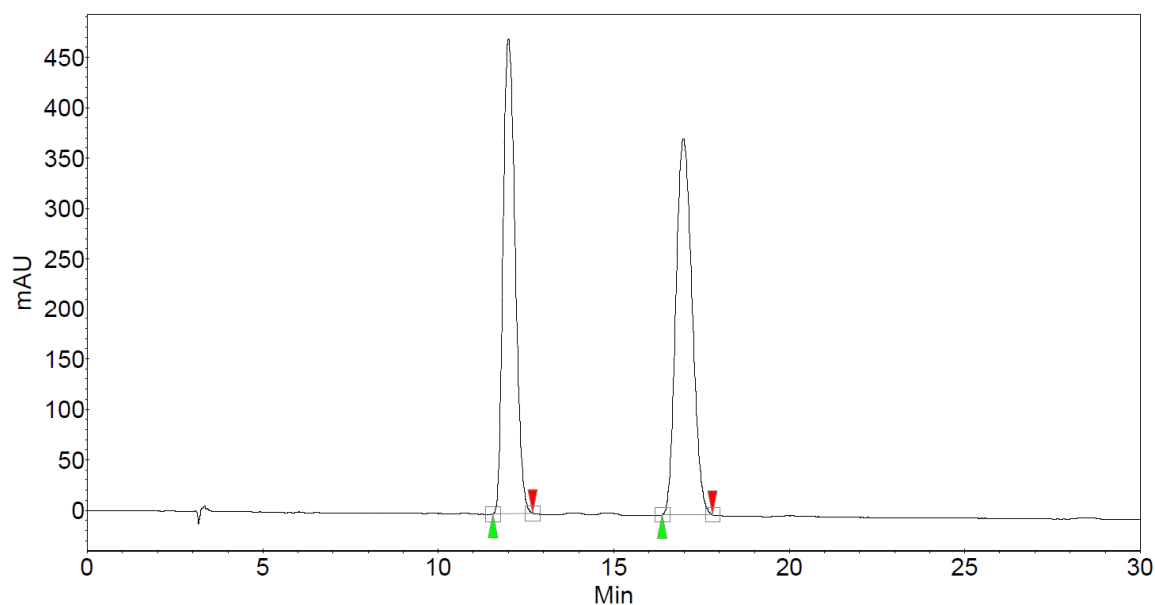
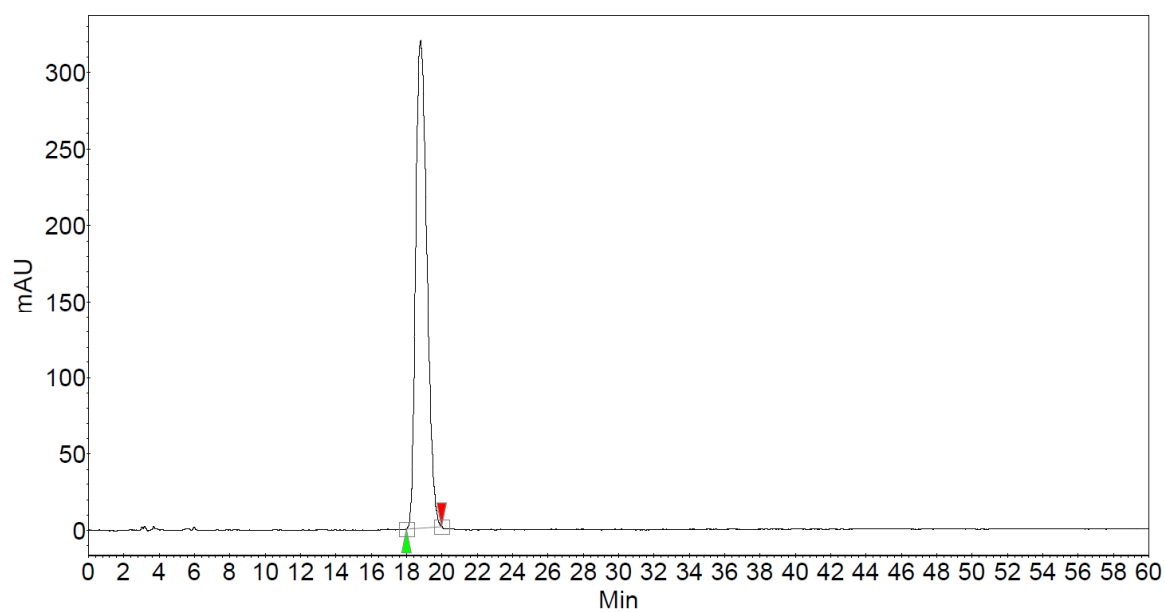**Figure 26.** Chiral HPLC Chromatogram of Compound **3at**.

(S)-Methyl(phenyl)((4-(trifluoromethyl)phenyl)imino)-λ⁶-sulfanone ((S)-3at)
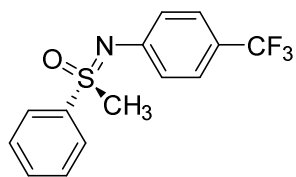
Table 13. Chiral HPLC Data of Compound **(S)-3at**.

Peak #	Retention Time [min]	Height [mAU]	Area [mAU * min]	Area% [%]
1	16.57	347.3	192.0	100
Total		347.3	192.0	100
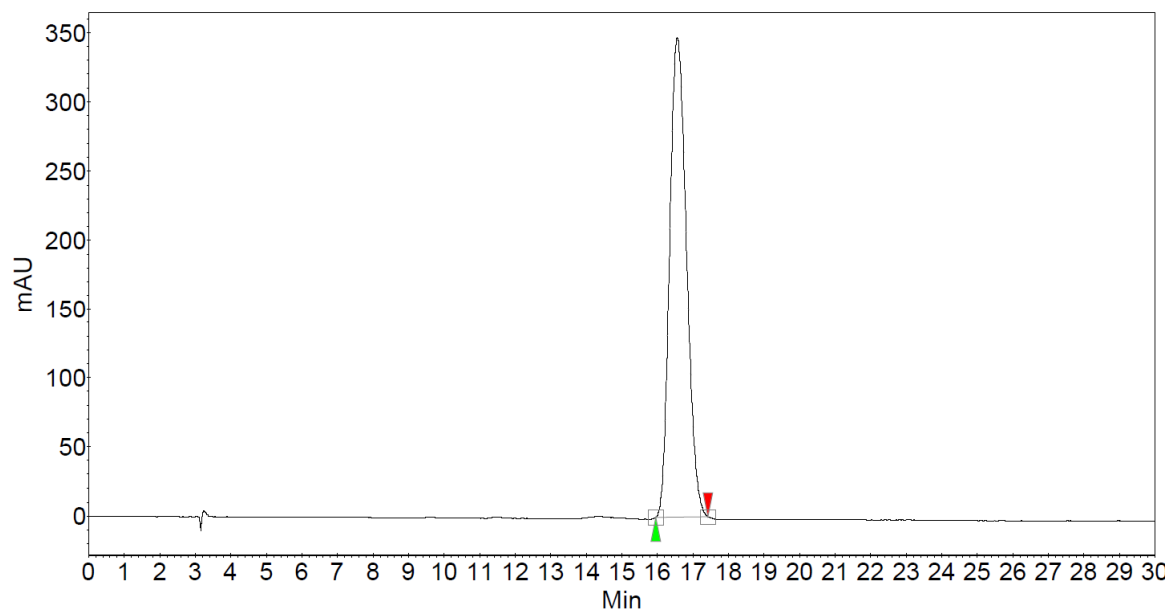
Figure 27. Chiral HPLC Chromatogram of Compound **(S)-3at**.

tert-butyl 6-((methyl(oxo)(phenyl)-λ⁶-sulfaneylidene)amino)-1*H*-indole-1-carboxylate (3au)
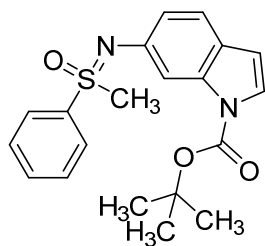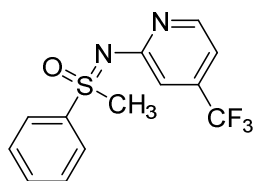

Table 14. Chiral HPLC Data of Compound **3au**.

Peak	Retention Time	Height	Area	Area%
#	[min]	[mAU]	[mAU * min]	[%]
1	16.87	104.0	60.7	50
2	18.91	93.0	61.3	50
Total		197.0	122.0	100
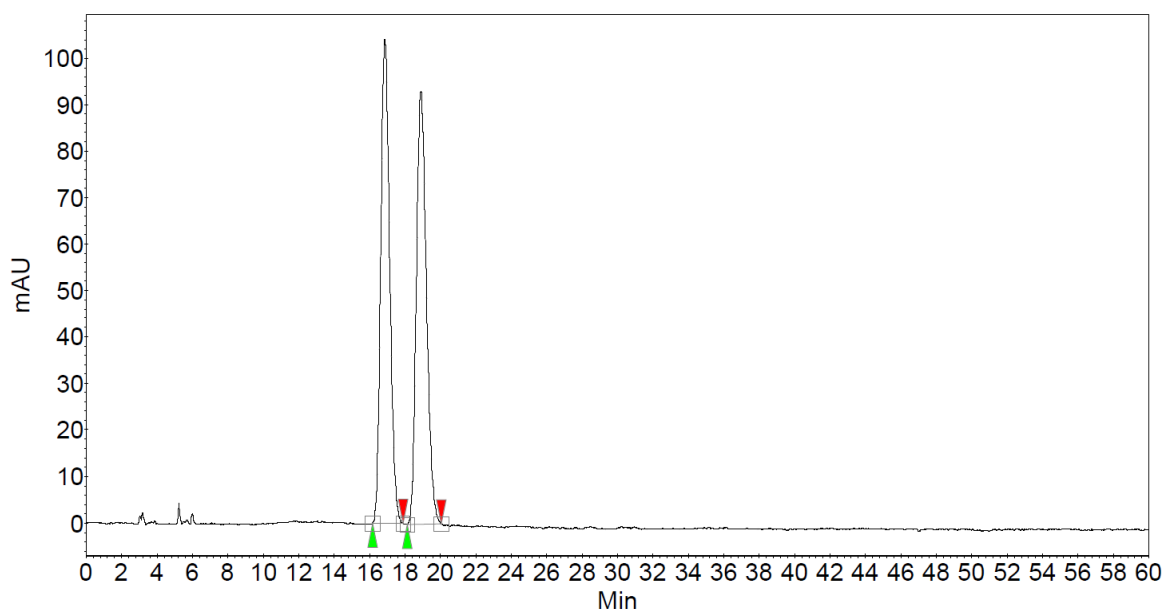
Figure 28. Chiral HPLC Chromatogram of Compound **3au**.

tert-butyl (*S*)-6-((methyl(oxo)(phenyl)-λ⁶-sulfaneylidene)amino)-1*H*-indole-1-carboxylate ((*S*)-3au)
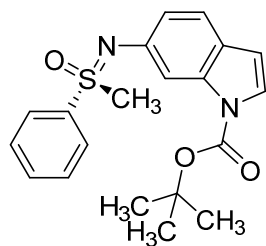
Table 15. Chiral HPLC Data of Compound **(*S*)-3au**.
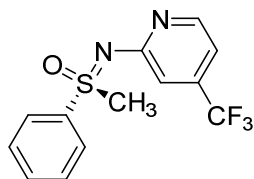
Peak	Retention Time	Height	Area	Area%
#	[min]	[mAU]	[mAU * min]	[%]
1	18.80	319.5	235.8	100
Total		319.5	235.8	100

Figure 29. Chiral HPLC Chromatogram of Compound **(*S*)-3au**.

Methyl(phenyl)(quinolin-3-ylimino)-λ^6-sulfanone (3av)
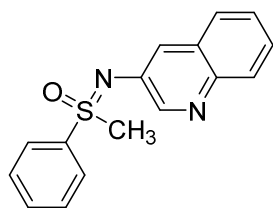
Table 16. Chiral HPLC Data of Compound **3av**.

Peak	Retention Time	Height	Area	Area%
#	[min]	[mAU]	[mAU * min]	[%]
1	18.76	594.3	468.2	48
2	22.32	541.2	503.3	52
Total		1135.6	971.5	100
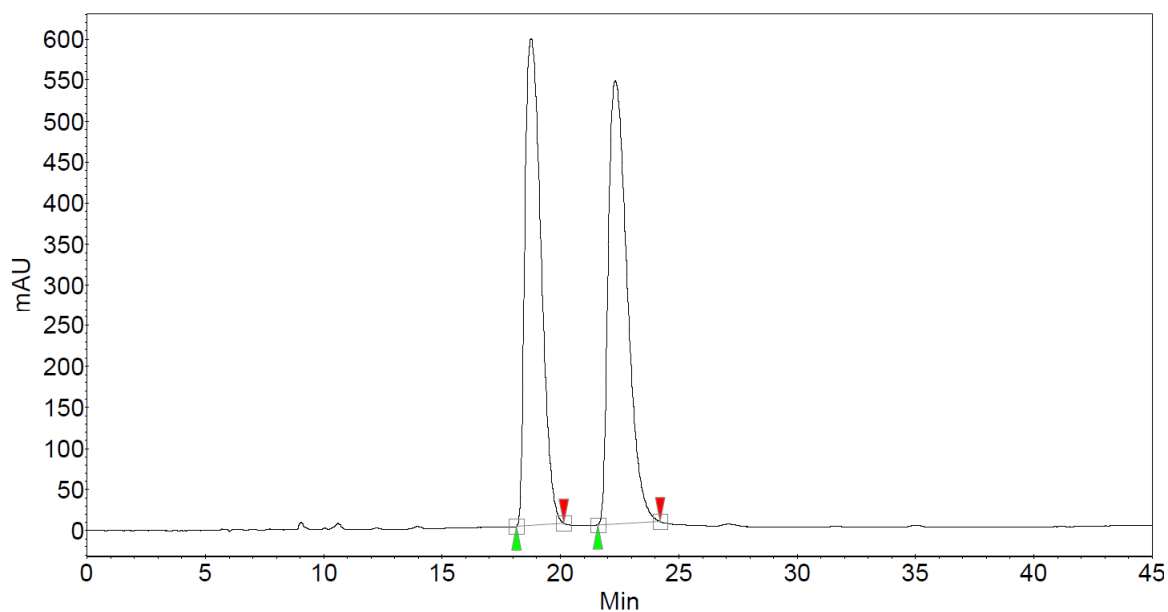
Figure 30. Chiral HPLC Chromatogram of Compound **3av**.

(*S*)-Methyl(phenyl)(quinolin-3-ylimino)-λ⁶-sulfanone ((*S*)-3av)
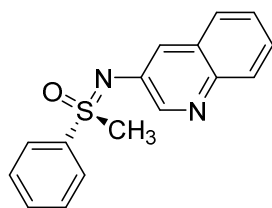
Table 17. Chiral HPLC Data of Compound **(*S*)-3av**.

Peak	Retention Time	Height	Area	Area%
#	[min]	[mAU]	[mAU * min]	[%]
1	22.17	620.7	701.5	100
Total		620.7	701.5	100
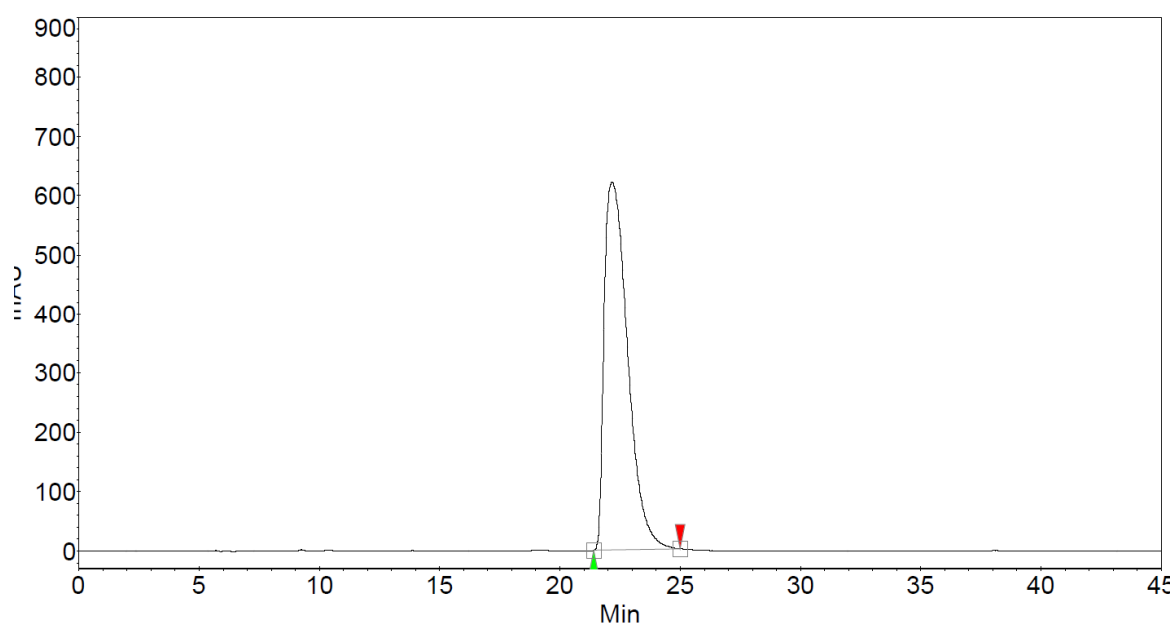
Figure 31. Chiral HPLC Chromatogram of Compound **(*S*)-3av**.

Methyl(phenyl)((4-(trifluoromethyl)pyridin-2-yl)imino)-λ^6-sulfanone (3aw)

Table 18. Chiral HPLC Data of Compound **3aw**.

Peak	Retention Time	Height	Area	Area%
#	[min]	[mAU]	[mAU * min]	[%]
1	15.28	176.4	80.1	50
2	20.47	133.7	81.7	50
Total		310.1	161.9	100
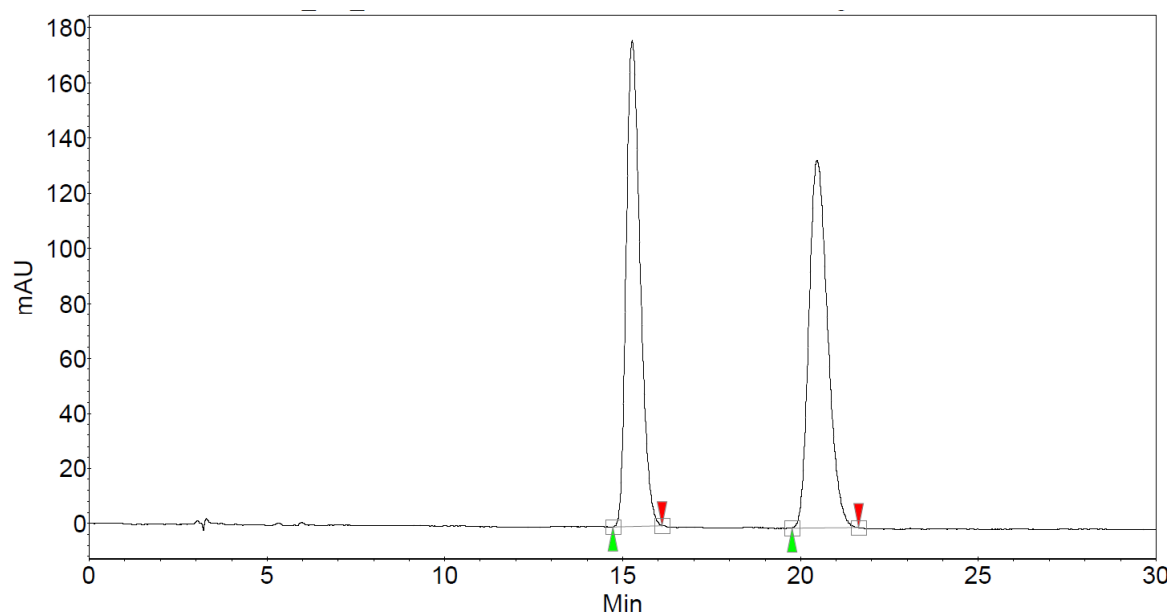
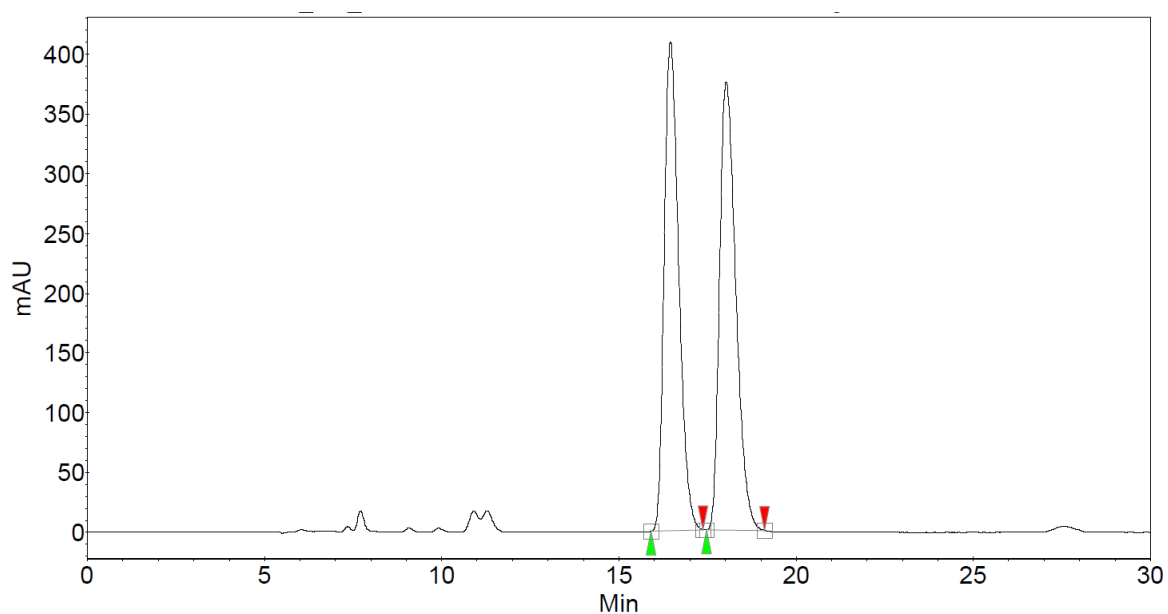**Figure 32.** Chiral HPLC Chromatogram of Compound **3aw**.

(*S*)-Methyl(phenyl)((4-(trifluoromethyl)pyridin-2-yl)imino)-λ^6-sulfanone ((*S*)-3aw

Table 19. Chiral HPLC Data of Compound **(*S*)-3aw**.

Peak	Retention Time	Height	Area	Area%
#	[min]	[mAU]	[mAU * min]	[%]
1	20.25	361.5	248.2	100
Total		361.5	248.2	100
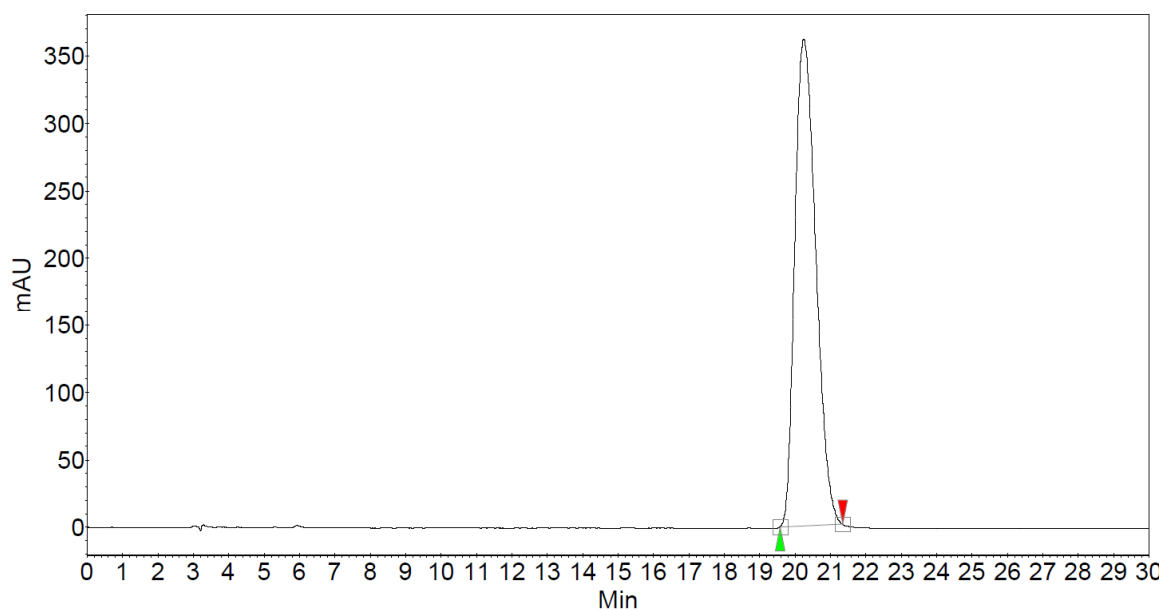
Figure 33. Chiral HPLC Chromatogram of Compound **(*S*)-3aw**.

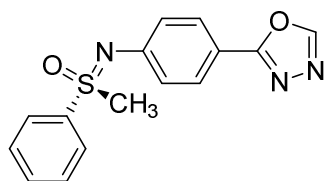**((4-(1,3,4-Oxadiazol-2-yl)phenyl)imino)(methyl)(phenyl)-λ⁶-sulfanone (3ax)**
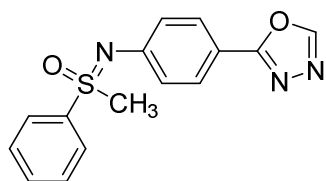
Table 20. Chiral HPLC Data of Compound **3ax**.

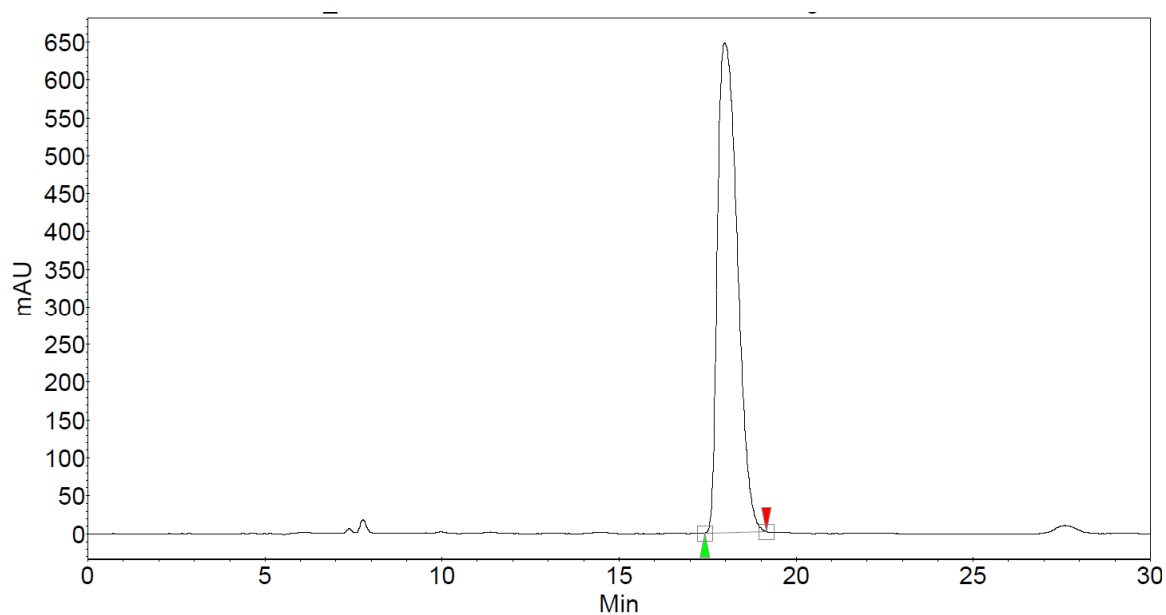| Peak	Retention Time	Height	Area	Area%
#	[min]	[mAU]	[mAU * min]	[%]
1	16.46	409.0	196.1	49
2	18.04	375.3	200.5	51
Total		784.3	396.6	100

Figure 34. Chiral HPLC Chromatogram of Compound **3ax**.

(*S*)-((4-(1,3,4-Oxadiazol-2-yl)phenyl)imino)(methyl)(phenyl)-λ⁶-sulfanone ((*S*)-3ax)

Table 21. Chiral HPLC Data of Compound **(*S*)-3ax**.

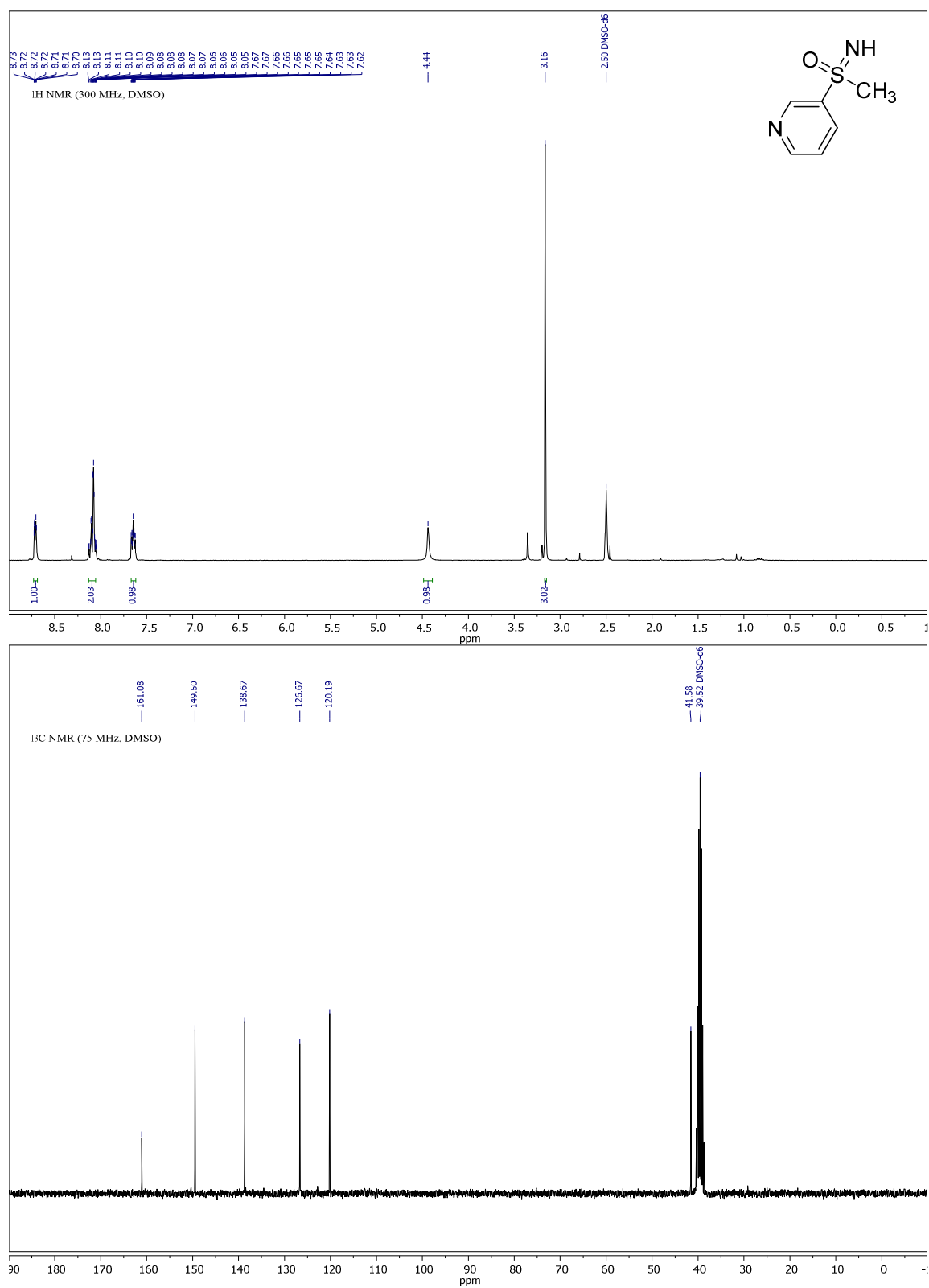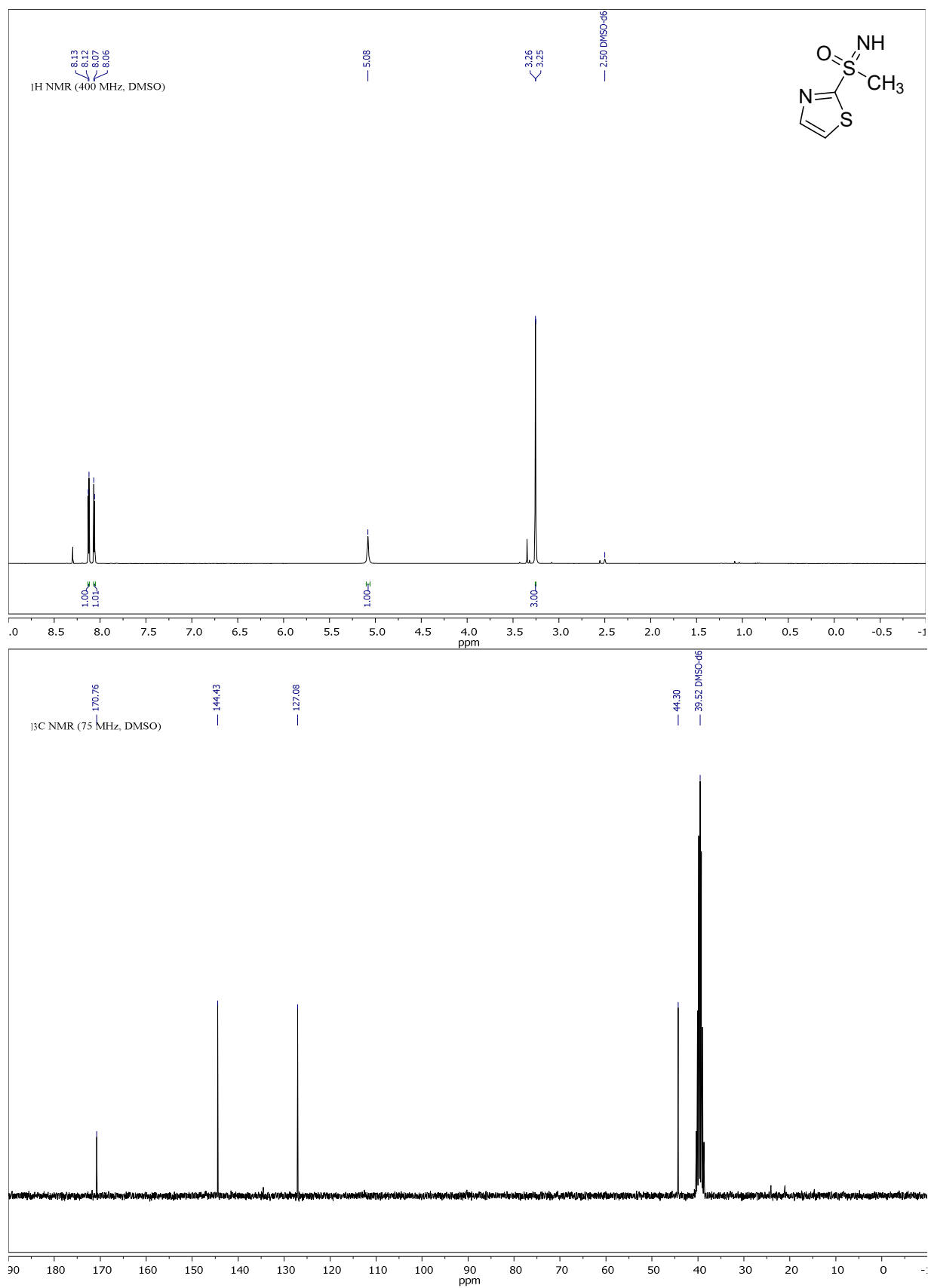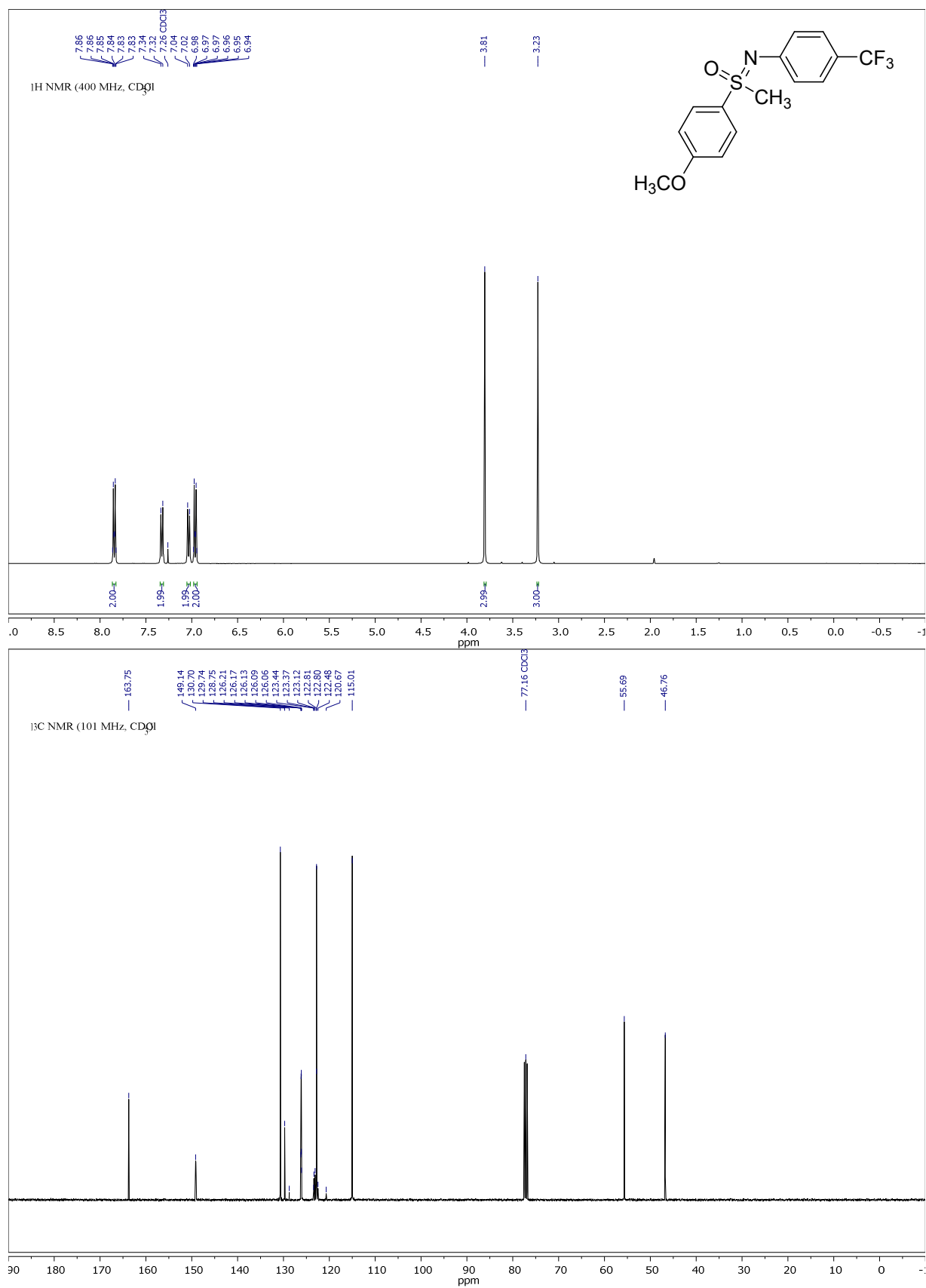| Peak	Retention Time	Height	Area	Area%
#	[min]	[mAU]	[mAU * min]	[%]
1	17.99	647.8	423.0	100
Total		647.8	423.0	100

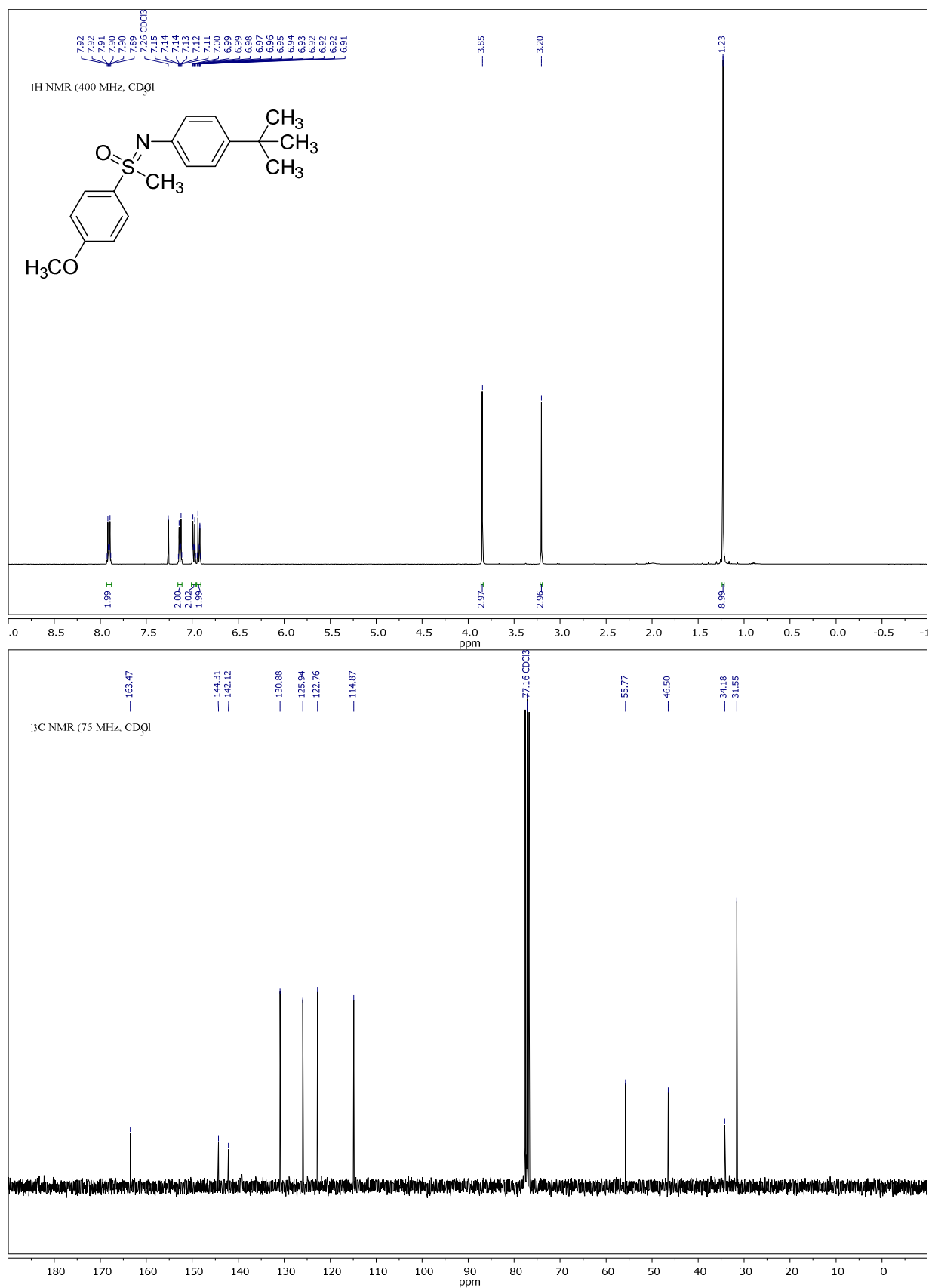**Figure 35.** Chiral HPLC Chromatogram of Compound **(*S*)-3ax**.

6.3.2 NMR Spectra

Compound 1ap, ^{1}H- and ^{13}C-NMR:

Compound 1aq, ^{1}H- and ^{13}C-NMR:

1H NMR (400 MHz, DMSO)

8.13
8.12
8.07
8.06

5.08

3.26
3.25

2.50 DMSO-d6

13C NMR (75 MHz, DMSO)

170.76

144.43

127.08

44.30

39.52 DMSO-d6

Compound 3a, ^{1}H-, ^{13}C- and ^{19}F-NMR:

19F NMR (376 MHz, CDCl₃)

— -62.15

3.00—

40 30 20 10 0 -10 -20 -30 -40 -50 -60 -70 -80 -90 -100 -110 -120 -130 -140 -150 -160 -170 -180 -190 -200 -2

ppm

Compound 3b, [^1]H- and [^13]C-NMR:

1H NMR (400 MHz, CDCl₃)

7.92, 7.92, 7.91, 7.90, 7.90, 7.89, 7.26 CDCl3, 7.15, 7.14, 7.13, 7.12, 7.11, 7.00, 6.99, 6.99, 6.98, 6.97, 6.96, 6.95, 6.94, 6.93, 6.92, 6.92, 6.91

3.85

3.20

1.23

1.99

2.00, 2.02, 1.99

2.97

2.96

8.99

13C NMR (75 MHz, CDCl₃)

163.47

144.31, 142.12

130.88, 125.94, 122.76

114.87

77.16 CDCl3

55.77

46.50

34.18, 31.55

Compound 3c, ^{1}H- and ^{13}C-NMR:

1H NMR (300 MHz, CDCl$_3$)

7.85, 7.85, 7.84, 7.83, 7.82, 7.82, 7.26 CDCl3, 7.06, 7.05, 7.05, 7.03, 7.03, 7.02, 6.96, 6.95, 6.95, 6.94, 6.94, 6.93, 6.93, 6.92, 6.91, 6.91, 6.90

3.80 3.19 2.35

2.00 2.01 3.98 3.00 2.99 3.00

13C NMR (101 MHz, CDCl$_3$)

163.45 143.35 130.77, 130.26, 129.75, 128.87 123.81 114.81 77.16 CDCl3 55.67 46.42 17.25

Compound 3d, ^{1}H-NMR:

1H NMR (400 MHz, CDCl₃)

Compound 3e, ^{1}H-NMR:

1H NMR (400 MHz, CDCl3)

Compound 3f, ^{1}H- and ^{13}C-NMR:

Compound 3g, ^{1}H-, ^{13}C- and ^{19}F-NMR:

1H NMR (300 MHz, CDCl3)

13C NMR (75 MHz, CDCl3)

19F NMR (377 MHz, CDCl3)

−63.55

6.00

30 20 10 0 -10 -20 -30 -40 -50 -60 -70 -80 -90 -100 -110 -120 -130 -140 -150 -160 -170 -180 -190 -200 -2

ppm

Compound 3h, ^{1}H- and ^{13}C-NMR:

Compound 3i, ^{1}H- and ^{13}C-NMR:

1H NMR (400 MHz, CDCl$_3$)

13C NMR (101 MHz, CDCl$_3$)

Compound 3j, ^{1}H- and ^{13}C-NMR:

1H NMR (300 MHz, CDCl$_3$)

13C NMR (75 MHz, CDCl$_3$)
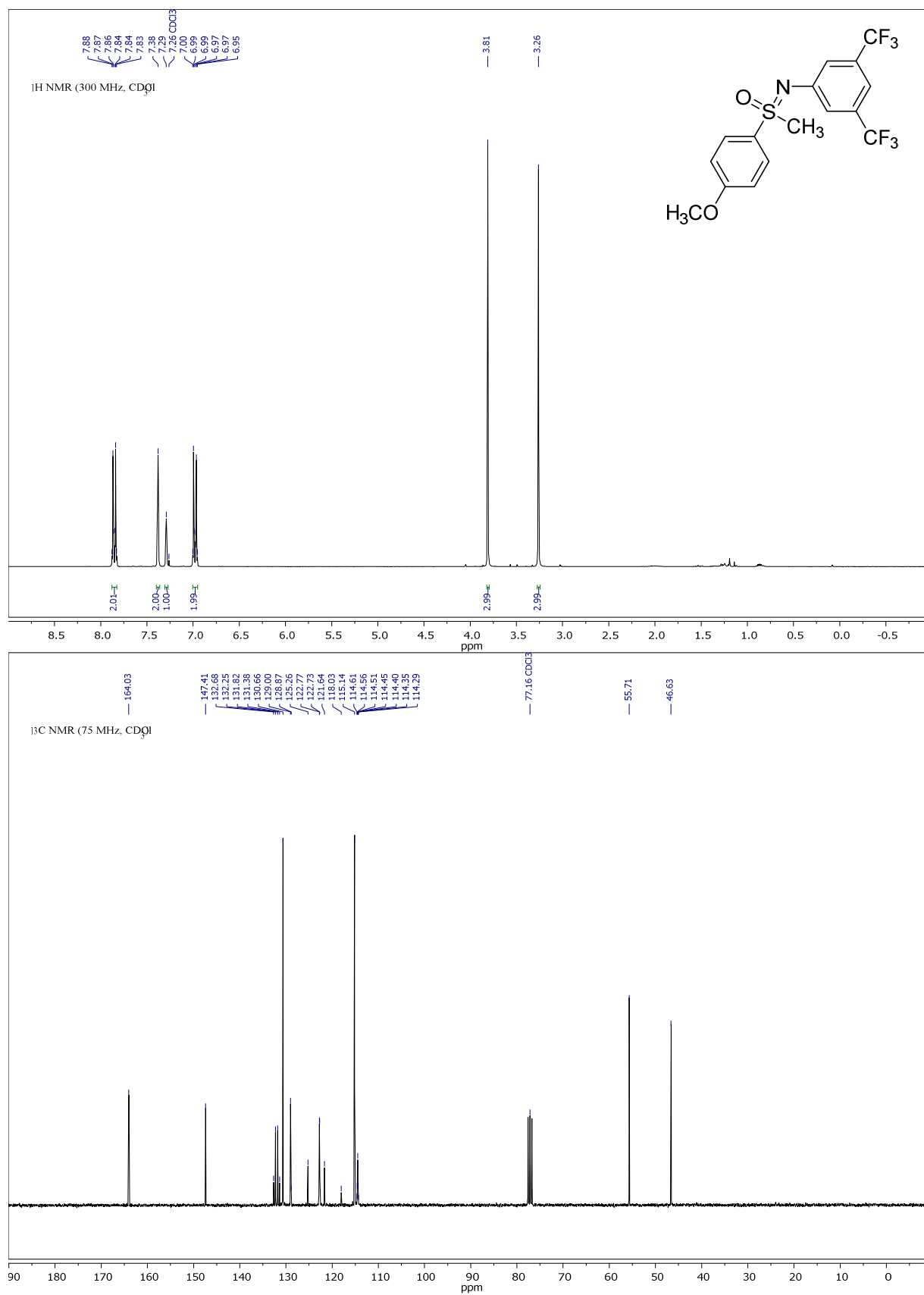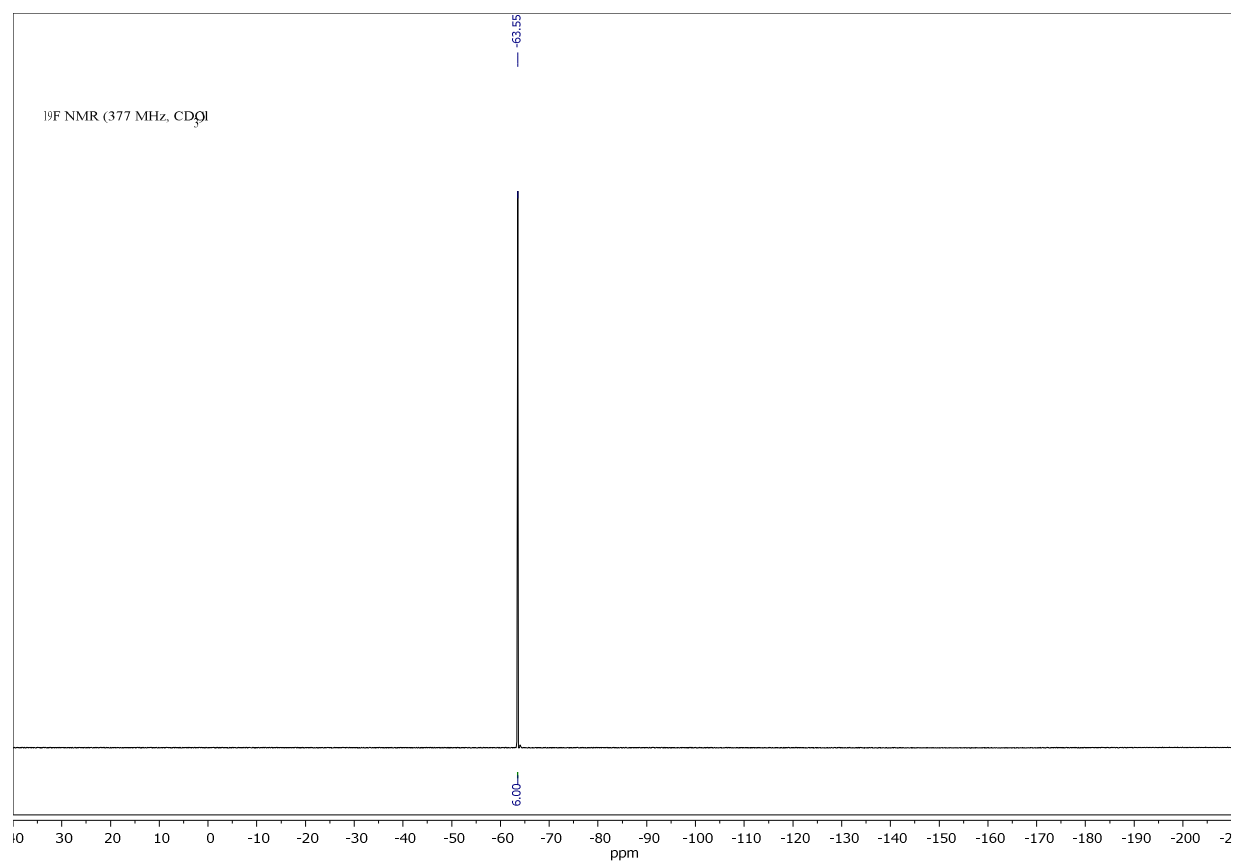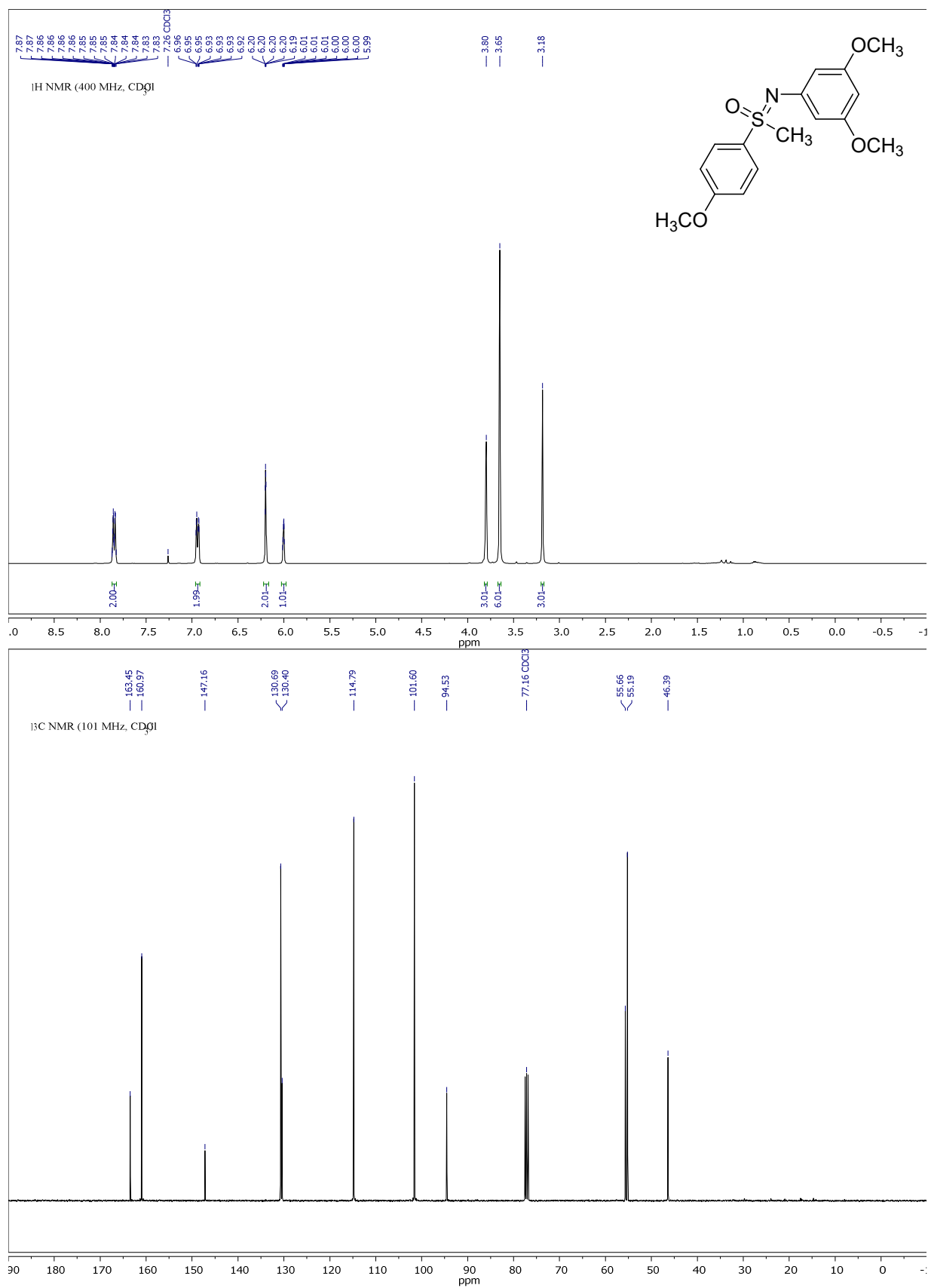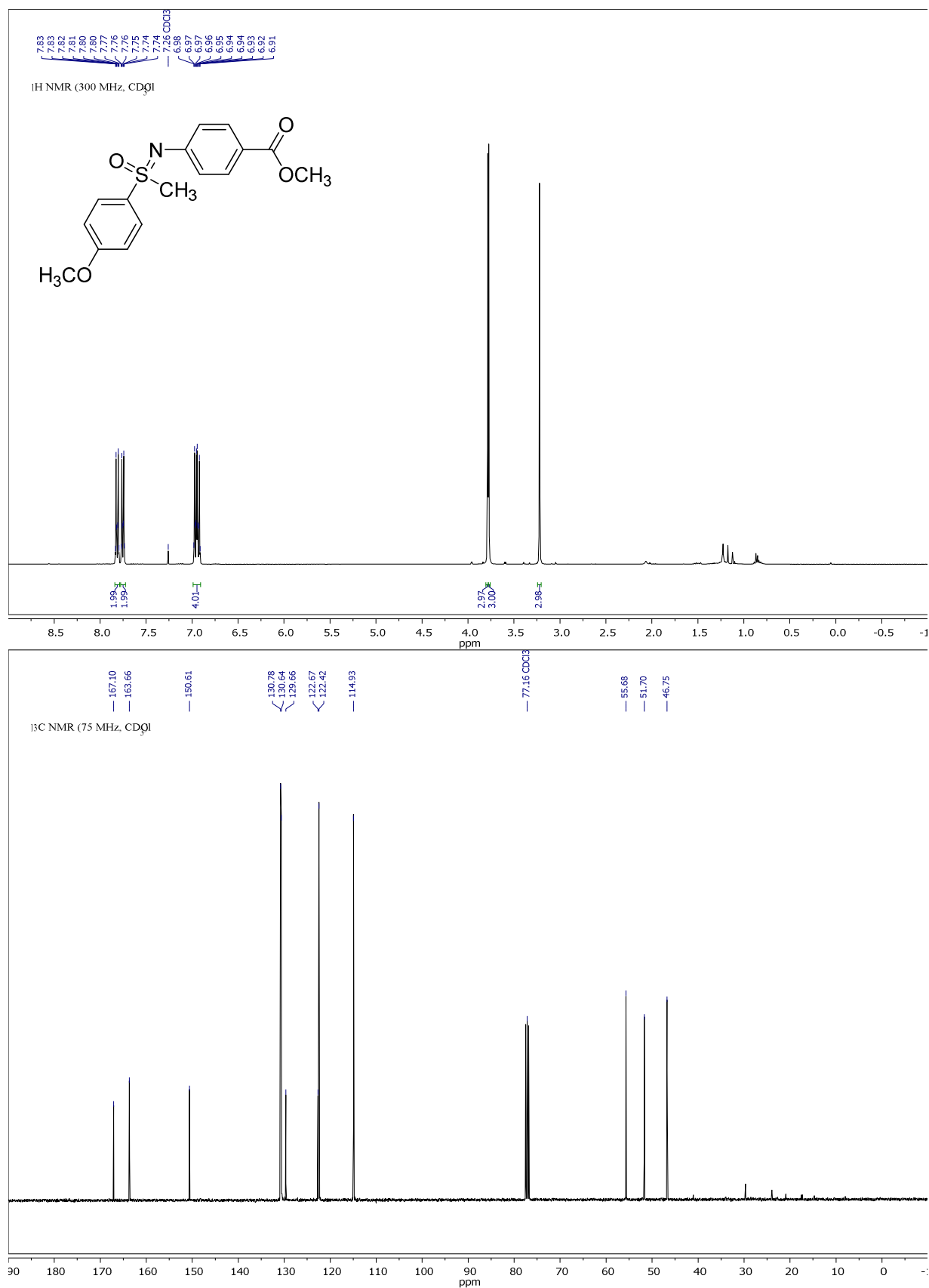
Compound 3k, ^{1}H- and ^{13}C-NMR:

Compound 3l, ^{1}H- and ^{13}C-NMR:

1H NMR (400 MHz, CD$_3$Cl)

13C NMR (101 MHz, CD$_3$Cl)

Compound 3m, ^{1}H- and ^{13}C-NMR:

1H NMR (300 MHz, CDCl$_3$)

13C NMR (101 MHz, CDCl$_3$)

Compound 3n, ^{1}H- and ^{13}C-NMR:

1H NMR (300 MHz, CDCl3)

13C NMR (75 MHz, CDCl3)
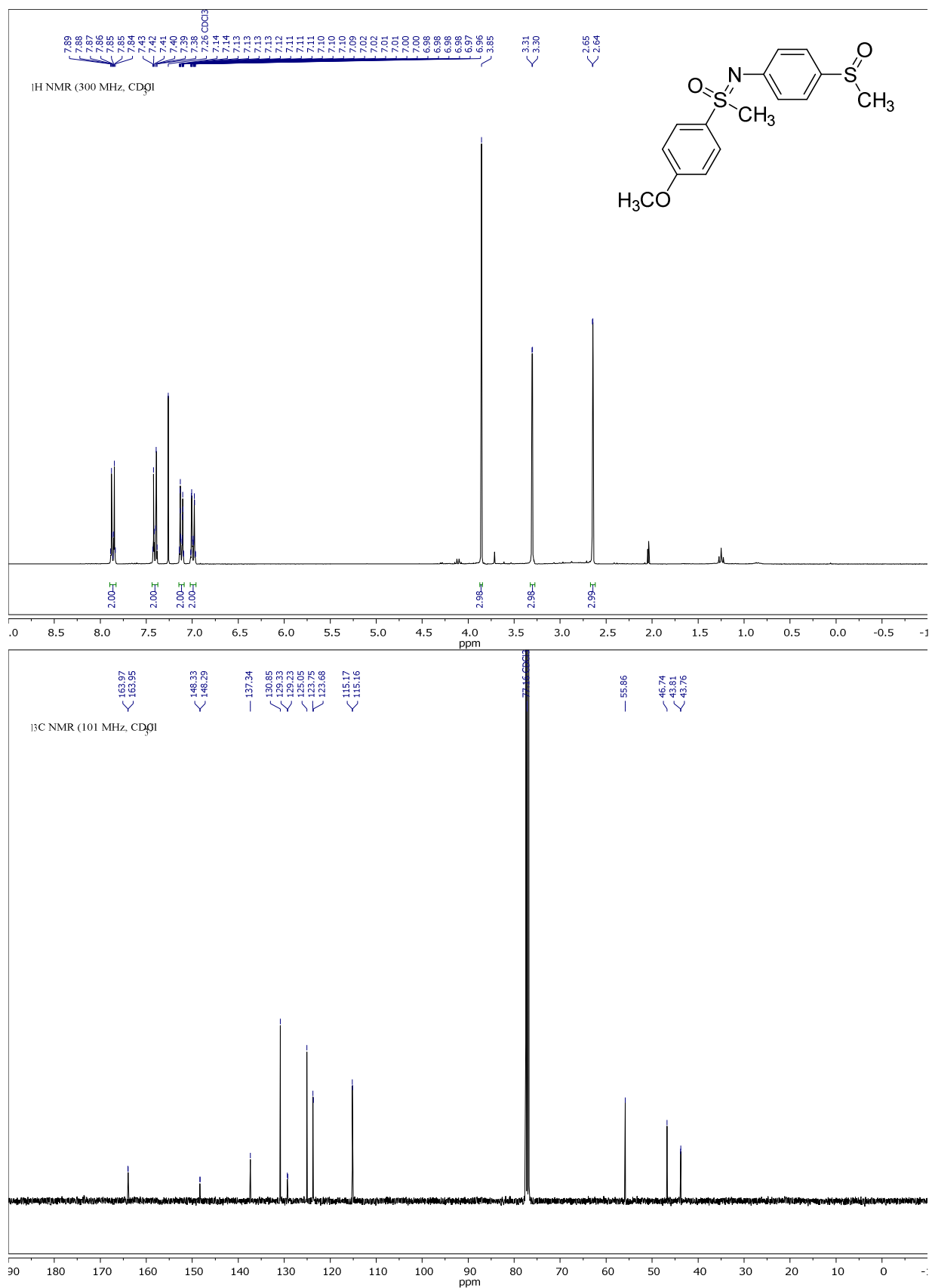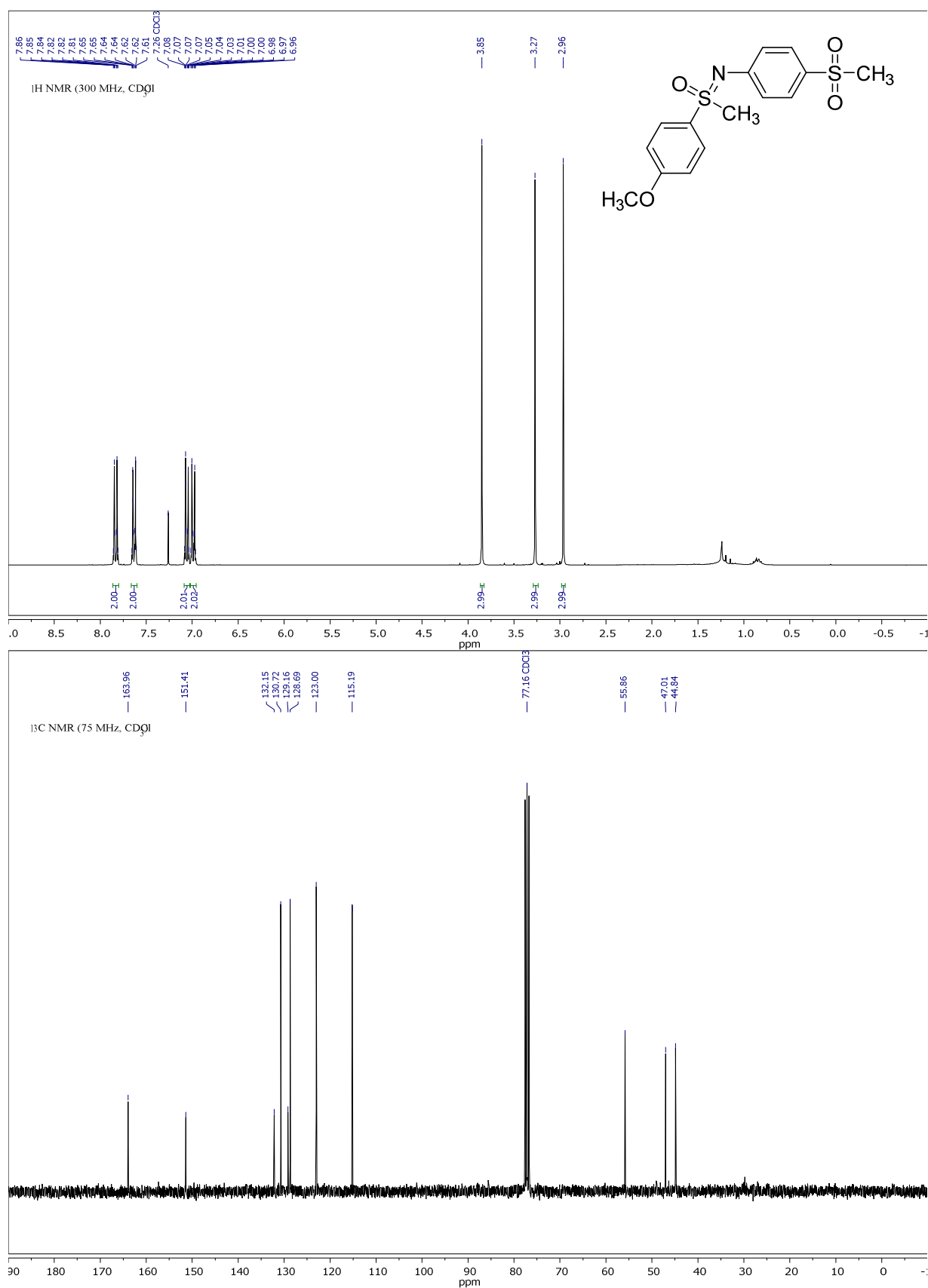
Compound 3o, ^{1}H-, ^{13}C- and ^{19}F-NMR:

19F NMR (377 MHz, CDCl₃)

−58.67

3.00

56.0   −56.5   −57.0   −57.5   −58.0   −58.5   −59.0   −59.5   −60.0   −60.5   −61.0
ppm
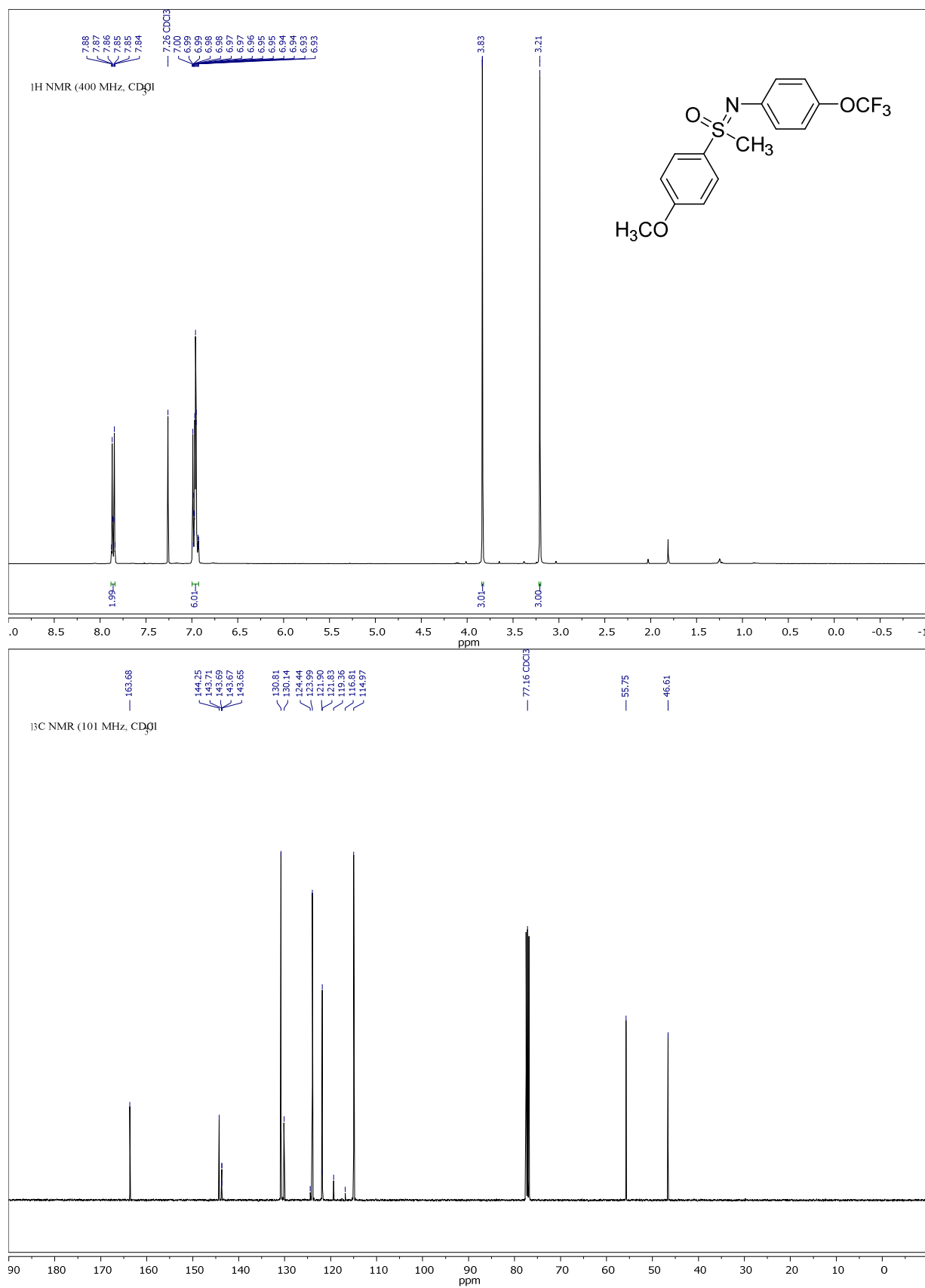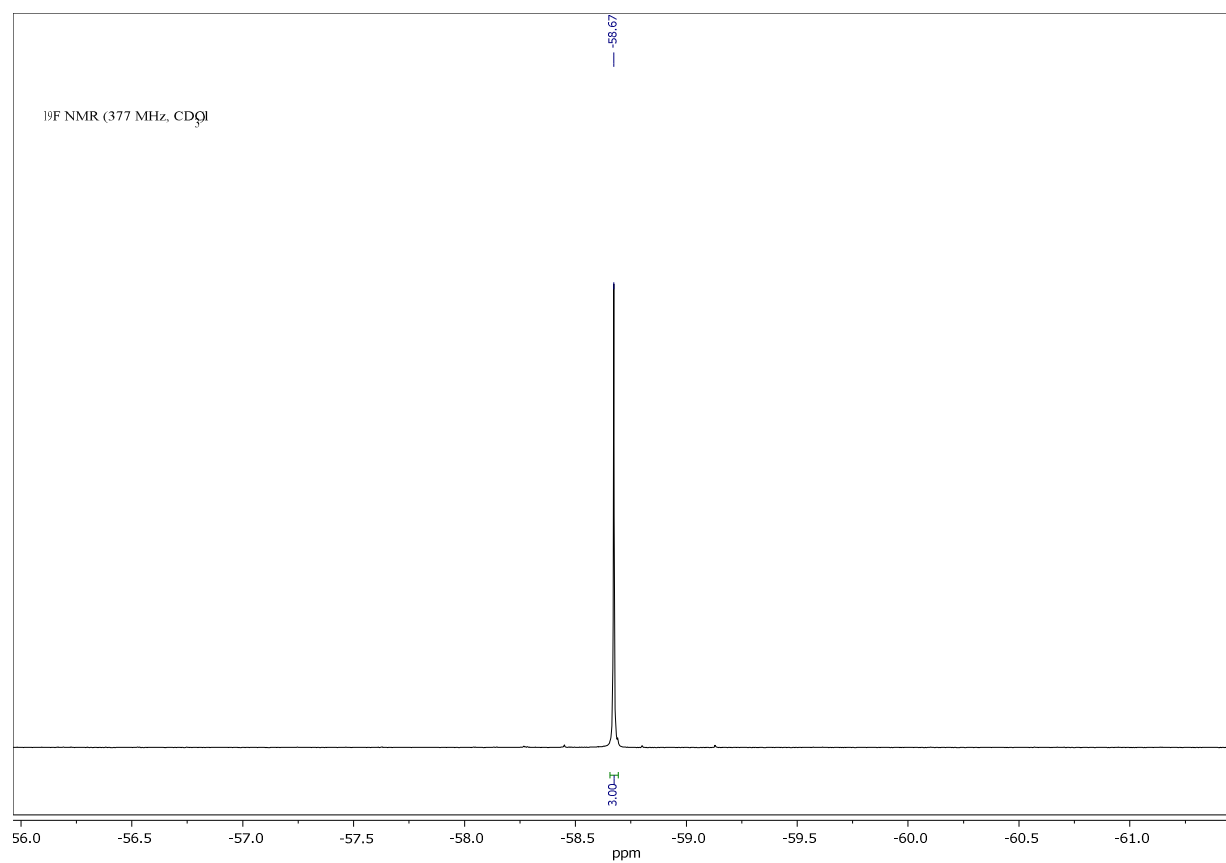
Compound 3p, ^{1}H-, ^{13}C- and ^{19}F-NMR:

19F NMR (282 MHz, CDCl₃)

-44.21

3.00

30 20 10 0 -10 -20 -30 -40 -50 -60 -70 -80 -90 -100 -110 -120 -130 -140 -150 -160 -170 -180 -190 -2

ppm
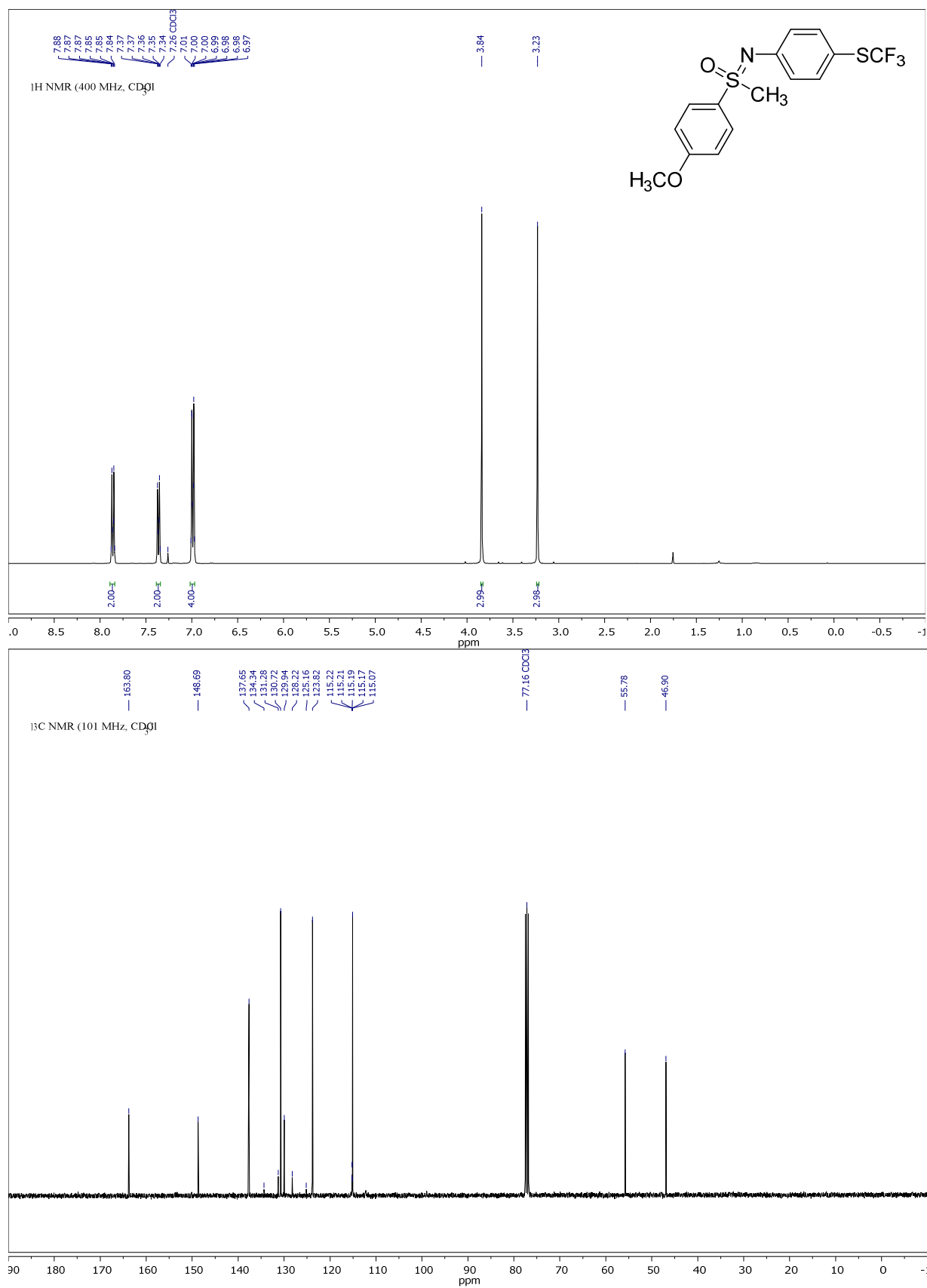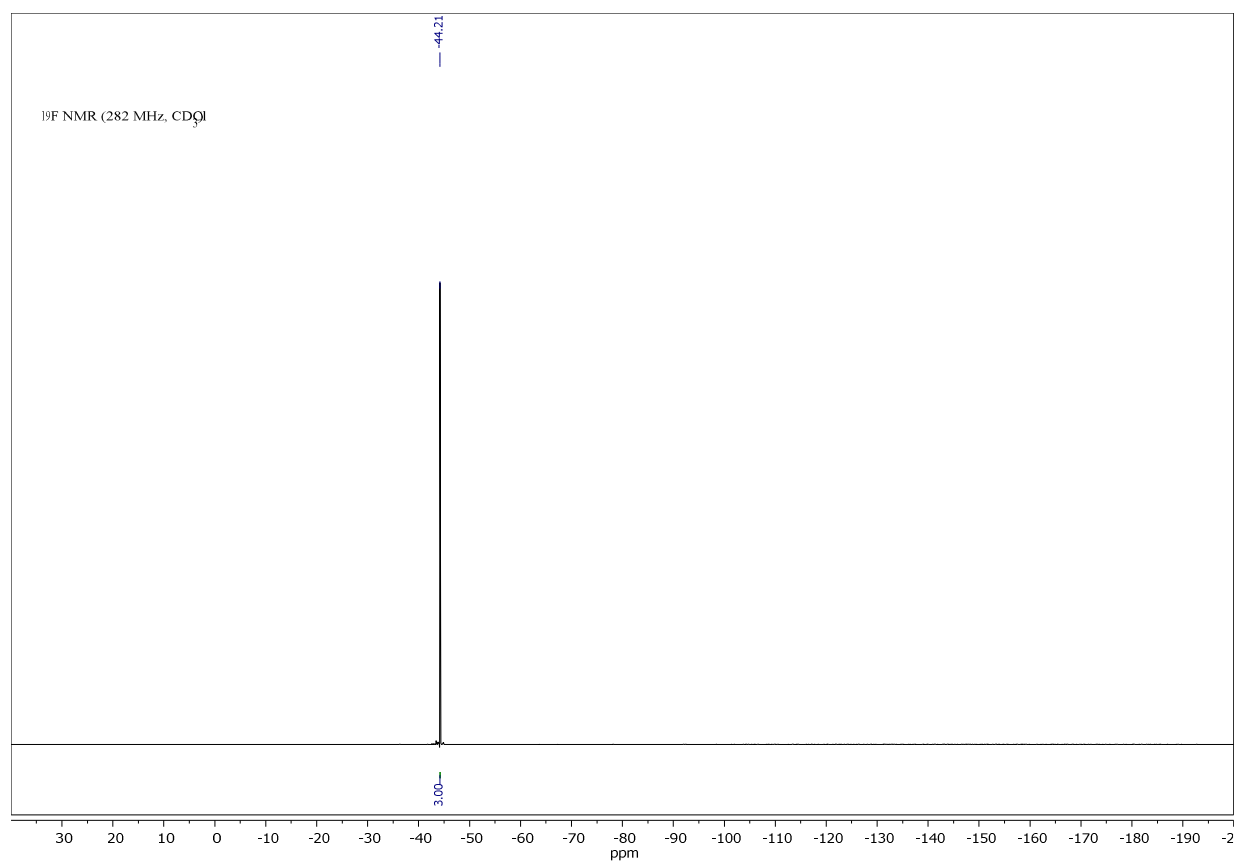
Compound 3q, ^{1}H-, ^{13}C- and ^{19}F-NMR:
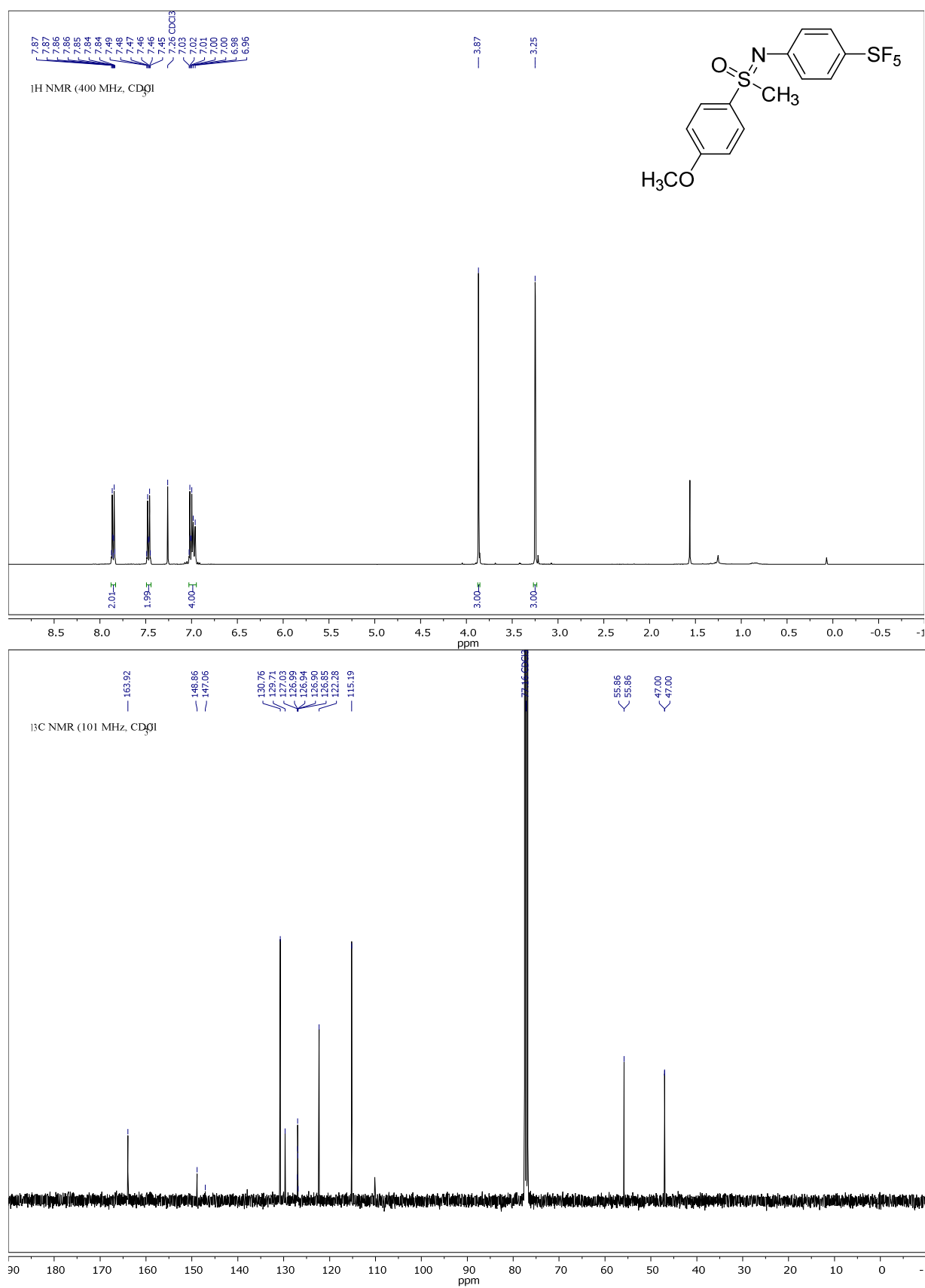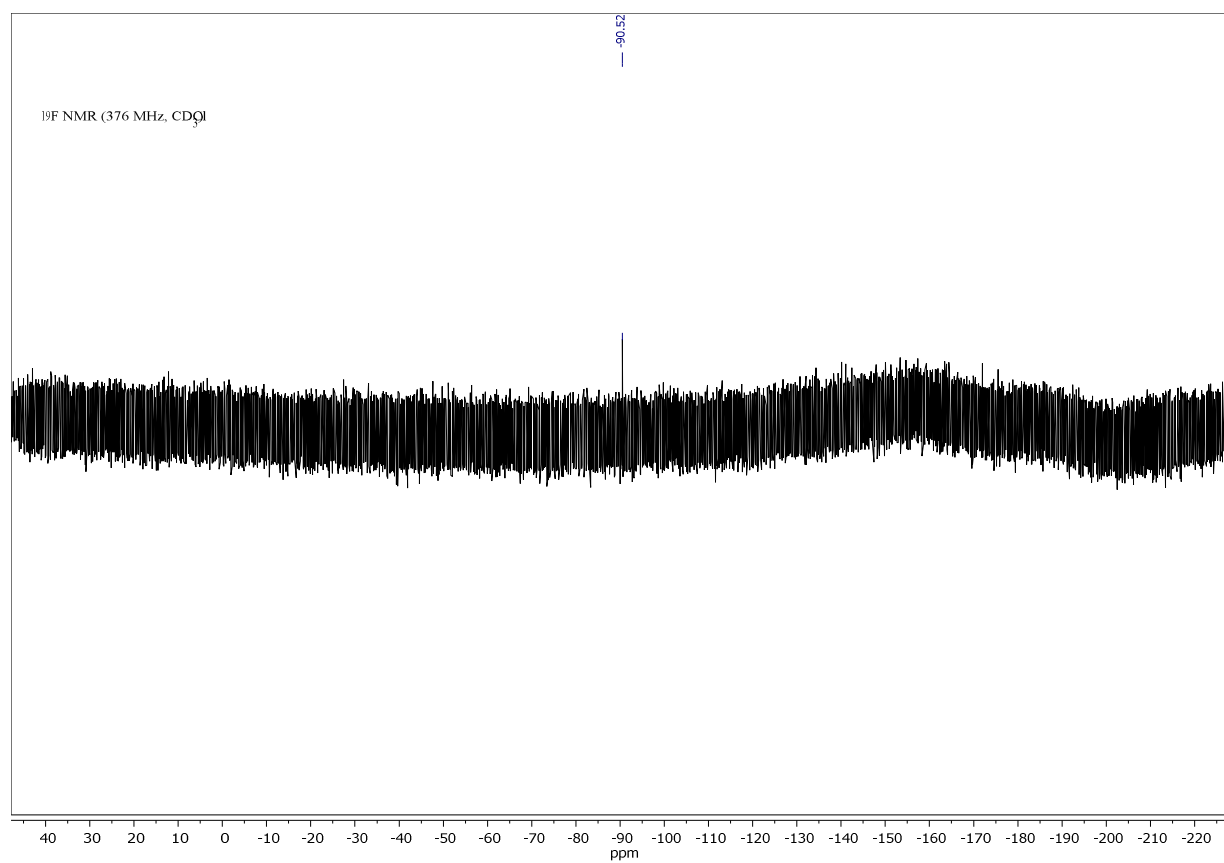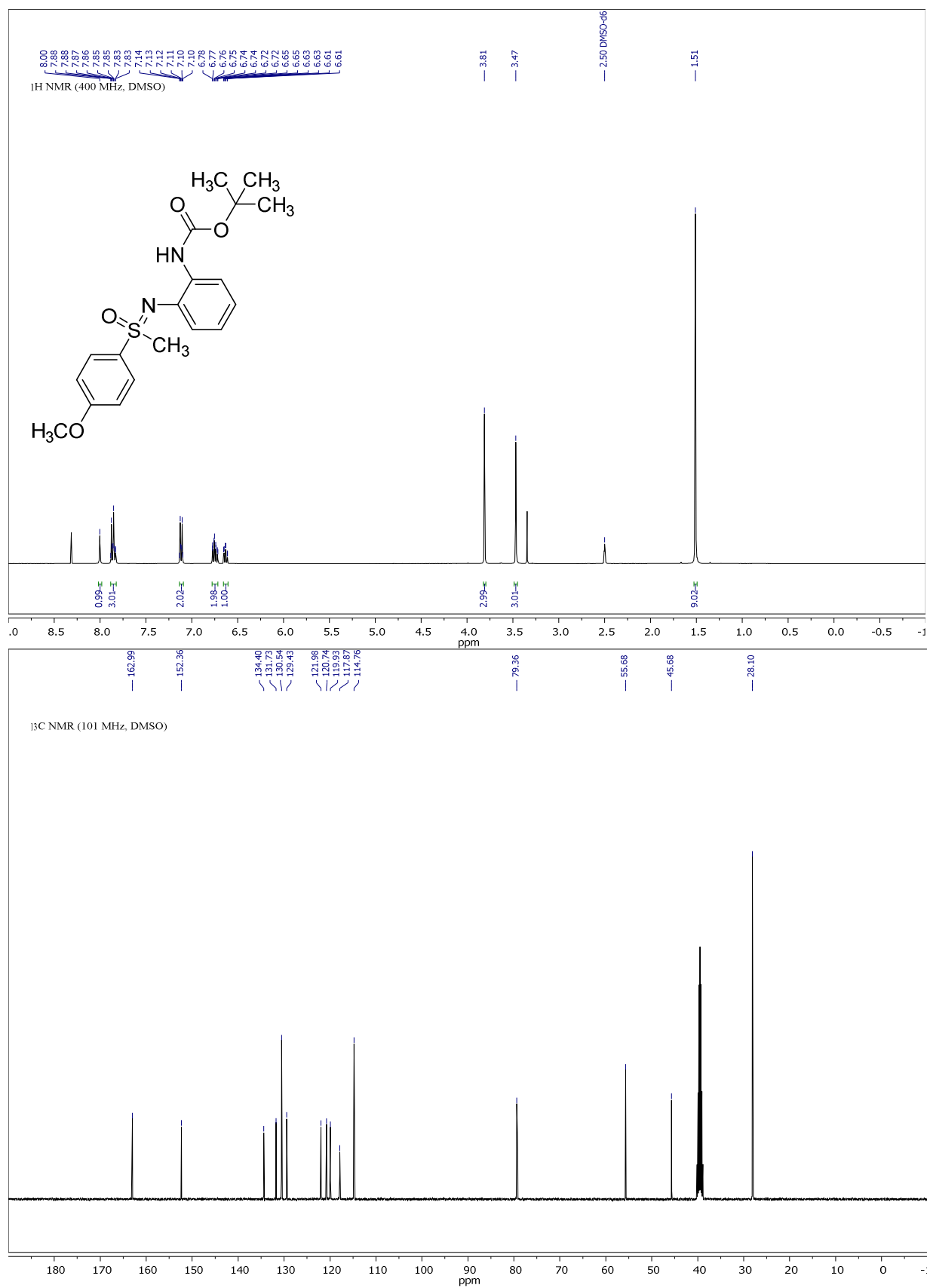
19F NMR (376 MHz, CDCl₃)

−90.52

40 30 20 10 0 -10 -20 -30 -40 -50 -60 -70 -80 -90 -100 -110 -120 -130 -140 -150 -160 -170 -180 -190 -200 -210 -220

ppm

Compound 3r, ^{1}H- and ^{13}C-NMR:

1H NMR (400 MHz, DMSO)

13C NMR (101 MHz, DMSO)

Compound 3s, ^{1}H- and ^{13}C-NMR:

1H NMR (400 MHz, CDCl₃)

13C NMR (101 MHz, CDCl₃)

Compound 3t, ^{1}H- and ^{13}C-NMR:

IH NMR (400 MHz, DMSO)

I3C NMR (101 MHz, DMSO)

Compound 3u, ^{1}H- and ^{13}C-NMR:

1H NMR (400 MHz, CDCl3)

13C NMR (101 MHz, CDCl3)
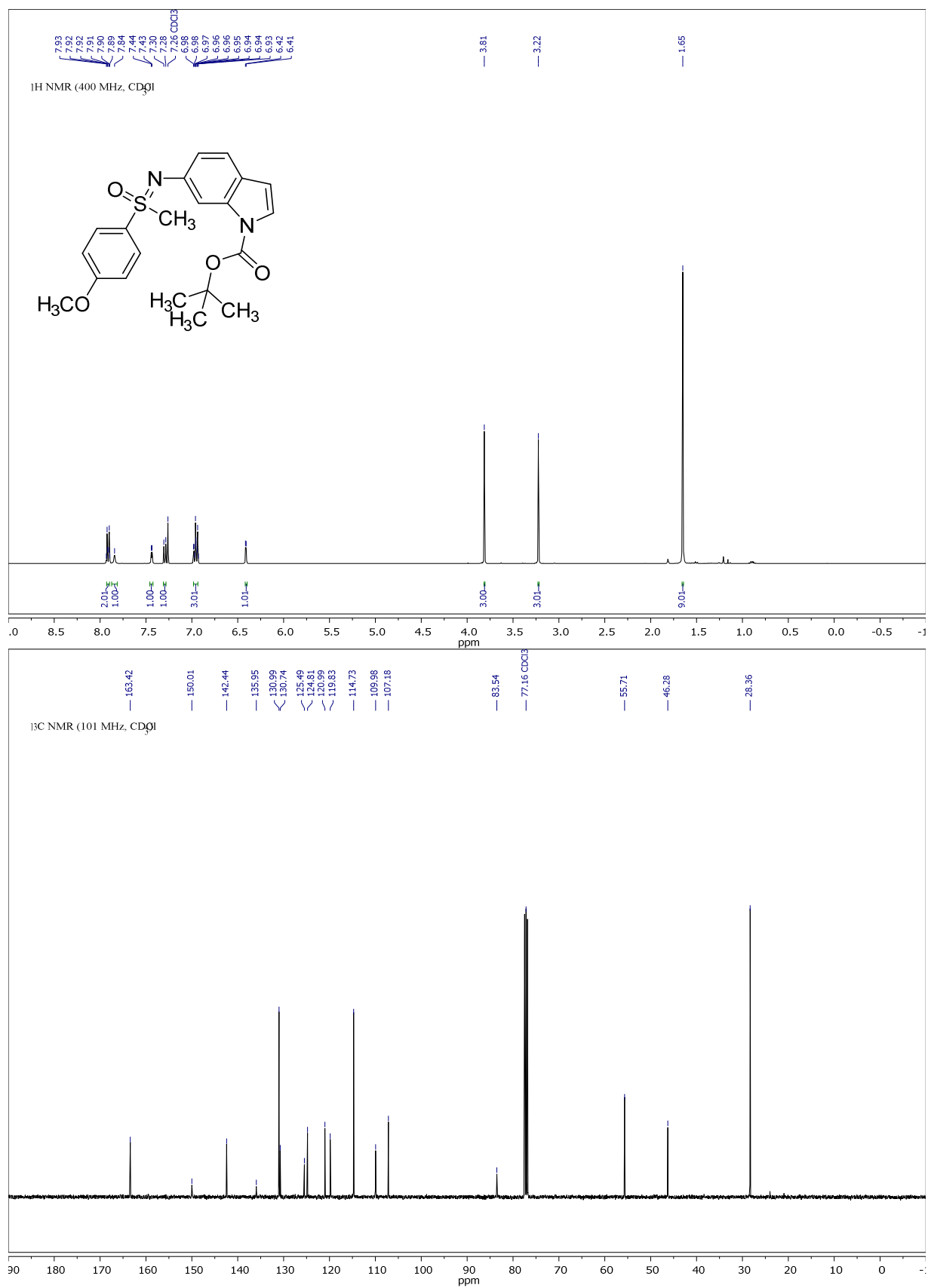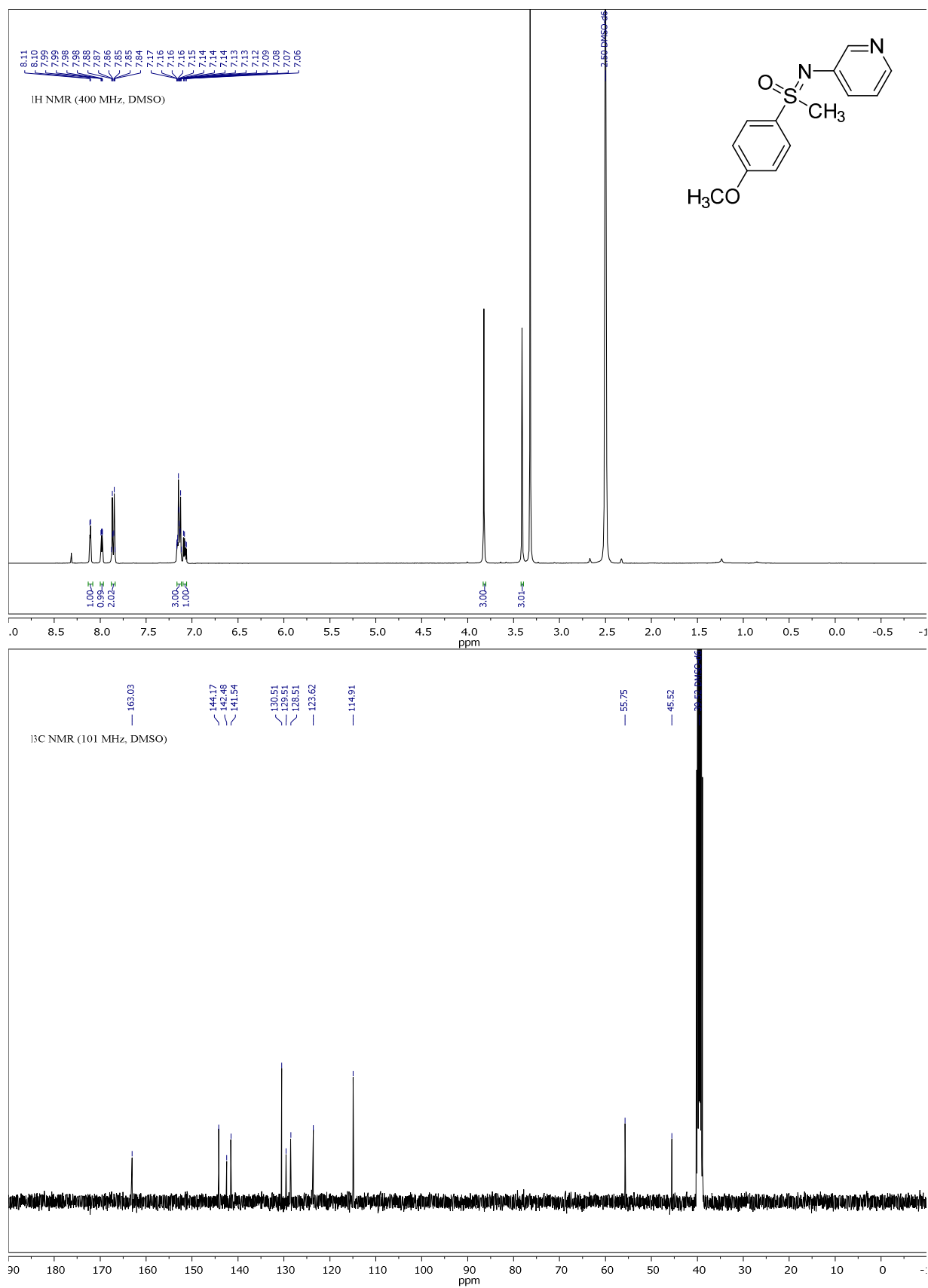
Compound 3v, ^{1}H-, ^{13}C- and ^{19}F-NMR:

19F NMR (376 MHz, CD₃Cl)

Compound 3w, ^{1}H- and ^{13}C-NMR:

Compound 3x, ^{1}H- and ^{13}C-NMR:

1H NMR (400 MHz, CDCl3)

13C NMR (101 MHz, CDCl3)
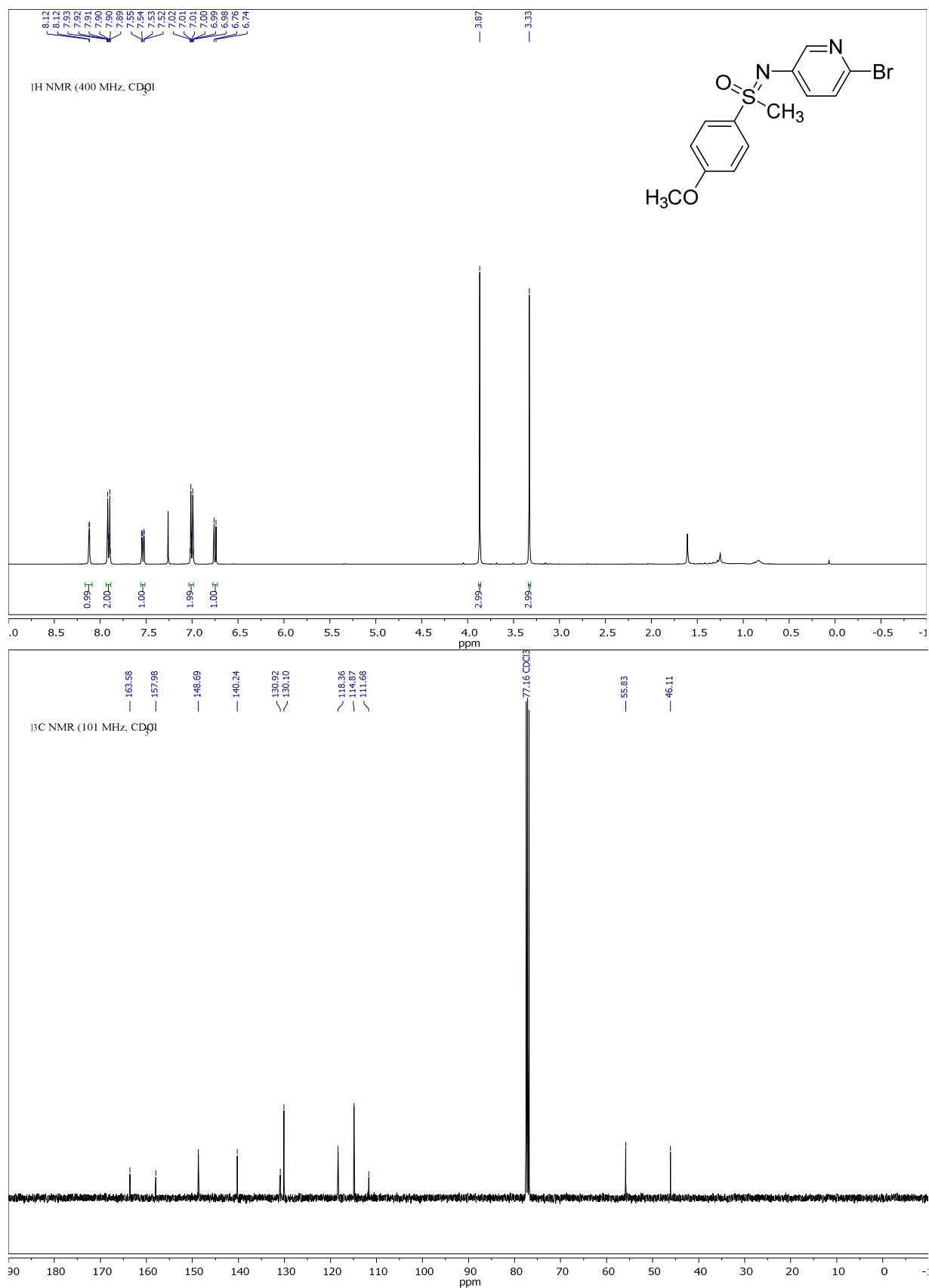
Compound 3y, ^{1}H- and ^{13}C-NMR:

Compound 3z, ^{1}H- and ^{13}C-NMR:

1H NMR (400 MHz, CD3Cl)

13C NMR (101 MHz, CD3Cl)

Compound 3aa, ^{1}H- and ^{13}C-NMR:

1H NMR (400 MHz, DMSO)

8.60
8.25
7.91
7.90
7.90
7.89
7.88
7.87
7.18
7.17
7.16
7.15
7.15
7.14
3.83
3.50
2.50 DMSO-d6

0.98
2.00
2.02
2.01
3.00
3.01

13C NMR (101 MHz, DMSO)

163.29
150.62
149.51
141.24
130.54
128.67
115.07
55.81
45.34
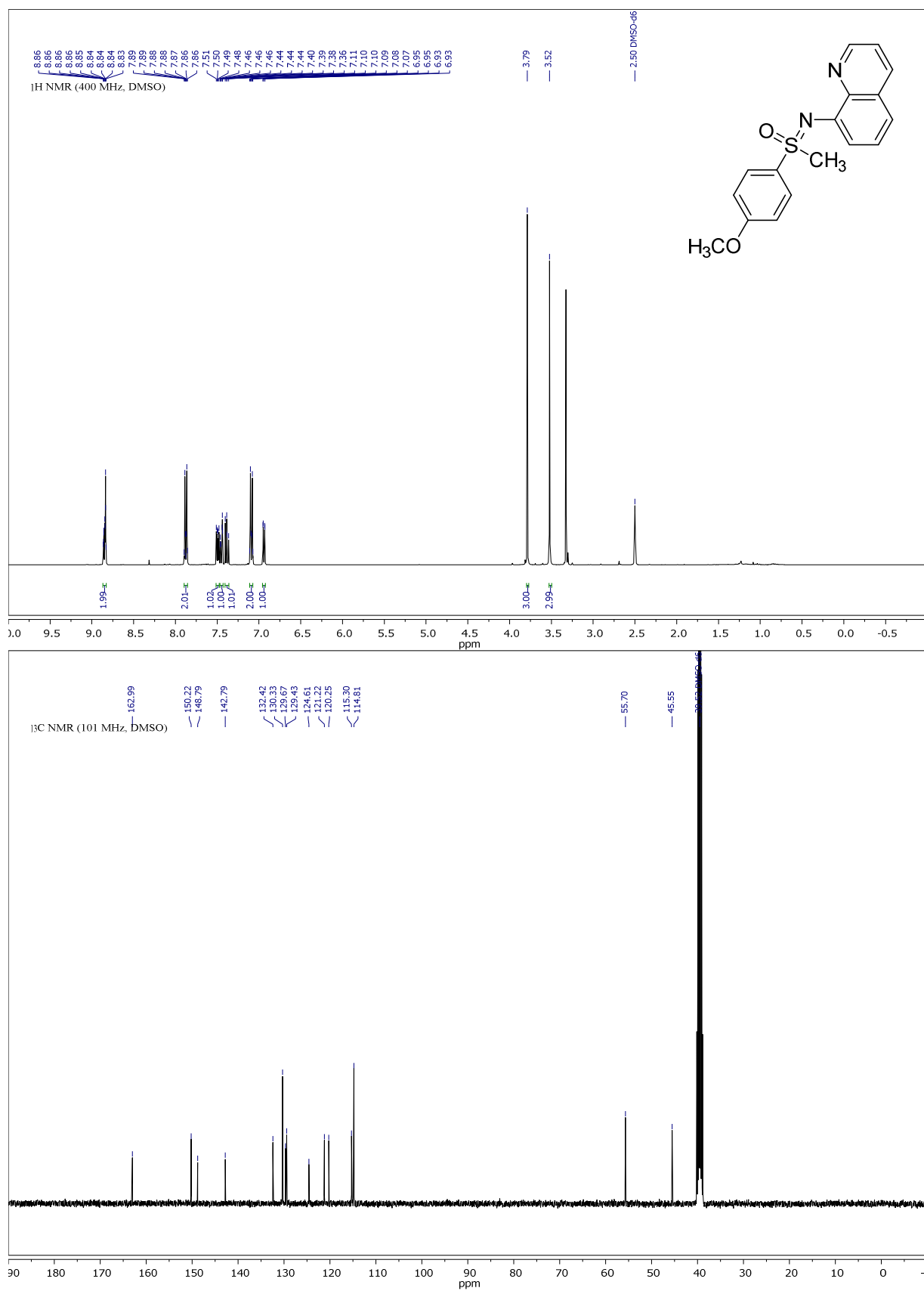
Compound 3ab, ^{1}H- and ^{13}C-NMR:
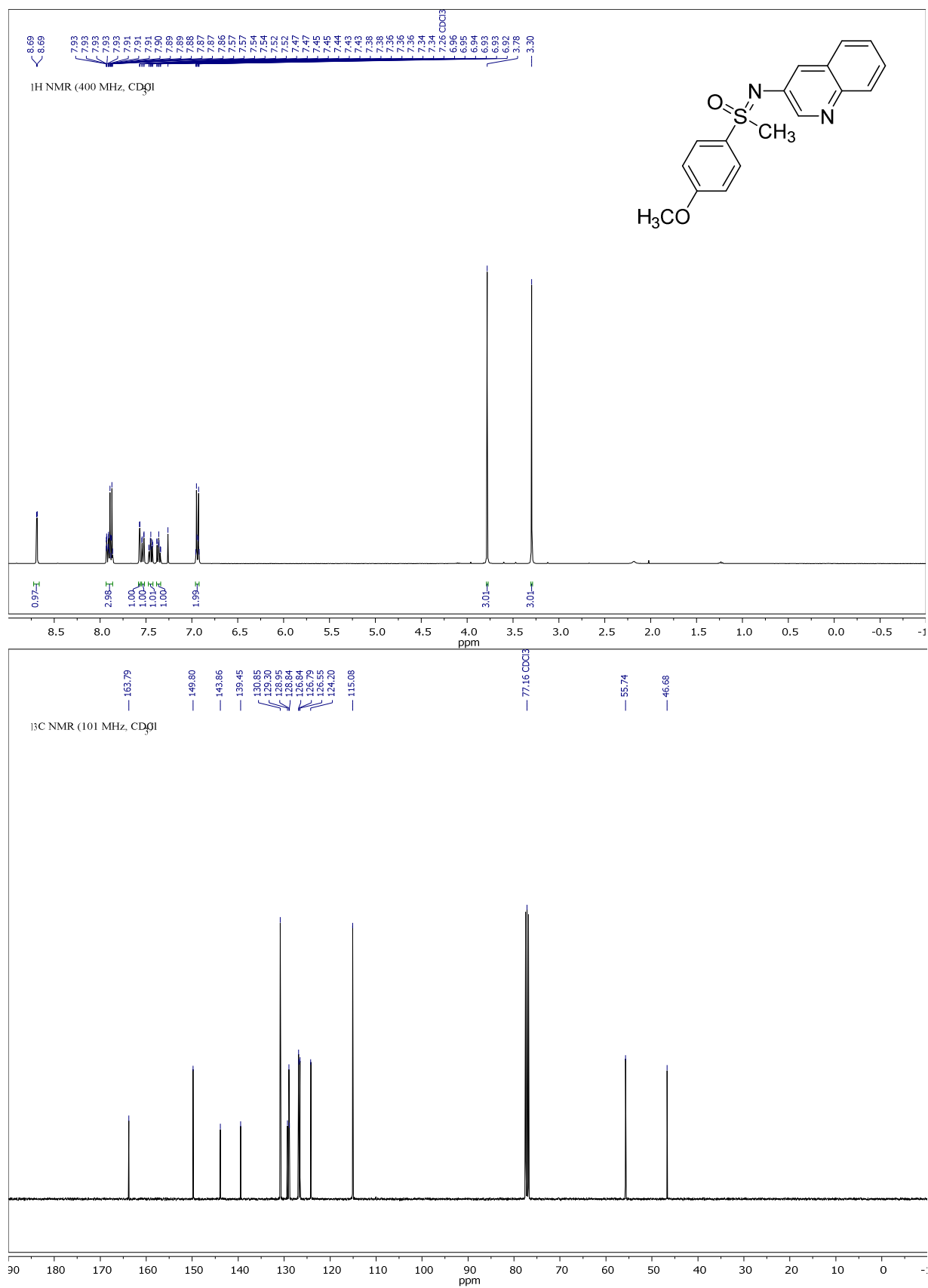
Compound 3ac, ^{1}H- and ^{13}C-NMR:
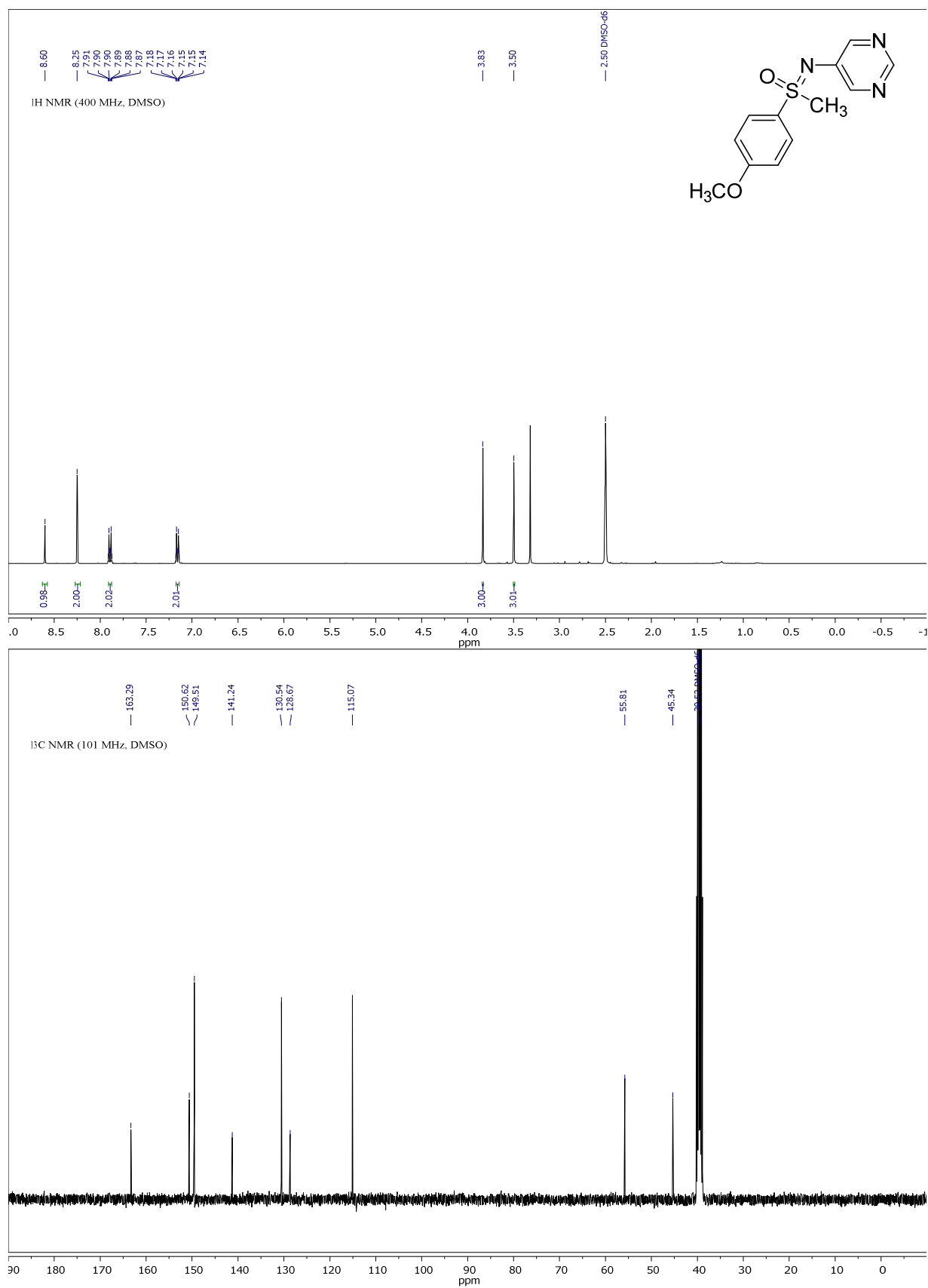
Compound 3ae, ^{1}H- and ^{13}C-NMR:

1H NMR (400 MHz, CDCl$_3$)

13C NMR (101 MHz, CDCl$_3$)
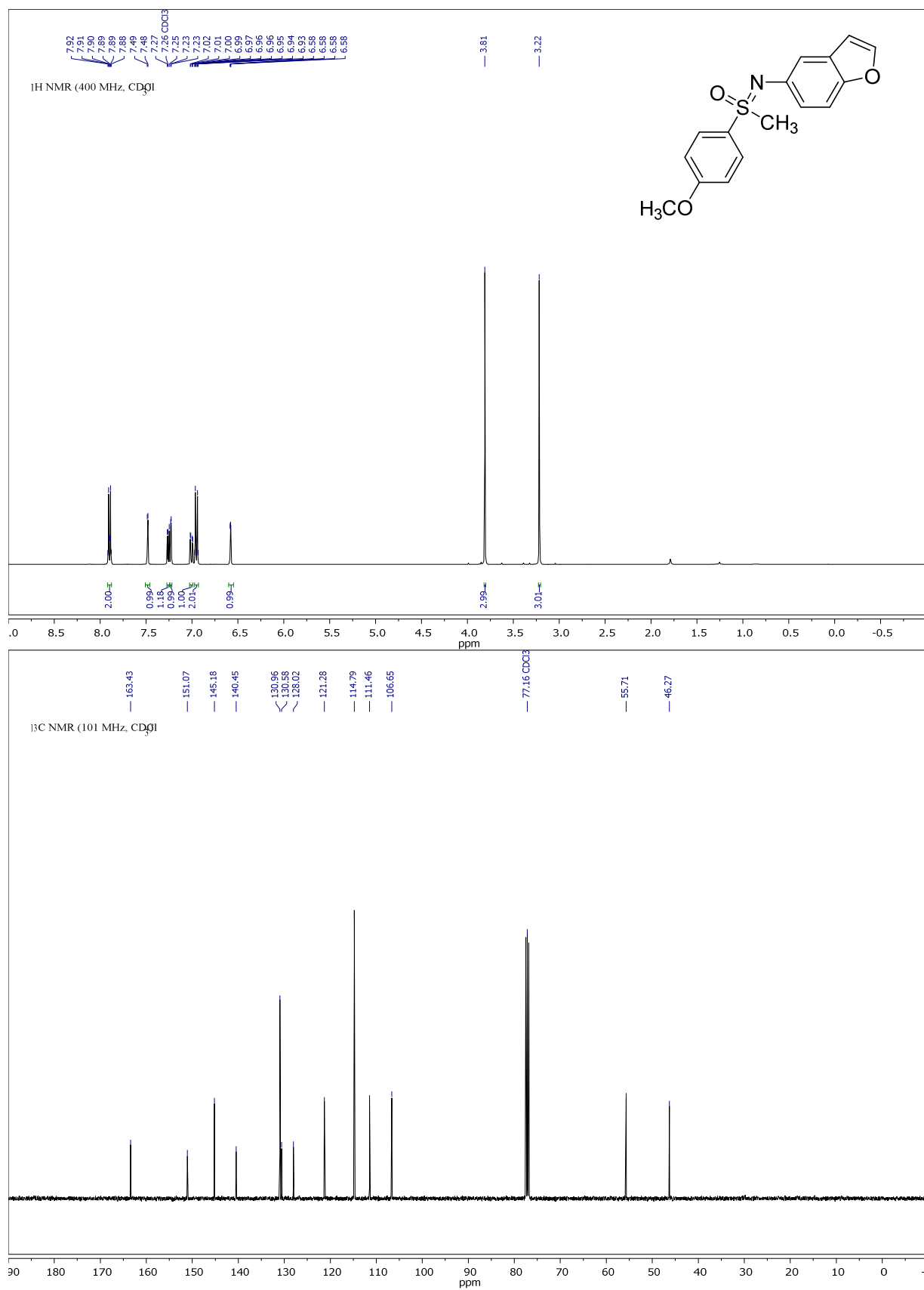
Compound 3af, ^{1}H- and ^{13}C-NMR:

1H NMR (400 MHz, CDCl3)

8.34
7.87
7.86
7.85
7.84
7.84
7.83
7.81
7.80
7.80
7.79
7.78
7.78
7.77
7.26 CDCl3
7.08
7.08
7.07
7.07
7.06
7.05
7.05
7.05
6.99
6.98
6.97
6.96
6.96
6.95

3.82
3.25

0.99
2.00
2.00
2.00
1.99

2.99
2.99

13C NMR (101 MHz, CDCl3)

165.01
163.77
152.10
149.75
130.72
129.67
128.19
123.32
116.14
115.04
77.16 CDCl3
55.77
46.87
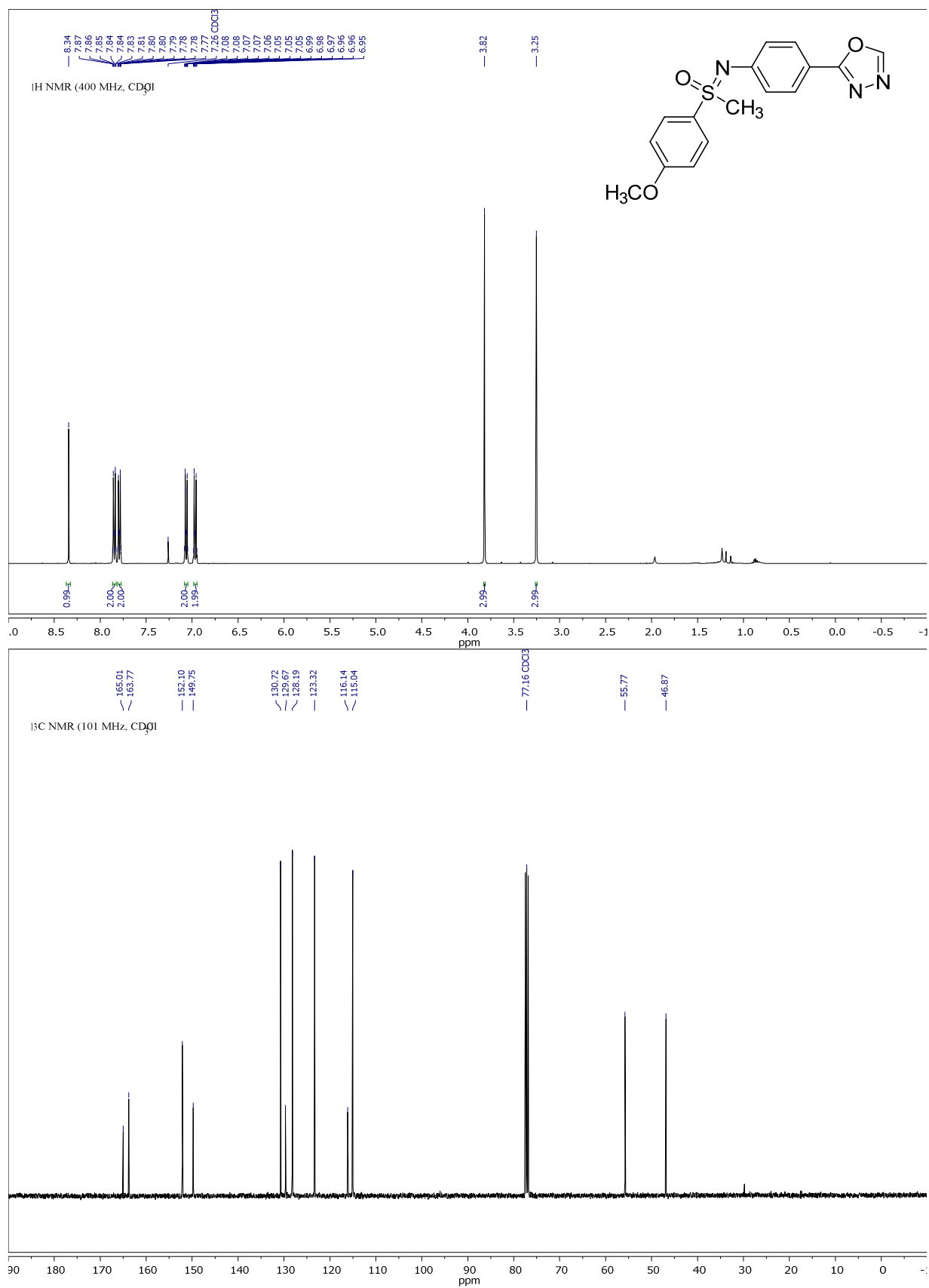
Compound 3ag, ^{1}H- and ^{13}C-NMR:

1H NMR (300 MHz, DMSO)

7.99
7.98
7.98
7.97
7.96
7.95
7.94
7.75
7.75
7.73
7.72
7.48
7.48
7.46
7.46
7.29
7.27
7.26
7.24
7.23
7.22
7.21
7.20
7.18
7.18
7.17
7.16
7.16
7.14
7.13
7.11
7.11

3.85
3.63

2.50 DMSO-d6

1.99
1.00
1.01
1.01
1.99
0.99

3.01
2.99

13C NMR (75 MHz, DMSO)

166.38
163.39

151.50

132.48
130.05
128.97
125.61
122.60
121.16
119.75

114.91

55.86

44.36
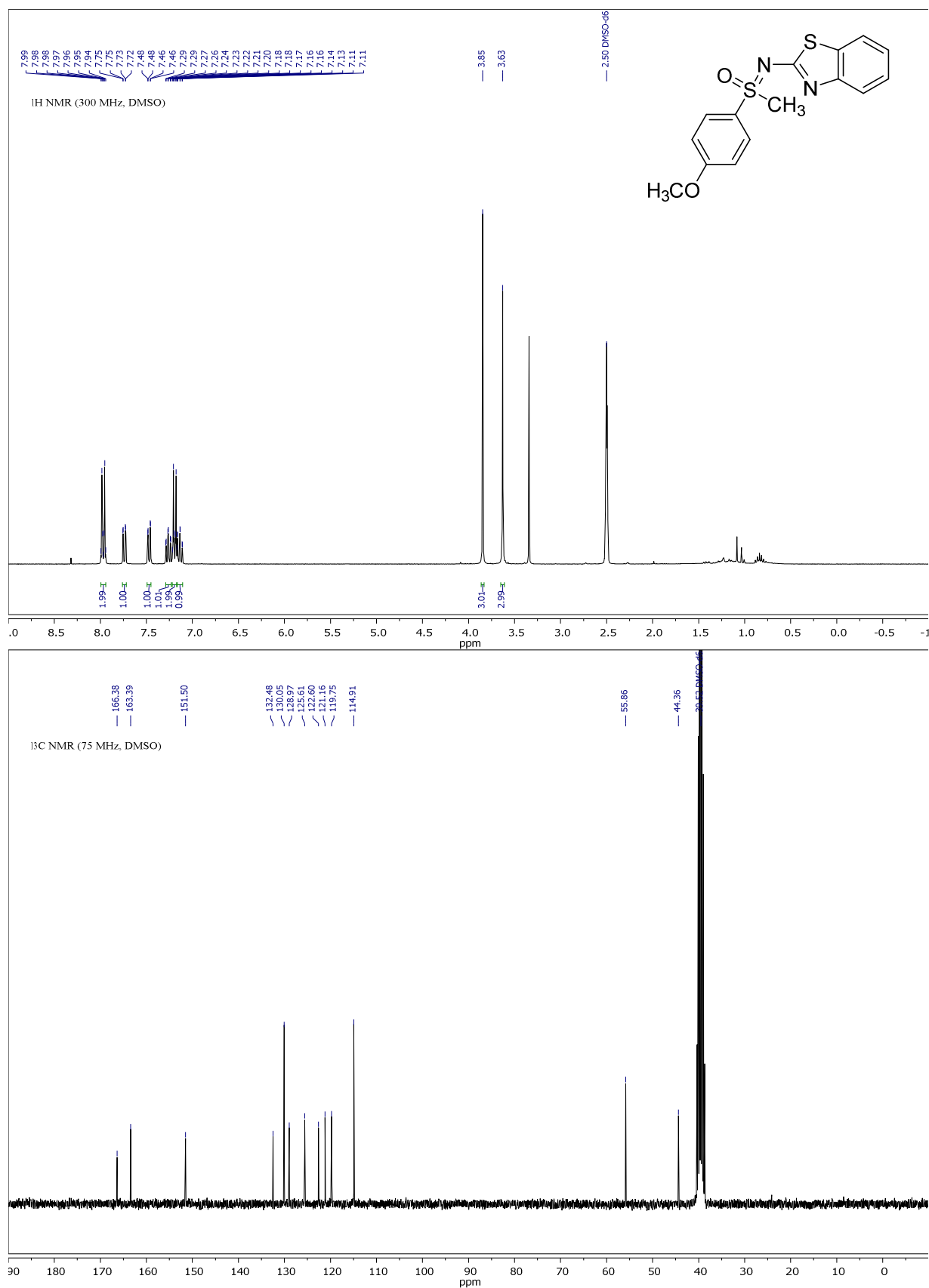
Compound 3ah, ^{1}H- and ^{13}C-NMR:

1H NMR (400 MHz, acetone)

13C NMR (101 MHz, DMSO)
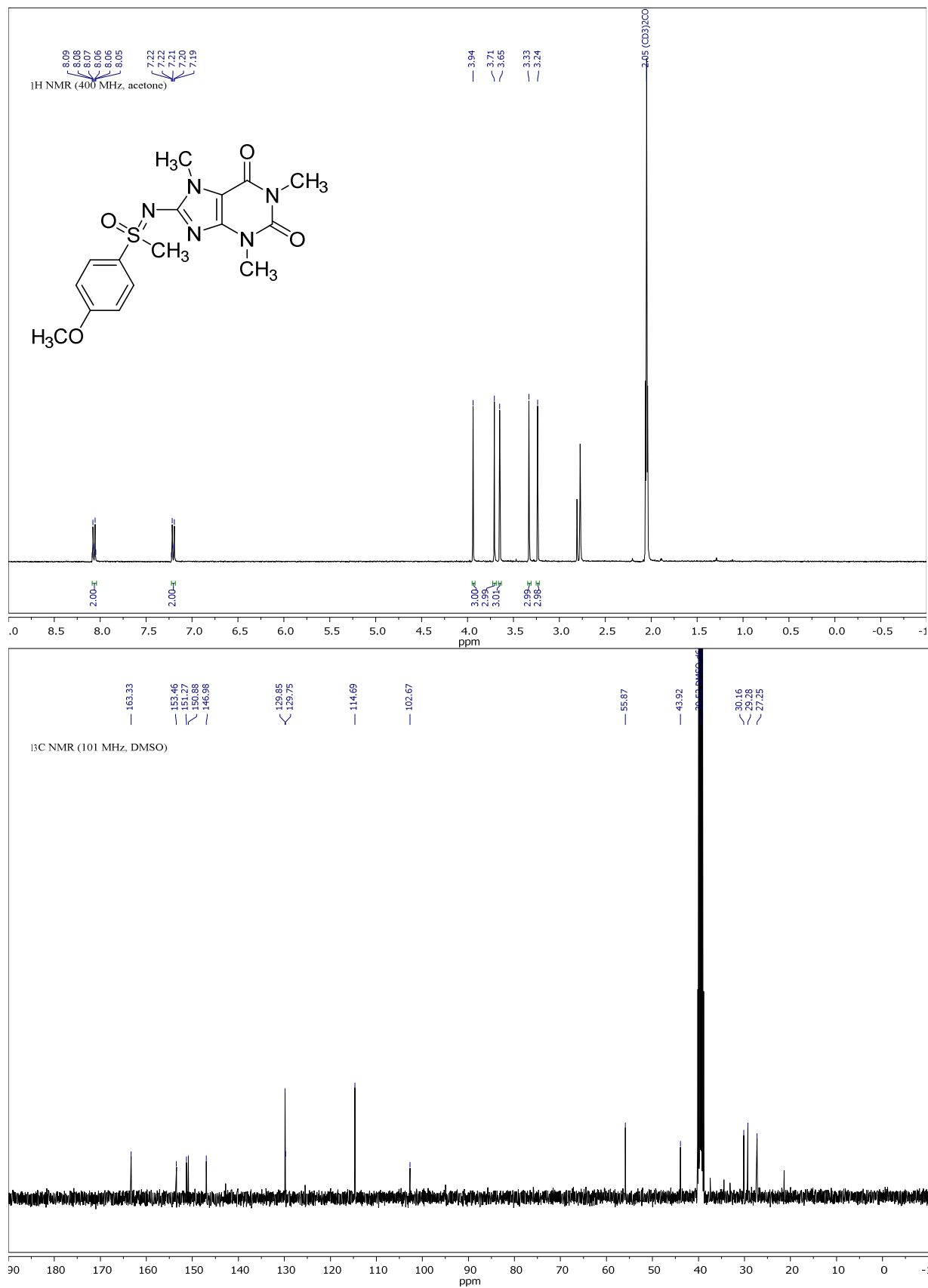
Compound 3ai, ^{1}H- and ^{13}C-NMR:

1H NMR (400 MHz, CDCl$_3$)

13C NMR (101 MHz, CDCl$_3$)
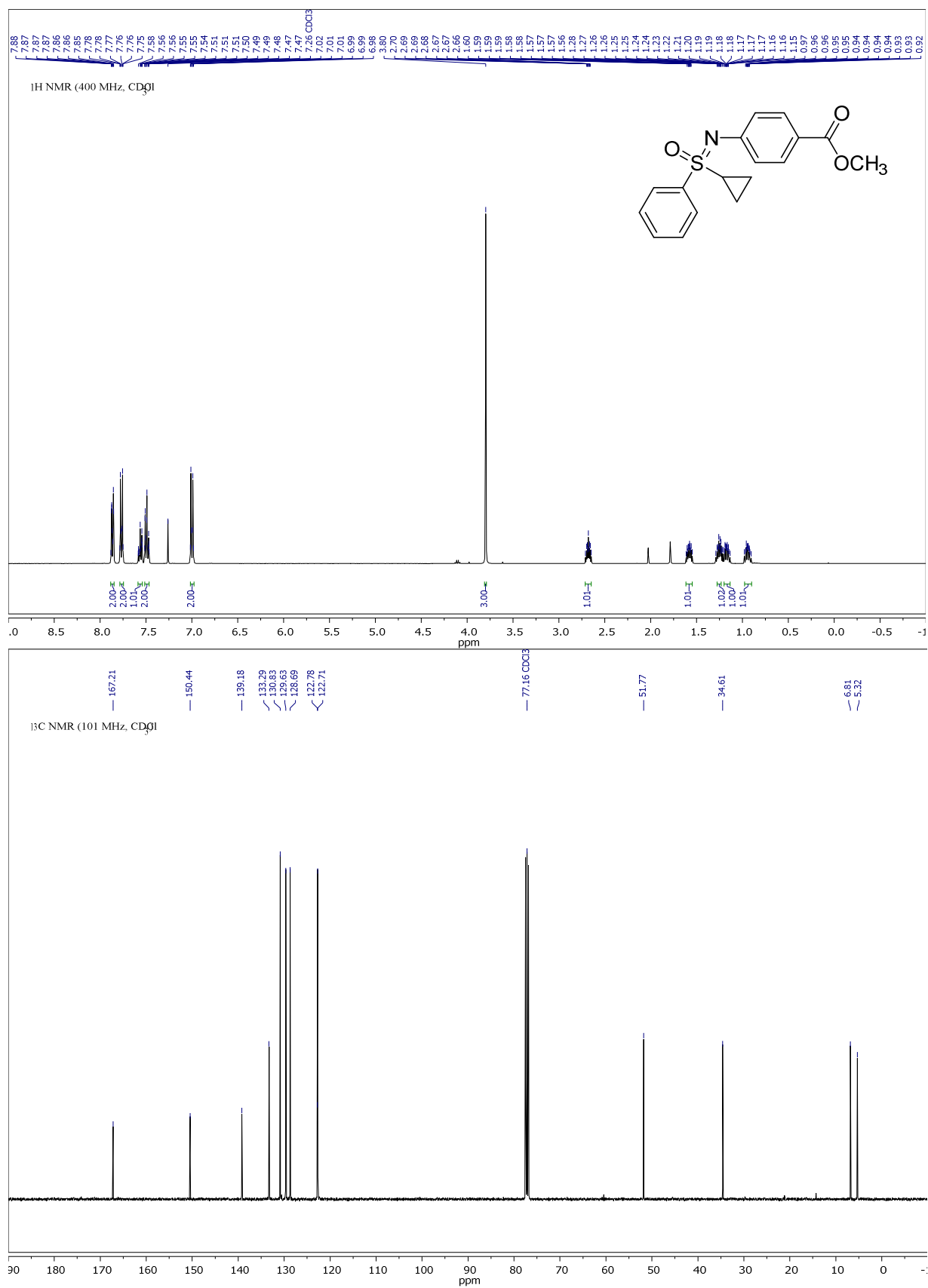
Compound 3aj, ^{1}H- and ^{13}C-NMR:
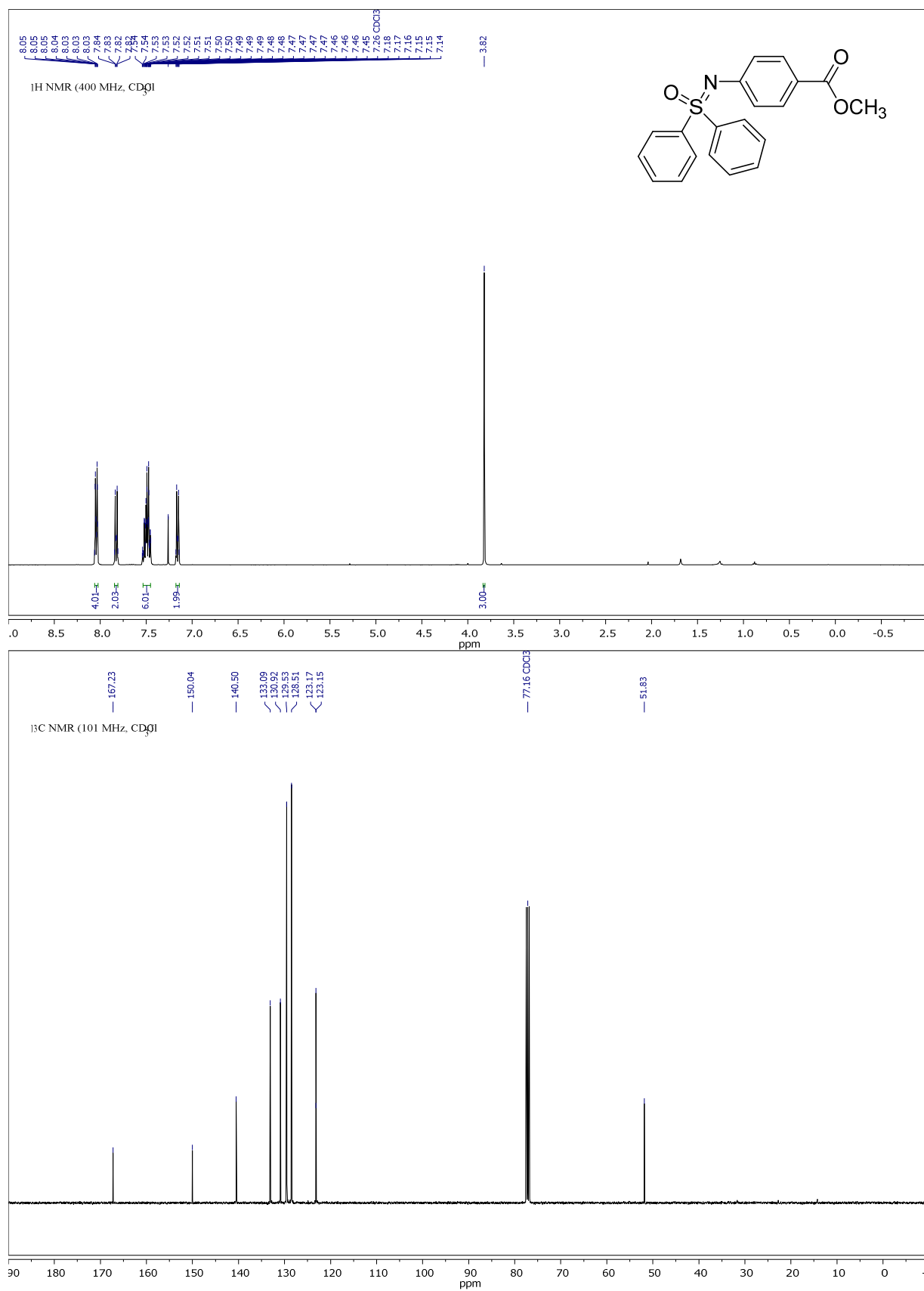
1H NMR (400 MHz, CDCl$_3$)

13C NMR (101 MHz, CDCl$_3$)

Compound 3ak, ^{1}H- and ^{13}C-NMR:

1H NMR (400 MHz, CDCl3)

13C NMR (101 MHz, CDCl3)

Compound 3al, ^{1}H- and ^{13}C-NMR:

1H NMR (400 MHz, CDCl$_3$)

Compound 3am, ^{1}H-, ^{13}C- and ^{19}F-NMR:

19F NMR (282 MHz, CDCl₃)

−104.16

1.00

0   -10   -20   -30   -40   -50   -60   -70   -80   -90   -100   -110   -120   -130   -140   -150   -160   -170   -180   -190   -2
ppm
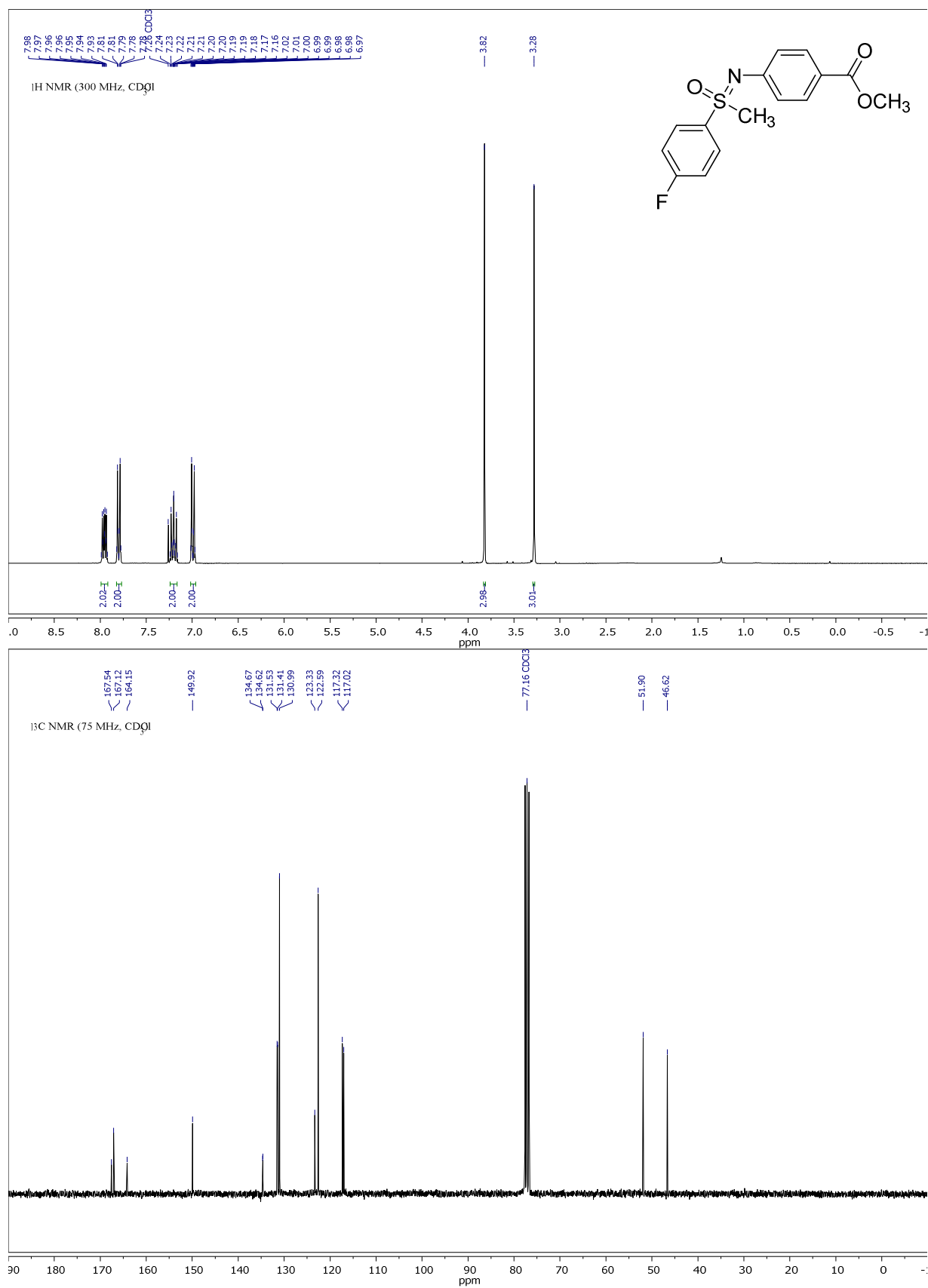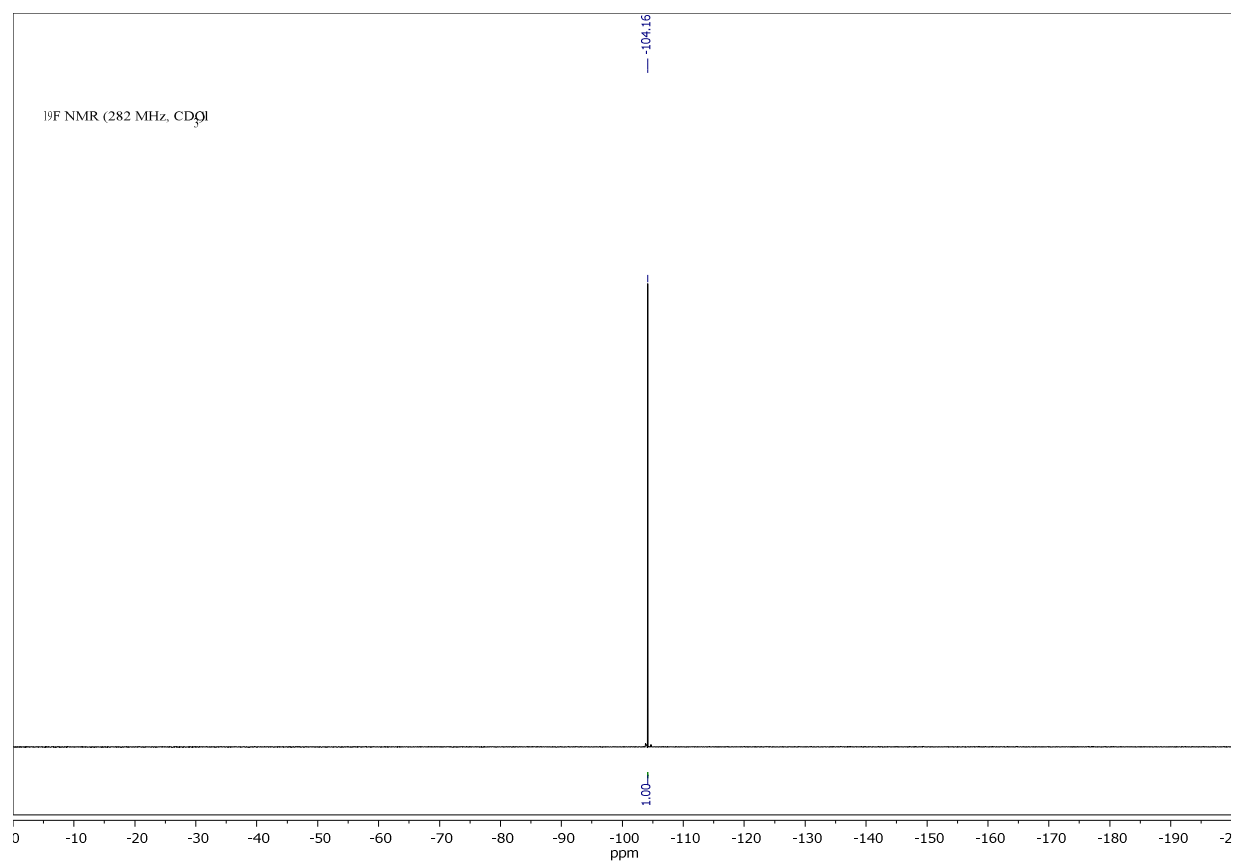
Compound 3an, ^{1}H- and ^{13}C-NMR:

1H NMR (300 MHz, CDCl3)

13C NMR (75 MHz, CDCl3)

Compound 3ao, ^{1}H- and ^{13}C-NMR:

1H NMR (400 MHz, CDCl3)

13C NMR (101 MHz, CDCl3)
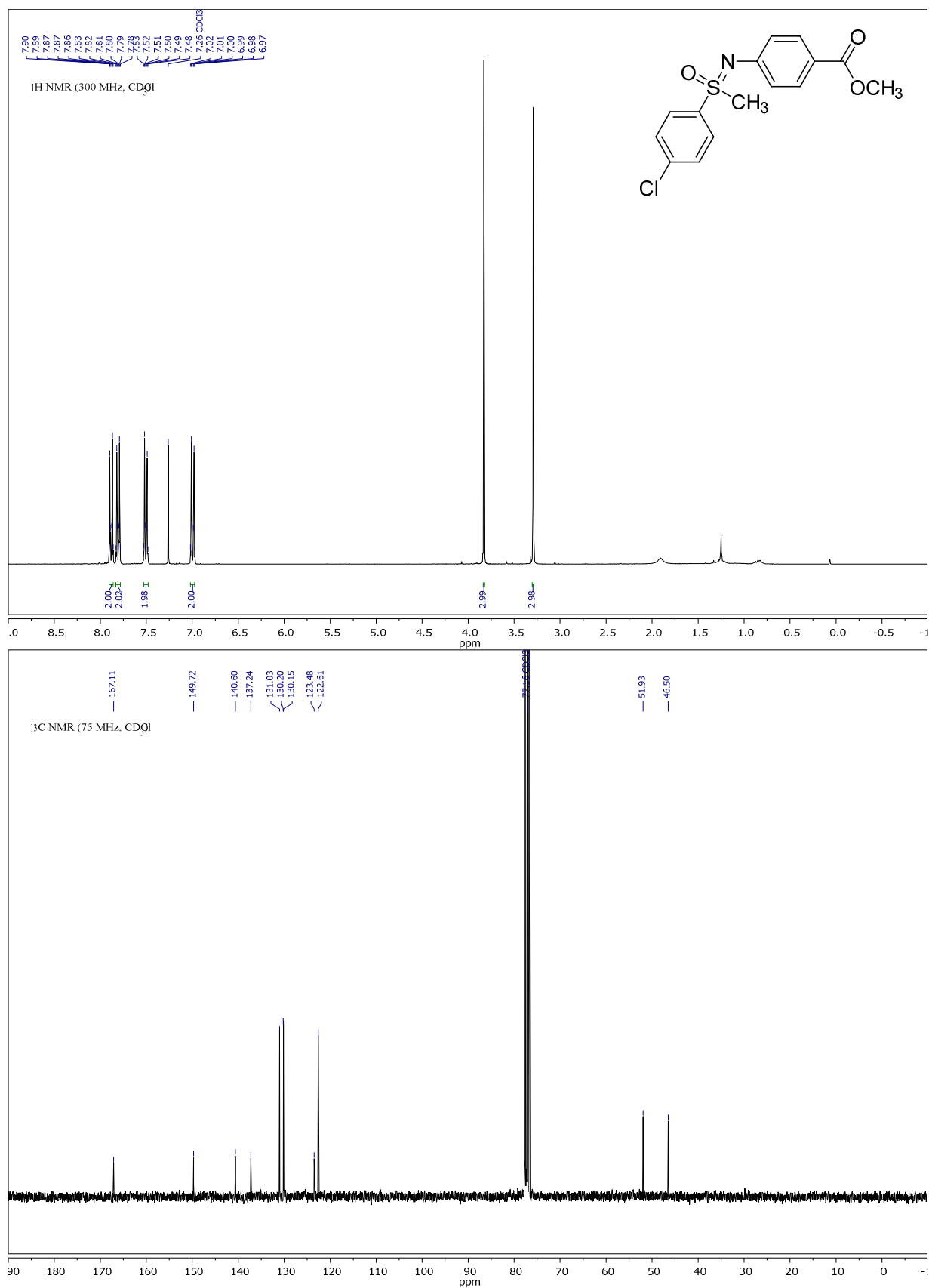
Compound 3ap, ^{1}H- and ^{13}C-NMR:

1H NMR (400 MHz, DMSO)

13C NMR (101 MHz, DMSO)
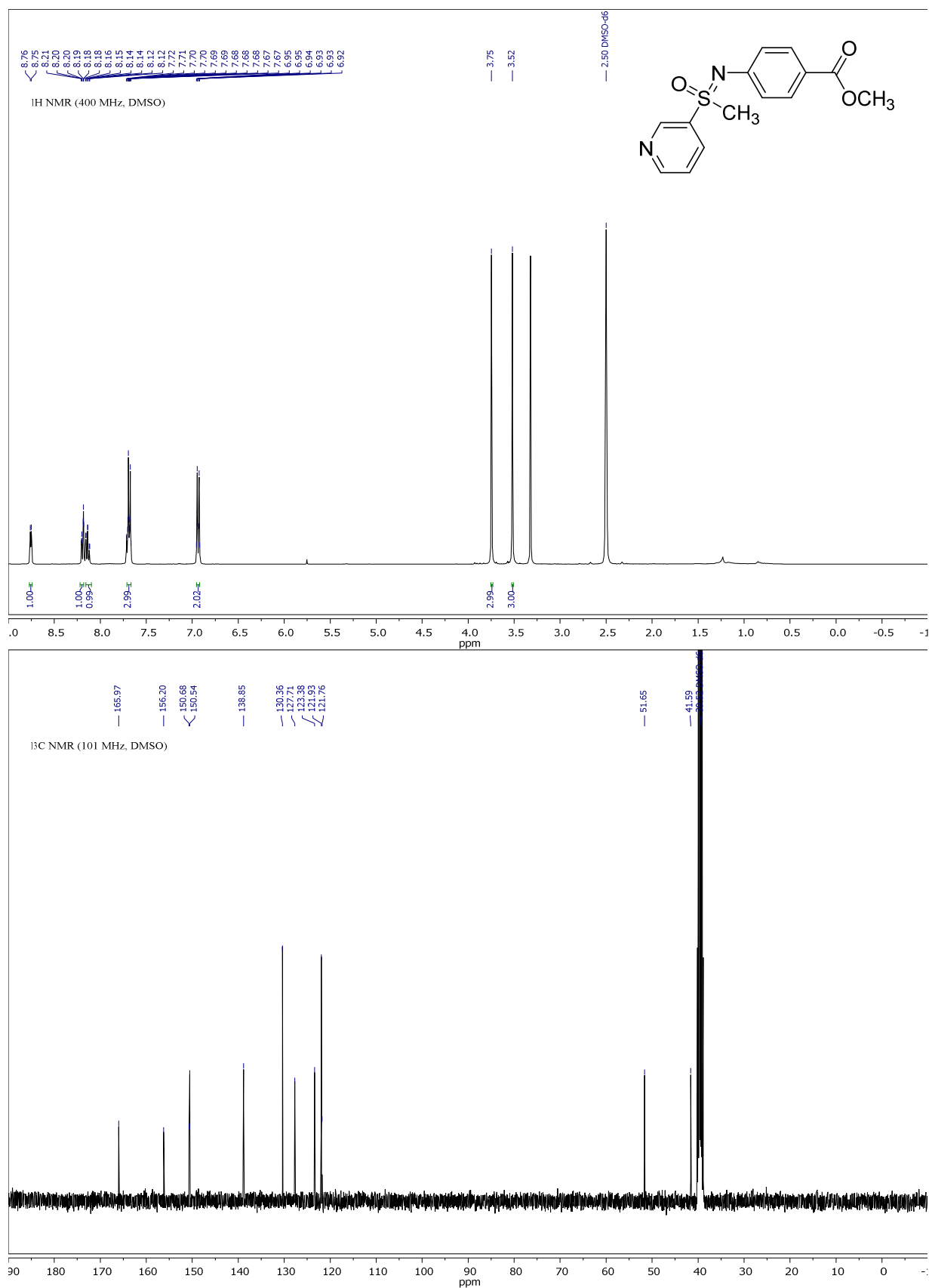
Compound 3aq, ^{1}H- and ^{13}C-NMR:

1H NMR (400 MHz, CDCl3)

8.00
7.99
7.86
7.85
7.84
7.83
7.82
7.68
7.67
7.26 CDCl3
7.12
7.11
7.11
7.10
7.09
7.08

3.84
3.52

1.00
2.02
1.00
2.01
3.00
3.00

13C NMR (101 MHz, CDCl3)

167.08
165.62
148.66
145.24
130.96
126.75
124.47
123.25
77.16 CDCl3
51.98
44.78
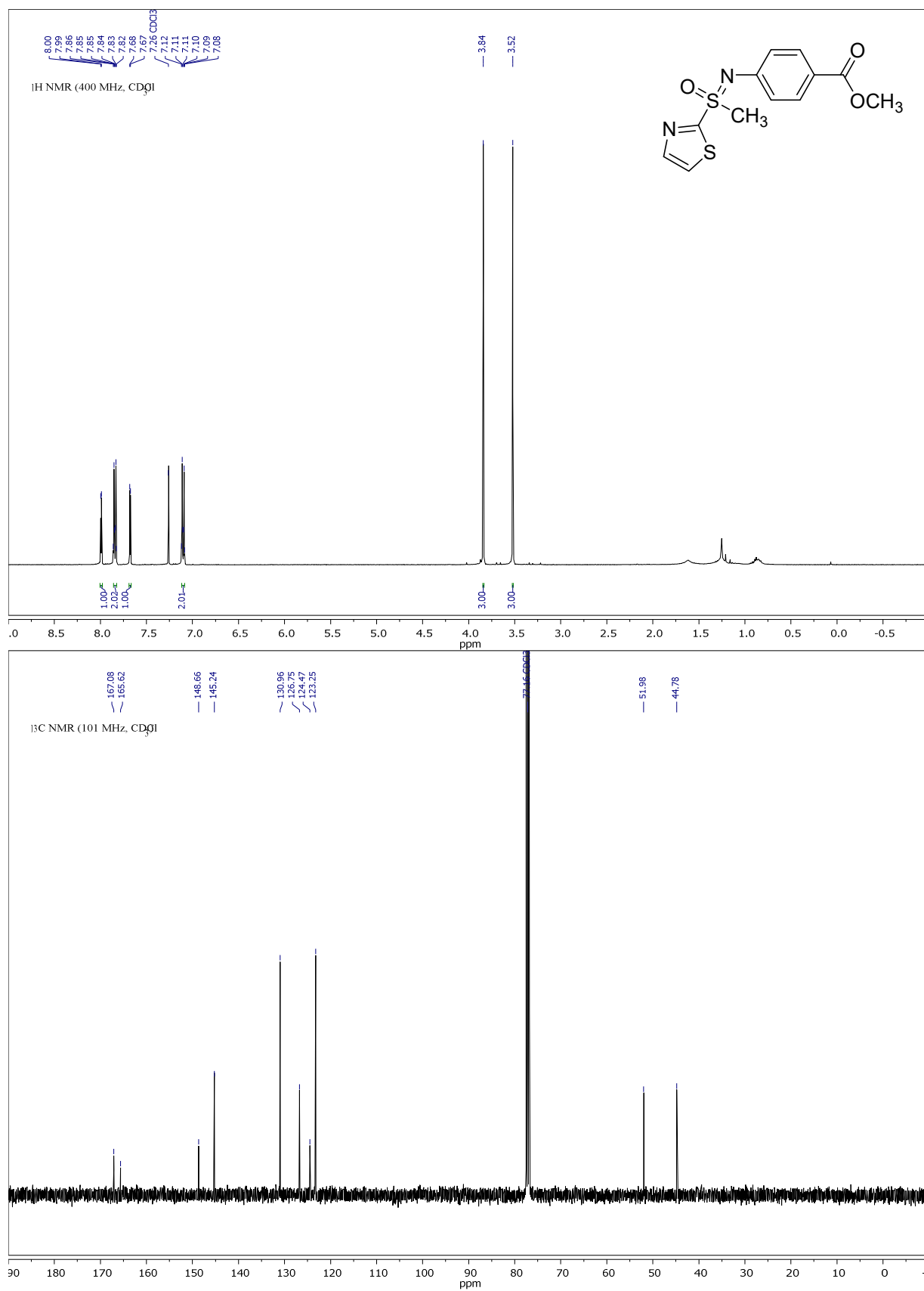
Compound 3ar, ^{1}H- and ^{13}C-NMR:

1H NMR (400 MHz, CDCl3)

7.93
7.92
7.91
7.90
7.89
7.26 CDCl3
7.11
7.10
7.09
7.08
7.07

3.87

3.20

2.01
2.00
3.01
5.98

8.5 8.0 7.5 7.0 6.5 6.0 5.5 5.0 4.5 4.0 3.5 3.0 2.5 2.0 1.5 1.0 0.5 0.0 -0.5
ppm

13C NMR (101 MHz, CDCl3)

167.19
150.26
131.20
123.60
122.45
77.16 CDCl3
51.96
42.50

180 170 160 150 140 130 120 110 100 90 80 70 60 50 40 30 20 10 0
ppm
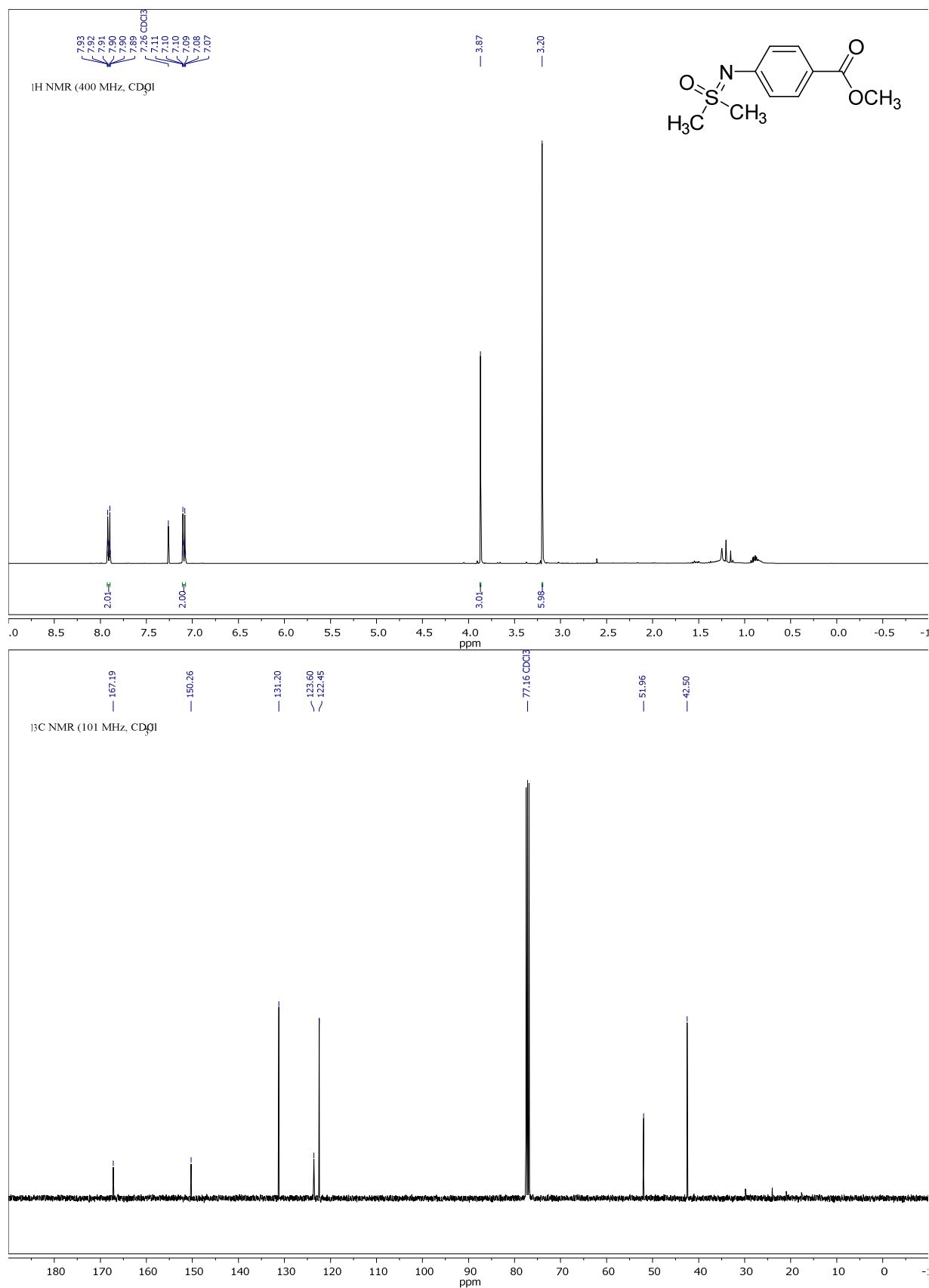
Compound 3as, ^{1}H- and ^{13}C-NMR:

1H NMR (400 MHz, CDCl3)

13C NMR (101 MHz, CDCl3)
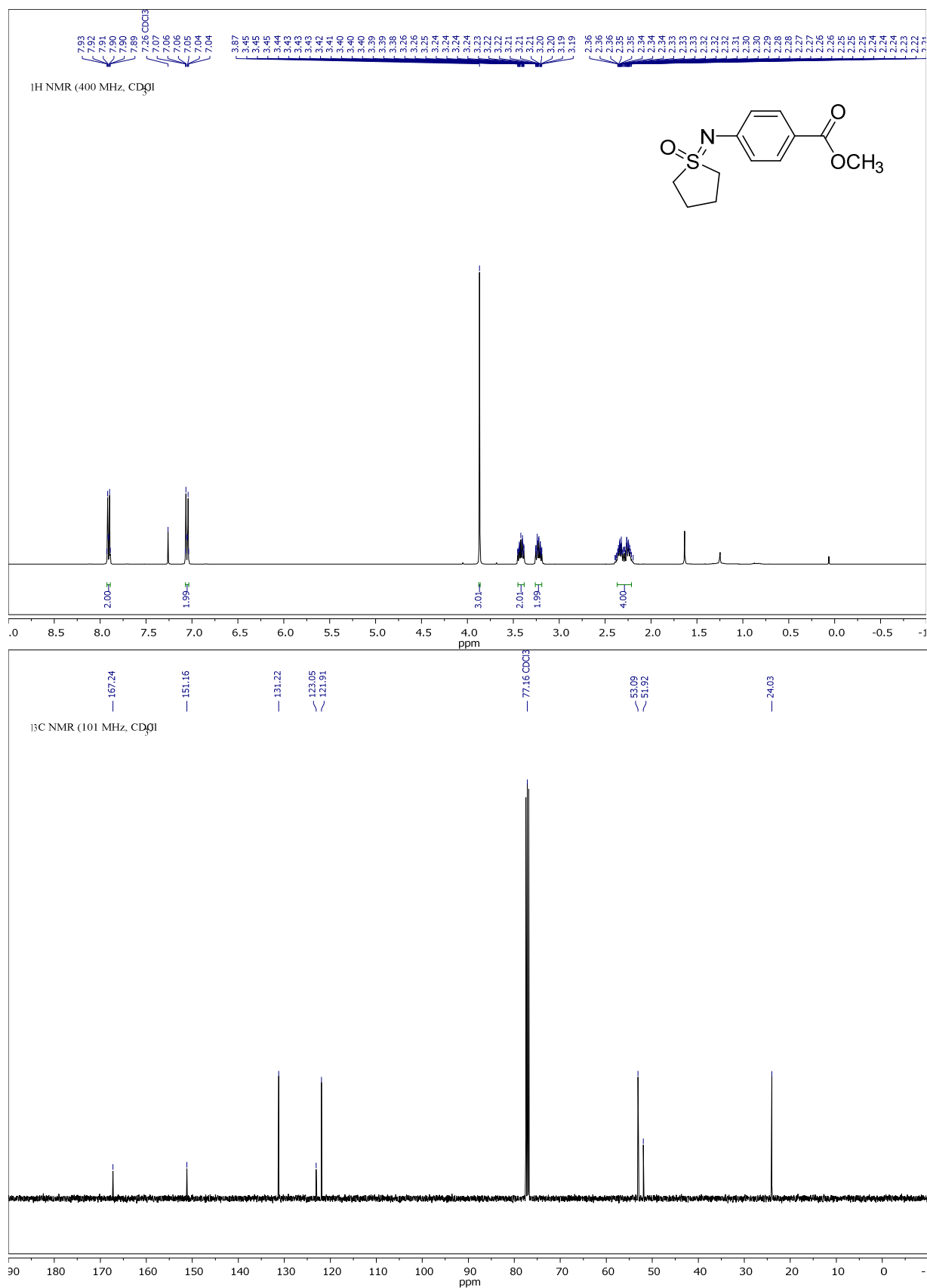
Compound 3at, ^{1}H-NMR:

1H NMR (400 MHz, CDCl$_3$)
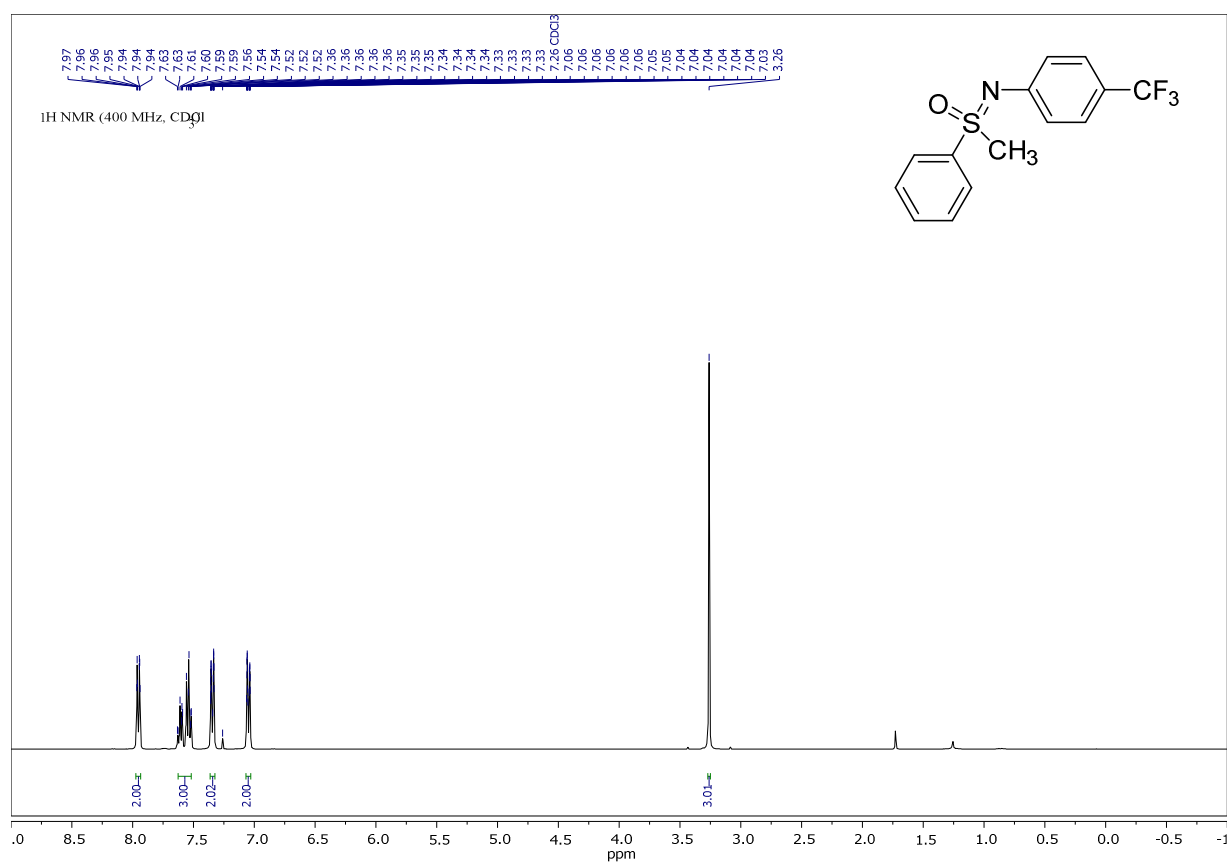
Compound 3au, ^{1}H- and ^{13}C-NMR:

1H NMR (400 MHz, CDCl$_3$)

8.02
8.02
8.01
8.00
7.99
7.86
7.58
7.57
7.57
7.56
7.55
7.54
7.54
7.53
7.52
7.51
7.50
7.50
7.48
7.47
7.45
7.44
7.31
7.29
7.26 CDCl3
6.99
6.97
6.97
6.42
6.42
6.41
6.41

3.24

1.65

2.00
0.95
4.02
1.02
0.99
1.01
2.98
9.01

13C NMR (101 MHz, CDCl$_3$)

149.96
142.15
139.62
135.91
133.20
129.50
128.83
125.57
124.86
121.02
119.79
109.97
107.15
83.54
77.16 CDCl3
45.88
28.33

267
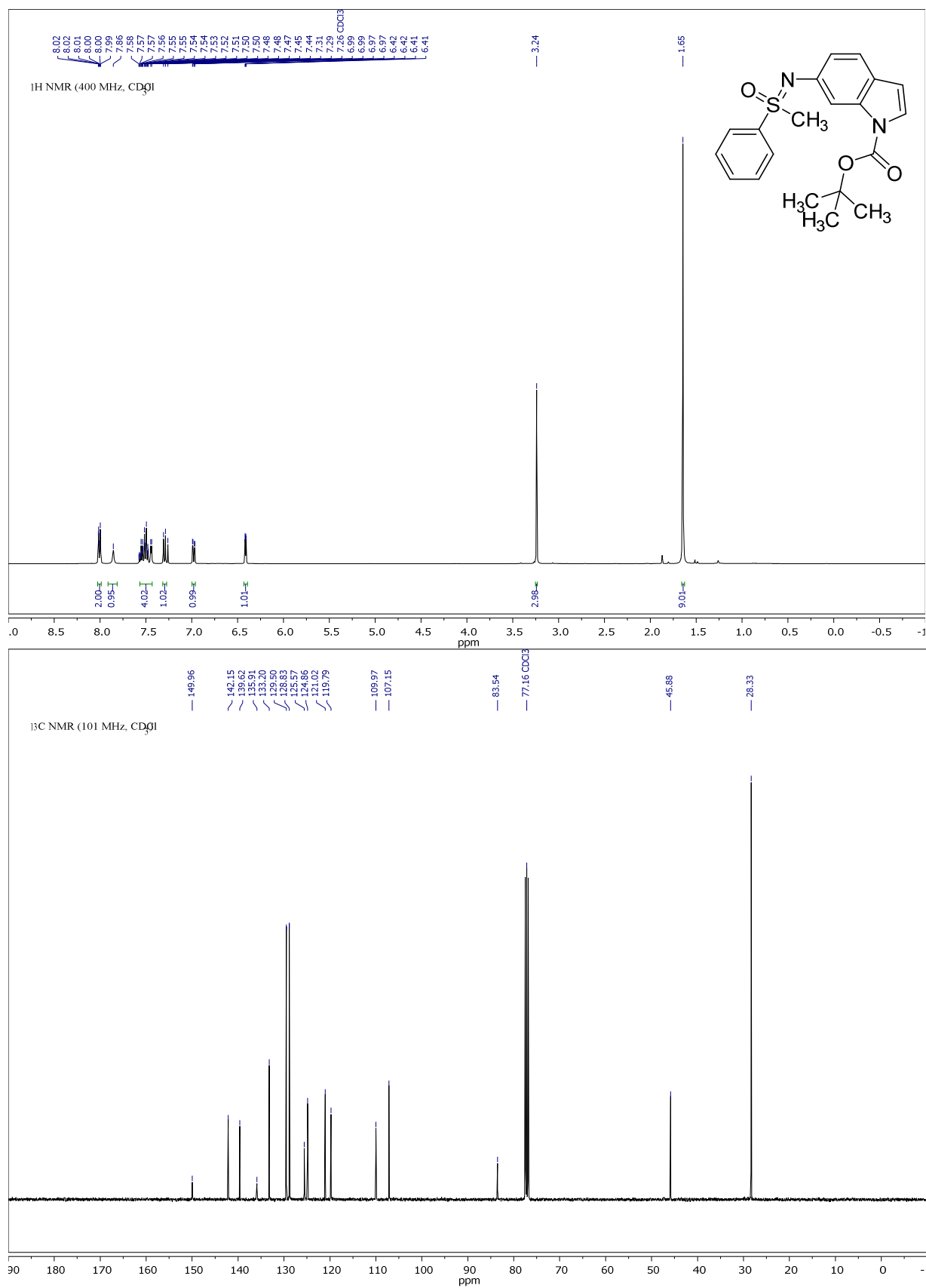
Compound 3av, ^{1}H- and ^{13}C-NMR:

1H NMR (400 MHz, CD$_3$l)

13C NMR (101 MHz, CD$_3$l)
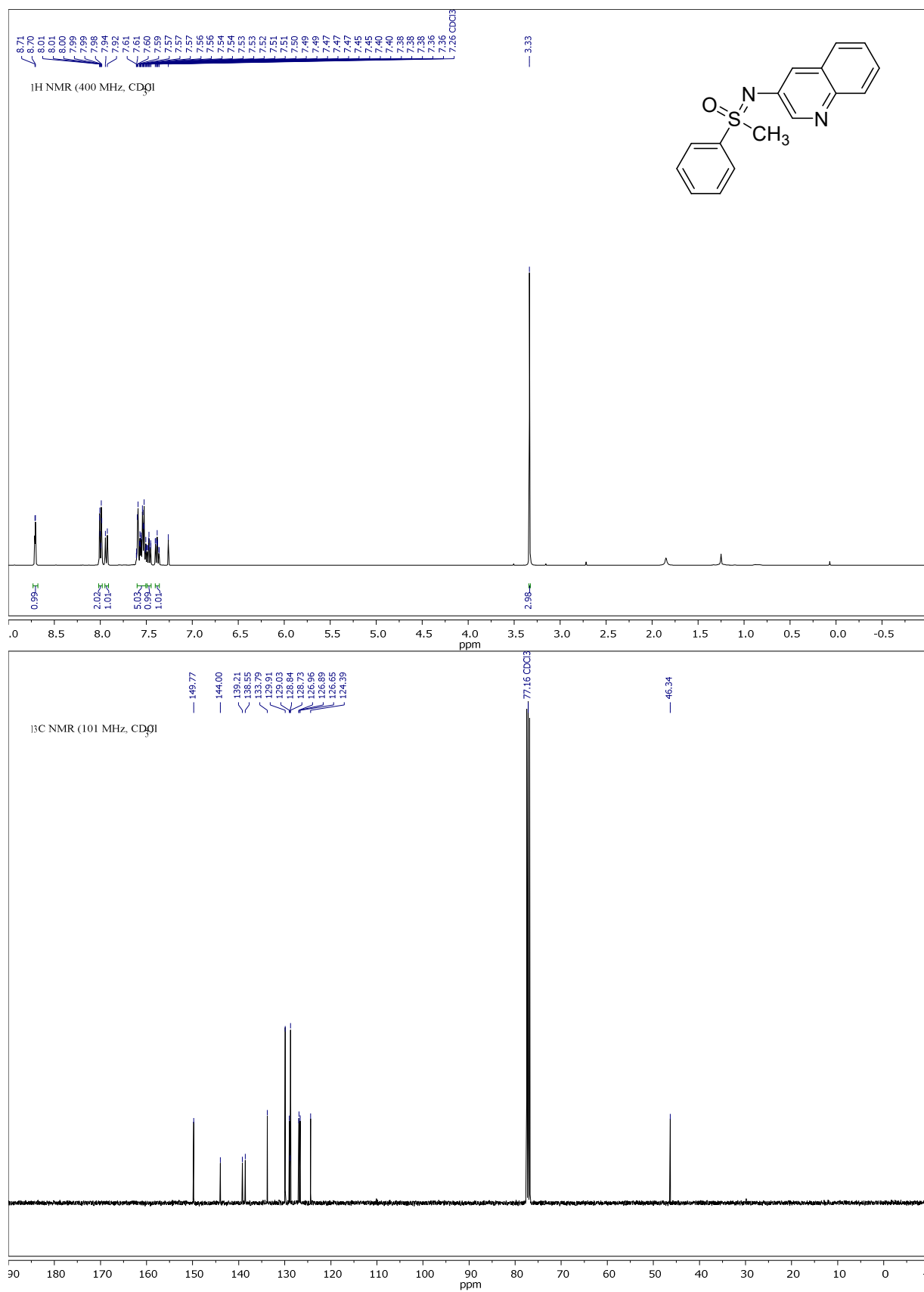
Compound 3aw, ^{1}H-, ^{13}C- and ^{19}F-NMR:

1H NMR (400 MHz, CDCl3)

13C NMR (101 MHz, CDCl3)

19F NMR (377 MHz, CDCl₃)

−65.62

3.00

40 30 20 10 0 -10 -20 -30 -40 -50 -60 -70 -80 -90 -100 -110 -120 -130 -140 -150 -160 -170 -180 -190 -200 -210 -220
ppm
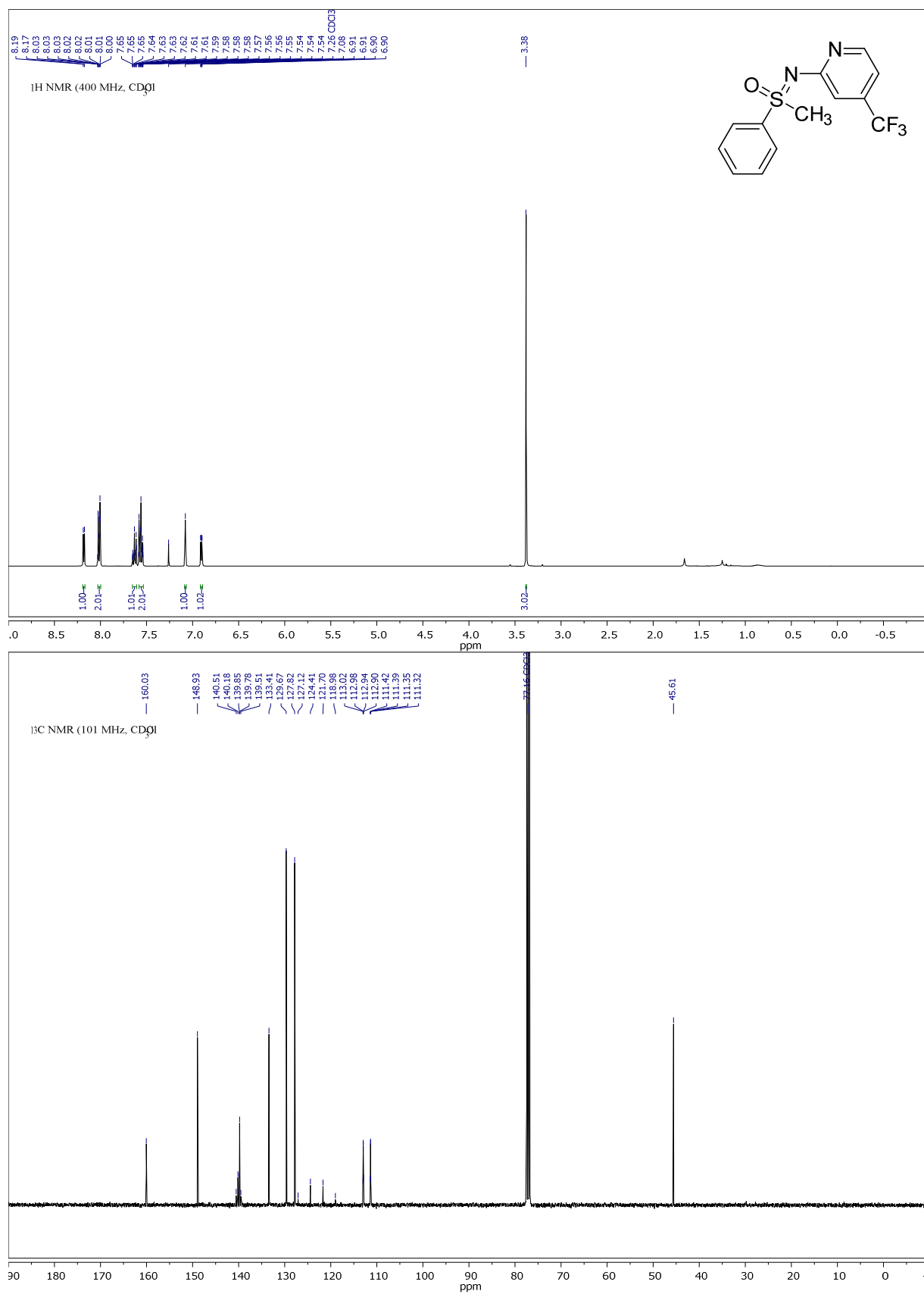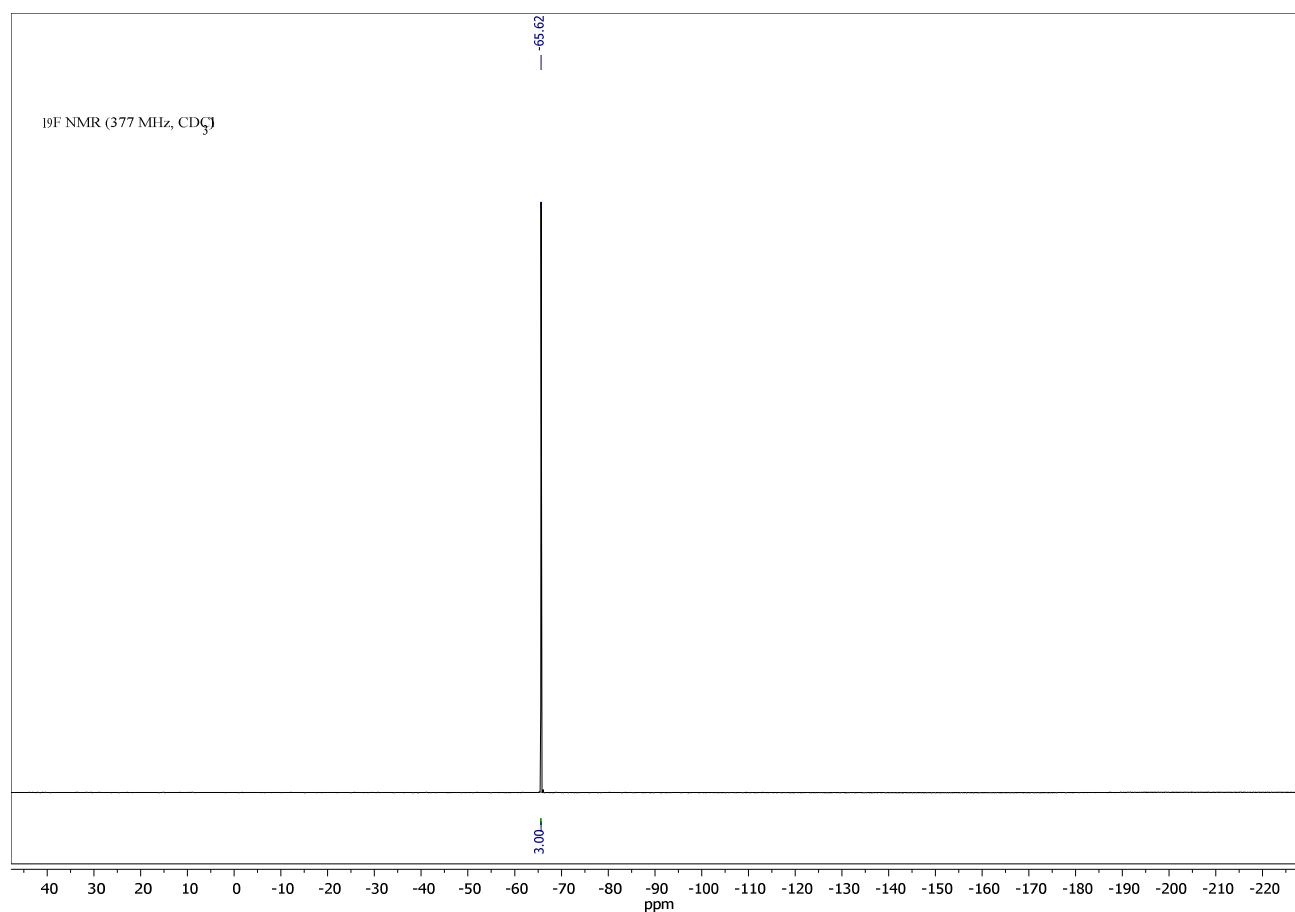
Compound 3ax, ^{1}H- and ^{13}C-NMR:

1H NMR (400 MHz, CDCl3)

13C NMR (101 MHz, CDCl3)

Compound 5, ^{1}H- and ^{13}C-NMR:

1H NMR (300 MHz, DMSO)

13C NMR (75 MHz, DMSO)

Compound 7, ^{1}H-NMR:

1H NMR (400 MHz, CDCl3)
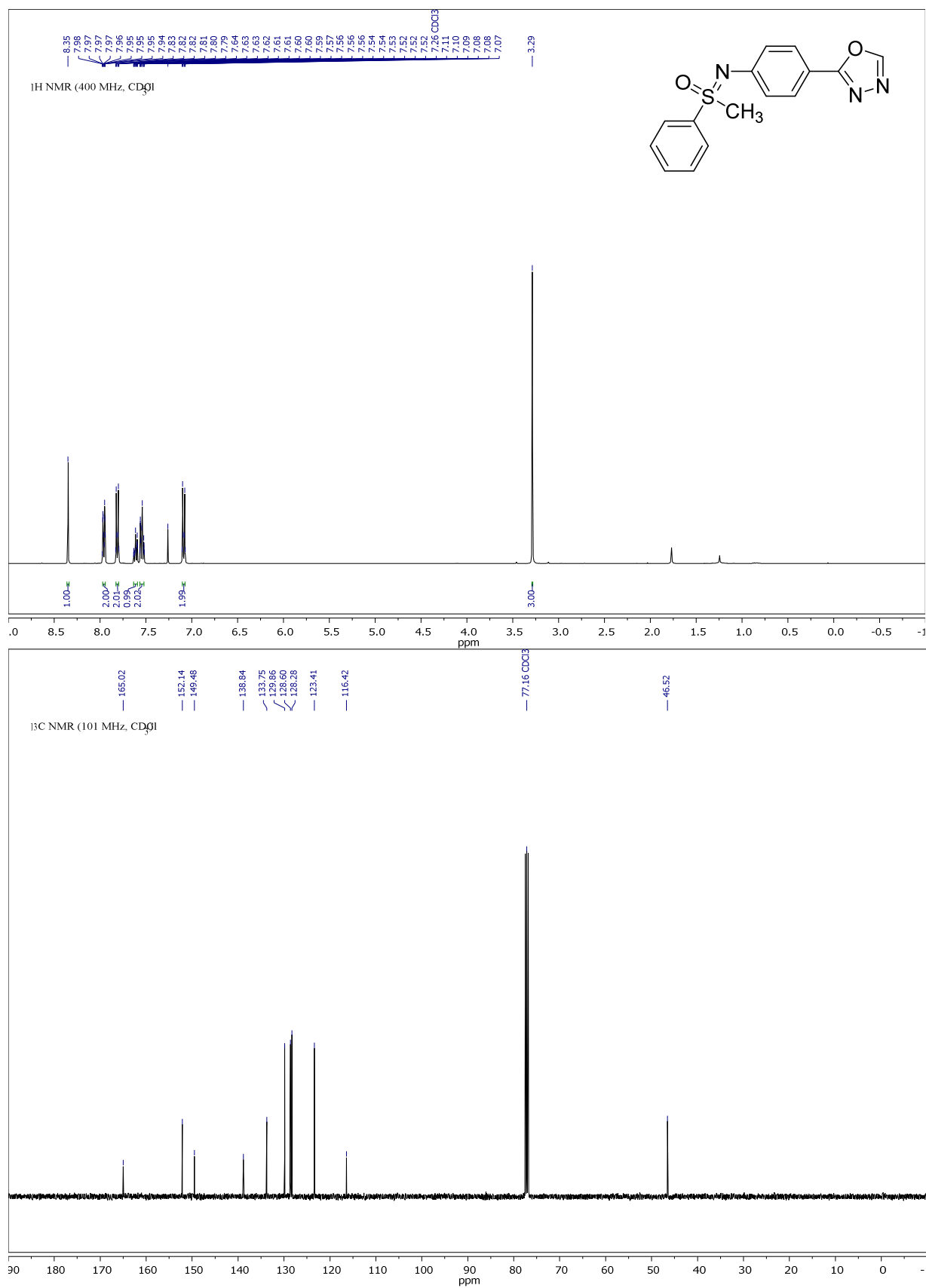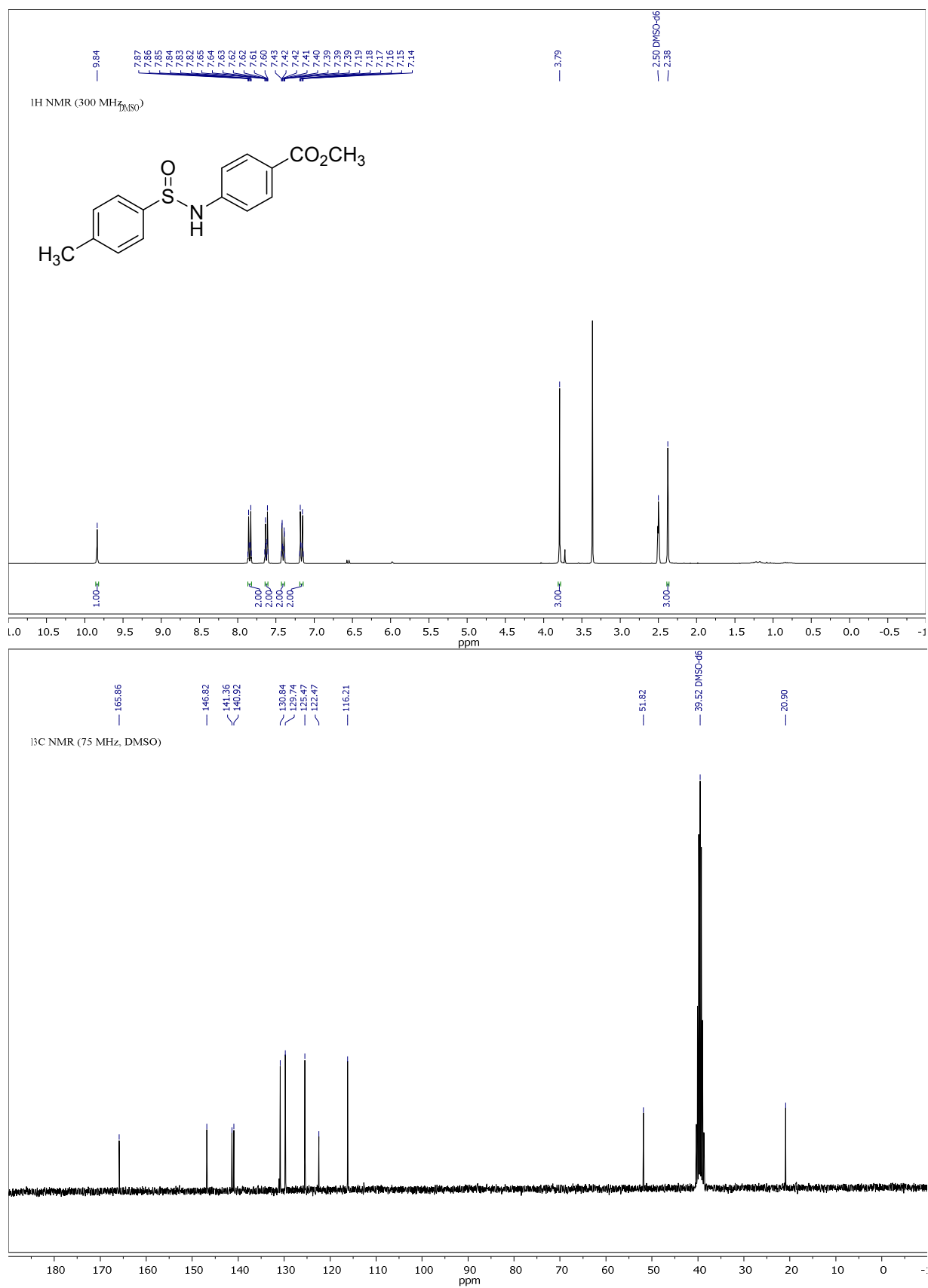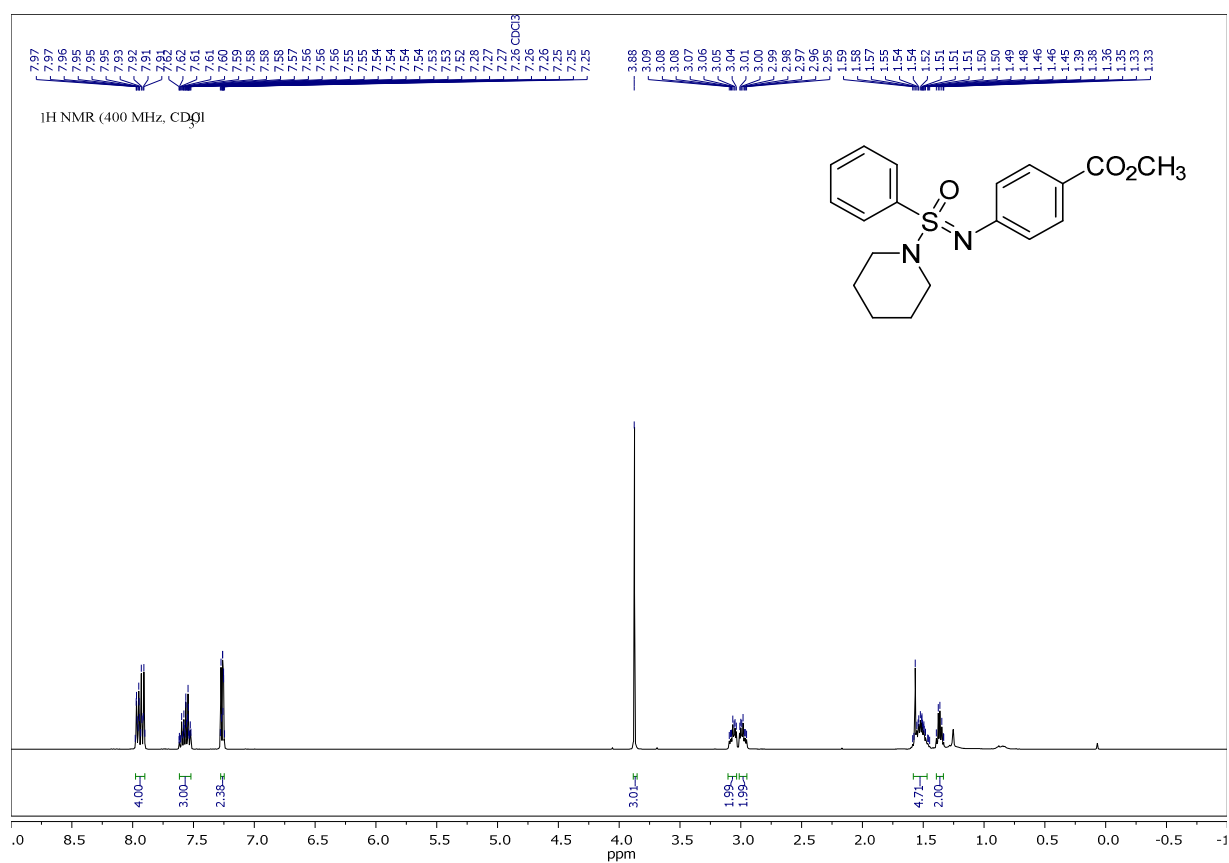
6.4   Appendix Chapter 3

6.4.1   Computational Details

DFT calculations were carried with the *Gaussian 09* software package,[1] using the (U)M06-2X DFT functional[2] (with an ultrafine integration grid of 99,590 points) with the 6-311++G(d,p) basis set for all atoms. Grimme's D3 version (zero damping) for empirical dispersion[3] was also included. Frequency calculations were conducted for all structures to confirm them as either a minimum or a Transition State (TS). Full (U)MP2[4] with cc-pVTZ basis set for all atoms was also employed in selected cases. Intrinsic Reaction Coordinates (IRC)[5] were determined for the TS of interest. Natural Bond Orbital[6] (NBO) analysis was performed on key intermediates and transition states. Spin density was evaluated from the NBO analysis data. The Gibbs Free energy values are reported at 298 K, unless noted otherwise. DLPNO-CCSD(T)[7] calculations (with Tight PNO) were performed with ORCA 4.0[8], with the aug-cc-pVTZ basis set for all atoms. RIJCOSX was used to accelerate the HF steps during the SCF evaluation. Three-dimensional structures and orbital plots were produced with CYLView 1.0.1,[9] Chemcraft 1.8[10] and UCSF Chimera.[11] Geometries, energies and frequencies presented in this SI were organized with ESIgen.[12]

6.4.2   CCSD(T) Corrections to the DFT Results

In order to evaluate the performance of the chosen DFT method, it has been compared with the results of DPLNO-CCSD(T) calculations. DLPNO-CCSD(T) can recover 99.9% of the CCSD(T) energy at a fraction of its computational cost.[13] The aug-cc-pVTZ basis set was chosen as a sufficiently large one to cover the orbitals involved in the systems of interest, particularly the ones for sulfur. The DLPNO-CCSD(T) (labelled as simply CCSD(T) in Figure 36) data suggest that M06-2X(D3)/6-311++G(d,p) (labelled as DFT in Figure 36) systematically overestimates endergonicity of the fragmentation. For fluorinated radicals, the CCSD(T) correction reaches up to 7.5 kcal/mol, with an average of 6.1 kcal/mol. Understanding of DFT's overestimation will be important for the formation of partially fluorinated radicals and other borderline cases (vide infra).
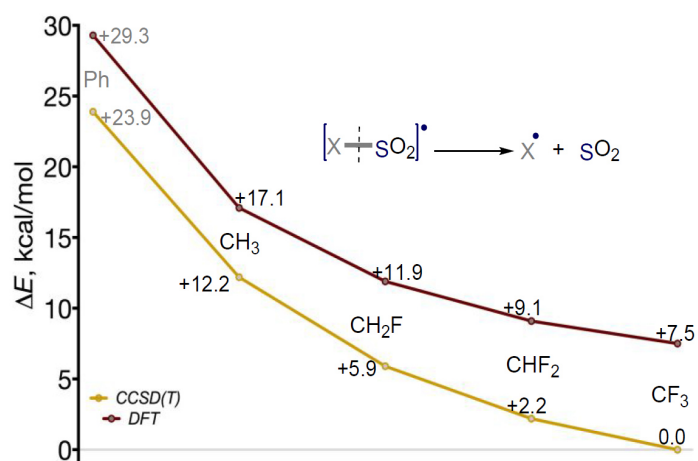
Figure 36. Comparison between UM06-2X(D3) and DLPNO-CCSD(T) reaction electronic energies for C–S scissions for fluorinated systems.

6.4.3 NMR Spectra

Compound 2a, ^{1}H-, ^{13}C- and ^{19}F-NMR:

1H NMR (300 MHz, CDCl)

CH$_3$CF$_2$

13C NMR (101 MHz, CDCl)

19F NMR (282 MHz, CDCl₃)

-96.02
-96.87
-97.05
-97.91

Compound 3a, ^{1}H-, ^{13}C- and ^{19}F-NMR:

1H NMR (400 MHz, CD$_2$Cl$_2$)

4.00

1.00

3.01
0.99
1.03
1.03
1.16

.0   8.5   8.0   7.5   7.0   6.5   6.0   5.5   5.0   4.5   4.0   3.5   3.0   2.5   2.0   1.5   1.0   0.5   0.0   -0.5   -1
ppm

13C NMR (101 MHz, CD$_2$Cl$_2$)

30 180 170 160 150 140 130 120 110 100 90 80 70 60 50 40 30 20 10 0 -
ppm

19F NMR (376 MHz, CDCl₃)

-122.60
-123.34
-123.81
-124.55
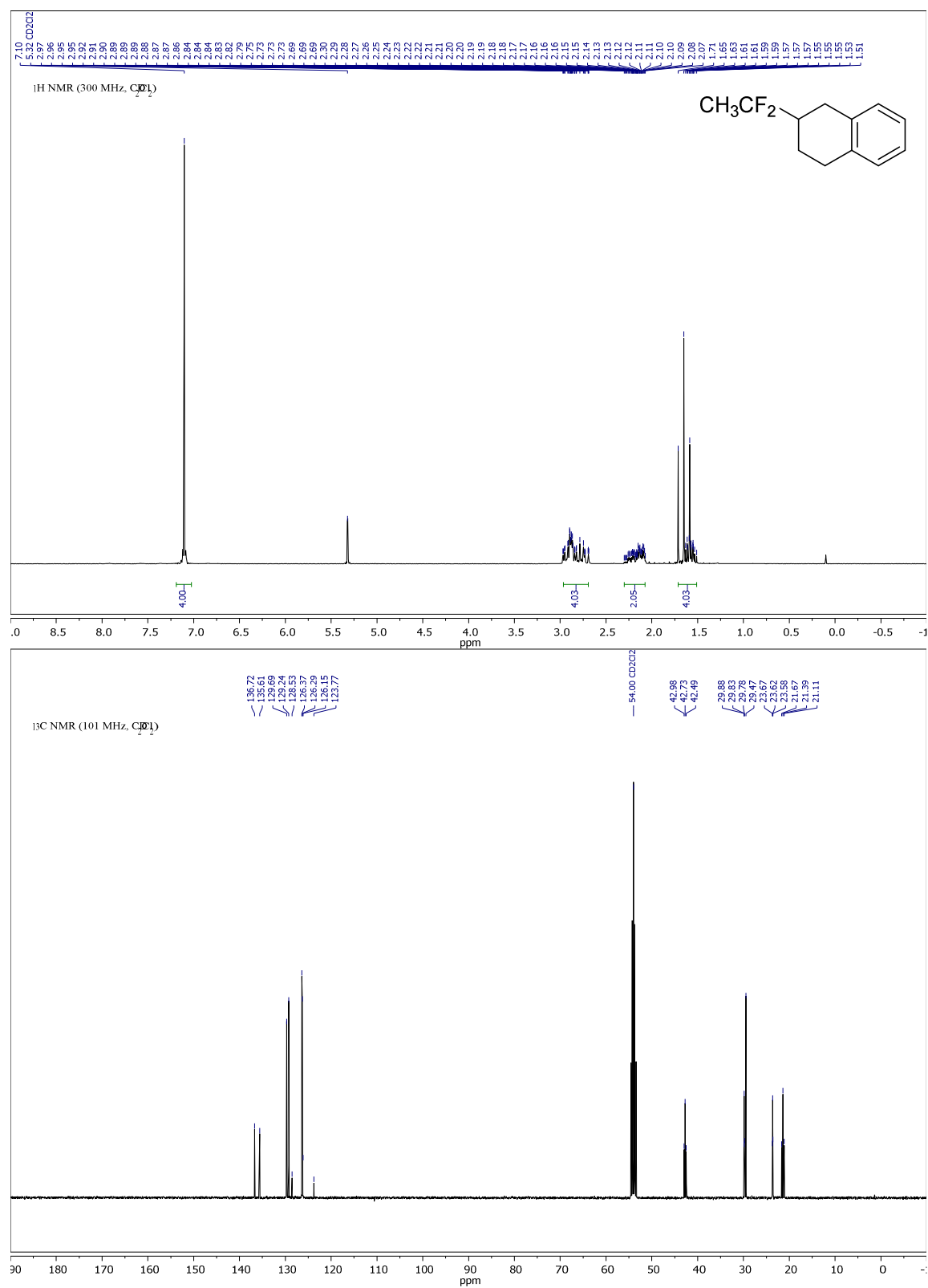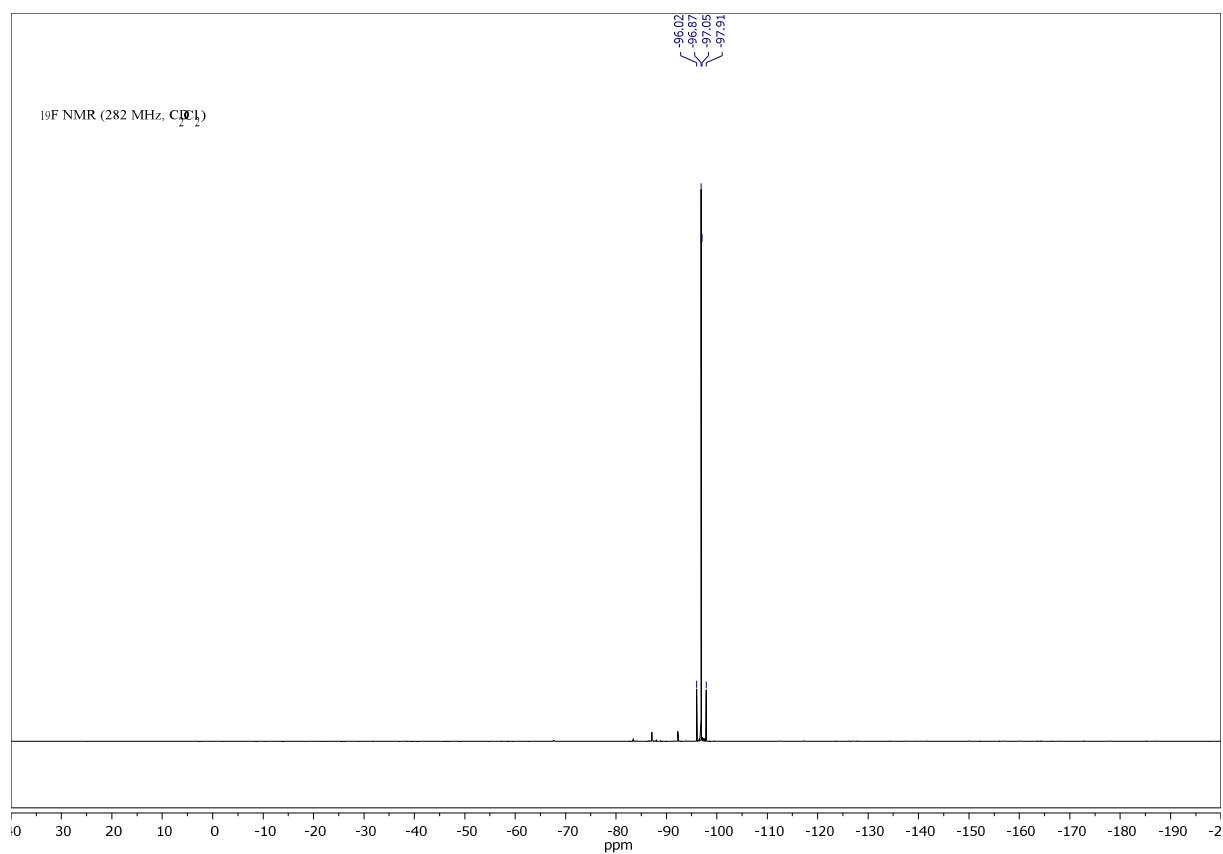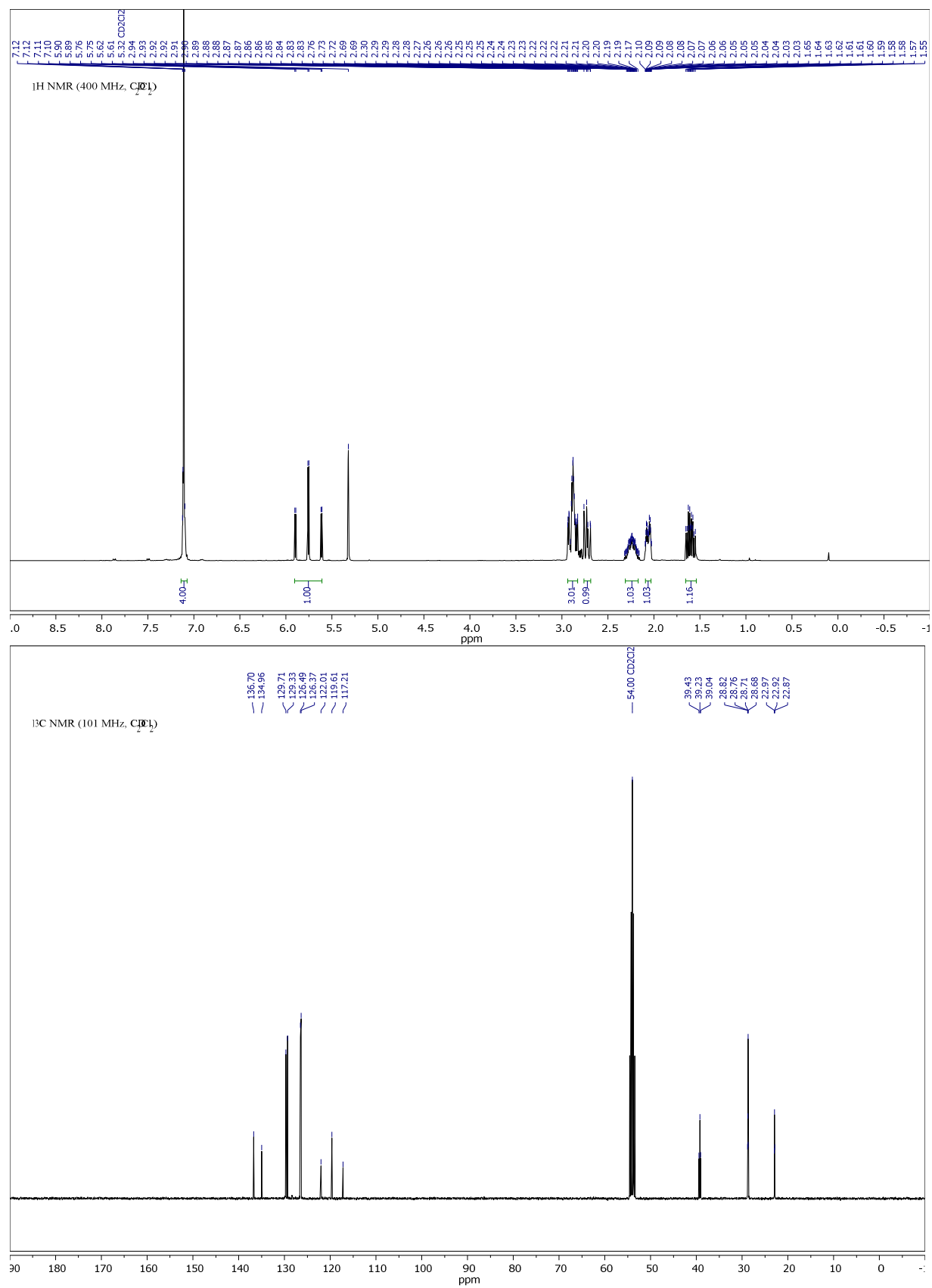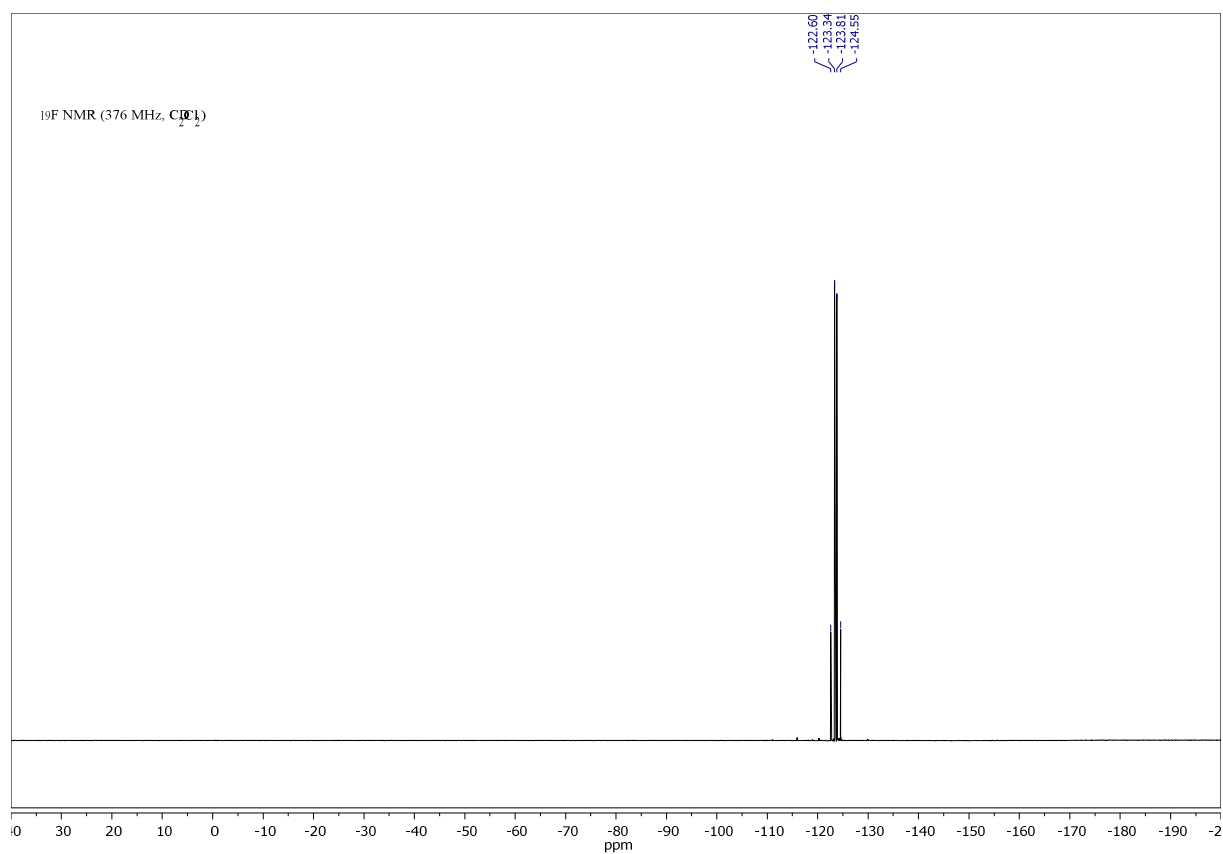
6.4.4   References and Notes

[1]   M. J. Frisch, G. W. Trucks, H. B. Schlegel, G. E. Scuseria, M. A. Robb, J. R. Cheeseman, G. Scalmani, V. Barone, G. A. Petersson, H. Nakatsuji, X. Li, M. Caricato, A. Marenich, J. Bloino, B. G. Janesko, R. Gomperts, B. Mennucci, H. P. Hratchian, J. V. Ortiz, A. F. Izmaylov, J. L. Sonnenberg, D. Williams-Young, F. Ding, F. Lipparini, F. Egidi, J. Goings, B. Peng, A. Petrone, T. Henderson, D. Ranasinghe, V. G. Zakrzewski, J. Gao, N. Rega, G. Zheng, W. Liang, M. Hada, M. Ehara, K. Toyota, R. Fukuda, J. Hasegawa, M. Ishida, T. Nakajima, Y. Honda, O. Kitao, H. Nakai, T. Vreven, K. Throssell, J. A. Montgomery, Jr., J. E. Peralta, F. Ogliaro, M. Bearpark, J. J. Heyd, E. Brothers, K. N. Kudin, V. N. Staroverov, T. Keith, R. Kobayashi, J. Normand, K. Raghavachari, A. Rendell, J. C. Burant, S. S. Iyengar, J. Tomasi, M. Cossi, J. M. Millam, M. Klene, C. Adamo, R. Cammi, J. W. Ochterski, R. L. Martin, K. Morokuma, O. Farkas, J. B. Foresman, and D. J. Fox, Gaussian, Inc., Wallingford CT, 2016.

[2]   a) Y. Zhao, D. G. Truhlar, Theor. Chem. Acc., 2008, 120, 215-241; b) Y. Zhao, D. G. Truhlar, Acc. Chem. Res., 2008, 41, 157-167.

[3]   S. Grimme, J. Antony, S. Ehrlich, H. Krieg, The Journal of Chemical Physics, 2010, 132, 154104.

[4]   M. Head-Gordon, J. A. Pople, M. J. Frisch, Chem. Phys. Lett., 1988, 153, 503-506.

[5]   K. Fukui, Acc. Chem. Res., 1981, 14, 363-368.

[6]   a) A. E. Reed, F. Weinhold, The Journal of Chemical Physics, 1985, 83, 1736-1740; b) A. E. Reed, F. Weinhold, Isr. J. Chem., 1991, 31, 277-285; c) A. E. Reed, L. A. Curtiss, F. Weinhold, Chem. Rev., 1988, 88, 899-926; d) J. Podlech, The Journal of Physical Chemistry A, 2010, 114, 8480-8487; e) M. P. Freitas, J. Org. Chem., 2012, 77, 7607-7611; f) K. T. Greenway, A. G. Bischoff, B. M. Pinto, J. Org. Chem., 2012, 77, 9221-9226; g) E. Juaristi, R. Notario, J. Org. Chem., 2015, 80, 2879-2883; h) G. d. P. Gomes, V. Vil, A. Terent'ev, I. V. Alabugin, Chem. Sci., 2015, 6, 6783-6791; i) D. V. Vidhani, M. E. Krafft, I. V. Alabugin, J. Am. Chem. Soc., 2016, 138, 2769-2779; j) V. A. Vil', G. dos Passos Gomes, O. V. Bityukov, K. A. Lyssenko, G. I. Nikishin, I. V. Alabugin, A. O. Terent'ev, Angew. Chem. Int. Ed., 2018, 57, 3372-3376.

[7]   C. Riplinger, F. Neese, The Journal of Chemical Physics, 2013, 138, 034106.

[8]   F. Neese, WIREs Comput. Mol. Sci., 2018, 8, e1327.

[9]   CYLview, 1.0b; Legault, C. Y., Université de Sherbrooke, 2009 (http://www.cylview.org).

[10]   ChemCraft 1.7, build number 405; http://www.chemcraftprog. com (accessed February 2015).

[11]   Spin densities plotted with UCSF Chimera, developed by the Resource for Biocomputing, Visualization, and Informatics at the University of California, San Francisco, with support from NIH P41-GM103311. E. F. Pettersen, T. D. Goddard, C. C. Huang, G. S. Couch, D. M. Greenblatt, E. C. Meng, T. E. Ferrin UCSF

Chimera—A visualization system for exploratory research and analysis J. Comput. Chem. 2004, 25, 1605–1612.

[12]   J. Rodríguez-Guerra Pedregal, P. Gómez-Orellana, J.-D. Maréchal, Journal of Chemical Information and Modeling, 2018, 58, 561-564.

[13]   E. Paulechka, A. Kazakov, The Journal of Physical Chemistry A, 2017, 121, 4379-4387.

6.4.5 Structural, Energetic and Spectroscopic Calculated Parameters for all Species

For all structural, energetic and spectroscopic calculated parameters for all species please visit the published online supporting information:

G. dos Passos Gomes, A. Wimmer, J. M. Smith, B. König, I. V. Alabugin, *J. Org. Chem.,* **2019**, *84*, 6232-6243 or DOI: 10.1021/acs.joc.9b00503

7. Curiculum Vitae

Name	Alexander Wimmer
Date of birth	14.02.1992
Place of birth	Rotthalmünster
Nationality	German

Education

11/2016 – 12/2019   **Ph.D. in Chemistry (Dr. rer. nat.)**

Institute of Organic Chemistry, University of Regensburg

"Preparation of Sulfoximines, Sulfoximidoyl Derivatives and Sulfones via Visible-Light Photocatalysis"

Supervisor: Prof. Dr. B. König

10/2014 – 09/2016   **Master of Science in Chemistry**

Institute of Organic Chemistry, University of Regensburg

"Visible-Light-Accelerated Sulfoxidation of Electron-Rich Arenes"

Supervisor: Prof. Dr. B. König

10/2011 – 10/2014   **Bachelor of Science in Chemistry**

Institute of Organic Chemistry, University of Regensburg

"Synthese und Anwendung von polyisobutylen-markierten fac-Ir(ppy)₃-Derivaten als homogene, leicht rückgewinnbare Photokatalysatoren."

Supervisor: Prof. Dr. O. Reiser

09/2002 – 05/2011   **Allgemeine Hochschulreife (A-Levels)**

Wilhelm-Diess-Gymnasium Pocking

Majors: Chemistry & Sports

International Experience

07/2019 – 09/2019   Research stay with Prof. Dr. S. K. Collins at the University of Montreal, Canada.

Scientific Publications

12/2016   „Visible-Light-Accelerated C–H Sulfinylation of Heteroarenes"

A. U. Meyer, A. Wimmer, B. König, *Angew. Chem. Int. Ed.*, **2017**, 56, 409-412; A. U. Meyer, A. Wimmer, B. König, *Angew. Chem.*, **2017**, 129, 420-423.

01/2018   "Photocatalytic formation of carbon-sulfur bonds"

A. Wimmer, B. König, *Beilstein J. Org. Chem.,* **2018**, *14*, 54-83.

Part of thematic series: „Modern aspects of catalysis in organic synthesis."

08/2018   "Visible-Light-Mediated Photoredox-Catalyzed *N*-Arylation of *NH*-Sulfoximines with Electron-Rich Arenes"

A. Wimmer, B. König, *Adv. Synth. Catal.,* **2018**, *360*, 3277-3285.

04/2019   „CO_2 or SO_2: Should It Stay, or Should It Go?"

G. dos Passos Gomes, A. Wimmer, J. M. Smith, B. König, I. V. Alabugin, *J. Org. Chem.,* **2019**, *84*, 6232-6243.

04/2019   „*N*-Arylation of *NH*-Sulfoximines *via* Dual Nickel Photocatalysis"

A. Wimmer, B. König, *Org. Lett.,* **2019**, *21*, 2740-2744.

08/2019   "Photo-Nickel Dual Catalytic Benzoylation of Aryl Bromides"

T. E. Schirmer, A. Wimmer, F. W. C. Weinzierl, B. König, *Chem. Commun.,* **2019**, DOI: 10.1039/C9CC04726C.

Conference Contributions

10/2016   **27th Seminar Days of the GRK 1626**, Regensburg, Germany
            oral contribution

03/2017   **29th Seminar Days of the GRK 1626**, Regensburg, Germany
            oral contribution

06/2017   **45th National Organic Chemistry Symposium**, Davies, USA
            poster presentation

09/2017   **26th International Conference on Heterocyclic Chemistry**,
            Regensburg, Germany
            poster presentation

06/2018   **33th Seminar Days of the GRK 1626**, Perasdorf, Germany
            oral contribution

06/2018   **EuCheMS Conference on Organic Free Radicals**, Marseille, France
            oral contribution

09/2018   **26th Lecture Conference on Photochemistry**, Munich, Germany
            poster presentation

Memberships

11/2016 – 03/2019   Associate member of the DFG Research Training Group GRK 1626
                  "Chemical Photocatalysis"

01/17 – present   Member of the GDCh (Gesellschaft Deutscher Chemiker e.V.)

8. Danksagung

Allen voran gilt mein besonderer Dank Prof. Dr. Burkhard König für die Möglichkeit, meine Master- und Doktorarbeit unter seiner Aufsicht anfertigen zu dürfen. Ich bedanke mich für seine Unterstützung während der gesamten Zeit, die hervorragende Betreuung und die wertvollen Diskussionen und Denkanstöße während der Arbeit. Darüber hinaus danke ich ihm für die Ermöglichung von zahlreichen Konferenz-Besuchen auf der ganzen Welt und meines Forschungsaufenthaltes in Montreal.

Weiterhin danke ich den Mitgliedern des Prüfungsausschusses, Herrn Prof. Dr. Frank-Michael Matysik für die Übernahme des Zweitgutachtens, Herrn Prof. Dr. Alexander Breder als Drittprüfer und Herrn Apl. Prof. Dr. Rainer Müller für die Übernahme des Vorsitzes meines Promotionskolloquiums.

Des Weiteren danke ich allen Kooperationspartnern, mit denen ich die Herausforderungen der Projekte der letzten Jahre gemeistert habe: Prof. Dr. Burkhard König, Dr. Andreas Meyer, Tobias Schirmer, Prof. Dr. Igor Alabugin, Dr. Gabriel dos Passos Gomes, Dr. Joel M. Smith und Prof. Dr. Shawn K. Collins.

Ich bedanke mich bei Britta Badziura, Regina Hoheisel, Ernst Lautenschlager, Katharina Nickl, Viola Rappenegger, Simone Strauß, Dr. Rudolf Vasold, Julia Zach und Roxane Harteis für ihre Hilfe in allen technischen und organisatorischen Dingen, CV-Messungen, Chemikalienbestellungen und GC-MS Messungen.

Außerdem danke ich den Mitarbeitern der Zentralen Analytik, der NMR-Abteilung sowie der Glasbläserei und der Elektronik- und Feinmechanikwerkstatt der Universität Regensburg für die stets schnelle Bearbeitung anfallender Aufträge.

Besonderer Dank geht an meine Praktikanten Susanne Märkl, Oguzhan Albayrak und Selina Eichinger für die Tatkräftige Unterstützung an meinen Forschungsprojekten.

DANKE